IDŐJÁRÁS

QUARTERLY JOURNAL
OF THE HUNGARIAN METEOROLOGICAL SERVICE

CONTENTS

IDŐJÁRÁS

Quarterly Journal of the Hungarian Meteorological Service

IDŐJÁRÁS

Creation of a representative climatological database for Hungary from 1870 to 2020

Beatrix Izsák[1, 2,*] , **Tamás Szentimrey** [3], **Mónika Lakatos**[1], **Rita Pongrácz** [4], and **Olivér Szentes**[1]

[1]*Hungarian Meteorological Service,*
Kitabel Pál Street 1, H-1024, Budapest, Hungary

[2] *ELTE Faculty of Science, Doctoral School of Earth Sciences, Budapest, Hungary*

[3] *Varimax Limited Partnership, Budapest, Hungary*

[4] *ELTE Department of Meteorology,*
Pázmány Péter st. 1/A, H-1117, Budapest, Hungary

*Corresponding author E-mail: izsak.b@met.hu

(Manuscript received in final form August 13, 2021)

Abstract— Climate studies, particularly those that are related to climate change, require long, high-quality controlled data sets, which are representative both spatially and temporally. Changing the conditions of measurements, for example relocating the station, or changing the frequency and timing of measurements, or changing the instruments used can cause breaks in the time series. To avoid these problems, data errors and inhomogeneities are eliminated and the data gaps are filled by using the MASH (Multiple Analysis of Series for Homogenization, *Szentimrey,* 1999, 2008) homogenization procedure. The Hungarian meteorological observation network was upgraded significantly in the last decades. Homogenization of the data series raises the question of how to homogenize long and short data series together within the same process. It is possible to solve this with the MASH method due it has solid mathematical foundations, which make it suitable for such purposes. The solution includes the synchronization of the common parts' inhomogeneities within three (or more) different MASH processing of the three (or more) datasets with different lengths depending on the time periods and elements. After the homogenization process, the station data series were interpolated to a 0.1 degree regular grid covering the whole area of Hungary. The MISH (Meteorological Interpolation based on Surface Homogenized Data Basis; *Szentimrey* and *Bihari,* 2007) program system was used for this purpose. The MISH procedure was developed specifically for the interpolation of various meteorological elements. In the case of mean temperature, we also renewed the MISH modeling, as compared to previous years, the number of homogenized stations doubled due to the new work, so it was expedient to model the climate statistical parameters with this extended station system. Time series of daily mean temperature and precipitation sum for the period 1870–2020 for Hungary were used in this study. As a result, the longest ever homogenized, gridded daily data sets became available for Hungary. The method described here can also be applied to produce representative datasets for other meteorological elements.

Key-words: homogenization, interpolation, quality control, climatological database, ANOVA method, gridding

1. Introduction

In recent years, as the importance of climate change research has grown, more and more databases for climatological purposes have emerged. These are mainly based on measurements, but the methodology itself can be quite different. Raw data sets contain errors, significant inhomogeneities are found in them, and missing data must be replaced. To get to know the climate of recent periods, we need a representative database in space and time based on measurements (*Izsák and Szentimrey,* 2020). In order to have a spatially and temporally representative database, the first step is to homogenize, check, and complete missing values in the station data series (*WMO,* 2020). Since we have data series of different lengths, this is not an easy task, because in order to create a representative database we need to use as much data and as long data series as possible.

Homogenization, quality control and completion of the daily data series were implemented by the method MASH (*Szentimrey,* 1999, 2008). The interpolation or gridding of the daily data series was carried out using the method MISH method (*Szentimrey* and *Bihari,* 2007). A general overview and evaluation of the homogenization methods and the theoretical background can be found in these references (*Venema et al.,* 2012; *WMO,* 2020). While the following references (*Cressie,* 1991; *Szentimrey et al.,* 2011) are suggested for studying the general theoretical questions and methods of spatial interpolation.

2. The software MASH v3.03

Changing measurement conditions, such as station relocation, changing measuring time, or changing the instrument, may result in undue fractures in time series. At the Hungarian Meteorological Service (HMS), data errors and inhomogeneities are eliminated and data gaps are filled using the MASH (Multiple Analysis of Series for Homogenization; *Szentimrey,* 1999, 2008, 2017) homogenization procedure. What kind of software is employed for homogenization is of great importance, because if not just inhomogeneities are removed from the data series, but also, the process unintentionally modifies the signal of climate change, the result will be misleading. Thanks to the mathematical model, using the MASH software, it is possible to detect climate change in the homogenized data set.

2.1. The main properties of MASHv3.03

The advantages of MASHv3.03 in the homogenization of monthly series are:

– It is a relative homogeneity test procedure.
– It is a step-by-step iteration procedure: the role of series (candidate, reference) changes step by step in the course of the procedure.

– Either an additive (e.g., temperature) or a multiplicative (e.g., precipitation) model can be used depending on the distribution of the target meteorological element.
– It includes quality control and missing data completion.
– It provides the homogeneity of the seasonal and annual series as well.
– Metadata (probable dates of break points) can be used automatically.
– The homogenization results can be evaluated on the basis of verification tables generated automatically during the procedure.

In the homogenization of daily series:
– The procedure is based on the detected monthly inhomogeneities.
– It includes quality control and the completion of missing data in daily data.

2.2. *The MASH procedure for daily series*

The MASH procedure developed for daily series (*Szentimrey*, 2008, 2013) consist of the following steps:

1. preparation of monthly series from daily series;
2. MASH homogenization procedure for monthly series, estimation of monthly inhomogeneities;
3. on the basis of estimated monthly inhomogeneities, smooth estimation for daily inhomogeneities;
4. homogenization of daily series;
5. quality control for homogenized daily data;
6. missing daily data completion;
7. monthly series from homogenized, quality-controlled, completed daily data;
8. test of homogeneity for the new monthly series by MASH.

The procedure repeats steps 2–8 if it is necessary.

2.3. *The verification statistics in MASH*

The test statistics generated automatically during the procedure are the following:
Test statistics for series inhomogenity:
– test statistics after homogenization,
– test statistics before homogenization,
– statistics for estimated inhomogeneities.

Characterization of inhomogenity:
– relative estimated inhomogeneities,

– relative modification of series,

– lower confidence limit for relative residual inhomogeneities.

Representativity of station network
Evaluation of meta data;

– test statistics,

– representativity of META data.

3. The software MISHv1.03

The method MISH (Meteorological Interpolation based on Surface Homogenized Data Basis; *Szentimrey* and *Bihari,* 2007, 2014) was developed specifically for the spatial interpolation of surface meteorological elements. This is a meteorological system not only in respect of the aim but in respect of the tools as well. It means that as well as the predictors, all the valuable meteorological information – climate statistical parameters, supplementary model variables, and possible background information – are included. For that purpose, developing an adequate mathematical background was also necessary of course. The main difference between MISH and the geostatistical interpolation methods can be found in the amount of information used for modeling the necessary statistical parameters (*Szentimrey et al.,* 2011). In general, when using the geostatistical methods built in GIS, the sample elements for modeling are only the predictors, which sample is merely a single realization in time. However, MISH method uses the spatio-temporal data for modeling since long data series form a sample in time and space as well. The long data series is such a specialty of meteorology, which enables efficient modelling of the statistical parameters in question.

The software version MISHv1.03 (*Szentimrey* and *Bihari,* 2014) consists of two units, the modeling and the interpolation systems. The interpolation system can be applied to the results of the modeling system. These two units of the software developed can be summarized as follows.

The modeling subsystem for climate statistical (local and stochastic) parameters:

– This is based on long homogenized data series and supplementary deterministic model variables. The model variables may include such elements as height, topography, distance from the sea, etc. Neighborhood modeling and correlation model are applied to each grid point.

– It is also a benchmark study, a cross-validation test for interpolation error or representativity.

– It should be noted that the modeling procedure must be executed only once before the interpolation applications.

The interpolation subsystem:

– Either additive (e.g., temperature) or multiplicative (e.g., precipitation) model and interpolation formula can be used, depending on the climate elements.

– Daily or monthly values and means from a number of years can be interpolated.

– Only a few predictors are sufficient for the interpolation, and no problem arises if the greater part of daily precipitation predictors is equal to 0.

– Representativity is also modeled.

– Supplementary background information (stochastic variables), e.g., satellite, radar, forecast data can also be used.

– Data series completion, namely, missing value interpolation, completion for monthly or daily station data series is possible.

– Interpolation, the gridding of monthly or daily station data series for given predictand locations is possible. In case of gridding, the predictand locations are the nodes of a relatively dense grid.

For this study, station datasets are interpolated to a 0.1 degree regular grid. We calculate regional and national averages from these gridded data series. In addition, in the case of temperature, modeling of the climate statistical parameters was also renewed, as the number of stations had increased significantly. In the case of precipitation, the number of homogenized data series used for modeling did not change, so here we interpolate with the previous modeling results.

The quality of interpolation can be characterized by the representativity value in the s_0 location (*Szentimrey* and *Bihari,* 2014):

$$\text{REP}(s_0) = 1 - \frac{\text{RMSE}(s_0)}{\text{D}(s_0)} \, ,$$

where $\text{RMSE}(s_0)$ is the root-mean-square error and $\text{D}(s_0)$ is the standard deviation in the s_0 location. We show the representativity values for the gridpoint databases obtained by gridding the different station systems.

4. ANOVA (analysis of variance) examination

Since the representativity values depend on the distribution of the given meteorological element, the comparison of the gridded data sets is supplemented. We focus on the ANOVA methodology that we used originally in the MISH procedure (*Szentimrey* and *Bihari,* 2014).

Using the basic theorem of ANOVA, the total spatiotemporal variance can be partitioned equivalently as follows.
- Sum of spatial variance of temporal means and spatial mean of temporal variances. The temporal means and temporal variances (or standard deviations) in the space can be visualized by maps.
- Sum of temporal variance of spatial means and temporal mean of spatial variances. The series of spatial means and spatial variances (or standard deviations) can be visualized by graphics.
- The above ANOVA methodology can be used for gridded monthly, seasonal, and annual series calculated from the daily series. Mean series are calculated for temperature, while sum series are calculated for precipitation.

4.1. Mathematical description

In our ANOVA examination, the following mathematical formulas are used:

- data series at s_j location and t time: $\quad Z(s_j, t)\ (j = 1, \ldots, N; t = 1, \ldots, n)$,

- temporal mean at location s_j: $\quad \hat{E}(s_j) = \frac{1}{n}\sum_{t=1}^{n} Z(s_j, t)\ (j=1,\ldots,N)$,

- temporal standard deviation at location s_j:
$$\hat{D}(s_j) = \sqrt{\frac{1}{n}\sum_{t=1}^{n}(Z(s_j, t) - \hat{E}(s_j))^2} \quad (j=1,\ldots,N)$$
,

- spatial mean at moment t: $\quad \hat{E}(t) = \frac{1}{N}\sum_{j=1}^{N} Z(s_j, t) \quad (t=1,\ldots,n)$,

- spatial standard deviation at moment t:
$$\hat{D}(t) = \sqrt{\frac{1}{N}\sum_{j=1}^{N}(Z(s_j, t) - \hat{E}(t))^2} \quad (t=1,\ldots,n)$$

- total mean: $\quad \hat{E} = \frac{1}{N\cdot n}\sum_{j=1}^{N}\sum_{t=1}^{n} Z(s_j, t) = \frac{1}{N}\sum_{j=1}^{N}\hat{E}(s_j) = \frac{1}{n}\sum_{t=1}^{n}\hat{E}(t)$

- total variance: $\quad \hat{D}^2 = \frac{1}{N\cdot n}\sum_{j=1}^{N}\sum_{t=1}^{n}(Z(s_j, t) - \hat{E})^2$

4.2. Partitioning of total variance (Theorem)

Using the formulas defined above, the following equation can be written:

$$\widehat{D}^2 = \frac{1}{N}\sum_{j=1}^{N}\left(\widehat{E}(s_j) - \widehat{E}\right)^2 + \frac{1}{N}\sum_{j=1}^{N}\widehat{D}^2(s_j) = \frac{1}{n}\sum_{t=1}^{n}\left(\widehat{E}(t) - \widehat{E}\right)^2 +$$

$$\frac{1}{n}\sum_{t=1}^{n}\widehat{D}^2(t)\,. \tag{1}$$

The analysis of the following terms is recommended to characterize the spatiotemporal variability:

Spatial terms: spatial variance of temporal means: $\qquad \frac{1}{N}\sum_{j=1}^{N}\left(\widehat{E}(s_j) - \widehat{E}\right)^2,$

and temporal mean of spatial variances: $\qquad \frac{1}{n}\sum_{t=1}^{n}\widehat{D}^2(t),$

Temporal terms: spatial mean of temporal variances: $\qquad \frac{1}{N}\sum_{j=1}^{N}\widehat{D}^2(s_j)$,

and temporal variance of spatial means $\qquad \frac{1}{n}\sum_{t=1}^{n}\left(\widehat{E}(t) - \widehat{E}\right)^2.$

We do not show the variances but the standard deviations to make the values easier to interpret, especially in the case of precipitation.

Total standard deviation: $\qquad \widehat{D} = \sqrt{\frac{1}{N \cdot n}\sum_{j=1}^{N}\sum_{t=1}^{n}\left(Z(s_j,t) - \widehat{E}\right)^2}.$

Spatial standard deviation of temporal means: $\qquad \sqrt{\frac{1}{N}\sum_{j=1}^{N}\left(\widehat{E}(s_j) - \widehat{E}\right)^2}.$

Root spatial mean of temporal variances: $\qquad \sqrt{\frac{1}{N}\sum_{j=1}^{N}\widehat{D}^2(s_j)}.$

Temporal standard deviation of spatial means: $\qquad \sqrt{\frac{1}{n}\sum_{t=1}^{n}\left(\widehat{E}(t) - \widehat{E}\right)^2}.$

Root temporal mean of spatial variances: $\qquad \sqrt{\frac{1}{n}\sum_{t=1}^{n}\widehat{D}^2(t)}.$

5. Homogenization of spatially and temporally expanded station systems

When the station network is upgraded and we have short data series along with the long series, the common section must be homogeneous together with the long as well as with the short data series, whilst the two or more systems have also to be homogeneous. MASH is able to fulfil these criteria, as it is based on hypothesis testing, and it involves an iteration procedure (*Szentimrey,* 1999, 2017). Because MASH is an iteration procedure, the series are examined and adjusted many times, therefore, the homogenization of the new system can be considered as a

continuation of the earlier homogenization procedure. The test of hypothesis, and throughout this test, the test statistics enable us to use the former results.

The solution is that we synchronize the inhomogeneities of the common part within two or more different MASH processings for two or more datasets with different length.

We have harmonized two MASH systems in the recent years. However, as a result of digitization undertaken for the 150th anniversary of the HMS, daily precipitation sums and mean temperature data for 11 stations, starting in 1870 are now available. Three and four MASH systems are used to combine the daily precipitation sum and mean daily temperature, respectively, into one homogeneous climate database. Therefore, we harmonize three MASH systems for the precipitation database. This year, on the basis of the larger daily mean temperature database, the task is to homogenize four MASH systems together. We first note that the selection of station systems is a difficult task, as we have to look for discontinued stations close to the automatic measuring stations launched a few years ago, or even to find a continuation data series for stations that have been discontinued for decades but had an 80- to100-year-long time series.

In order to update our database annually or to homogenize several MASH systems together, test statistics must be studied at each step so that the homogenization can be continued based on these, or it can be decided that the overall homogeneity of the station network is acceptable at a given significance level.

5.1. Quality control of daily data

The data check section of MASH is very useful not only for checking archive data, but also for a comprehensive examination of daily data for the entire period. When checking the data of recent years, we can more easily examine the suspicious data marked in automatically generated error.res file of MASH, as we have additional data from radar or satellite measurements, or from other information sources. For example, in the case of temperature, if a measurement point has a much lower value than the nearest stations, looking at the satellite image, it is clear that this could be possible due to the lack of cloud and snow cover, so the data in the error file is actually extreme and not an error (*Fig. 1*). There are also cases where the value in the error file is indeed erroneous, such as when there is a large discrepancy based on comparison with neighboring stations, and from a meteorologist's point of view there is nothing to justify this difference. There are many such examples from the present, while the more difficult task is to examine the data measured 100 and more years ago, as there were no satellites or radars at that time. There are cases where statistical calculation indicates an error, but the meteorologist is unable to make a decision due to the small amount of information. For instance, if the nearest stations (distance $\geq$ 100 km, as the station network was even less dense 150 years ago) show 20 °C and the given

station shows 10 °C, this is possible in the Carpathian Basin (e.g., due to a cold front), but it may also be a measurement error. (Mathematical procedures cannot distinguish between extreme values and data errors.) Recording errors are easily found by MASH, in which case we can correct the data based on the annual books. In several cases, we found errors of varying magnitude and sign for the entire month, and now we know that in all of these cases, data for the previous or following month were recorded. Typical errors are the sign error and the absence of the decimal point. It can be seen from these examples, that professional analyses are needed after the automatic data verification, and the two together ensure a comprehensive examination. A major advantage of quality control in MASH is that only a few percent of the millions of data need to be subjected to further analysis, and if we have checked past data, we do not have to re-examine them again, only the new year or years have to be examined, which does not exceed 10 such examinations per year per meteorological variable.

Fig. 1. Satellite image, captured on December 5, 2019. In the area marked with a red circle, a very low daily average temperature was measured compared to the nearest stations.

5.2. *Quality control of monthly data*

In the MASH system, errors in the monthly data are displayed as outliers. However, it is also worth exploring large inhomogeneities over several months or even years. Here are a few examples.

As it can be seen in *Fig. 2*, Miskolc station has high inhomogeneity values for the period 1901–1908. We found an explanation for these about 20 years later, in the paper archives. At that time they were not measured in Celsius, but in Réaumur scale (*Fig. 3*). When checking the precipitation data archive, we found the same discrepancies due to the fact that the unit of measurement was different, e.g., Paris line or inch. In these cases, converting the basic data to the appropriate unit, give us

valid data. The significant monthly and annual inhomogeneities detected at the Nyíregyháza station can also be easily explained, as we found in the annual books that the observation time was 1 hour later in the morning and 1 hour earlier in the evening between 1890–1901, so the high inhomogeneity found by MASH does not indicate erroneous data (*Fig. 4*). These are inhomogeneities, which resulted in much higher daily averages than if they had been detected at the standard time.

It also shows that the models based on the classical mathematical theories which forms the basis of the MASH system work very efficiently, but human intervention is also needed!
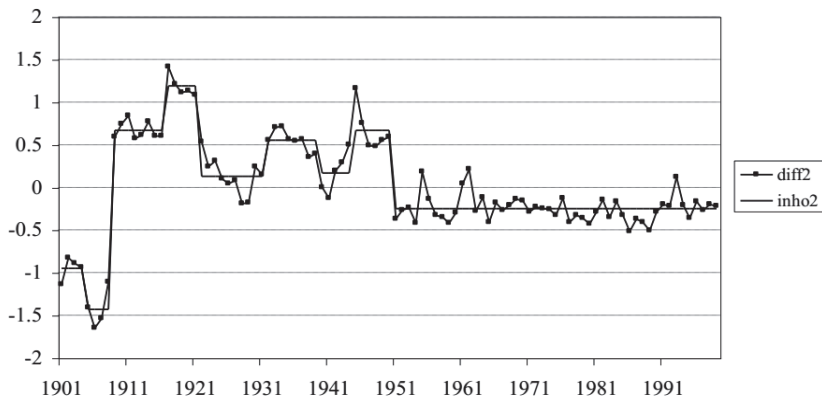
Fig. 2. The original graph of the MASH manual (*Szentimrey,* 2017): the difference series for Miskolc station and the estimated inhomogeneity.

Fig. 3. The observations of May 1902 at Miskolc station. It is clear that instead of the °C already widely used at that time, the air temperature values are given in Réaumur scale. (Source: HMS)

10
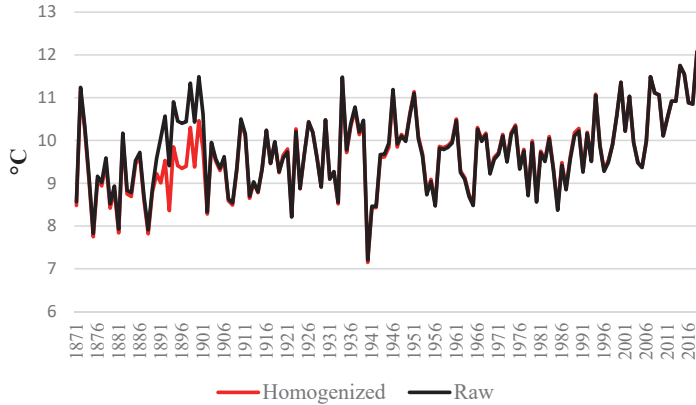
Fig. 4. Spatial mean series of annual mean temperature calculated from raw and homogenized data series at Nyíregyháza station, 1871–2019.

5.3. Automatic use of metadata in MASH

One of the great benefits of MASH is that it handles metadata (i.e., station history information) automatically, so we created these meta-files as well. However, we know that these are often incomplete, and we also know that not all changes cause inhomogeneity. The decision mechanism in MASH ensures that breakpoints are detected (*Szentimrey,* 2017), the user can choose between basic, strict, and light versions, and MASH evaluates the metadata with automatically generated statistics (*Szentimrey,* 2017). In the case of the three longer systems the representativity values of the metadata are below 0.4, in the case of the shortest system they are less than 0.5, but even in this case we cannot say that the inhomogeneities themselves can be well explained with this information. However, if the annual breakpoints are searched for and treated as metadata, the verification statistics will improve significantly (around 0.8), but still there are stations that cannot be explained with metadata at all, and there are several stations where all breakpoints can be explained with metadata.

6. Creation of a representative climatological database

6.1. Joint homogenization of time series with unequal length in the case of mean temperatures

We use the MASH system at the Climate Department of the Hungarian Meteorological Service to check, homogenize, and complete the daily station data sets. As the database is constantly updated, it is necessary to complete and verify

them, not only with the data of the past year, but also with the archive data being continuously digitized. Our goal is to use as many station data sets as possible for climatological analyses each year. So far, in the case of mean temperatures, we used the data of 25 stations from 1901 to 2020, and from 1971 to 2020 a further 33 stations were added, i.e., a total of 58 stations were included, to compile our database for climatological purposes.

This year, we reviewed our station system and significantly expanded it (*Fig. 5*). From 1870, data sets from 11 stations were checked, homogenized, and completed. For the period starting in 1901, we also use the data of an additional 22 stations, so from 1901 our homogenized, completed, and quality controlled database is based on the long data series of 33 stations. The next time step was chosen to be 1951, when the number of available station data sets was significantly expanded, with a further 22 stations, i.e., 55 station data sets altogether. The shortest period starts from 1975 and includes 110 stations. (Note here that we also use data from 4 other stations, which have too many missing data to be included in the short system, but their geographical location justifies taking their data into account. We will discuss this issue later.) So, our task was to homogenize the data sets of the four MASH systems together, i.e., the common part should be homogeneous in each system.
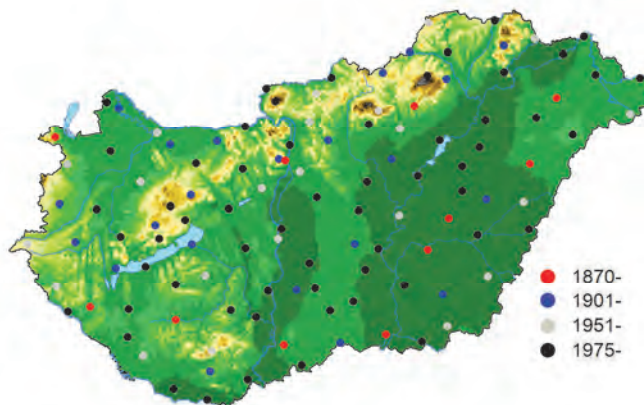
Fig. 5. Location of the stations in case of temperature.

6.1.1. Homogenization steps using four MASH systems

Step zero is to compile the station systems, since we cannot predict in advance how much missing data the MASH will work with, i.e., when the data series will be dependent. The methodology for station selection is a complex task, as data

gaps, relocation, and closure of stations are common. Thus, in many cases, it is necessary to concatenate the data of a station closed with the data of a station located 10–20 km apart. Such as Zirc and Tés, or Salgótarján and Zabar, for instance. These station pairs are both at high elevations in the data-sparse mountainous regions of Bakony and Börzsöny, respectively, so it is important to included them in the analysis. Station selection is very important in order to end up with a coherent dataset. Stations where missing data are utmost have to be left out from the process. The 4 systems used in the homogenization process are presented in *Fig. 6.*
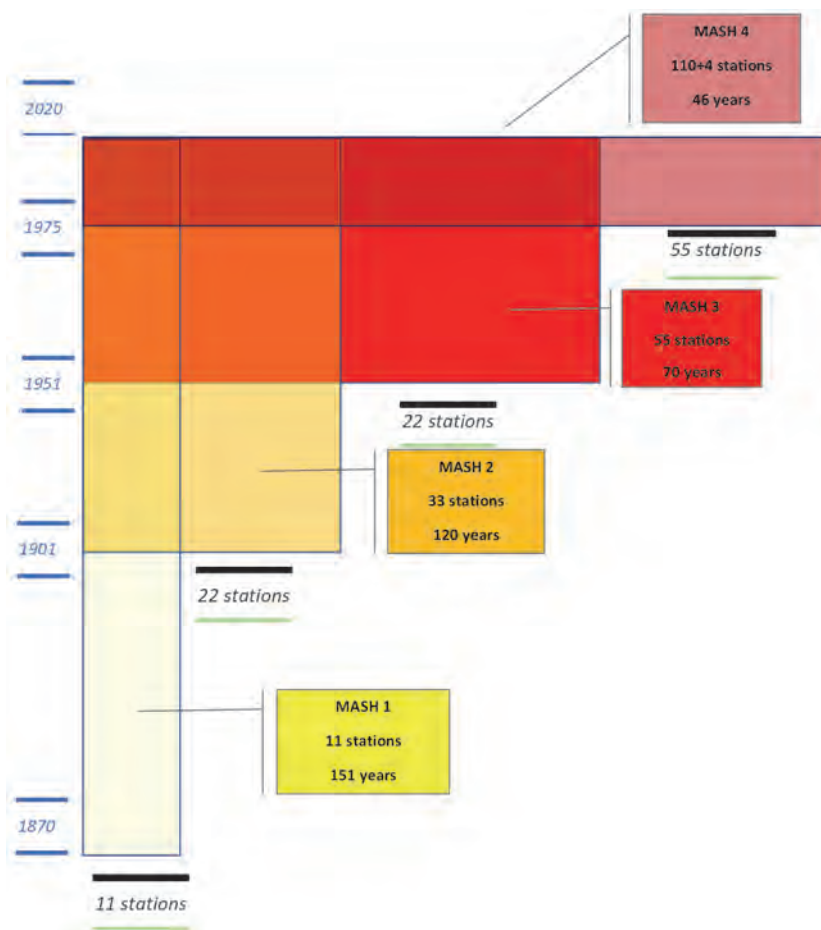
Fig. 6. The scheme of the four different station systems for the MASH procedure in the case of temperature.

The steps for homogenization of the temperature station data series are as follows:

1. MASH1: homogenization of monthly data;
2. Cutting out the inhomogeneities of the common part and inserting it into the other three MASHs (i.e., MI1, ...MI12 in the SAM directory);
3. MASH2: homogenization of monthly data;
4. Cutting out the inhomogeneities of the common part and inserting them into the other three MASHs;
5. MASH3: homogenization of monthly data;
6. Cutting out the inhomogeneities of the common part and inserting them into the other three MASHs;
7. MASH4: homogenization of monthly data;
8. Cutting out the inhomogeneities of the common part and inserting them into the other three MASHs;
9. If statistics are acceptable in MASH1: go to step 10, if not, go to step 1;
10. If statistics are acceptable in MASH2: go to step 11, if not, go to step 3;
11. If statistics are acceptable in MASH3: go to step 12, if not, go to step 5;
12. Homogenization of daily data in MASH1, MASH2, MASH3, MASH4;
13. Gathering the homogenized data sets from the different MASH systems.

Summarizing the steps 1–12: we homogenized the data series from the longest to the shortest ones. In this case, two runs provided good results as after inserting the common inhomogeneities, the test statistics no longer increased.

Overall, we can say that the co-homogenization was successful, the data sets can be considered homogeneous at the 0.05 level of significance. The most important verification statistics are summarized in *Table 1*.

Table 1. The most important verification statistics in case of annual mean temperature

MASH	MASH1	MASH2	MASH3	MASH4
Significance level: 0.05	Critical value: 22.05	Critical value: 21.76	Critical value: 21.31	Critical value: 20.86
Test statistics before homogenization	1253.08	877.95	357.2	257.49
Test statistics after homogenization	44.89	29.1	24.83	21.81
Relative modification of series	0.43	0.48	0.39	0.38
Representativity of station network	0.83	0.87	0.89	0.89

6.1.2. Some examples of manual correction

Here we note, that we took advantage of the possibilities of the interactive program system, since we needed manual correction in many cases. The subroutines and subdirectories built into the MASH provide this option. (This, in turn, requires a thorough study of the mathematical background.) As mentioned earlier, we have added several stations to the new system that have a significant lack of data, in which case the completion of missing values takes place from neighboring stations. The test statistics after homogenization value can be very high without having an actual breakpoint for that data set. In this case, the built-in graphics program, *mashex1-2* subroutines, can help us to decide whether to look for an additional breakpoint. It may also be necessary to manually exclude a particular station (e.g., one which we completed from the candidate series), in order to find the new breakpoint. We have the opportunity to do this with the *mashgame* program, and in many cases we have found a breakpoint. However, we may also need to manually delete a breakpoint with the *mashcor* program. For example, if the test statistics did not change before and after homogenization, despite the relative modification of series, value increased significantly. The principle of MASH is to homogenize the station data series with the slightest change in the data series. In months where the relative modification of the series value is very high for a station, it is always worth looking at what happened.

In our work, we omitted two stations from the older system that were homogenized, but the 80-100-year-old coherent data set has been discontinued for more than 20 years, and there is no continuation (Mencshely and Hárskút). Two more stations have data sets only from the last 10 years, but these are also in locations where data are highly needed. Thus, at the very end of the homogenization, these were inserted next to the homogenized data sets, and the verification statistics were regenerated. This year, these did not increase, and we did not receive any indication of inhomogeneity at the given stations, so we completed them based on the neighboring data series, and thus, finally the data set of 114 stations is included in the homogenized station database. Of course, if the statistics for these stations increase in the coming years, we will have to examine them thoroughly, as a new breakpoint may appear after new data is added.

6.2. Gridding in the case of mean temperature and the ANOVA results

Through homogenization and missing data completion, the station data set was completed and finalized. These homogenized station data series formed inputs to the MISH interpolation procedure (*Szentimrey* and *Bihari,* 2007, 2014), which is applied for gridding. Because far fewer stations were considered in the previous modeling procedure, we updated the results of the MISH model using the new homogenized data sets. These results were applied to gridding in all four cases. The resulting gridded dataset has acceptable quality, it is representative spatially

as well as temporally, therefore, it can be used for climate change studies. Since during the MISH modeling the resolution is set to a very fine 0.5´ grid, the information obtained in this way can be applied to any location within Hungary in the future. The gridded datasets from the four different station networks (*Figs. 5, 7*) were compared. Considering the representativity values for these data sets, a significant improvement is obvious, especially in the northern counties (*Fig. 8*). However, the representativity values themselves are not yet sufficient to characterize the created database. The ANOVA methodology (see Section 4), among others, enables us to compare the grid point databases. We looked at the ANOVA results for the common period 1975–2020. Temporal mean values and temporal standard deviation values of annual mean temperature for the four different station systems are shown in *Fig. 9*. The difference between the temporal means of the systems, which consists of stations 11 or 114, is illustrated in *Fig. 10.* Lower annual mean temperatures appear in extended regions with the denser station system. Higher values were obtained mainly in the central and southern areas of Transdanubia. Regarding the time series of spatial statistics, while the spatial means are almost identical, the spatial standard deviations are slightly different for the four different systems (*Fig. 11*). From this, we can conclude that as a result of MISH modeling, indeed, few predictors are sufficient to calculate a national average. In order to analyze the climatic conditions of a smaller area, it is no longer sufficient to use a less dense station system, but in this case the system of 33 and 55 stations also returns the spatial variability obtained from the system of 114 stations. Further ANOVA results are listed in *Table 2*.

Finally, the four gridded datasets are merged to a common database by taking grid point values from the dataset, which consists of most stations in the given time period (*Fig. 7*). The spatial mean series of annual mean temperature obtained with the merged dataset are shown in *Fig. 12*.
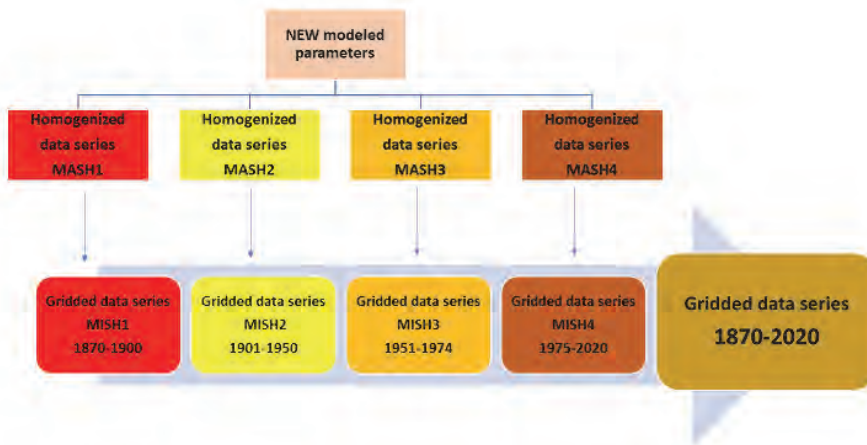
Fig. 7. The shematic diagram of creating the gridded database.

Fig. 8. Representativity values for the year for the four different station systems.
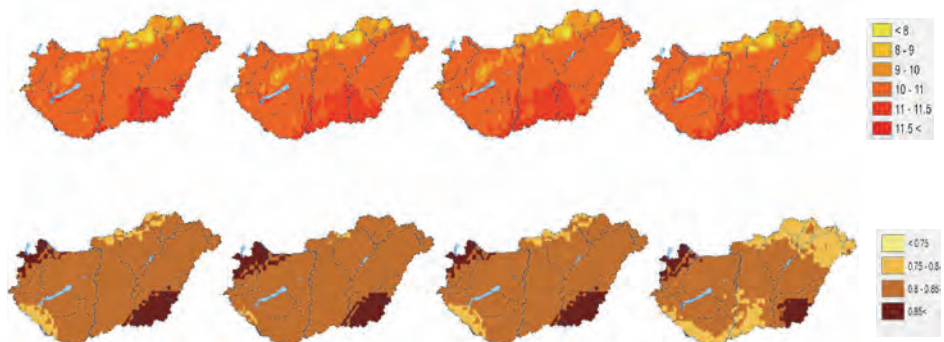
Fig. 9. Temporal mean values of annual mean temperature (top, in °C) and temporal standard deviation values of annual mean temperature (bottom, in °C) for the period 1975–2020 for the four different station systems.

Fig. 10. The difference between the temporal mean values of annual mean temperature based on 114 or 11 gridded stations for the common period 1975–2020 (in °C).
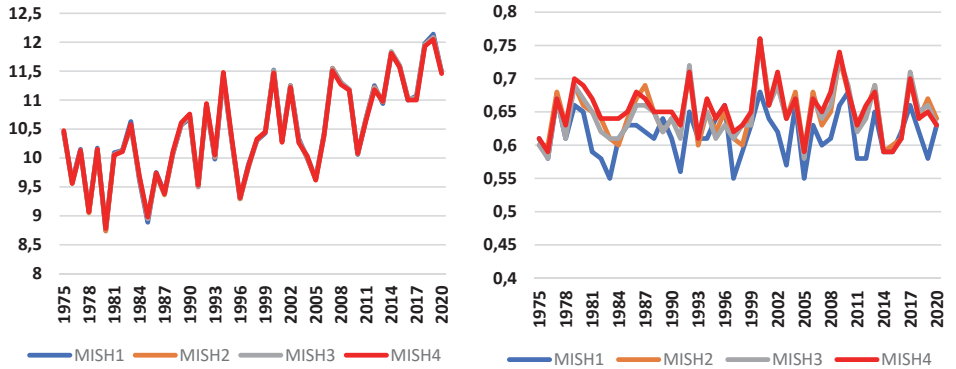
Fig. 11. Spatial mean series (left) and spatial standard deviation series (right) of annual mean temperature for the different systems (in °C).
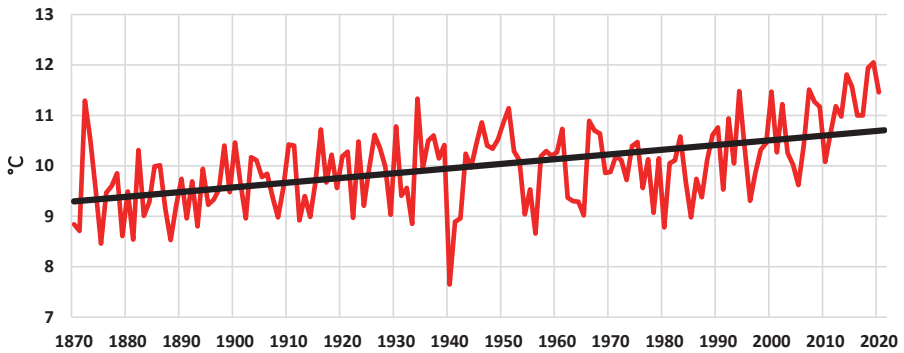
Fig. 12: Spatial mean series of annual mean temperature for Hungary from 1870 to 2020 with the estimated linear trend.

Table 2. The most important ANOVA results for the gridded annual mean temperature series for the different station systems computed for the common time period 1975–2020

	MISH1	MISH2	MISH3	MISH4
Total mean	10.47	10.46	10.47	10.46
Total standard deviation	3.25	3.23	3.24	3.23
Spatial standard deviation of temporal means	1.04	1.10	1.07	1.08
Root spatial mean of temporal variances	0.62	0.72	0.66	0.69
Temporal standard deviation of spatial means	0.83	0.84	0.84	0.83
Root temporal mean of spatial variances	0.82	0.83	0.83	0.82

6.3. Joint homogenization of time series with unequal length in the case of precipitation

The task is much simpler in the case of precipitation than in case of temperature, as the list of precipitation stations which could be used for homogenization and gridding remained unchanged compared to previous years (*Fig. 13*). The only new issue comes from the inclusion of the recently digitized data from 1870–1900 into the homogenization and gridding process. Quality control, data homogenization, and data completion are the first steps to execute here as well. Three MASH systems were built and harmonized for precipitation time series. *Fig. 14* illustrates the periods and the number of stations that were used in this process.
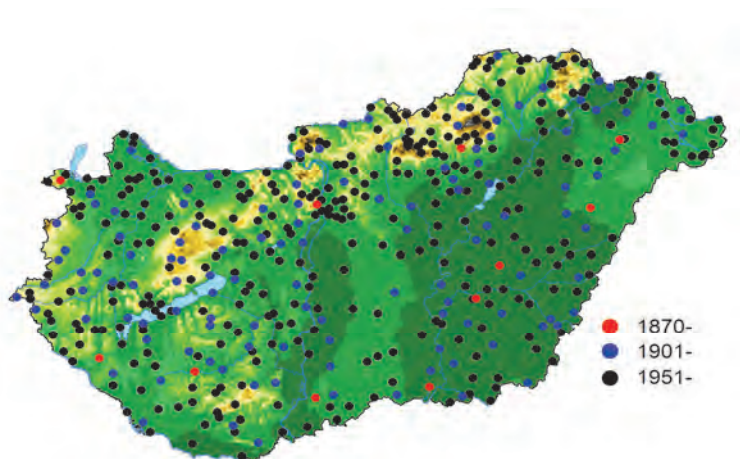
Fig. 13. Location of the stations in the case of precipitation.
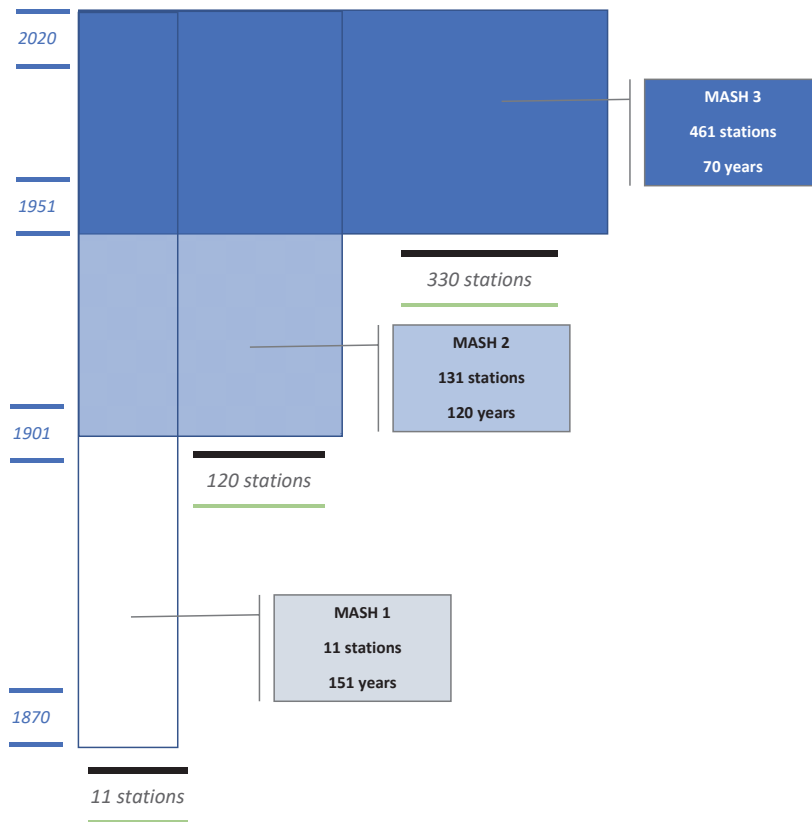
Fig. 14. The scheme of the three station systems for the MASH procedure, in the case of precipitation.

The steps of homogenization of precipitation station data series are as follows:

1. MASH1: homogenization of monthly data;
2. Cutting out and inserting the inhomogeneities of the common part into MASH2 and MASH3;
3. MASH2: homogenization of monthly data;
4. Cutting out the inhomogeneities of the common part and inserting them into MASH3 and MASH1;
5. MASH3: homogenization of monthly data;
6. Cutting out the inhomogeneities of the common part and inserting them into MASH1 and MASH2;

7. If statistics are acceptable in MASH1: go to step 8, if not, go to step 1;

8. If the statistics are acceptable in MASH2: go to step 9, if not, go to step 3;

9. Homogenization of daily data in MASH1, MASH2, and MASH3;

10. Gathering the homogenized data sets from the different MASH systems.

The most important verification statistics are listed in *Table 3*. Obviously, using data from 461 stations brings an improvement over using only 131 stations. Not surprisingly the representativity values of the station system consisting of 11 data series are very low. The reason for this is that precipitation varies more both spatially and temporally than the mean temperature, therefore, a much denser network of stations is needed to characterize well the distribution of precipitation. Similarly to temperature, we do not recommend the mere use of automatic algorithms in the case of precipitation either, even though in this case we are much more careful and use a significance level of 0.01. In each case, it is necessary to study the test statistics and, on this basis, the homogenized station data series is prepared. The great advantage of MASH is that we can correct not only automatically but also manually at almost every step, however of course, the biggest help is the study of verification statistics. The advantage of this is that the database can be updated every year without having to restart homogenizing again from the beginning.

Table 3. The most important verification statistics for annual precipitation sum

MASH	MASH1	MASH2	MASH3
Significance level: 0.01	Critical value: 28.00	Critical value: 28.00	Critical value: 30.00
Test statistics before homogenization	45.46	63.42	42.19
Test statistics after homogenization	18.79	27.91	26.75
Relative modification of series	0.23	0.18	0.11
Representativity of station network	0.46	0.63	0.7

6.4. Gridding in the case of precipitation and the ANOVA results

Using the previous modeling results in MISH, the grid point data sets in all three station networks were created by applying MISH interpolation procedure (*Figs. 13, 15*). The representativity values for January and July can be seen in the maps of *Fig. 16*. It is clear that the representativity values are smaller in July than in January. As the station density increases, the spatial pattern is more accurate.
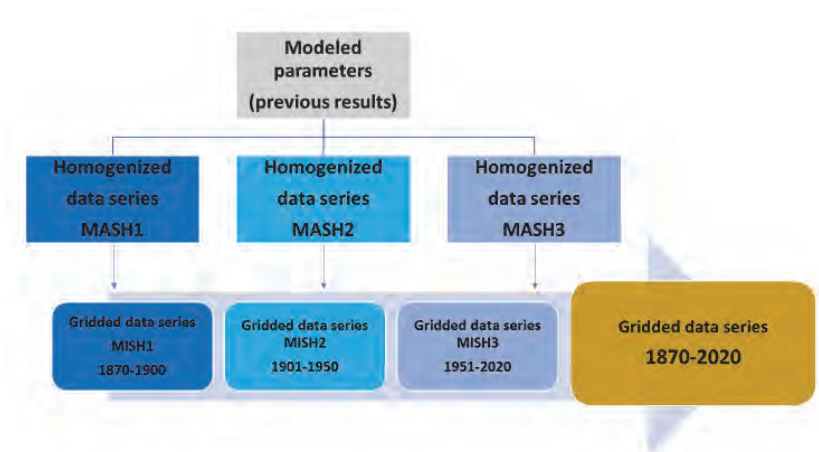
Fig 15. The shematic diagram of creating the gridded database.
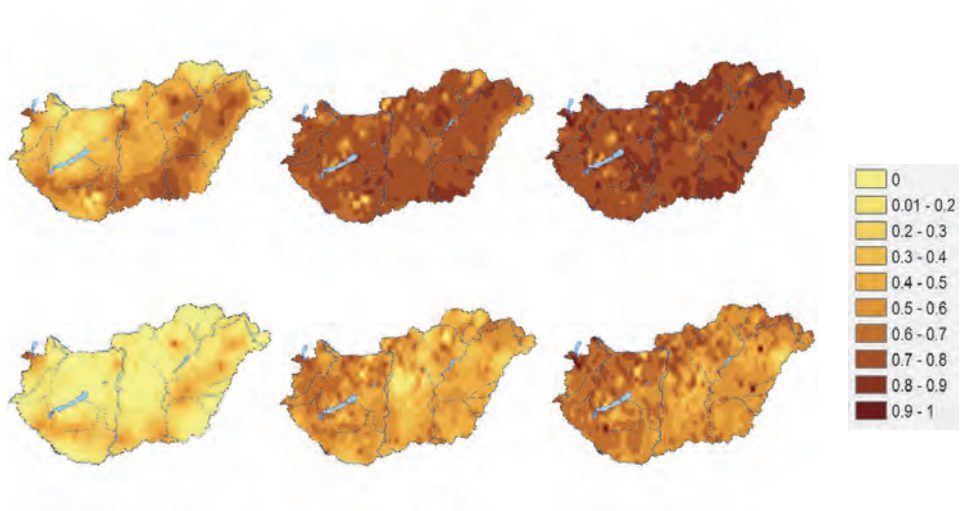
Fig. 16. January (top) and July (bottom) representativity values for the different station systems.

The ANOVA (see Section 4) results for the three precipitation station systems were compared (*Table 4*). The temporal means and standard deviations based on the common period of all three datasets are visualized in the maps of *Fig. 17*. The maps in *Fig. 18* enable us to identify the areas where more or less precipitation sums appear depending on the station systems. The spatial means are almost identical, the spatial standard deviations are slightly different for the three different systems (*Fig. 19*).

Table 4: The most important ANOVA results for the gridded annual precipitation sum series for the different station systems

	MISH1	MISH2	MISH3
Total mean	591.42	603.74	601.65
Total standard deviation	132.51	135.02	135.48
Spatial standard deviation of temporal means	68.85	66.23	65.46
Root spatial mean of temporal variances	113.22	117.66	118.62
Temporal standard deviation of spatial means	99.05	101.38	101.07
Root temporal mean of spatial variances	88.02	89.17	90.22
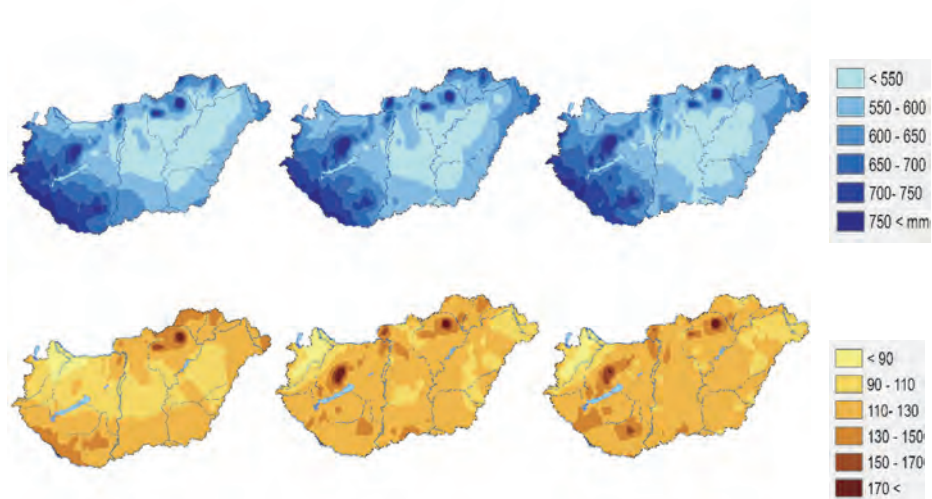
Fig. 17. Temporal mean values of annual precipitation sum (top, in mm) and temporal standard deviation values of annual precipitation sum (bottom, in mm) for the period 1975–2020 for the different station systems.
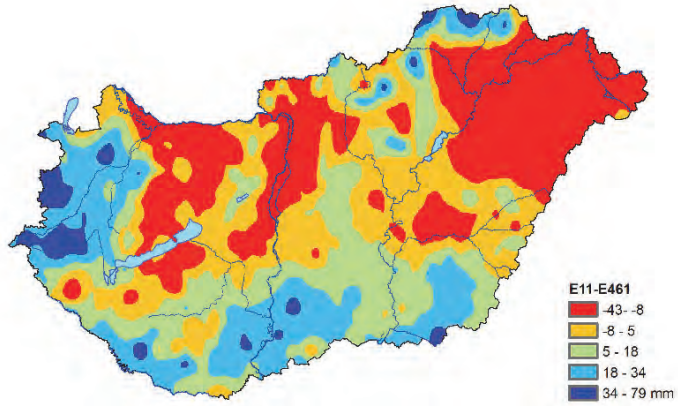
Fig. 18. The difference between the temporal mean values of annual precipitation sum based on 461 or 11 gridded stations for the common period 1975–2020 (in mm).
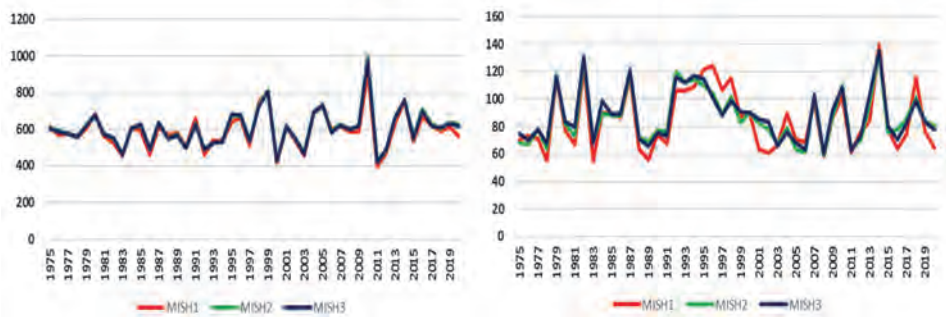
Fig. 19. Spatial mean series (left) and spatial standard deviation series (right) of annual precipitation sum for the different systems (in mm).

The three gridded precipitation datasets can be merged by taking the values from the most dense station systems for specific time periods (*Fig. 15*). Finally, the spatial mean series obtained with the merged dataset can be seen in *Fig. 20*.
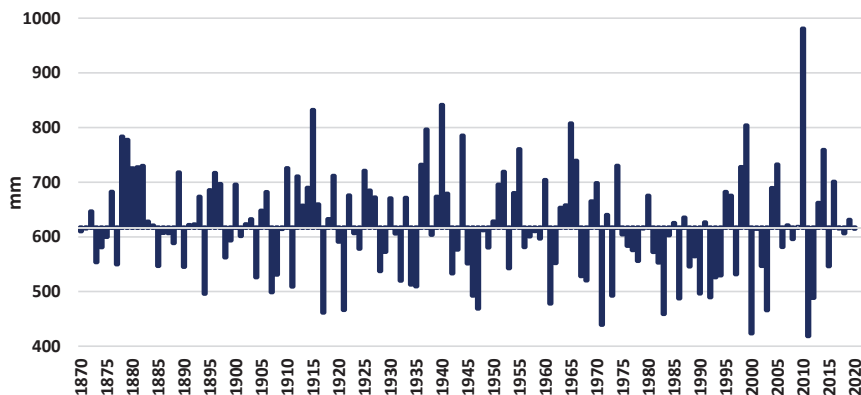
Fig 20. Spatial mean series of annual precipitation sum for Hungary, relative to the 1991-2020 normal, from 1870 to 2020.

We can conclude that we were able to harmonize station data series of different lengths, gaining as much information as possible from the measurements in order to characterize the precipitation. However, the station density for the period 1870–1900 is too sparse for quality checks, data completion, and homogenization. Thereby the quality of the time series from 1870–1900 is lower than the quality of data of the other two systems.

7. *Summary*

Homogenized, completed, and quality-controlled station datasets were derived from the daily mean temperature and daily precipitation sums for Hungary for different time periods. One of the most important achievements is that 151-years-long climate data series were homogenized for Hungary. Three MASH systems for the three different time intervals were harmonized for precipitation and four MASH systems for daily mean temperature. In the case of temperature, the daily data of 11 meteorological stations from 1870, 33 from 1901, 55 from 1951, and 114 from 1975 were used in this process. Daily precipitation sums of 11 stations from 1870, 131 from 1901, and 461 from 1951 were quality-controlled, homogenized, and completed. Significant quality improvement was achieved by expanding the station system in the case of temperature. We used unprocessed archived data for the creation of the datasets for temperature and precipitation. This work will allow us to study the climate change in Hungary over a longer period of time than it was previously possible.

References

Cressie, N., 1991: Statistics for Spatial Data., Wiley, New York, p. 900.

Izsák, B. and *Szentimrey, T.*, 2020: To what extent does the detection of climate change in Hungary depend on the choice of statistical methods? *Int. J. Geomath. 11*, 17.
https://doi.org/10.1007/s13137-020-00159-7

Szentimrey, T., 1999: Multiple Analysis of Series for Homogenization (MASH), Proceedings of the Second Seminar for Homogenization of Surface Climatological Data. Budapest, Hungary; WMO, WCDMP-No. 41, pp. 27-46.

Szentimrey, T., 2008: Development of MASH homogenization procedure for daily data. Proceedings of the Fifth Seminar for Homogenization and Quality Control in Climatological Databases, Budapest, 2006, WCDMP-No. 71, WMO/TD-NO. 1493, 123–130.

Szentimrey, T., 2013: Theoretical questions of daily data homogenization, *Időjárás 117*, 113–122.

Szentimrey, T., 2017: Manual of homogenization software MASHv3.03, Hungarian Meteorological Service, p.71.

Szentimrey, T. and *Bihari, Z.*, 2007: Mathematical background of the spatial interpolation methods and the software MISH (Meteorological Interpolation based on Surface Homogenized Data Basis), Proceedings of the Conference on Spatial Interpolation in Climatology and Meteorology, Budapest, Hungary, 2004, COST Action 719, COST Office, 2007, pp. 17–27.

Szentimrey, T. and *Bihari, Z.*, 2014: Manual of interpolation software MISHv1.03, Hungarian Meteorological Service, p. 60.

Szentimrey, T, Bihari, Z., Lakatos, M., and *Szalai, S.*, 2011: Mathematical, methodological questions concerning the spatial interpolation of climate elements. Proceedings of the Second Conference on Spatial Interpolation in Climatology and Meteorology, Budapest, Hungary, 2009, *Időjárás 115*, 1–11.

Venema V, Mestre O, Aguilar E, Auer I, Guijarro JA, Domonkos P, Vertacnik G, Szentimrey T, Štěpánek P, Zahradnicek P, Viarre J, Müller-Westermeier G, Lakatos M, Williams CN, Menne M, Lindau R, Rasol D, Rustemeier E, Kolokythas K, Marinova T, Andresen L, Acquaotta F, Fratianni S, Cheval S, Klancar M, Brunetti M, Gruber C, Duran MP, Likso T, Esteban P, Brandsma, T., 2012: Benchmarking monthly homogenization algorithms. *Clim. Past* 8, 89–115.
https://doi.org/10.5194/cp-8-89-2012

World Meteorological Organization (WMO), 2020: Guidelines on Homogenization, WMO-No. 1245.

IDŐJÁRÁS

Regionalization of low flow for chosen catchments of the upper Vistula river basin using non-hierarchical cluster analysis

Agnieszka Cupak* and **Grzegorz Kaczor**

University of Agriculture in Cracow
Faculty of Environmental Engineering and Land Surveying
Department of Sanitary Engineering and Water Management
30-059 Cracow, Poland

*Corresponding author E-mail: a.cupak@ur.krakow.pl

Abstract— The aim of this work was the regionalization of low flow for chosen catchments located in the upper Vistula river basin using non-hierarchical cluster analysis. Next, with such creative clusters, the regional relationships were determined between the specific low flow discharge q_{95} and the meteorological and physiographic parameters of the catchment. The study evaluated regional regression models for low flow (specific q_{95} discharge) in selected, 30 catchments located in the upper Vistula river basin. The data for calculations were a series of observations of daily discharge from the multiannual period of 1963–2016 and were obtained from the Institute of Meteorology and Water Management – National Research Institute in Warsaw. The study showed, that the k-means method can be used for regional regression determination. The parameters which influenced the catchments grouping in clusters were the specific low flow discharge q_{95}, precipitation, median catchment altitude, mean catchment slope, soil, and land use. The study indicated that k-means method may be an effective tool for evaluating low flow in rivers of the southern parts of Poland.

Key-words: low flow, cluster analysis, morphoclimatic parameters, catchments grouping

1. Introduction

The flow in a river is the sum of natural processes that take place within the catchment, such as: supplying, storing, and outflowing of water. Supply of water depends highly on precipitation, landscape and use of the area, and the roughness coefficient. Storage of water and its flow are dependent on complex physiographic elements of the catchment. The natural factors that affect the low flow in the river are: the type and infiltration capacity of the soil, deposition of aquifers, speed and frequency of water supply, evapotranspiration, management and topography of the area, and the climate. In many cases, ground waters provide supply of water for streams during the time of low flows. Low flows do not unbalance the ecology at such times. Therefore, it is important for aquifer layers to have access to sufficient volume of water, the level of ground waters to be sufficiently low to cross the watercourse, and the size and hydraulic conditions of the aquifer to be sufficient to maintain the flow during dry time. Supply of water for low flows may also come from the nearby surface of the valley bottom, where water is stored in the form of saturated soil, alluvial area, and wetlands. These are places saturated with water during or right after precipitation (*Smakhtin*, 2001; *Ziernicka-Wojtaszek* and *Kaczor*, 2013). The geological structure of the catchment also significantly affects the appearance of low flows. *Armbruster* (1976) and *Smith* (1981) confirmed in their study the direct relationships between the geological structure of the catchment and the speed of outflow at low flow time.

Modern society faces the common phenomenon of shortage of water. This problem is enhanced with the fact that water deficits occur in many parts of the world at the same time (*Bates et al.,* 2008). Shortage of water is related to drought that affects resources of surface and underground waters and can lead to reduction of the supply of water, deterioration of its quality, crop failure, and disturbances in habitats (*Mishra* and *Singh,* 2011).

The water balance is the main and commonly used model to determine low flows in controlled catchments. It requires entering some data, which in most cases are easily available, and the method is relatively simple and easy (*Merz* and *Blöschl*, 2004). In general, hydrometric gauging records are not available at the site of interest. Where these records are available, they may be of short length, leading high uncertainties in the selection of the probability distribution and the estimation of the parameters of selected model. When the observed streamflow records are unavailable or inadequate for a proper local frequency analysis, other approaches must be used (*Ouarda et al.,* 2008). In uncontrolled catchments, the relevant parameters are acquired from other sources of information, such as the neighboring catchments or the data concluded on the basis of literature information (*Merz* and *Blöschl*, 2004; *Wałega* and *Młyński*, 2017). In Poland, in case of controlled catchments, statistical methods based on different type of distribution of extreme value are in use, i.e., Gumbel method for low flow calculation (*Byczkowski,* 1972). For uncontrolled catchments, empirical formulas are used. There are few formulas

to low and average flow calculations, but they were worked out based on hydrological data for years 1950–1980 by the 20th century, for example the Punzet formula (*Punzet,* 1981). At present there is a need of verification or updating of these formulas, especially since actual hydrological data sequence are much longer at present (*Wałęga et al.,* 2014).

The regional frequency analysis is the most commonly used tool for the estimation of extreme hydrological events (floods, droughts) at sites, where little or no reliable data are available (*Vogel* and *Kroll*, 1990; *Tucci et al.* 1995; *Durrans* and *Tomic,* 1996; *Hamza et al.,* 2001; *Ouarda et al.,* 2005; *McLean* and *Watt*, 2005; *Laaha* and *Blöschl*, 2006). In general, a regional frequency analysis procedure is composed of two main steps: the identification of groups of hydrologically homogenous catchments (or regions) and the application of a regional estimation method within each delineated region (*Ouarda et al.,* 2008). Regionalization of catchments is founded on the premise, that catchments of the same climate, geology and topography, vegetation and soils have similar values of low flow parameters. It is possible to define the homogenous regions in a variety of manners: as geographically contiguous region, as geographically non-contiguous regions (*Ouarda et al.,* 2008). Regions grouped in this way are not always strictly homogeneous, but this approach may produce sufficient results when availability of data is limited. A homogeneous region can be also perceived as a group of catchments hydrologically similar, but not necessarily geographically neighboring. Multidimensional statistical analyses are often used to group catchments. cluster analysis is the general name of multidimensional statistical techniques that are used to study, interpret, and classify the data with those of a similar group or groups. The data from one cluster should be as close to each other as possible, whereas parameters from different clusters should differ, if possible.

Non-hierarchical methods of grouping require the initial determination of the number of clusters. They may be classified based on the techniques used to initiate the clusters, the criteria for cluster creation, and the types of the data for which they are appropriate (*Rao* and *Srinivas*, 2008). One of the most frequently used and the best known of the non-hierarchical clustering methods, i.e., for catchments grouping for the sake of flooding, is the k-means method (*Lecce*, 2000; *Burn* and *Goel*, 2000). In India, *Ahuja* (2012) used the k-means method for data regionalization of Godaravi catchments. In Poland, *Cupak* (2017) used it for low flow grouping. This method is effective for grouping large sets of data with numerical attributes. However, there are some limitations to this method in the breaking down of the data into categories. The method is also sensitive to presence of errors (*Rao* and *Srinivas,* 2008).

The objective of this work was the regionalization of low flow in chosen catchments located in in the area of the upper Vistula river basin with use of the non-hierarchical cluster analysis – the k-means method. Next, with such creative clusters, the regional relationships were determined between low flow q_{95} and the meteorological and physiographic parameters of the catchment.

2. Material and methods

The analysis was conducted for 30 selected catchments of the upper Vistula river basin (*Fig. 1*). The source material for the analysis were daily flows from the period 1963–2016 (*Table 1*). It was assumed, as a criterion of catchments' selection, that for analysis, only those catchments will be taken, for which daily streamflows are available with a minimum record length of 20 years. 13 physiographic and meteorological characteristics of catchments were also used (*Table 1*) in the analysis. The data related to daily flows, temperature, and precipitation were obtained from the Institute of Meteorology and Water Management, National Research Institute in Warsaw.
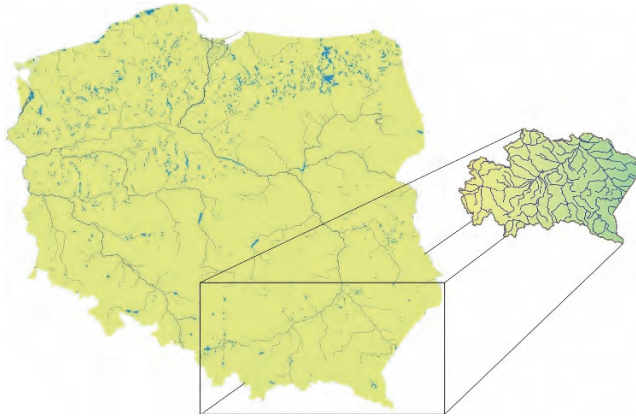
Fig. 1. Location of the upper Vistula river basin
(https://pl.wikipedia.org/wiki/Plik:Polska_hydrografia2.jpg)

The first step was to determine $Q_{95\%}$, that is the flow achieved during 95% of days in the studied timeframe. This low flow characteristic is widely used in Europe and was chosen because of its relevance for multiple choices of water management, among other things in case of projection of water supply systems. Then, $Q_{95\%}$ was subsequently standardized by the catchment area resulting in specific low flow discharges q_{95} ($dm^3 \cdot s^{-1} \cdot km^{-2}$). The data were standardised on the basis of Eq.(1) in order to obtain average values expected for the individual variables, which were given in various units.

$$x_{ij} = \frac{w_j}{\sigma_j} \left[f(y_{ij}) \right] \quad for \ \ j = 1, ..., n \ , \tag{1}$$

where
    $f(y_{ij})$ is the function subject to transformation,
    y_{ij} is the value of the feature j, in n – dimensional function of the vector y_i,
    w_j is the weight assigned to the given feature,
    σ_j is standard deviation.

In the k-means method, the first step is to determine the number of clusters. The center is determined for each group, which is defined as the function of the vector between the clusters. After assigning the variables to the clusters, the function of the vector is calculated again to redetermine the location of the center of the cluster. The variables are again assigned to the groups, according to the position of the new cluster (*Dikbas et al.*, 2013). The Euclidean distance was used to calculate the distance of the objects from the centers of the clusters.

The calculation procedure was run four times – for two, three, four, and five clusters. First, two clusters are generated. In the last step, analysis of correlations was conducted and models of correlations were defined. The coefficient of correlation was calculated, which describes the relationship between the unit outflow q_{95} and selected meteorological and physiographic features of the catchment. The coefficient of determination R^2 was also determined for the level of confidence $\alpha = 0.05$. Regional regression is built as a multiply regression (Eq.(4)), which shows relationships between low flow (as a dependent variable) and morphoclimatic parameters (as independent variables). It is used to identify the parameters that most strongly influence the low flow. To determine the power of regression equation, adjusted coefficient of determination R^2_{adj} for the level of significance 0.05 was calculated. The best results were obtained while using stepwise regression:

$$q_{95} = \beta_0 + \beta_1 \cdot x_1 + \beta_2 \cdot x_2 + \cdots + \beta_{p-1} \cdot x_{p-1}, \qquad (2)$$

where
    x_i are the morphoclimatic parameters of a catchment,
    β_i is the regression coefficient.

The statistical calculation were made using STATISTICA 13 software. *Figs. 2* and *4* were made in Inkscape.

2.1. Model performance criteria

The performance measures used in this study were the Nash–Sutcliffe efficiency (E), the percent bias ($PBIAS$), and the adjusted coefficient of determination (R^2_{adj}). Additionally to the regression model the goodness of fit was tested in case, when uncontrolled catchment will be included to a region.

The value of percent bias (Eq.(3)) and a root mean sum of squares error (Eq.(4)) were calculated for each clusters obtained with use cluster analysis (*Patel,* 2007).

$$PBIAS = \frac{1}{n}\sum_{i=1}^{n}(\frac{q_{95}^{obs} - q_{95}^{sim}}{q_{95}^{obs}}) \cdot 100\% \,, \tag{3}$$

$$RMSE = \sqrt{\frac{1}{n}\sum_{i=1}^{n}(q_{95}^{obs} - q_{95}^{sim})^2} \,, \tag{4}$$

where

q_{95}^{obs} is the observed specific low flow discharge q_{95} for catchment i,

q_{95}^{sim} is the model prediction.

$RMSE$ and $PBIAS$ values of 0 indicate a perfect fit. $PBIAS$ measures the average tendency of the simulated data to be larger or smaller than observed ones. The optimal value of PBIAS is 0. Positive values indicate model underestimation, while negative values indicate model overestimation (*Fang et al.,* 2014). For the assessment under $PBIAS$ a classification was used suggested by *Van Liew et al.* (2007), described as follows: $PBIAS<10\%$: it is a very good model, $10\% < PBIAS < 15\%$: the model is good; $15\% < PBIAS < 25\%$: the model is satisfactory, and when $PBIAS \geq 25\%$: the model is unsatisfactory model (*Pereira et al.,* 2016).

The E value (Eq.(5)) is a normalized statistic, that expresses the relative magnitude of the residual variance compared to the variance of the measured data (*Nash* and *Sutcliffe,* 1970; *Tegegne et al.,* 2017). E indicates how well a plot of observed versus simulated data fits a 1:1 line (*Tegegne et al.,* 2017). E was recommended for two major reasons: it is recommended for use by *ASCE* (1993) and *Legates* and *McCabe* (1999), and it is very commonly used, which provides extensive information on reported values (*Moriasi et al.,* 2007). It is calculated as:

$$E = 1 - (\frac{\sum_{i=1}^{n}(q_{95}^{obs} - q_{95}^{sim})^2}{\sum_{t=1}^{Nn}(q_{95}^{obs} - \overline{q_{95}^{obs}})^2}) \,, \tag{5}$$

where

q_{95}^{obs} is the observed specific low flow discharge,

q_{95}^{sim} is the predicted specific low flow discharge,

$\overline{q_{95}^{obs}}$ is the average value.

The range of E lies between 1.0 (perfect fit) and $-\infty$. An efficiency of lower than zero indicates that the mean value of the observed time series would have been a better predictor than the model (*Krause et al.,* 2005).

3. The description of the study area

The research included 30 selected catchments located in the upper Vistula river basin (*Fig. 2*). This area is spread within three great Carpathian physiographic units: the Carpathians (40% of the basin area), the Subcarpathian valleys (about 35% of the basin area), and the Małopolska Upland (about 25% of the basin area). The Carpathians and the Upland are the source areas for most of the upper Vistula tributaries, while the Subcarpathian valleys are a transit area for the Vistula and an estuary area for the rivers and streams formed in the Carpathians and Subcarpathian Uplands (*Chełmicki,* 1991).

Fig. 2. Location of analyzed catchments in the upper Vistula river basin, where: 1 – Dłubnia, 2 – Opatówka, 3 – Biała Tarnowska, 4 – Szreniawa, 5 – Wieprzówka, 6 – Łeg, 7 – Tanew, 8 – Biała, 9 – Pszczynka, 10 – Skawa, 11 – Łososinka, 12 – Biała Nida, 13 – Trzebośnica, 14 – Czarna, 15 – Soła, 16 – Wisła, 17 – Dunajec, 18 – Koprzywianka, 19 – Skawica, 20 – Czarna Nida, 21 – Wschodnia, 22 – Ropa, 23 – Jasiołka, 24 – Solinka, 25 – Osława, 26 – Stupnica, 27 – Mleczka, 28 – Łubinka, 29 – Grabinianka, 30 – Wielkopolska

Catchments (*Fig. 2*) chosen for analysis are diverse in respect of analyzed parameters. The average annual precipitation amounted more than 1000 mm for the Carpathian inflows of Vistula river, and in case of other catchments it is about 600–800 mm (*Table 1*).

Table 1. Statistical summary of catchments' characteristics

Variable	Variable description	Units	Min.	Mean	Max.
A	Catchment area	km^2	66.3	472.8	2034.0
L	Length of the watercourse	km	8.8	33.2	72.0
T	Mean annual air temperature	˚C	5.0	7.0	8.0
P	Mean annual precipitation	mm	603.8	796.6	1192.6
I	Mean catchment slope	–	0.002	0.022	0.091
H_{me}	Median catchment altitude	m a.s.l.	202.0	391.5	836.0
$LU1$	Coniferous forests	%	0.0	16.0	77.6
$LU2$	Mixed forests	%	0.0	13.0	53.1
$LU3$	Grassland	%	0.0	8.3	30.0
$LU4$	Arable land	%	7.4	57.2	87.0
$S1$	Fluvisols	%	0.0	15.6	34.0
$S2$	Cambisols	%	0.0	28.0	100.0
$S3$	Luvisols	%	0.0	17.1	73.4

Catchments with different area were also chosen, from small ones (like Łubinka with an area of 66.3 km^2) to large ones (like Tanew – 2093 km^2 or Biała Tarnowska – 957 km^2). The mean slope is in range from 0.002 for Łęg river to 0.091 for Biała river. In case of some catchments, cambisols and arable land dominates (*Table 1*).

In the analysis, data of precipitation and temperature were also used for the meteorological station located in the area of the upper Vistula river basin (*Table 2*).

Table 2. Meteorological stations used in this study

Station	Altitude	Latitude	Longitude
Annopol	165	50 53	21 50
Frampol	245	50 40	22 40
Gorlice	439	49 40	21 10
Jarocin	187	50 34	22 18
Jasło	228	49 44	21 29
Jawiszowice	265	49 58	19 08
Kalwaria Zebrzydowska	339	49 52	19 42
Kamesznica	821	49 36	19 04
Kańczuga	237	49 59	22 24
Klimontów	258	50 40	21 27
Konieczno	256	50 48	20 03
Kowaniec	672	49 30	20 02
Maków Podhalański	578	49 44	19 41
Osielec	525	49 41	19 45
Pilzno	193	49 59	21 18
Radomyśl Wielki	189	50 12	21 18
Radziemice	249	50 15	20 15
Raków	265	50 41	21 03
Rozdziele	375	49 48	20 27
Rudzica	272	49 51	18 53
Rybotycze	301	49 39	22 39
Sandomierz	217	50 41	21 42
Skoczów	302	49 47	18 47
Szaflary	686	49 25	20 02
Szczawne	463	49 24	22 09
Terka	668	49 18	22 26
Tuchów	223	49 54	21 03
Wadowice	257	49 52	19 30
Zawichost	139	50 48	21 52
Żabnica	824	49 34	19 11

4. Results

To facilitate the identification of clusters, the following symbols were applied for the individual groups:
- for two clusters: 2a, 2b,
- for three clusters: 3a, 3b, 3c,
- for four clusters: 4a, 4b, 4c, 4d,
- for five clusters: 5a, 5b, 5c, 5d, 5e.

As a result of classification, clusters were obtained with the catchments of similar values of the analyzed parameters (*Fig. 3*).
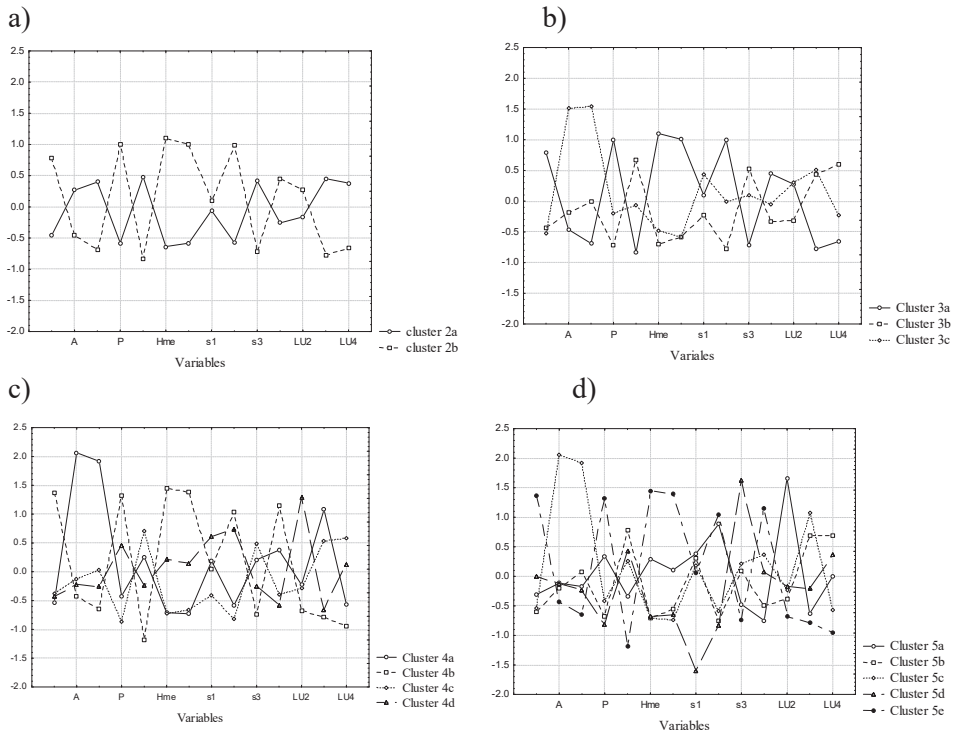
Fig. 3. Chart of the centers of the individual parameters for: a – two clusters, b – three clusters, c – four clusters, d – five clusters.

Fig. 4 presents the distribution of the analyzed catchments assigned to the individual clusters. cluster 2a includes 19 catchments located in the northern and central parts of the upper Vistula river basin. These are catchments varied in terms of area: from middle-size catchments of approximately 160 km^2 to large ones, whose area exceeds 800 km^2. In terms of the length of the streams, this cluster (*Fig. 4a*) includes varied catchments: from 17 km in case of Czarna river to 72 km in case of

Tanew river. In terms of the specific low flow discharge q_{95}, the cathments are in the range from 1 to 4 $dm^3 \cdot s^{-1} \cdot km^{-2}$. The parameters according to which catchments were classified in this cluster are: low median altitude of the catchment, which was up to 380 m a.s.l., the slope of the catchment (<0.03), with luvisols soils dominant in the catchments, as well as the catchment use, where arable lands are dominant, which constitute 64% of the catchment area on average. The parameters, which had the greatest influence on the shaping of the specific outflow in the cluster 2a, were the mean catchment slope and the median catchment altitude, for which the partial correlation coefficient resulted in 73%. A similar partial correlation value of 70% for this cluster was obtained for the mean annual air temperature and luvisols. In the cluster 2b, 11 catchments were included (*Fig. 4a*), similar in terms of median catchment altitude (over 390 m a.s.l.), large catchment slope (over 0.02), as well as soil type – cambisols prevail in the area of the catchments in the cluster 2b. However, similarly to the cluster 2a, catchments varied in terms of area (from 66 to 681 km^2) as well as specific low flow discharge q_{95} (in the range from 1.78 to 7.98 $dm^3 \cdot s^{-1} km^{-2}$). The parameters, which in the cluster 2b and 3b had the greatest influence on the shaping of the q_{95} outflow, had a mean catchment slope for which the partial correlation coefficient was 53%.

Fig. 4. Localization of the investigated catchments forming the clusters identified with the k-means method for: a – two clusters, b – three clusters, c – four clusters, d – five clusters

In the next step, three clusters were composed. cluster 3b (*Fig. 4b*) included 11 catchments, the same that created the cluster 2b. In the cluster 3a, 14 catchments were included, similar in terms of precipitation (averaged at about 700 mm), median catchment altitude (200 m a.s.l. > H_{me} > 340 m a.s.l.), and with the domination of luvisols and arable land. These catchments were similar also in terms of specific low flow discharge q_{95} (averaged at 2 $dm^3 \cdot s^{-1} km^{-2}$), and catchment area – compared to clusters 3b and 3c, the catchments in this cluster feature average areas from 154 to 755 km^2. cluster 3b including the catchments with the smallest area, and the cluster 3c – the largest ones. Also, the streams were the shortest ones in this cluster (the longest ones were in case of the catchments in the cluster 3c). The parameter, which in the cluster 3a had the greatest influence on the shaping of the specific outflow, was the mean annual air temperature, for which the partial correlation coefficient was 74%.

cluster 3c is composed of 5 catchments similar in terms of specific low flow discharge q_{95} (with the average of 2 $dm^3 \cdot s^{-1} km^{-2}$), precipitation (750 mm on the average), and the largest catchment areas (> 600 km^2), and stream lengths (> 40 km). Further delineation of clusters (four – *Fig. 4c* and five – *Fig. 4d*) was not successful due to the creation of clusters with a small number of catchments. Additionally, the catchments included in the new clusters, whose analyzed parameters, on the basis of which the given catchment was assigning into the group, did not significantly differ from other clusters, e.g., the catchments in the clusters 4b, 4c, and 4d, as well as for the clusters 5a, 5c, and 5d featured very similar values of specific low flow discharge (in both cases in the range from 1 to 4 $dm^3 \cdot s^{-1} km^{-2}$), average annual precipitation (700 mm in case of the clusters 4a, 4c, 5a, and 5c), median catchment altitude (about 260 m a.s.l. in case of clusters 4a, 4c, 5a, 5c, and 5d) (*Fig. 3c* and *3d*). The parameters, which in the cluster 4a had the greatest influence on the shaping of the specific outflow q_{95}, were the coniferous forests (r = 97%). An equally high partial correlation coefficient of 95% was obtained for the length of the watercourse and 93% for luvisols. In turn, for the cluster 5a, for the mean annual air temperature the particle correlation was 76%.

Then regression dependences were determined for selected clusters, for which more than 10 catchments were included (*Table 3*), between the specific discharge q_{95} and the individual parameters.

Table 3. Components of the regional regression model based on the k-means method

cluster	R_2 (%)	R^2_{adj} (%)	Model
2a	87	75	$q_{95} = 6.906^* - 0.0272 \cdot S1^* - 0.003 \cdot P - 75.916 \cdot I^*$ $+ 0.018 \cdot S3^* + 0{,}017 \cdot H^*_{me} + 1.245 \cdot T^*$ $- 0.029 \cdot LU4^* - 0.005 \cdot LU2 + 0.026 \cdot S2$
2b, 3b	85	75	$q_{95} = 27.9383 - 50.581 \cdot I - 0.1579 \cdot LU4 + 0.1681 \cdot S1$ $- 0.0807 \cdot LU2 - 0.013 \cdot P - 0.003 \cdot A - 0.0418$ $\cdot S2 + 0.0199 \cdot LU1 - 0.0221 \cdot L + 0.0197 \cdot T$
3a	69	59	$q_{95} = -11.1668^* - 0.0385 \cdot S1^* + 1.7797 \cdot T^* + 0.0147$ $\cdot S3^*$
4a	98	95	$q_{95} = -12.223^* + 0.0022 \cdot P + 0.0912 \cdot LU1^* + 0.0841 \cdot L^*$ $- 0.0016 \cdot A^* + 0.0181 \cdot S3^* + 0.834 \cdot T$ $+ 0.0441 \cdot LU3^* + 0.0106 \cdot H^*_{me}$
5a	57	52	$q_{95} = -15.3857^* + 2.2687 \cdot T^*$

R^2_{adj} denotes the goodness of fit coefficient of determination
*Parameter statistically significant at level α=0.05

The best regression model resulted in the case of the cluster 4a ($R^2_{adj} = 95\%$) – *Table 3,* for the level of confidence 0.05. Also, a strong adjusted coefficient of determination, with the value of 75%, was obtained for clusters 2a, 2b, and 3b.

The scatter plots allow a detailed examination of the performance of individual catchments including the existence of outliers and a potential heteroscedasticity of the observations and the predictions (*Laaha* and *Blöschl,* 2006). Overall, the relative scatter of the method (*Fig. 5*) corresponds well with the coefficient of determination in *Table 3*. The model fit was the best for the catchments closest to the diagonal line.

In case of other clusters (with less than 10 catchments each), models of correlation dependence were determined between specific low flow discharge q_{95} and individual independent variables. *Table 4* summarizes only those correlation dependences whose coefficient of correlation (*r*) exceeded the average value (> 0.5). A pretty strong dependence (0.7>*r*>0.9) was obtained in case of the cluster 3c, 5b, and 5d (for such variables as average precipitation, median catchment altitude, mean catchment slope, coniferous forests, and grassland). On the other hand, almost full correlation (for *r*>0.9) was obtained in the case of the clusters 4b and 5c (the variables: catchment area, length of the watercourse, and fluvisols) and the cluster 5d in case of mean annual air temperature.
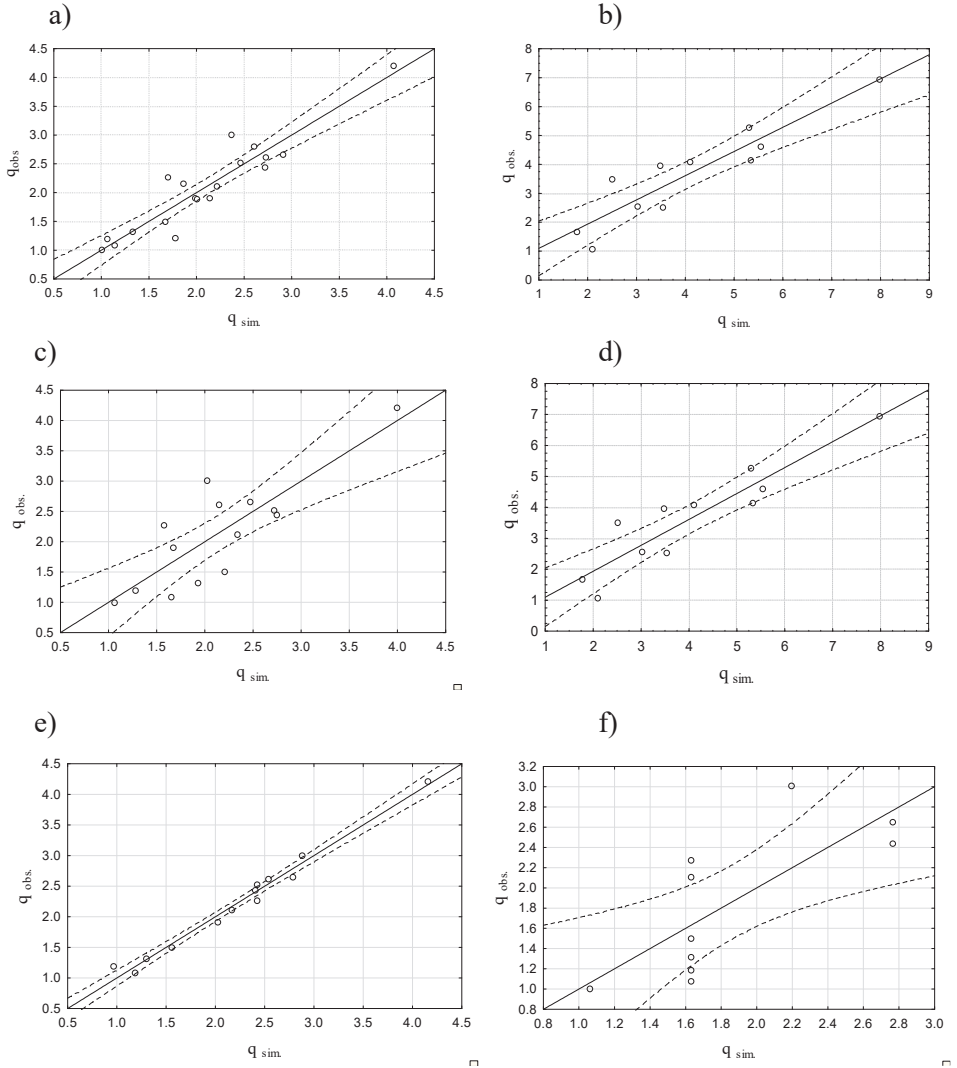
Fig. 5. Differences between observed and calculated q_{95} (dm^3·s^{-1}·km^{-2}) for clusters: a – 2a, b – 2b, c – 3a, d – 3b, e – 4a, and f – 5a.

Table 4. Correlation models between q_{95} and each parameters

cluster	Correlation model	Correlation coefficient	R^2
3c	$q_{95} = 3.31 - 0.067 \cdot S1$	-0.83	0.69
	$q_{95} = 1.174 - 0.0078 \cdot A$	0.78	0.61
4b	$q_{95} = 0.54 + 0.0011 \cdot A$	0.94	0.88
	$q_{95} = -2.57 + 0.73 \cdot L$	0.97	0.94
	$q_{95} = 3.59 - 0.094 \cdot S1$	-0.98	0.96
	$q_{95} = 1.25 + 0.031 \cdot LU1$	0.63	0.40
	$q_{95} = 2.69 - 0.0038 \cdot LU3$	-0.50	0.25
4c	$q_{95} = 2.72 + 42.47 \cdot I$	0.58	0.34
	$q_{95} = 6.88 - 0.048 \cdot LU4$	-0.56	0.31
4d	$q_{95} = 8.01 - 0.007 \cdot P$	-0.58	0.34
	$q_{95} = 1.29 + 0.016 \cdot S2$	0.51	0.26
	$q_{95} = 2,.41 - 0.024 \cdot S3$	-0.55	0.30
	$q_{95} = 2.40 - 0.057 \cdot LU1$	-0.64	0.41
	$q_{95} = 1.19 + 0.029 \cdot LU2$	0.69	0.48
5b	$q_{95} = -5.37 + 1.16 \cdot T$	0.79	0.62
5c	$q_{95} = 0.54 + 0.0011 \cdot A$	0.94	0.88
	$q_{95} = -2.57 + 0.73 \cdot L$	0.97	0.94
	$q_{95} = 3.59 - 0.094 \cdot S1$	-0.98	0.96
	$q_{95} = 1.25 + 0.031 \cdot LU1$	0.63	0.40
	$q_{95} = 2.69 - 0.0038 \cdot LU3$	-0.50	0.25
5d	$q_{95} = 3.90 - 0.0026 \cdot A$	-0.62	0.38
	$q_{95} = -3.88 + 0.01 \cdot P$	0.88	0.77
	$q_{95} = -11.60 + 1.97 \cdot T$	0.95	0.90
	$q_{95} = 17.45 - 0.055 \cdot H_{me}$	-0.79	0.62
	$q_{95} = 3.69 - 113.0 \cdot I$	-0.71	0.50
	$q_{95} = 3.11 - 0.46 \cdot S1$	-0.61	0.37
	$q_{95} = 0.73 + 0.04 \cdot S3$	0.60	0.36
	$q_{95} = 6.13 - 0.19 \cdot LU1$	-0.81	0.66
	$q_{95} = 2.01 + 0.13 \cdot LU3$	0.78	0.61
5e	$q_{95} = 2.72 + 42.47 \cdot I$	0.58	0.34
	$q_{95} = 6.88 - 0.048 \cdot LU4$	-0.56	0.31

A summary of the performance indicator statistics such as percentage bias (*PBIAS*) and the root mean sum of squares error (*RMSE*) for the models presented in this study is given in *Table 5*.

Table 5. Values of *BIAS*, *RMSE* and *E* for clusters obtained with the use of the k-means method

cluster	PBIAS [%]	RMSE [dm^3·s^{-1}·km^{-2}]	E
2a	-22.2	0.68	0.81
2b, 3b	9.9	0.79	0.79
3a	-6.10	0.48	0.69
4a	-1.50	0.11	0.98
5a	-6.62	0.45	0.57

The highest value of *PBIAS* was obtained in the case of cluster 2a (*Table 4*). For clusters 2a, 3a, 4a, and 5a, the predicted values of the specific low flow discharge q_{95} were overestimated, only in case of clusters 2b and 3b, the estimated values were underestimated. According to *Liew et al.* (2007) classification, the models for cluster 2b, 3b, 4a, and 5a are very good, and for cluster 2a they are satisfactory. According to the criterion in (*Pereira et al.,* 2016), the results obtained with the use of cluster analysis for almost every cluster, for which regional regression was made, except cluster 2a, are equal to a very good model. The values of the *E* coefficient were similar to the adjusted determination coefficient R^2. For cluster 4a we got the highest value of *E*, what corresponds with the value of R^2_{adj} (95%) and *PBIAS* (the lowest value equal -1.50), which means that in case of this cluster, we got the best fit of the regression model.

5. Discussion and conclusion

This paper discusses the regionalization of the specific low flow discharges q_{95} in chosen 30 catchments located in the in the area of upper Vistula river basin with use the non-hierarchical cluster analysis - the k-means method. Our research confirms that this method can be used for grouping of watersheds, according to hydrological characteristics. It is also important that this method can be a useful and interesting tool for low flow estimation in uncontrolled catchments. The positive aspect of this method is that we can determine the number of groups. However, when the number of clusters is too large, there is probably no training data in the cluster. Another disadvantage of the method is the lack of an unambiguous criterion on the basis of which the number of clusters can be determined (*Lin* and *Chen*, 2006). In the analysis, 13 physiographic and meteorological characteristics of catchments were also used. We started with two clusters and finished with five. The assumption of two clusters is too small number, because the given group includes catchments varied in terms of some parameters, for example for cluster 2a, in which the catchment areas ranged from about 160 km^2 to more than 800 km^2, while the strean length ranged from 17 km

to 72 km. In turn, defining four and five clusters resulted in the situation when they included catchments, whose analyzed parameters, on the basis of which the given catchment was included in the group, did not significantly differ from the other clusters. Additionally, these clusters featured a low number of catchments, e.g., clusters 4c and 5c had only 3 catchments.

In our research, we got similar relationship to those got by *Cupak* (2017). In case of grassland, coniferous forests, median catchment altitude, mean annual air temperature, and eutric cambisols, the relationship had a positive character, that is the greater the value of each analyzed parameters, the greater the value of low flow is. For parameters, like mean catchment slope and fluvisols, we also got similar – negative relationship, which means, that the value of low flow increases as the value of these parameters decreases.

We also got similar values of R^2, in case of regression models got from cluster analyses, which are in the literature, but for hierarchical cluster analyses. For example in Austria, *Laaha* and *Blöschl* (2006) obtained R^2 varying from 32% to 75% for clusters got with the use of Ward's method between specific low flow discharge q_{95} and catchment characteristics. However, in their study, 325 catchments were taken into research.

In summary, the parameters which influenced the catchments grouping in clusters were the specific low flow discharge q_{95}, precipitation, median catchment altitude, mean catchment slope, soil, and land use.

The best fitting of the model was obtained in the case of cluster 4a, for which the adjusted coefficient of determination and the coefficient E rated high, at 95% and 0.98, respectively. The parameters, which had the greatest influence on the shaping of the specific outflow q_{95} in the cluster 4a were the coniferous forests (r = 97%). An equally high partial correlation coefficient of 95% was obtained for the length of the watercourse and 93% for luvisols. However, despite the high value of the obtained coefficients, optimum results (in our opinion: assigning individual catchments to clusters so that the given cluster includes only catchments most similar to each other in terms of hydrological, meteorological, and physiographic parameters, and definitely different from those included in the other catchments), was obtained in case of generation of three clusters, despite lower values of R^2_{adj} (75% and 59%) and the coefficient E (0.69 and 0.79). The parameter, which had the greatest influence on the shaping of the specific outflow in the cluster 3a had the mean annual air temperature, for which the partial correlation coefficient was 74%, while in the cluster 3b, the parameter with the greatest influence was the mean catchment slope for which the partial correlation coefficient was 53%.

References

Ahuja, S., 2012: Regionalization of River Basins Using cluster Ensemble. *J. Water Res. Protect. 4,* 560–566.

Armbruster, J.T., 1976: An infiltration index useful in estimating low-flow characteristics of drainage basins. *J. Res., USGS 4,* 533–538.

ASCE, 1993: Criteria for evaluation of watershed models. *J. Irrigation Drainage Eng. 119,* 429–442.

Bates, B.C., Kundzewicz, Z.W., Wu, S., and *Palutikof,, S.,* 2008: Climate change and water. Technical Paper of the Intergovernmental Panel on Climate Change. IPCC Secretariat, Geneva.

Burn, D.H. and *Goel, N.K.,* 2000: The formation of groups for regional flood frequency analysis. *Hydrol. Sci. J. 45,* 97–112.

Byczkowski, A., 1972: Hydrologiczne podstawy projektowania budowli wodno-melioracyjnych. PWRiL, Warszawa (in Polish).

Chełmicki, W., 1991: Położenie, podział I cechy dorzecza. In (eds.: *Dynowska I.* and *Maciejewski M.*) Dorzecze górnej Wisły. PWN Kraków (in Polish).

Cupak, A., 2017: Initial results of nonhierarchical cluster methods use for low flow grouping. *J. Ecol. Engin. 18,* 44–50.

Dikbas, F., Firat, M., Koc, C.A., and *Gungor, M.,* 2013: Defining homogenous regions for streamflow processes In Turkey Rusing k – means clustering method. *Civil Engin. 38,* 1313–1319.

Durrans, S.R. and *Tomic, S.,* 1996: Regionalisation of Low-Flow Frequency Estimates: An Alabama Case Study. *Water Resour. Bull. 32,* 23–37.

Fang, G.H., Yang, J., Chen Y.N., and *Zammit, C.,* 2014: Comparing bias correction methods in downscaling meteorological variables for hydrologic impact study in an arid area in China. *Hydrol. Earth Syst. Sci. Discuss. 11,* 12659–12696.

Hamza, A., Ouarda, T.B.M.J., Durrans, R.S., and *Bobée, B.,* 2001: Développement de modèles de queues et d'invariance d'échelle pour l'estimation régionale des débits d'étiage. *Rev. Canadienne de Génie Civil 28,* 291–304. (In France)

Krause, P., Boyle, D.P., and *Bäse, F.,* 2005: Comparison of different efficiency criteria for hydrological model assessment. *Adv. Geosci. Europ. Geosci. Union 5*, 89–97.

Laaha, G. and *Blöschl, G.,* 2006: A Comparison of Low Flow Regionalisation Methods—Catchment Grouping. *J. Hydrol. 323,* 193–214.

Lecce, S.A., 2000: Spatial variations in the timing of annual floods in the southeastern United States. *J. Hydrol. 235,* 151–169.

Legates, D.R. and *McCabe, G.J.,* 1999: Evaluating the use of "goodness-of-fit" measures in hydrologic and hydroclimatic model validation. *Water Resour. Res., 35,* 233–241.

Lin, G.F., Chen, and *L.H.,* 2006: Identification of homogenous regions for regional frequency analysis using the self-organizing map. *J. Hydrol. 324,* 1–9.

McLean, R.K. and *Watt, W.E.,* 2005: Regional Low Flow Frequency Relations for Central Ontario. *Canad. Water Resour. J. 30,* 179–196.

Merz, R. and *Blöschl, G.,* 2004: Regionalisation of catchment model parameters, *J. Hydrol. 298,* 95–123.

Mishra, A.K. and *Singh, V.P.,* 2011: Drought modeling – A review, *J. Hydrol. 403,* 157–175.

Moriasi, D.N., Arnold, J.G., Van Liew, M.W., Bingner, R.L., Harmel, R.D., and *Veith, T.L.,* 2007: Model evaluation guidelines for systematic quantification of accuracy in watershed simulations. Transactions of the ASABE. *Amer. Soc. Agricult. Biol. Engin. 50*, 885–900.

Nash, J.E. and *Sutcliffe, J.,* 1970: River flow forecasting through conceptual models part I – A discussion of principles. *J. Hydrol., 10,* 282–290.

Ouarda, T.B.M.J., Charron, Ch., and St-Hilaire, A., 2008: Statistical models and the estimation of low flows. Canad. Water Resour. J. 33, 195–206.

Ouarda, T.B.M.J., V. Jourdain, N. Gignac, H. Gingras, H. Herrera, and Bobée, B. 2005: Développement d'un modèle hydrologique visant l'estimation des débits d'étiage pour le Québec habité. INRS-ETE, Rapport de recherche No R-684-f1 (in French).

Patel, J.A., 2007: Evaluation of low flow estimation techniques for ungauged catchments. *Water Environ. J. 21,* 41–46.

Pereira, D. dos R., Martinez, M. A., da Silva, D.D., and *Pruski, F.F.,* 2016: Hydrological simulation in a basin of typical tropical climate and soil using the SWAT Model Part II: Simulation of hydrological variables and soil use scenarios. *J. Hydrol.: Regional Studies 5,*149–163.

Punzet, J., 1981: Empiryczny system ocen charakterystycznych przepływów rzek i potoków w karpackiej części Dorzecza Wisły. *Wiadomości IMGW, zeszyt 1 – 2,* 31 – 39 (in Polish).

Rao, A.R. and *Srinivas, V.V.,* 2008: Regionalization of Watersheds. An approach based on cluster analysis, Springer.

Smakhtin, V.U., 2001: Low flow hydrology: a review. *J. Hydrology 240,* 147–186.

Smith, R.W., 1981: Rock type and minimum 7-day/10-year flow In Virginia streams. Virginia Water Resource Research Center, Virginia Polytechnology Institute and State University, Blacksburg, Bulletin, vol. 116.

Tegegne, G., Park D.K., and *Kim, Y.,* 2017: Comparison of hydrological models for the assessment of water resources in a data-scarce region, the Upper Blue Nile River Basin. *J. Hydrol.: Regional Studies 14,* 49–66.

Tucci, C., A. Silveira, J. Sanchez, and *Albuquerque, F.,* 1995: Flow Regionalization in the Upper Paraguay Basin, Brazil. *Hydrol. Sci. J. 40,* 485–497.

Van Liew, M.W., Veith, T.L., Bosch, D.D., and *Arnold, J.G.,* 2007. Suitability of SWAT for the conservation effects assessment project: A comparison on USDA-ARS experimental watersheds. *J. Hydrologic Eng., 12,* 173–189.

Vogel, R.M. and *Kroll C.N.,* 1990: Generalised Low-Flow Frequency Relationships for Ungauged Sites in Massachusetts. *Water Resour. Bull. 26,* 241–253.

Wałęga, A., Młyński, D., and *Kokoszka, R.,* 2014: Weryfikacja wybranych metod empirycznych do obliczania przepływów minimalnych i średnich w zlewniach dorzecza Dunajca. *Infrastructure and Ecology of Rural Areas, No II/3,* 825–837 (in Polish).

Wałęga, A. and *Młyński, D.,* 2017. Seasonality of media monthly discharge in selected Carpathian rivers of the upper Vistula basin. *Carpathian J. Earth Environ. Sci. 12,* 61.

Ziernicka-Wojtaszek, A. and *Kaczor, G.,* 2013. Wysokość i natężenie opadów atmosferycznych w Krakowie i okolicach podczas powodzi w okresie maj-czerwiec 2010.. *Acta Sci. Pol., Formatio Circumiectus, 12 (2),* 143 (in Polish).

IDŐJÁRÁS

Assessment of observed and projected climate changes in Bačka (Serbia) using trend analysis and climate modeling

Nikola Milentijević[1,*], **Aleksandar Valjarević**[2], **Nikola R. Bačević**[1],
Dušan Ristić[1], **Kristina Kalkan**[3], **Marija Cimbaljević**[3], **Jovan Dragojlović**[1],
Stevan Savić[3], and **Milana Pantelić**[3]

[1] *University of Priština in Kosovska Mitrovica,*
Faculty of Sciences and Mathematics, Department of Geography,
Lole Ribara 29, 38220 Kosovska Mitrovica, Serbia

[2] *University of Belgrade, Faculty of Geography,*
Studentski Trg 3/III, 11000 Belgrade, Serbia;

[3] *University of Novi Sad, Faculty of Sciences,*
Department of Geography, Tourism and Hotel Management,
Trg Dositeja Obradovića 3, 21000 Novi Sad, Serbia;

*Corresponding author E-mail: nikola.milentijevic@pr.ac.rs

(Manuscript received in final form October 27, 2020)

Abstract— Climate change is one of the largest environmental issues causing hydroclimatological extremes such as floods, droughts, and aridity. The aim of this study is to assess the observed and projected climate changes in Bačka (Serbia). Detailed trend analyses and possible climate scenarios over Bačka has not been presented up to now. In this paper, four data sets were extracted and calculated: mean annual air temperature, mean air temperatures during the vegetation period, mean annual precipitation and total precipitation during the vegetation period. The presented parameters were obtained from the annual meteorological reports of the Republic Hydrometeorological Service of Serbia. Trend equation based on linear regression, trend magnitude according to the trend equation, and Mann-Kendall statistics have been used for trend analysis of climatic parameters. A GIS modeling of the possible climate scenario was created according to the Beijing Climate Center Climate System Model (BCC-CSM2-MR). Based on the trend equations, positive trends related to air temperature and precipitation variables are dominant. The trend magnitude shows the largest mean increase in all time series related to air temperature during the vegetation period. The highest mean precipitation increase occurs only in two time series. The Mann-Kendall statistics showed significantly positive trends in 11 cases and no changes in 9 cases. According to BCC-CSM2-MR, changes will be especially dominant in case of air temperatures. The expected changes in the total precipitation during the vegetation period show a tendency towards semiarid conditions. The presented results of observed and projected climate changes demand adaptation measures, especially from the aspect of sustainable agriculture.

Key-words: air temperature, precipitation, GIS modeling, trends, semiaridity, agriculture

1. Introduction

Climate change refers to a statistically significant variation in climate averages or its variability persisting for decades or a longer period of time (*Hulme*, 2017). Although climate change occurred on a global scale, its impacts often vary from region to region (*Arnell et al.,* 2019). Therefore, the analysis of changes in meteorological variables represents an important task in detection of observed and projected climate changes.

In recent years, various studies for detecting possible climate trends and changes across the world have been performed. Examining long-term trends of air temperature on annual and seasonal scales in Iran, *Ahmadi et al*. (2018) revealed that the highest increasing trends were observed in the south and southeast regions of Iran. The results showed statistically significant positive trends during autumn, spring, and especially summer. Some authors analyzed selected hydro-climatological variables (precipitation, streamflow, air temperature, and humidity) over the Middle East (*Nourani et al*., 2018, 2019). In these papers, the monthly, annual, and seasonal trends at Urmia Lake Basin from 1971 to 2013 were examined together with correlated mentioned variables. The results identified statistically significant decreasing trends in the streamflow, moderate decreasing trends in the precipitation and relative humidity, and increasing trends in the observed temperature data. *Sa´adi et al*. (2019) analyzed trends of precipitation and precipitation extremes using a modified Mann-Kendall test in Sarawak (Malaysia). The modified Mann-Kendall test detected an annual precipitation increasing trend only at one station and no significant trend on seasonal scale at any stations. However, authors revealed the statistically significant trends of the 1-hour maximum precipitation mainly at the stations located in urban areas. This implicates the possibility of flash floods. Monthly precipitation and temperature time series from 6 meteorological stations were used to calculate meteorological drought indices over Ankara Province in Turkey (*Danandeh Mehr* and *Vaheddoost*, 2020). In the methodological sense, the well-known standardized precipitation (SPI) and precipitation-evapotranspiration (SPEI) indices were used in examining drought events. The results showed that the province suffered from 5 drought events during the period of 1971 to 2016. However, the results of examining the trends of the SPEI indicated a slight decrease trend during the observed interval; the SPI did not show the same pattern.

The patterns of projected changes of air temperature and precipitation will be intensive over many regions of the world. For example, China could be faced with an increase in temperature extremes and intensification of precipitation extremes according to CMIP5 climate model simulations (*Zhou et al*., 2014). Applied CMIP3 models (*Almazroui et al*., 2017) over the Arabian Peninsula revealed a continuous increase in projected annual air temperature and precipitation during the 21st century (2070–2099). *Bucchiagnani et al*. (2018) investigated the future climate conditions over the Middle East - North Africa

region using the IPCC RCP4.5 scenario (from 1979 to 2100). Their results showed that the temperature and precipitation projections are statistically significant and generally highlight a strong warming (especially in summer) along with a reduction in precipitation. *Zittis et al.* (2019) examined the climate projections for the Mediterranean according to the CORDEX model. General warming can be expected by the end of the century (2081–2100). It is considered, that air temperature will increase by 1–5 °C with respect to the 1986–2005 reference period. A general drying (between 10% and 40%) is also inferred for the Mediterranean. *Touseef et al.* (2020) investigated the historical and future precipitation trends on water resources over the Xiajing River basin. According to the results, a decreasing trend was observed for the past 50 years over the basin with negative values of The Mann-Kendall test and Sen's slope. The future projections from CMIP5 (2020–2099) will likely be positive trends for annual precipitation. Significant positive trends were observed in monsoon and winter seasons while premonsoon and postmonsoon seasons, will likely slightly decrease.

Some authors made a contribution in detecting air temperature and precipitation trends in Vojvodina (*Tošić et al.*, 2014; *Gavrilov et al.*, 2015, 2016), some climate characteristics of Bačka (*Rakićević*, 1988; *Berić et al.*, 1990; *Lazić et al.*, 2004; *Rajić*, 2004, *Rajić* and *Rajić*, 2005; *Rajić* and *Štula*, 2007), and climate projections in Serbia (*Kržič et al.*, 2011; *Vuković et al.*, 2018; *Janković et al.*, 2019). *Rakićević* (1988) used drought indices and classified Northeastern Bačka as one of the regions most affected by drought in Serbia. *Hrnjak et al.* (2014) identified the lowest values of the De Martonne aridity index in the northeast part of Vojvodina (including the northeastern parts of Bačka). Investigating the forestry aridity index (FAI) in Vojvodina *Gavrilov et al.* (2019) classified the northern parts of Vojvodina (parts of Bačka) as forest-steppe climate. Authors correlated the FAI values lower of the De Martonne and Pinna indices, which indicate semi-humid conditions or semi-dry Mediterranean climate, respectively. Identified lower values are caused by a lower amount of precipitation. Region of Bačka was identified as the part of the so-called R1 sub-region that includes the northern part of Serbia. The R1 is characterized by the lowest total precipitation and mostly intensive agriculture (*Gocić* and *Trajković,* 2014a; *Gocić et al.*, 2020). Therefore, drought and aridity in the region of Bačka are frequent, intensive, and depending on the duration, so they could have impact on agricultural production. Also, in terms of detailed trend analysis and climate modeling, Bačka region has not been investigated yet. Thus, this paper could provide a basis to a future research of interaction between climate projections and sustainable agriculture.

The purpose of this paper is to analyze the variability of air temperature and precipitation variables at 5 meteorological stations in the region of Bačka (Serbia) during two intervals: 1949 to 2018 and 2018 to 2050. Besides, the objectives of this study are: (1) to analyze and discuss the trend characteristics of meteorological

variables in detail; (2) to quantify the significance of changes by the trend equations, the trend magnitude, and the Mann-Kendall statistics; and (3) to use GIS modeling in order to detect the projected climate scenario (from 2018 to 2050) according to the Beijing Climate Center Climate System Model (BCC-CSM2-MR).

2. Research area

Bačka represents historical and geographical area in the northwest of Serbia (the western part of the Autonomous Province of Vojvodina). The borders of Bačka with the neighboring areas are of two different types: natural and artificial. The river Tisza towards Banat in the east, and the Danube towards Srem in the south are the natural borders of Bačka. Furthermore, the border with Croatia is also natural marked by the Danube (in the south and in the west). The borderline with Hungary is of an artificial type. It cuts transversely and then again merges the two biggest rivers of the Pannonian basin, rivers Danube and Tisza. In terms of climate, the northern border of Bačka does not represent a zone of separation of the neighboring climatic regions, since it belongs to the Pannonian plain, where the climatic conditions are similar. Administratively, the territory of Bačka is divided into three districts: the northern, the western, and the southern Bačka. It occupies an area of 8,671 km^2, i.e., 40.3% of the territory of Vojvodina (*Urban Institute of Vojvodina*, 2011). Spatial distribution of the selected stations is shown in *Fig. 1*, while their description is given in *Table 1*.
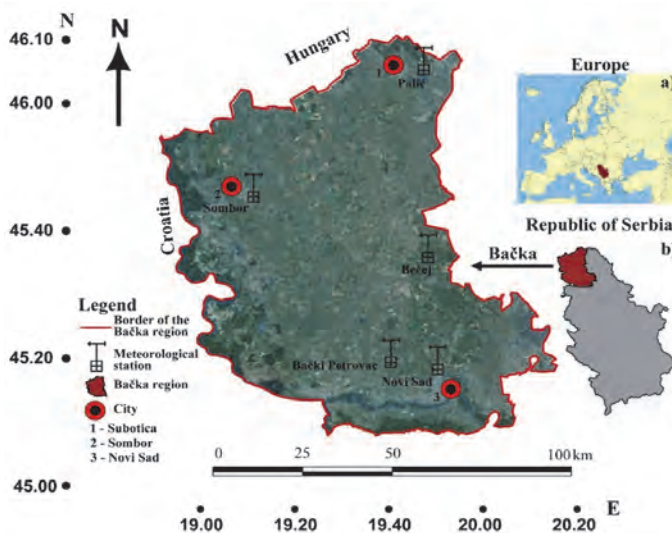
Fig. 1. Location map of Bačka with the distribution of meteorological stations.

These locations were chosen according to three parameters: (1) each of them should have good quality datasets; (2) the data should be reliable; and (3) the data should have adequate record length.

Table 1. List of used meteorological stations in Bačka with their abbreviations and geographic features, length of instrumental measurements and type (o.m.s.: ordinary meteorological station; p.m.s.: principal meteorological station)

No.	Station name	Abbreviation	Longitude (E)	Latitude (N)	Altitude (m)	Length of measurements	Type
1.	Bački Petrovac	BP	45º20′	19º40′	80	1948–2018	o.m.s
2.	Bečej	B	45º37′	20º04′	75	1948–2015	o.m.s
3.	Novi Sad	N	45º19′	19º50′	86	1948–2018	p.m.s.
4.	Palić	P	46º06′	19º46′	102	1945–2018	p.m.s.
5.	Sombor	S	45º46′	19º09′	87	1949–2018	p.m.s.

3. Materials and methods

3.1. Materials

Trend analysis of air temperature and annual total precipitation have been performed in the period of 70 years (from 1949 to 2018). Data from 5 meteorological stations were used, based on the Annual Meteorological Report (*Republic Hydrometeorological Service of Serbia*, 2019). Apart from the meteorological station Bečej, continuous instrumental observations were performed in all other analyzed stations. In case of Bečej, the meteorological station data have not been kept for three years (2016, 2017, and 2018). Since there was a small amount of data gaps (up to 4.3% of data), there was no significant bias of the final results. The missing data were supplemented by the method of linear interpolation. This simple statistical procedure is defined as arithmetic mean of linear interpolants between the two neighboring data sets (*Hazewinkel*, 1990). The software used for interpolation was EXCEL.

In this study, before previous calculations, statistical significance of the mean change and distribution from two different datasets was tested using the Kolmogorov–Smirnov (KS) test. The KS test is an empirical distribution function test in which the theoretical cumulative distribution function of the test distribution is compared to the empirical distribution function of the series

(*Javari*, 2016). The null hypothesis (*Ho*) is that the two dataset values are from the same continuous distribution. The alternative hypothesis (*Ha*) is that these two datasets come from different continuous distributions. The hypothesis test can be carried out at a specific statistical significance level (5%) (*Teegavarapu*, 2019). The KS test, performed using these two datasets, led to the result that the null hypothesis is not rejected suggesting that the two samples are drawn from the same continuous distribution. Therefore, it was concluded that the quality of air temperature and precipitation data was consistent and eligible for further data quality analysis, no corrections needed. For measuring the normality of the time series, the SPSS software was used.

Climate variables were categorized into 4 data sets: mean annual air temperatures (YT), mean air temperatures during the vegetation period (T_{mean}-VP), mean annual precipitation (YP), and total precipitation during the vegetation period (P_Σ-VP). The analysis of data, especially during the vegetation period (April-October) is very significant for agriculture.

3.2. Methods

In this paper, three statistical approaches were used, previously performed in similar researches: a) the trend equation (tendency was calculated for each time series using the method of linear regression (*Mudelsee*, 2019); b) in all cases the trend magnitude was calculated using the trend equation (*Gavrilov et al.*, 2018); c) finally, all trends were assessed using the MK non-parametric test (*Zeleňáková et al.*, 2018). Software EXCEL was used for the purpose of calculating the air temperature and precipitation trends. For determining the probability of confidence *p*, as well as for the purpose of hypothesis testing, the software XLSTAT was used.

3.2.1. The trend equation

The first statistical approach was to calculate the trend equation of the mentioned parameters using linear regression (*Mudelsee*, 2019). The selected approach has been long utilized in this type of research (*Feidas et al.*, 2004), because it gives results which are simple to interpret; both graphically and analytically based on the shape and parameters of the trend equation. For instance, the temperature trend sign depends on the value of the slope. There are three possible scenarios: if the size of slope is greater than zero, the sign of trend is *positive* (increase); b) if it is equal to zero there *is no trend* (no changes); and c) if it is less than zero, the sign of trend is *negative* (decrease).

3.2.2. The trend magnitude

In the second statistical approach, the trend magnitude was defined as the difference in variables between the beginning and the end of the period. It was

obtained from the linear trend equation (*Gavrilov et al.*, 2015). For a better understanding of the trend magnitude, in this paper the following statement was followed. First, when Δy is greater than zero, less than zero, or equal to zero, the sign of the trend is *negative* (decrease), *positive* (increase), or *no trend* (no change), respectively.

3.2.3. The Mann-Kendall (MK) non-parametric test

The Mann-Kendall (MK) test is a popular non-parametric alternative which tests the presence of a trend, or nonstationarity of the central tendency of a time series. In a parallel to the alternative parametric regression approach, the Man-Kendall test arises as a special case of the Kendall's τ, reflecting a tendency for monotone association between two variables (*Wilks*, 2011). The MK test has been widely used in hydrometeorological trend detection studies: for the magnitude and frequency of flood occurence (*Zadeh et al.*, 2020), air temperature and precipitation (*Panda* and *Sahu*, 2019), and aridity (*Nouri* and *Bannayan*, 2018). The test statisics for the Mann-Kendal trend test is (*Wilks*, 2011):

$$S = \sum_{i=1}^{n-1} sgn\,(x_{i+1} - x_i)\,, \qquad (1)$$

where

$$sgn(\Delta x) = \begin{cases} +1, & \Delta x > 0 \\ 0, & \Delta x = 0 \\ -1, & \Delta x < 0 \end{cases}. \qquad (2)$$

That is, the statistic in Eq.(1) counts the number of adjacent data pairs in which the first value is smaller than the second, and subtracts the number of data pairs in which the first is larger than the second. If the data x_i is serially independent and drawn from the same distribution, then the numbers of adjacent data pairs for which $sgn(\Delta x)$ is positive and negative should be nearly equal.

For moderate (*n* equals to about 10) or larger series length, the sampling distribution of the test statistic in Eq.(2) is approximately Gaussian, and if the null hypothesis is true, this Gaussian null distribution will have zero means. The variance of this distribution depends on whether all the *x*'s are distinct, or if some *x* are repetaed values. If there is no ties, the variance of the sampling distribution of *S* is:

$$Var(S) = \frac{n(n-1)(2n+5)}{18}. \qquad (3)$$

Otherwise the variance is:

$$Var\ (S) = \frac{n(n-1)(2n+5)-\sum_{J=1}^{J} t_j\,(t_j-1)(2t_j+5)}{18}, \tag{4}$$

where J represents the number of groups of repetaed values, and t_j is the number of repeated values in the jth group. The statistic S is approximately normally distributed provided that the following Z-transformation is employed:

$$Z = \begin{cases} \frac{S-1}{[(Var(S)]} & if \quad S>0 \\ 0 & if \quad S=0 \\ \frac{S+1}{[(Var(S)]} & if \quad S<0 \end{cases}. \tag{5}$$

Finally, the measure of significance of variables, the probability p is computed as:

$$p = [1 - f(Z)] \times 100\ . \tag{6}$$

The probability density function for a normal distribution with a mean of 0 and a standard deviation of 1, is given by the following equation:

$$f(Z) = \frac{1}{\sqrt{2\pi}} exp\left(-\frac{Z^2}{2}\right). \tag{7}$$

By using MK test, two hypotheses were tested: the zero hypothesis (H_o) pointed to the inexistence of trend in time series; and the alternative hypothesis (H_a) pointed to the existence of a statistically significant trend in time series for the chosen level of significance (α). The main role in MK test belongs to the value of p (*Razavi et al.*, 2016). The value of p determines the accuracy of the hypothesis. If the value p is lower than the chosen level of significance α (it is common that α=0.05 or 5%), the hypothesis H_o should be rejected and hypothesis H_a accepted. In case of p having the value larger than the level of significance, then the hypothesis H_o is accepted (*Gavrilov et al.*, 2018).

3.2.4. *The geographical information system (GIS) and the modeling of data*

The geographical information system (GIS) is an important tool, and with the help of geostatistical and statistical methods, it may give important and valuable results. GIS may show the climate properties from the past and present and also give possibility to predict future climate. Many climate models are present today, while some of them are present with grid data. These grid data may show future climate predictions (*Li* and *Cheng*, 1999). In this research, we used GIS advanced methods and procedures to estimate climate change properties of Bačka region. GIS advanced methods present very important way of calculating and estimating

annual climate properties. Climate features, which are the main reason, can not be detected without digitization and visualization for drought or hazardous weather. The relevant GIS spatial algorithms used in this research are: global kriging, semi-kriging, kriging, spatial interpolation, interpolation, and light buffer analysis. In this paper we gave priority to the global kriging algorithm, because it is useful, easy, and transparent (*Orus et al.*, 2005). Standard kriging and semi-kriging were used for climatological calculations in this research. Other techniques which may improve climatological estiamtion and performed general analysis of climate properties are interpolation technics (*Tomaszkiewicz et al.*, 2016). The semi-kriging method and nugget values between -0.5 and +1.0 on Z axis and between 0.2 and -0.5 on X axis were used. In addition, modified Gaussian regression and Kolmogorov prediction were used as well. The Beijing Climate Center Climate System Model (BCC-CSM2-MR) was used in this research. This model predicts data between 2081 and 2100. The resolution of the grid of this data is 2.5 minutes. This resolution is 5 km × 5 km in longitude and latitude. The main advancement of the BCC model from phase 5 of the Coupled Model Intercomparison Project (CMIP5) to phase 6 (CMIP6) is its precise physical parameterizations and model performance (*Wu et al.*, 2019). The 114 grid cells covering the Bačka region with an average area of 5 km^2 were used for climatological projections. This grid included analyzed climate variables for air temperature and precipitation.

With the help of a specially created computer *Tesla L3* with parallel functions of the operations, we estimated a very precise grid of 1 km^2. In that way it is possible to find all the positions and data obtained from the meteorological station at global, regional, and local scales. QGIS software was used to estimate grid for future predictions. Model projections of selected climate parameters include large uncertainties. Disagreement between individual simulations primarily arises from internal variability, whereas models agree remarkably well on the forced signal, the change in the absence of internal variability (*Fischer et al.*, 2014). For this reason, the GIS tool gave an advantage in climate projections. The error in predictions presented by GIS software is between 3% and 5%.

4. Results

4.1. Trend parameters and estimation of trends

In this paper, the results for twenty time series are presented. For each of the series, the trend equation as well as the linear trend for the interval from 1949 to 2018 were performed. The magnitude of trend (Δy), the probability of trend (*p*) for each time series, and Mann-Kendall statistics were used for the estimation of trends. These results summed up in *Tables 2, 3,* and *4* and *Fig. 2*.

The largest mean temperature increase *Δy* (*Table 2* and *3*) was recorded in the case of mean air temperature during the vegetation period (T$_{mean}$-VP) at

stations Bački Petrovac (BP) and Bečej (B) (time series BP-T_{mean}-VP and B-T_{mean}-VP). Minor changes were identified in case of time series N-T_{mean}-VP and S-YT. In case of precipitation, the magnitude of trend is the largest in the case of time series N-YP and N-P_{Σ}-VP. The time series BP-YP is characterized by a decrease in mean precipitation.

Table 2. Trend equation (*y*), trend magnitude (Δ*y*), and probability of confidences (*p*) for air temperature time series (from 1949 to 2018) in Bačka. Abbreviations are listed in Section 3.1. and *Table 1*.

Time series	Trend equation	Δ*y* (℃)	*p* (%)
BP-YT	$y = 0.0237x + 10.546$	1.6	< 0.0001
BP-T_{mean}-VP	$y = 0.0269x + 16.291$	1.9	< 0.0001
B-YT	$y = 0.0217x + 10.494$	1.5	0.0002
B-T_{mean}-VP	$y = 0.0262x + 16.339$	1.8	< 0.0001
N-YT	$y = 0.0217x + 10.557$	1.5	< 0.0001
N-T_{mean}-VP	$y = 0.0201x + 16.52$	1.4	0.0001
P-YT	$y = 0.0242x + 10.188$	1.7	< 0.0001
P-T_{mean}-VP	$y = 0.026x + 16.149$	1.8	< 0.0001
S-YT	$y = 0.0211x + 10.29$	1.5	< 0.0001
S-T_{mean}-VP	$y = 0.0215x + 16.164$	1.5	< 0.0001

Table 3. Trend equation (*y*), magnitude of trend *(*Δ*y)*, and probability of confidences (*p*) for precipitation time series (from 1949 to 2018) in Bačka. Abbreviations are listed in Section 3.1. and *Table 1*.

Time series	Trend equation	Δ*y* (mm)	*p* (%)
BP-YP	$y = -0.0792x + 616.86$	-5.5	0.8480
BP-P_{Σ}-VP	$y = 0.8409x + 365.96$	58.0	0.2438
B-YP	$y = 0.0684x + 590.86$	4.7	0.8520
B-P_{Σ}-VP	$y = 0.5936x + 365.6$	40.9	0.2954
N-YP	$y = 1.4727x + 572.45$	101.6	0.1455
N-P_{Σ}-VP	$y = 1.712x + 349.03$	118.1	0.0586
P-YP	$y = 1.4039x + 509.03$	96.9	0.0615
P-P_{Σ}-VP	$y = 1.3171x + 318.84$	90.9	0.0963
S-YP	$y = 1.2902x + 555.14$	89.0	0.1304
S-P_{Σ}-VP	$y = 1.2298x + 351.17$	84.9	0.0450
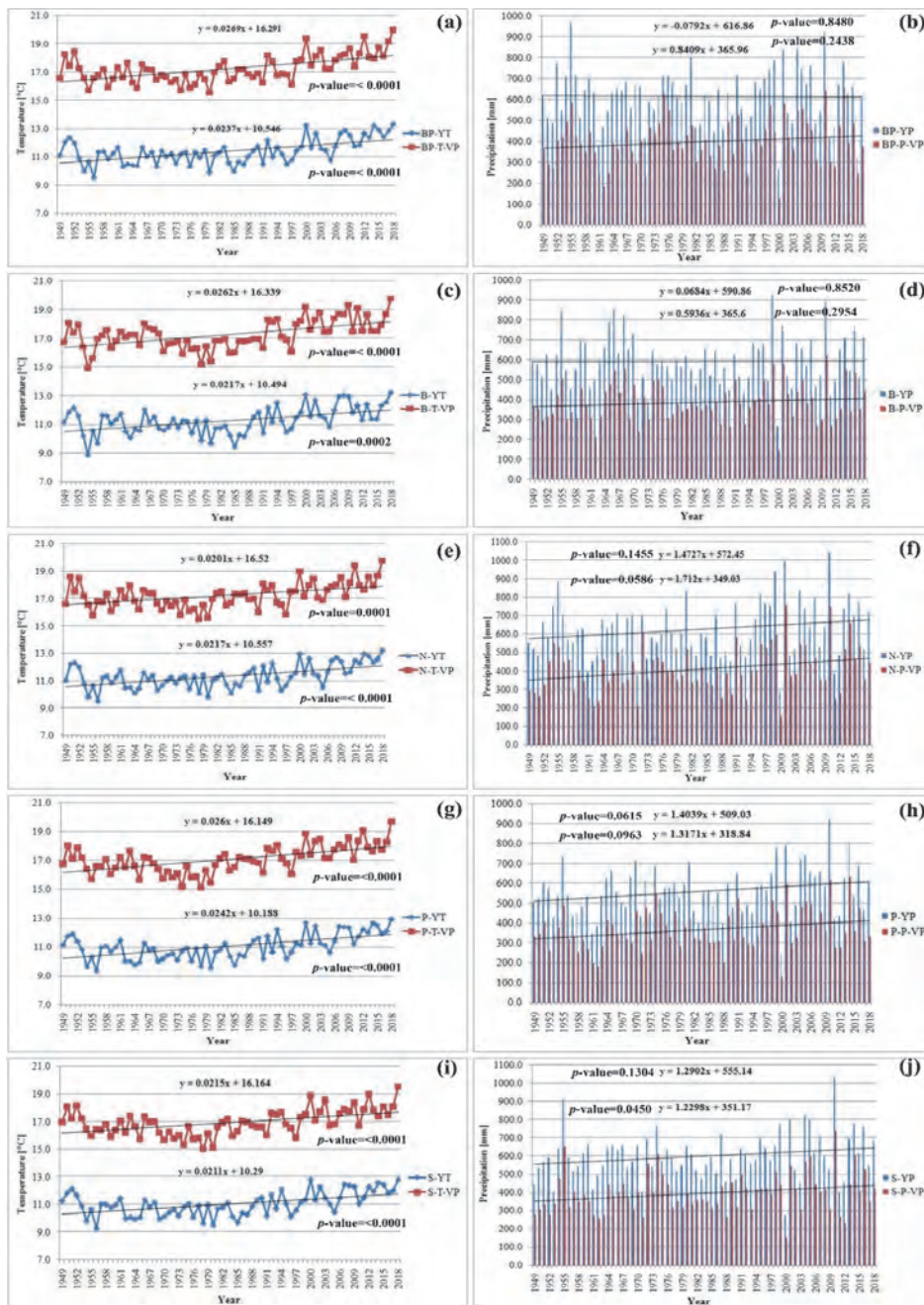
Fig. 2. Mean annual air temperature (YT), mean air temperature during the vegetation period (T$_{mean}$-VP), trend equation and trend lines (left column) and mean annual precipitation (YP), total precipitation during the vegetation period (P$_\Sigma$-VP), trend equation and trend lines (right column) from 1949 to 2018 at selected meteorological stations in Bačka.

The main results (*Table 4, Fig. 2*) for the trend equations in twenty time series are: a) in nineteen time series the trend is positive; b) in one of the time series the trend is negative (BP-YT). The analysis based on MK test has led to the following conclusions: a) in eleven out of twenty time series, there is a statistically significant positive trend, where it is necessary to apply the hypothesis *Ha*; b) in nine out of twenty time series there is no trend, therefore it is necessary to accept the hypothesis *Ho*.

Table 4. The main results of the analysis of air temperature and precipitation trends for 20 time series

Time series	Trend equation	Classical MK test
BP-YT	*Negative trend*	*significantly positive trend*
BP-T_{mean}-VP	*Positive trend*	*significantly positive trend*
BP-YP	*Positive trend*	*no trend*
BP-P_{Σ}-VP	*Positive trend*	*no trend*
B-YT	*Positive trend*	*significantly positive trend*
B-T_{mean}-VP	*Positive trend*	*significantly positive trend*
B-YP	*Positive trend*	*no trend*
B-P_{Σ}-VP	*Positive trend*	*no trend*
N-YT	*Positive trend*	*significantly positive trend*
N-T_{mean}-VP	*Positive trend*	*significantly positive trend*
N-YP	*Positive trend*	*no trend*
N-P_{Σ}-VP	*Positive trend*	*no trend*
P-YT	*Positive trend*	*significantly positive trend*
P-T_{mean}-VP	*Positive trend*	*significantly positive trend*
P-YP	*Positive trend*	*no trend*
P-P_{Σ}-VP	*Positive trend*	*no trend*
S-YT	*Positive trend*	*significantly positive trend*
S-T_{mean}-VP	*Positive trend*	*significantly positive trend*
S-YP	*Positive trend*	*no trend*
S-P_{Σ}-VP	*Positive trend*	*significantly positive trend*

According to the analyzed time series, the value of *p* is less than 0.0001 in eight cases. Such value was recorded in the following time series: BP-YT, BP-T_{mean}-VP, B-T_{mean}-VP, N-YT, P-YT, P-T_{mean}-VP, S-YT, and S-P_{Σ}-VP. The results obtained using MK test point to the existence of trend, according to which hypothesis *Ho* should be rejected and hypothesis *Ha* should be accepted. The risk

of rejecting the hypothesis *Ha* in previously presented time series is less than 0.01%. For the time series N-T_{mean}-VP, the value of *p* is 0.0001. MK test points to the existence of trend, thus hypothesis *Ho* should be rejected and hypothesis *Ha* should be accepted. The risk of rejecting the hypothesis *Ha* is less than 0.01%. Furthermore, for the time series B-YT, the recorded value of *p* is 0.0002. The MK test points to the existence of trend, so hypothesis *Ho* should be rejected and hypothesis *Ha* should be accepted. The risk of rejecting hypothesis *Ha* is less than 0.02%. The MK test points out that there is only positive trend, when it comes to mean precipitation during the vegetation period for the time series S-P_{Σ}-VP. The recorded value of *p* is 0.045. In this case, we should reject the hypothesis *Ho* and accept the hypothesis *Ha*. The risk of rejecting the hypothesis *Ha* is 4.5%.

In the remaining time series related to mean annual precipitation and total precipitation during the vegetation period there is no trend, so the dominant hypothesis is *Ho*. The value of *p* for the time series N-P_{Σ}-VP is 0.0586, while the dominant hypothesis is *Ho*, and it should not be rejected. The risk of rejecting the hypothesis *Ho* is 5.87%. For the time series P-YP, the value of *p* is 0.0615, the dominant hypothesis is the *Ho,* and it should not be rejected. The risk of rejecting the hypothesis *Ho* is 6.15%. For the time series P-P_{Σ}-VP, the value of *p* is 0.0963, the dominant hypothesis is *Ho,* and it should not be rejected. The risk of rejecting the hypothesis *Ho* is 9.64%. For the time series S-YP, the value of *p* is 0.1304, the dominant hypothesis is *Ho,* and it should noy be rejected. The risk of rejecting the hypothesis *Ho* is 13.04%. For the time series N-YP, the value of *p* is 0.1455, the dominant hypothesis is *Ho,* and it should not be rejected. The risk of rejecting the hypothesis *Ho* is 14.55%. For the time series BP-P_{Σ}-VP, the value of *p* is 0.2438, the dominant hypothesis is *Xo,* and it should not be rejected. The risk of rejecting the hypothesis *Xo* is 24.39%. For the time series B-P_{Σ}-VP, the value of *p* is 0.2954, the dominant hypothesis is *Xo* and it should not be rejected. The risk of rejecting the hypothesis *Xo* is 29.54%. For the time series BP-YP, the value of *p* is 0.8480, the dominant hypothesis is *Xo,* and it should not be rejected. The risk of rejecting the hypothesis *Xo* is 84.80%. For the time series B-YP, the value of *p* is 0.8520, the dominant hypothesis is *Xo,* and it should not be rejected. The risk of rejecting the hypothesis *Xo* is 85.20%.

4.2. *The geographical information system (GIS) and the modeling of data*

The spatial distribution of mean annual air temperature (YT) and mean air temperature during the vegetation period (T_{mean}-VP) from 1949 to 2018, as well as the projection of the chosen variables from 2018 to 2050 are shown in *Fig. 3*.
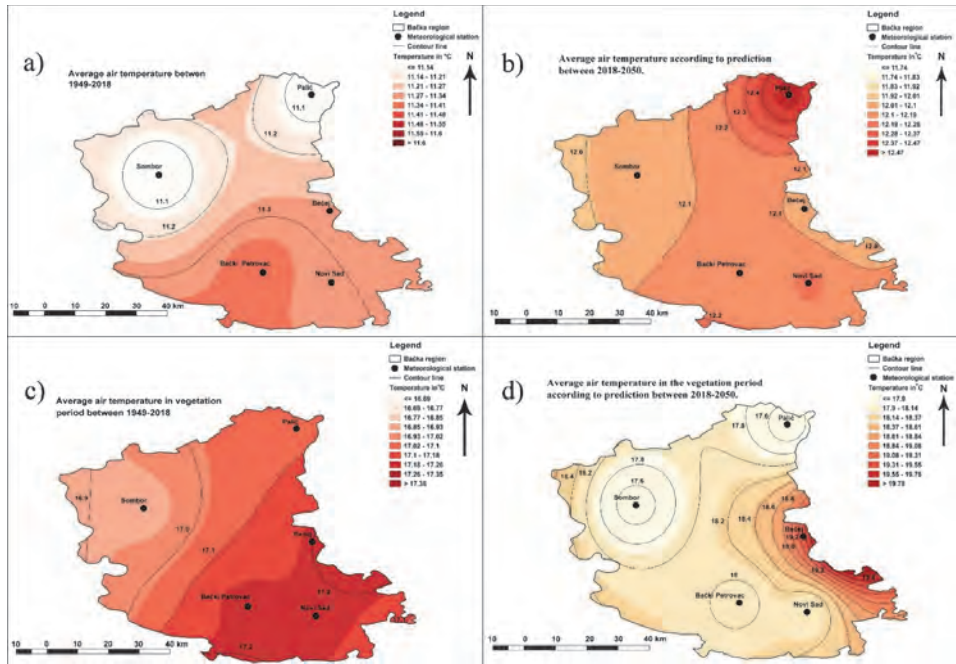
Fig. 3. Spatial distribution of air temperature values in Bačka: a) mean annual air temperature (YT) from 1949 to 2018; b) mean annual air temperature (YT) from 2018 to 2050; c) mean air temperature during the vegetation period (T_{mean}-VP) from 1949 to 2018; d) mean air temperature (T_{mean}-VP) during the vegetation period from 2018 to 2050.

During the reference period, the southern parts are characterized by prominent air temperature (above 11.3 ℃). The values of temperature are the lowest in the area of Palić and Sombor (above 11.1 ℃). In the projections of YT, there is a prominent increase comparing to the period 1949–2018, especially in the northern part of Bačka (above 12.4 ℃). Isotherms above 12.1 ℃ occupie the central part of the research area. Increasing of air temperature is more prominent in the eastern and western parts of Bačka (12.0 ℃).

Mean air temperatures during the vegetation period (T_{mean}-VP) in the wider area of Bački Petrovac, Novi Sad, and Bečej are limited by the 17.2 ℃ isotherm. Northern and central parts have similar values (17.1 ℃), whereas the lowest detected values are in the west (16.9 ℃). The projection of mean temperature during the vegetation period implicates dynamic changes in the air temperature. The projected values reach 19.4 ℃ in the eastern part of Bačka. Minor changes are expected in the northern part of Bačka (17.6 ℃). The area around Bački Petrovac and Novi Sad is limited by the 18.0 ℃ isotherm. Air temperature changes would be more intensive in the western parts of analyzed study area (18.4 ℃).

The mean annual precipitation (YP) from 1949 to 2018 (*Fig. 4*) indicates semiarid conditions in the northern part of Bačka (below 560 mm). Results in western, southern, and eastern parts of Bačka are similar (below 600 mm). The projected values of mean annual precipitation indicates moderate increase in the northern part (below 570 mm). In the western, southern and eastern parts of Bačka, pluviometric changes will be almost identical to those from 1949 to 2018 (610 mm isohyet). In case of total precipitation, during the vegetation period (P$_\Sigma$-VP) the values are increased in the southern parts (400 mm), and mildly decreased in the western (390 mm) and northern parts (370 mm). Projected values of total precipitation during the vegetation period are not in accordance with the values of this variable from 1949 to 2018. It implicates that aridity in the northern part of Bačka would reach even more extreme values (310 mm isohyet). These phenological conditions would have consequences on vegetation, especially in agriculture. Semiarid conditions will mildly decrease in the eastern parts (410 mm), while its values will increase on the southern part of Bačka. Decrease of precipitation will be particularly intensive in Bački Petrovac (300 mm isohyet).
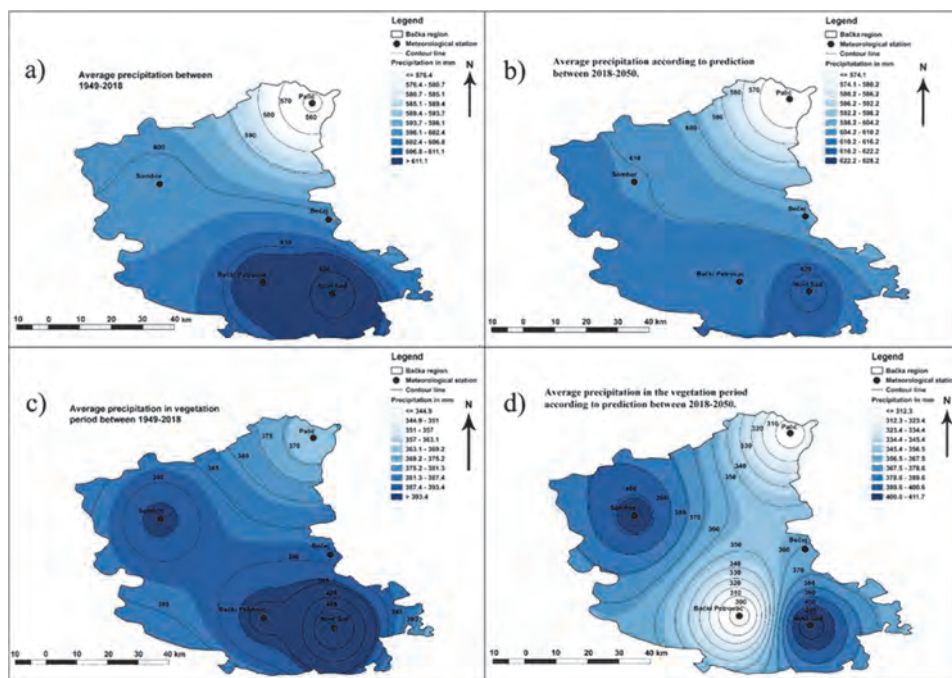
Fig. 4. Spatial distribution of precipitation values in Bačka: a) mean annual precipitation (YP) from 1949 to 2018; b) mean annual precipitation (YP) from 2018 to 2050; c) total precipitation during the vegetation period (P$_\Sigma$-VP) from 1949 to 2018; d) total precipitation during the vegetation period (P$_\Sigma$-VP) from 2018 to 2050.

5. Discussion

According to the Mann-Kendall test, all time series related to air temperature recorded a significantly increasing trend, while in nine out of ten precipitation time series did not detect any changes. It is difficult to find identical results accross the world, but certain similar patterns exist. *Wu et al*. (2016) detected significantly increasing annual air temperature and precipitation over the Dadu River basin in China. Analyzing the observed trends of precipitation and air temperature in the northeast part of Iran, *Minaei* and *Irannezhad* (2018) revealed: a) statistically increasing trend in case of annual precipitation (12.5% of the stations) and b) warming trend in case of annual air temperature (31% of the stations). *Tongal* (2019) investigated spatio-temporal changes of precipitation in the Antalya basin (Turkey). While the classical Mann-Kendall trend analysis could not reveal a significant trend for the stations, the modified Mann-Kendall test showed several significant increasing and decreasing trends in the precipitation values. Over the Mediterranean region, *Bilbao et al*. (2019) examined spatiotemporal patterns of air temperature in Spain (from 1950 to 2011) using the Mann-Kendall test. The decreasing trend of air temperature over Spain was recorded between 1950 and 1980, while significant warming was observed between 1980 and 2011. *Scorzini* and *Leopardi* (2019) detected a general, although not significant, negative trend in mean annual precipitation and significant warming in mean annual air temperature over the central part of Italy (Abruzzo region). However, this tendency has not been uniform from 1951 to 2012, but it has been characterized by a cooling phenomenon in the first 30 years (1951–1981), followed by an even stronger warming during the last three decades (1982–2012).

According to the possible climate scenario derived from the BCC Climate System Model (BCC-CSM2-MR), the increasing of air temperature will be pronounced, especially during the vegetation period. It is expected that, northern parts of Bačka become warmer compared to the reference period. The projected changes of mean precipitation will be similar in comparasion to the presented results from 1949 to 2018. Different results compared to the reference period could be expected in the total precipitation during the vegetation period. Changes will be manifested through a reduction of total precipitation. Projections of selected parameters represent the part of regional climate scenario. *Tarawneh* and *Chowdhury* (2018) examined future trends of climate changes in Saudi Arabia. For the RCP8.5 scenario, an increase of temperature occurred in the ranges from 0.8 to 1.6 ℃ (2025–2044) from 0.9 to 2.7 ℃ (2045–2064), and from 0.7 to 4.1 ℃ (2065–2084), respectively. However, precipitation showed variable patterns with respect to emission scenarios and assessment periods. In most regions, the RCP6 scenario showed a decrease in the rainfall from the reference period, while RCP8.5 and RCP2.6 showed variable patterns. For example, *Lionello* and *Scarascia* (2018) considered that air temperature will increase 20% more than the

global average, while precipitation will decrease at a rate around 20 mm during the 21st century over the Mediterranean region. Climate conditions will be more severe on the territory of Iran (*Senatore et al.*, 2019). According to the RCP4.5 scenario (from 2070 to 2099), the mean annual air temperature will increase by 2.4 ℃, while the mean annual precipitation will decrease by 20%. *Yin et al.* (2020) examined the long-term projections derived from a regional climate model (RCM) in the northwestern part of China. It is expected that the annual precipitation will rise by about 23.6 and 35.3 mm under the RCP 4.5 and 8.5 scenarios, respectively, while spatially averaged annual temperature will rise by about 1.95 and 1.10°C. On the territory of Serbia, *Kržič et al.* (2011) implicated: a) a projected increase in the air temperature from 2 ℃ to 4 ℃ based on regional climate models EBU-POM, b) a decrease in the precipitation from 13 mm to 6 mm (2071 to 2100). *Vuković et al.* (2018) predicted that global warming in Serbia would cause an increase in the mean annual air temperature by over 2.5 ℃ according to the stable scenario (RCP4.5) and over 5 ℃ according to the scenario of constant rise (RCP8.5). Total ammounts of precipitation do not display any significant change, apart from the reduction in the summer precipitation, along with the increase of intensity and frequency.

Analyzed results in terms of increasing trends of air temperature and no changes in precipitation trends indicate less available water resources for vegetation. For this reason, a possible aridity condition is a function of evapotranspiration rather than just a function of precipitation. These facts were confirmed in the paper of *Gocic* and *Trajkovic* (2014b). Authors noticed the statistically significant positive trends of reference evapotranspiration (ET_o) accross meteorological stations located in Bačka (Novi Sad, Sombor, and Palić). However, in order to confirm these facts in future research on the relationship between air temperature, precipitation, and evapotranspiration, it is necessary to include a larger number of meteorological stations in the territory of Bačka.

Sustainable agricultural production demands some adaptation measures in terms of drought and aridity. Possible negative effects of these phenomena can be mitigated by appropriate monitoring. From the above mentioned aspect, *Jovanović et al.* (2013) proposed the WAHASTRAT (*"Water shortage hazard and adaptive water management strategies in the Hungarian-Serbian crossborder region"*) project. The aim of this project was to find integrated water management solutions for the increasing problem of water shortage. In order to implement the project, a network of eight automatic measurement stations was set up in Southeast Bačka. Study area covers about 1,000 km² or 12% of Bačka. The presented results indicate that it would be necessary to expand the existing network of stations on the whole territory of Bačka in order to adeaqutely monitor the moisture deficit. Two important indicators make the agricultural production unsustainable nowadays: a) neglect or absence of irrigation systems, b) absence of adequate methodology of forecast of natural hazards, such drought and aridity,

while such methodologies could help in prevention and reduction of damage caused by these hazards (*Armenski et al.*, 2014).

Interaction between manifested climate changes and sustainability issues can also be reflected on tourism and on Ramsar wetland areas over the Bačka region. According to the observed and projected values of air temperatures, the effects of the urban heat island (UHI) can be manifested in urbas areas of Novi Sad, Subotica, and Sombor. For example, *Milošević et al*. (2020) noticed the existence of discomfort zones in urban area of Novi Sad by analyzing human thermal comfort that can affect tourism activity. On the territory of Bačka three Ramsar wetlands are located: the Special Nature Reserve "Gornje Podunavlje" (19,605 ha), the Special Nature Reserve "Koviljsko-petrovaradinski rit (5,895 ha), and the Special Nature Reserve "Ludaško jezero" (846 ha) (*Panjković* and *Stojnić*, 2014). The mentioned wetlands are climate sensitive, thus the manifested climatic patterns can lead to: a) the reduction of areas under hydrophilic vegetation and b) can cause uneven water regime. These areas are centers of heterogeneous biodiversity, so endangerment or extinction of plant and animal species is possible (*Stojanović*, 2005). Such problems must also be addressed through the preparation of planning documents in order to take adequate measures and to propose appropriate solutions. Therefore, results presented in this way could be used as a basis of policy, spatial planning, and regional development.

6. Conclusions

This paper provided the analysis of mean annual air temperature, mean air temperature during the vegetation period, mean annual precipitation, and total precipitation during the vegetation period (from 1949 to 2018). Beside statistical analysis of observed changes, in this paper a GIS modeling of a possible climate scenario over Bačka region (from 2018 to 2050) was performed. Selected trends in 20 time series were analyzed using (1) the trend equation, (2) the trend magnitude calculated from the trend equation, and (3) the MK test in the classical declaration. The main conclusions can be summarized as follows:

a) In accordance with the trend equations, positive trends were found in 18 out of 20 time series; in one of the time series there is no trend.
b) Negative trend was found only in one case.
c) Using the classical MK test, significant positive trends were found in 11 series, while in 9 cases there is no change.
d) A possible climate scenario (from 2018 to 2050) implicates that the increase in mean air temperatures would be dominant in comparison with the period from 1949 to 2018.

e) The changes of mean temperature during the vegetation period would be more intensive. The largest differences in a possible scenario would be in the eastern and western parts of Bačka.

f) Changes in the total precipitation during the vegetation period will give more certain image in comparasion with the mean annual precipitation. Semiarid conditions will be recorded in most parts of the region. Therefore, adaptation measures against potential drought and aridity problems are needed.

In this paper, the priority was given to the GIS method of climate projections rather than to the existing numerical models. In order to present the advantages and disadvantages of the GIS method, it is necessary to have more studies involving its application. Although Bačka occupies 9.8% of the territory of Serbia, it is of great importance to take into consideration smaller regions with specific features (e.g., agricultural significance of Bačka) for the purpose of future studies of climate projections on a national scale.

References

Ahmadi, F., Nazeri Tahroudi, M., Mirabbasi, R., Khalili, K., and *Jhajharia, D.,* 2018: Spatiotemporal trend and abrupt change analysis of temperature in Iran. *Meteorol. Appl. 25*, 314–321. https://doi.org/10.1002/met.1694

Almazroui, M., Saeed, S., Islam, M.N., Khalid, M.S., Alkhalaf, A.K., and *Dambul, R.,* 2017: Assessment of uncertainties in projected temperature and precipitation over the Arabian Peninsula: a comparison between different categories of CMIP3 models. *Earth Syst. Environ. 1*, 12. https://doi.org/10.1007/s41748-017-0012-z

Armenski, T., Stankov, U., Dolinaj, D., Mesaroš, M., Jovanović, M., Pantelić, M., Pavić, D., Popov, S., Popović, L., Frank, A., and *Ćosić, Đ.,* 2014: Social and economic impact of drought on stakeholders in agriculture. *Geographica Pannonica 18*(2), 34–42. https://doi.org/10.5937/GeoPan1402034A

Arnell, N.W., Lowe, J.A., Challinor, A.J., and *Osborn, T.J.,* 2019: Global and regional impacts of climate change at different levels of global temperature increase. *Climat. Change 155,* 377–391. https://doi.org/10.1007/s10584-019-02464-z

Berić, M., Zelenhasić, E., and *Srđević, B.,* 1990: Extreme Dry Weather Intervals of the Growing Season in Bačka, Yugoslavia. *Water Resour. Manage. 4*, 79–95. https://doi.org/10.1007/BF00429799

Bilbao, J., Román, R., and *De Miguel, A.,* 2019: Temporal and spatial variability in surface air temperature and diurnal temperature range in Spain over the period 1950 2011. *Climate 7*(1),16. https://doi.org/10.3390/cli7010016

Bucchignani, E., Mercogliano, P., Panitz, J.H., and *Montesarchio, M.,* 2018: Climate change projections for the Middle East–North Africa domain with COSMO-CLM at different spatial resolutions. *Adv. Climate Change Res. 9*, 66–80. https://doi.org/10.1016/j.accre.2018.01.004

Danandeh Mehr, A. and *Vaheddoost, B.,* 2020: Identification of the trends associated with the SPI and SPEI indices across Ankara, Turkey. *Theor. Appl. Climatol. 139*, 1531–1542. https://doi.org/10.1007/s00704-019-03071-9

Feidas, H., Makrogiannis, T., and *Bora-Senta, E.,* 2004: Trend analysis of air temperature time series in Greece and their relationship with circulation using surface and satellite data: 1955–2001. *Theor. Appl. Climatol. 79*, 185–208. https://doi.org/10.1007/s00704-004-0064-5

Fischer, E.M., Sedláček, J., Hawkins, E., and *Knutti, R.,* 2014: Models agree on forced response pattern of precipitation and temperature extremes. *Geophys. Res. Lett. 41*, 8554–8562. https://doi.org/10.1002/2014GL062018

Gavrilov, M.B., Lukić, T., Janc, N., Basarin, B., and *Marković, S.B.,* 2019: Forestry Aridity Index in Vojvodina, North Serbia. *Open Geosci. 11*(1), 367–377. https://doi.org/10.1515/geo-2019-0029

Gavrilov, M.B., Marković, S.B., Janc, N., Nikolić, M., Valjarević, A., Komac, B., Zorn, M., Punišić, M., and Bačević, N., 2018: Assessing average annual air temperature trends using the Mann–Kendall test in Kosovo. *Acta Geographica Slovenica 58*(1), 8–25. https://doi.org/10.3986/AGS.1309

Gavrilov, M.B., Marković, S.B., Jarad, A., and *Korać, V.M.,* 2015: The analysis of temperature trends in Vojvodina (Serbia) from 1949 to 2006. *Thermal Sci. 19*, 339–350. https://doi.org/10.2298/TSCI150207062G

Gavrilov, M.B., Tošić, I., Marković, S.B., Unkašević, M., and *Petrović, P.,* 2016: The analysis of annual and seasonal temperature trends using the Mann-Kendall test in Vojvodina, Serbia. *Időjárás 122*, 203–216. https://doi.org/10.28974/idojaras.2018.2.6

Gocić, M., and *Trajković, S.,* 2014a: Spatiotemporal characteristics of drought in Serbia. *J. Hydrol. 510*, 110–123. https://doi.org/10.1016/j.jhydrol.2013.12.030

Gocic, M. and *Trajkovic, S., 2014b*: Analysis of trends in reference evapotranspiration data in a humid climate. *Hydrol. Sci. J. 59*, 165–180. https://doi.org/10.1080/02626667.2013.798659

Gocic, M., Trajkovic, S., and *Milanovic, M.,* 2020: Precipitation and Drought Analysis in Serbia for the Period 1946–2017. In (eds: *Negm, A., Romanescu, G.,* and *Zelenakova, M.*) Water Resources Management in Balkan Countries. Springer Water. Springer, Cham. https://doi.org/10.1007/978-3-030-22468-4_11

Hazewinkel, M., 1990: Encyclopaedia of Mathematics. Kluwer Academic Publishers, Dordrecht. https://doi.org/10.1007/978-94-009-5991-0

Hrnjak, I., Lukić, T., Gavrilov, M.B., Marković, S.B., Unkašević, M., and *Tošić, I.,* 2014: Aridity in Vojvodina, Serbia. *Theor. Appl. Climatol. 115*, 323–332. https://doi.org/10.1007/s00704-013-0893-1

Hulme, M., 2017: Climate Change, Concept of. In (eds: *Richardson, D., Castree, N., Goodchild, M.F., Kobayashi, A., Liu, W.,* and *Marston, R.A.*) International Encyclopedia of Geography: People, the Earth, Environment and Technology. Black Wiley & Sons, Oxford. https://doi.org/10.1002/9781118786352.wbieg0343

Janković, A., Podraščanin, Z., and *Djurdjević, V.,* 2019: Future climate change impacts on residential heating and cooling degree days in Serbia. *Időjárás 123*, 351–370. https://doi.org/10.28974/idojaras.2019.3.6

Javari, M., 2016: Trend and homogeneity analysis of precipitation in Iran. *Climate 4*(3), 23. https://doi.org/10.3390/cli4030044

Jovanović, M., Pavić, D., Mesaroš, M., Stankov, U., Pantelić, M., Armenski, T., Dolinaj, D., Popov, S., Ćosić, Đ., Popović, Lj., Frank, A., and Crnojević, V., 2013: Water shortage and drought monitoring in Bačka region (Vojvodina, North Serbia) – setting-up measurement stations network. *Geographica Pannonica 17*(4), 114–124. https://doi.org/10.5937/GeoPan1304114J

Kržič, A., Tošić, I., Djurdjević, V., Veljović, K., and *Rajković, B.,* 2011: Changes in climate indices for Serbia according to the SRES-A1B and SRES-A2 scenarios. *Climate Res. 49*, 73–86. https://doi.org/10.3354/cr01008

Lazić, L., Marković, S., and *Pavić, D.,* 2004: Average and extreme precipitation heights in Bačka (1951-1990). *Geographica Pannonica 8*, 4–10. https://doi.org/10.5937/GeoPan0408004L

Li, X., and *Cheng, G.,* 1999: A GIS-aided response model of high-altitude permafrost to global change. *Sci. China Ser. D: Earth Sci. 42*, 72–79. https://doi.org/10.1007/BF02878500

Lionello, P., and *Scarascia, L.,* 2018: The relation between climate change in the Mediterranean region and global warming. *Regional Environ. Change 18*, 1481. https://doi.org/10.1007/s10113-018-1290-1

Milošević, D., Savić, S., Arsenović, D., Lužanin, Z., and *Dunjić, J.*, 2020: Analysis of human thermal comfort in Central European City during summer of 2015: A case of Novi Sad (Serbia). *Bulletin of the Serbian Geographical Society 100*(1), 31-39. https://doi.org/10.2298/GSGD2001031M

Minaei, M., and *Irannezhad, M.,* 2018: Spatio-temporal trend analysis of precipitation, temperature, and river discharge in the northeast of Iran in recent decades. *Theor. Appl. Climatol. 131*, 167–179. https://doi.org/10.1007/s00704-016-1963-y

Mudelsee, M., 2019: Trend analysis of climate time series: A review of methods. *Earth-Sci. Rev. 190*, 310–322. https://doi.org/10.1016/j.earscirev.2018.12.005

Nourani, V., Danandeh Mehr, A., and *Azad, N.,* 2018: Trend analysis of hydroclimatological variables in Urmia lake basin using hybrid wavelet Mann–Kendall and Şen tests. *Environ. Earth Sci. 77*, 207. https://doi.org/10.1007/s12665-018-7390-x

Nourani, V., Ghasemzade, M., Danande Mehr, A., and *Sharghi, E.*, 2019: Investigating the effect of hydroclimatological variables on Urmia Lake water level using wavelet coherence measure. *J. Water Climate Change 10*, 13–29. https://doi.org/10.2166/wcc.2018.261

Nouri, M., and *Bannayan, M.,* 2018: Spatiotemporal changes in aridity index and reference evapotranspiration over semi-arid and humid regions of Iran: trend, cause, and sensitivity analyses. *Theor. Appl. Climatol.136*, 1073–1084. https://doi.org/10.1007/s00704-018-2543-0

Orus, R., Hernandez-Pajares, M., Juan, J.M., and *Sanz, J.,* 2005: Improvement of global ionospheric VTEC maps by using kriging interpolation technique. *J. Atmos. Solar-Terr. Phys. 67*, 1598–1609. https://doi.org/10.1016/j.jastp.2005.07.017

Panda, A., and *Sahu, N.,* 2019: Trend analysis of seasonal rainfall and temperature pattern in Kalahandi, Bolangir and Koraput districts of Odisha, India. *Atmosp. Sci. Lett. 20*(10), e932. https://doi.org/10.1002/asl.932

Panjković, B., and *Stojnić, N.,* 2014: Biodiversity and protected areas. In (eds: *Puzović, S.*, and *Radovanović-Jovin, H.*) Environment in Autonomous Province of Vojvodina: state, challenges-perspectives. Provincial Secretariat for Urbanism, Construction and Environmental Protection, Novi Sad. 168–211.

Rajić, M., 2004: Klimatske promene i potrebe za vodom u regionu Južne Bačke. *Letop. naučn. rad. Poljoprivrednog fakulteta*, *28*(1), 137–145. (In Serbian)

Rajić, M., and *Rajić, M.,* 2005: Prosečne padavine na području Bačke. *Letop. naučn. rad. Poljoprivrednog fakulteta*, *29*(1), 178-186. (In Serbian)

Rajić, M., and *Štula, S.*, 2007: Klimatske promene i pojava suša na području Južne Bačke. *Letop. naučn. rad. Poljoprivrednog fakulteta*, *31*(1), 80–89. (In Serbian)

Rakićević, T., 1988: Regionalni raspored suše u SR Srbiji. *Glasnik Srpskog geografskog društva, 68*(1), 9-18. (In Serbian)

Razavi, T., Switzman, H., Arain, A., and *Coulibaly, P.,* 2016: Regional climate change trends and uncertainty analysis using extreme indices: A case study of Hamilton, Canada. *Climate Risk Manage. 13*, 43–63. https://doi.org/10.1016/j.crm.2016.06.002

Republic Hydrometeorological Service of Serbia, 2019: Meteorological Yearbook – Climatological Data. http://www.hidmet.gov.rs/ciril/meteorologija/klimatologija_godisnjaci.php Accessed 18 January 2020.

Sa'adi, Z., Shahid, S., Ismail, T., Chung, E., and *Wang, X.,* 2019: Trends analysis of rainfall and rainfall extremes in Sarawak, Malaysia using modified Mann–Kendall test. *Meteorol. Atmosph. Phys. 131*, 263–277. https://doi.org/10.1007/s00703-017-0564-3

Scorzini, A.R. and *Leopardi, M.,* 2019: Precipitation and temperature trends over central Italy (Abruzzo Region):1951–2012. *Theor. Appl. Climatol. 135*, 959–977. https://doi.org/10.1007/s00704-018-2427-3

Senatore, A., Hejabi, S., Mendicino, G., Bazrafshan, J., and *Irannejad, P.,* 2019: Climate conditions and drought assessment with the Palmer Drought Severity Index in Iran: evaluation of CORDEX South Asia climate projections (2070–2099). *Climate Dynam. 52*, 865–891. https://doi.org/10.1007/s00382-018-4171-x

Stojanović, V., 2005: Degradation and protection of wetlands in special nature reserves in Vojvodina. *Geographica Pannonica 9*, 24–28. https://doi.org/10.5937/GeoPan0509024S

Tarawneh, Q.Y., and *Chowdhury, S.,* 2018: Trends of climate change in Saudi Arabia: Implications on water resources. *Climate 6*(1), 8. https://doi.org/10.3390/cli6010008

Teegavarapu, S.V.R., 2019: Chapter 1-Methods for Analysis of Trends and Changes in Hydroclimatological Time-Series In (ed: *Teegavarapu, S.V.R.*)Trends and Changes in Hydroclimatic Variables. Elsevier. 1–89. https://doi.org/10.1016/B978-0-12-810985-4.00001-3

Tomaszkiewicz, M., Abou Najm, M., Beysens, D., Alameddine, I., Bou Zeid, E., and *El-Fadel, M.,* 2016: Projected climate change impacts upon dew yield in the Mediterranean basin. *Sci. Total Environ. 566–567*, 1339–1348. https://doi.org/10.1016/j.scitotenv.2016.05.195

Tongal, H., 2019: Spatiotemporal analysis of precipitation and extreme indices in the Antalya Basin, Turkey. *Theor. Appl. Climatol. 138*, 1735–1754. https://doi.org/10.1007/s00704-019-02927-4

Tošić, I., Hrnjak, I., Gavrilov, M.B., Unkašević, M., Marković, S.B., and Lukić, T., 2014: Annual and seasonal variability of precipitation in Vojvodina. *Theor. Appl. Climatol. 117*, 331–341. https://doi.org/10.1007/s00704-013-1007-9

Touseef, M., Chen, L., Yang, K., and *Chen, Y.,* 2020: Long-Term Rainfall Trends and Future Projections over Xijiang River Basin, China. *Adv. Meteorol. 2020* (article ID 6852148). https://doi.org/10.1155/2020/6852148

Urban Institute of Vojvodina, 2011: Regional Spatial Plan of AP Vojvodina until 2020. Novi Sad, Serbia. https://www.zavurbvo.co.rs/rppapv_cir.php. Accessed 02 March 2020.

Vuković, A.J., Vujadinović, M.P., Rendulić, S.M., Djurdjević, V.S., Ruml, M.M., Babić, V.P., and *Popović, D.P.,* 2018: Global warming impact on climate change in Serbia for the period 1961-2100. *Thermal Sci. 22*, 2267–2280. https://doi.org/10.2298/TSCI180411168V

Wilks, D., 2011: Frequentist Statistical Inference. In (ed: *Wilks, D.*) Statistical Methods in the Atmospheric Sciences (vol. 100, 3rd edition). Academic Press, United States. 133–185. https://doi.org/10.1016/B978-0-12-385022-5.00005-1

Wu, T., Lu, Y., Fang, Y., Xin, X., Li, L., Li, W., Jie, W., Zhang, J., Liu, Y., Zhang, L., Zhang, F., Zhang, Y., Wu, F., Li, J., Chu, M., Wang, Z., Shi, X., Liu, X., Wei, M., Huang, A., Zhang, Y., and Liu, X., 2019: The Beijing Climate Center Climate System Model (BCC-CSM): the main progress from CMIP5 to CMIP6. *Geosci. Model Develop*. 12, 1573–1600. https://doi.org/10.5194/gmd-12-1573-2019

Wu, Y., Wang, W., and *Wang, G.,* 2016: Detecting variation trends of temperature and precipitation for the Dadu River Basin, China. *Adv. Meteorol. 2016*, 11. https://doi.org/10.1155/2016/2564586

Yin, Z., Feng, Q., Yang, L., Deo, C.R., Adamowski, F.J., Wen, X., Jia, B., and *Si, J.,* 2020: Projected spatial patterns in precipitation and air temperature for China's northwest region derived from high-resolution regional climate models. *Int. J. Climatol. 40*, 3922–3941. https://doi.org/10.1002/joc.6435

Zadeh, M.S., Burn, H.D., and *O'Brien, N.,* 2020: Detection of trends in flood magnitude and frequency in Canada. *J. Hydrol.: Regional Studies 28*, 100673. https://doi.org/10.1016/j.ejrh.2020.100673

Zeleňáková, M., Purcz, P., Blišťan, P., Vranayová, Z., Hlavatá, H., Diaconu, D.C., and *Portela, M.M.,* 2018: Trends in precipitation and temperatures in Eastern Slovakia (1962–2014). *Water 10*, 727. https://doi.org/10.3390/w10060727

Zhou, B., Wen, H.Q., Xu, Y., Song, L., and *Zhang, X.,* 2014: Projected Changes in Temperature and Precipitation Extremes in China by the CMIP5 Multimodel Ensembles. *J. Climate 27*, 6591–6611. https://doi.org/10.1175/JCLI-D-13-00761.1

Zittis, G., Hadjinicolaou, P., Klangidou, M., Proestos, Y., and *Lelieveld, J.,* 2019: A multi model, multi-scenario, and multi-domain analysis of regional climate projections for the Mediterranean. *Regional Environmental Change 19*, 2621–2635. https://doi.org/10.1007/s10113-019-01565-w

IDŐJÁRÁS

Influence of meteorological conditions on the use of coercive interventions

Jakub Lickiewicz[1,*], **Katarzyna Piotrowicz**[2], **Patricia Paulsen Hughes**[3],
Agnieszka Micek[4], and **Marta Makara-Studzińska**[1]

[1] *Department of Health Psychology,*
Institute of Nursing and Midwifery, Faculty of Health Sciences,
Jagiellonian University Medical College, Krakow, Poland

[2] *Department of Climatology,*
Institute of Geography and Spatial Management,
Jagiellonian University, Krakow, Poland

[3] *Oklahoma State University, Stillwater, USA*

[4] *Department of Nursing Management and Epidemiology Nursing,*
Faculty of Health Sciences,
Jagiellonian University Medical College, Krakow, Poland

*Corresponding author E-mail: jlickiewicz@cm-uj.krakow.pl

(Manuscript received in final form October 15, 2020)

Abstract— Aggressive behavior in psychiatric care is a serious problem. The causes of aggression may be ambiguous, including behaviors gender, age, or atmosphere on the ward. Other risk factors, usually not mentioned, include meteorological conditions, such as air temperature and humidity, pressure or wind. The available literature suggests a link between meteorological conditions and the use of coercive interventions in psychiatric care. In this study, we examined meteorological conditions that correlated with an increased number of cases of aggressive behavior leading to coercive interventions. The relationships between the studied variables were determined using linear correlation tests and cluster analysis. The study draws on coercive intervention records from The Józef BabiánskiPsychiatric Hospital in Krakow, spanning 27 months. The hospital's seventeen in-patient treatment wards, six day-care centers, nine community treatment teams, and six outpatient clinics have a capacity of 790 patients. Among patients who were susceptible to weather changes, specific weather types were identified as being related to more cases of aggressive behavior.

Key-words: meteorological conditions, physical coercion, aggressive behavior, psychiatric patients

1. Introduction

Aggressive patient behavior presents a serious problem for medical staff. Some negative consequences may be identified, including healthcare professionals' reluctance to work, professional burn-out, or compromised healthcare quality (*Chamberset al.*, 2015)

The risk factors of aggression and of the exacerbation of symptoms of mental disease also include weather conditions, i.e., air temperature and humidity, pressure, wind (especially foehn wind), sunshine duration, and storms (*Almendra et al.*, 2019; *Belleville et al.*, 2013; *Dominiak et al.*, 2015; *Manning* and *Clayton*, 2018; *McWilliams, et al.,* 2014; *Nastos et al.,* 2017; *Santiago, et al.*, 2005; *Shiloh et al.*, 2005).

The variability of meteorological conditions over the course of the year and the occurrence of seasonal weather events has a strong impact on the human body. Such adverse meteorological conditions exacerbate disease symptoms and may increase the frequency of aggressive behavior among susceptible individuals. Strong atmospheric stimuli have an especially strong impact on the human nervous system, especially in highly excitable people (*Vida et al*., 2012). Researchers in Netherlands, Germany, Belgium, England, and Poland have found that patients suffering from depression, schizophrenia, as well as alcohol and drug addiction, are the most susceptible to weather conditions and their abrupt changes. The researchers have also confirmed the periodic nature of nervous system conditions (*Shiue, et al.*, 2016).

There are researchers, who suggest an increased number of aggressive incidents between January and April, in the summer season, and in autumn (*Peluola, et el., *2013; *Weizmann-Henelius*, 2000). Finnish research has found that fewer coercive interventions were required in January (*Kuivalainen et al.*, 2017). Coercion was more often used in psychiatric wards in Finland between June and November, and during the summer in Norway (*Reitan, et al.*, 2018).

Atmospheric factors have an impact not only on the number of aggressive incidents, but also on self-destructive behavior and the use of coercion. Research conducted in many countries suggests that patients suffering from mental diseases are the most sensitive to weather (*McWilliams et al*., 2014). This relationship has also been noted in regard to self-aggressive behavior (*Yackerson, et al.,* 2014).

The aim of the paper was to determine meteorological conditions prevailing during periods with more cases of aggressive behavior leading to coercive interventions in patients treated at a psychiatric hospital in Krakow (Poland, Central Europe).

2. Material and methods

The study was carried out at the largest psychiatric care facility in the Lesser Poland Region – the Józef Babiński Psychiatric Hospital in Krakow. It's

seventeen inpatient treatment wards, six day-care centers, nine community treatment teams, and six outpatient outpatient clinics can receive up to 790 patients. Annually, the hospital provides more than 8500 inpatient treatment services, and 85,000 people receive care out-patients as outpatients.

To determine the impact of weather conditions on the frequency of coercive interventions, "coercion sheets" filled out between January 1, 2015 and March 31, 2017 were analyzed. The paper has been approved by the Ethics Committee. During the studied period, the principles of recording coercive interventions were modified, enabling a more precise description of individual cases. A period of 27 months allowed the authors to take into account both relatively warm winter seasons, atypical considering the climatic conditions of Central Europe, as well as normal ones with characteristic frost waves.

When analyzing the data, the authors considered the date and time when the coercive intervention started, suggesting that the aggressive behavior occurred immediately beforehand. The researchers paid special attention to days, where a large number (N>8) of coercive interventions occurred. The adopted threshold resulted from the distribution of frequencies and values exceeding the mean daily number of events within the analyzed period.

The weather conditions prevailing in Krakow on the analyzed days were determined on the basis of meteorological measurements and observations taken at the Climatology Station of the Jagiellonian University. The daily values of air temperature: daily average, maximum, and minimum (ºC), air pressure (hPa), relative humidity (%), average wind speed (m/s), cloud cover (%), and sunshine duration (hours) were used in the analysis.

In order to determine the cumulative impact of weather on the number of coercive interventions, the reserachers used the Synoptic Situations Calendar prepared by *Niedźwiedź* (2020), which can be used to identify types of circulation over southern Poland (the presence of anticyclones or cyclones), the direction of advection and type of air mass, as well as the presence of weather fronts (*Table 1*). Conditional probability of the occurrence of days with an increased number of coercive interventions (N>8) was calculated in particular synoptic situations. Meteorotropic situations include, above all, cyclonic situations (lows), passage of weather fronts (especially cold ones), and advection of air masses with contrasting physical characteristics, as well as stormy weather (unstable state of the atmosphere) and foehn situations (foehn is a dry and warm wind blowing from the mountains). The above synoptic situations involve rapid changes in meteorological conditions which have a strong stimulating effect on the human body.

Symbol	Name
Circulation types	
E+SEa	Anticyclonic situations with an advection of air masses from east and south-east
Ca+Ka	Central anticyclonic situation, anticyclonic wedge
Cc+Bc	Central cyclonic situation, trough of low pressure
S+SWc	Cyclonic situations with an advection of air masses from south and southwest
S+SWa	Anticyclonic situations with an advection of air masses from south and southwest
E+SEc	Cyclonic situations with an advection of air masses from east and southeast
W+NWc	Cyclonic situations with an advection of air masses from west and northwest
W+NWa	Anticyclonic situations with an advection of air masses from west and northwest
N+NEa	Anticyclonic situations with an advection of air masses from north and northeast
N+NEc	Cyclonic situations with an advection of air masses from north and northeast
x	Unclassified situation
Air masses	
PPk	Polar continental
PPms	Polar maritime old (transformed)
PPmc	Polar maritime warm
PPm	Polar maritime (fresh)
rmp	Various air masses in day
PZ	Tropical air masses
PA	Arctic air masses
Atmospheric fronts	
-	Day without front
z	Cold front
c	Warm front
st	Stationary front
r	Several various fronts in day
o	Occluded front (occlusion)

In order to explore the relationship between the weather conditions on days with a larger number of coercive interventions, the differences between the average value of individual meteorological elements for each day in the years 1981–2010 and the value of a given day with N>8 (daily anomaly) were calculated (N is the number of coercive interventions). Spearman's rank linear correlation and multiple correlation coefficients were used. The statistical significance was determined as $p<0.05$. A cluster analysis was also performed to explore the relationship between meteorological conditions and the number of cases of aggressive behavior which resulted in coercive interventions. This statistical method is especially useful in the analysis of multiple variables, just as in the case of this study. Thus, each day with more than eight coercive interventions had

certain weather conditions characterized by a set of individual meteorological elements. These can be grouped into clusters if treated as multi-property objects. Objects which belong to the same group (cluster) are the most similar to one another (in our case, they had similar weather conditions), while those which belong to different groups differ most from each other. This method also allows for the identification of dominant elements, which have the greatest influence on, and which distinguish, a particular group.

A hierarchical (agglomeration) method of cluster analysis and tree diagram (Word's method) was used in the first step. Four clusters were selected, which very well represented the weather conditions in the seasons. The method of k-average allowed to add each day into a separate group. Grouping was carried out for all meteorological elements and their deviations from the 30-year average (1981–2010).

3. Results

There were 329 days with a large number of cases of aggressive behavior leading to coercive intervention (N>8) in the period from January 1, 2015 to March 31, 2017. Such days accounted for 40.1% of all analyzed days in analyzed period, out of which 21.3% were days with 9 or 10 coercive situations, 16.9% with 11–15 and 1.8% with more than 15 coercive situations. The greatest number of coercive interventions on a single day, namely 19, occurred on July 10, 2016. Their distribution in the analyzed months is presented in *Fig. 1*. On average, there were 13 days per month, with the largest number occurring in April 2016 (20 days) and the smallest in April 2015 (2 days). No clear difference in the course of such days during the year was identified. On average, there was only one further similar day in autumn and 2 in spring, fewer than the average for the entire period (*Fig. 1*).
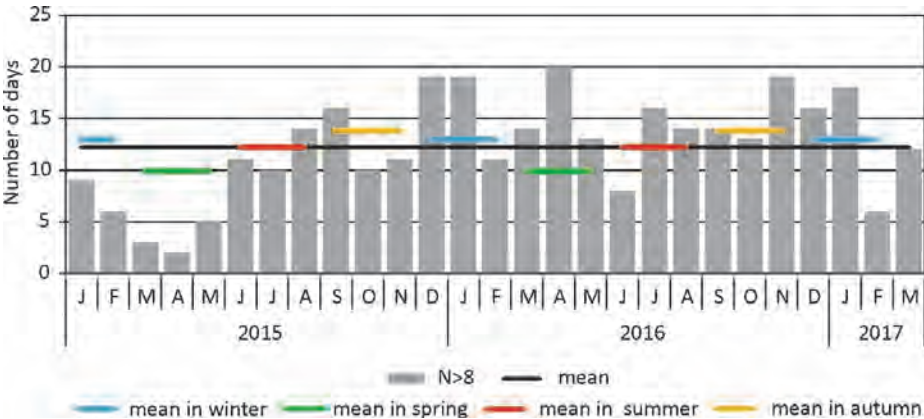
Fig. 1. Number of days on which physical coercion was used towards at least 9 hospital patients (N>8) and mean number of this days in particular seasons in the period from January 1, 2015 to March 31, 2017.

Few such studies, especially those conducted in the context of diseases of the nervous system, investigate the combined impact of a number of elements based on synoptic situations prevailing over a given area (pressure system with advection directions of specific air masses and the presence of weather fronts). Information about synoptic situations on a given day and those expected over the next few days is widely available since it serves as a basis of weather forecasts.

For southern Poland, *Niedźwiedź* (2020; *Table 1*) has prepared a calendar of synoptic situations, using which the synoptic situation on a given day was determined in the present study. A slightly higher conditional probability of the occurrence of days with N>8 was found for cyclonic situations, i.e., those with low atmospheric pressure (43.1%), than for anticyclonic situations (high atmospheric pressure; *Fig. 2a*). Probability of over 50% occurred with the following types of circulation: Nc (cyclonic situations with advection of air masses from the west; 64.3%), NWc (cyclonic situations with advection of air masses from the northwest; 61.8%) and NWa (anticyclonic situations with advection of air masses from the northwest; 51.7%). Therefore, with these three types of circulation, a rise in the frequency of days with a high number of coercive situations can be expected.

In biometeorological analyses, in addition to conditions prevailing on a given day, rapid changes over a short spell and/or from day to day, are also important. Therefore, the next step involved analyzing the types of circulation on a day with N>8 and on the preceding day. It was found that the conditional probability of coercive interventions was over 70% when the synoptic situation over southern Poland changed from one day to another from a cyclonic center to a cyclonic trough (Ca-Bc) or from a cyclonic situation with advection of air masses from the northwest to an anticyclonic trough with advection from the west (NWc-Wa). A high number of N>8 was also observed at times when the direction of air masses changed during cyclonic and anticyclonic situations. This included changes of advection from the west to the southwest (Wa-SWa), the east to the southeast (Ec-Sec), the northwest to the west (NWc-Wc), and from the east to an advectionless situation (Ea-Ka). The changes in the types of circulation thus distinguished occurred at least three times during the study period.

A similar analysis of the correlation between N>8 and the accompanying types of circulation was conducted for air masses and weather fronts moving over Krakow. Even though the results do not demonstrate clearly which air masses predominated on the days with N>8, since the conditional probability ranged from 35.9% for old maritime polar air masses (PPms) to 48.7% for various air masses (rmp) (*Fig. 2b*), it must be emphasized that the passage of various air masses over a given area during the day is indicative of rapid weather changes, and such meteorological conditions are strongly stimulating ones. In addition, Arctic air masses (PA), which form the type of air mass accompanying days with N>8, which ranked third in terms of conditional probability, are rather rare in Poland.

In the period under analysis, their frequency was at a level of 7%, which indicates a fairly strong correlation with coercive measures.

As regards fronts, the conditional probability indicates that days with N>8 could be correlated with the passage of a cold front (z; 46.0%) or several fronts on one day (rf; 45.6%) (*Fig. 2c*). These two cases are associated with dynamic change in the weather, which has an irritating effect on humans.
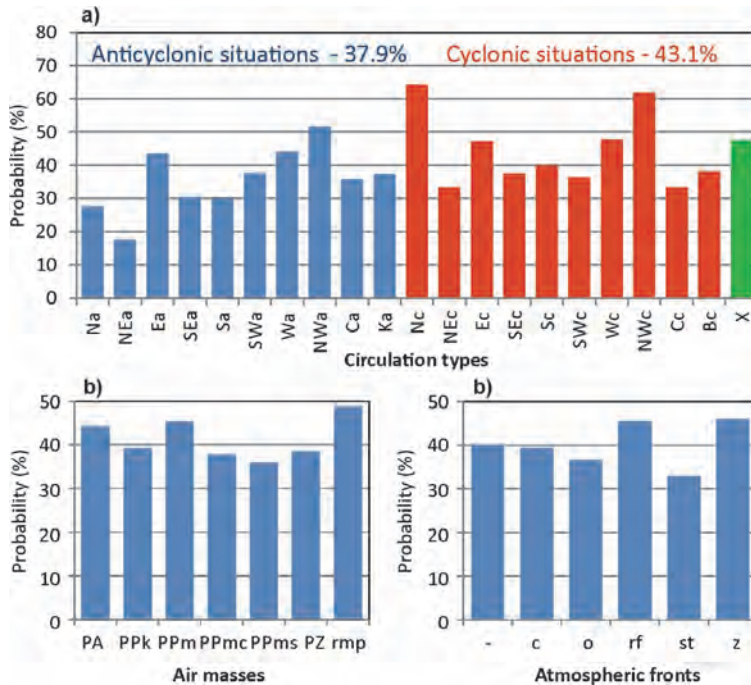
Fig. 2. Conditional probability of the occurrence of days with an increased number of coercive interventions (N>8) and associated circulation types (a), air masses (b) and atmospheric fronts (c) in the period from January 1, 2015 to March 31, 2017 (explanation of circulation types is presented in *Table 1*).

In order to explore the relationship between the weather conditions on days with a larger number of coercive interventions, the differences between the average value of individual meteorological elements for each day in the years 1981–2010 and the value of a given day with N>8 (daily anomaly) were a given meteorological element calculated. For this, the coefficients of the correlation

between the above mentioned differences for the individual meteorological elements were calculated first. The only statistically significant relationships ($p<0.05$) were: a positive anomaly for the mean and maximum air temperatures (0.113–0.116), and a negative one (-0.116; $p<0.05$) for the atmospheric pressure, i.e., the lower the pressure values, the larger the number of cases of aggressive behavior leading to coercive interventions. Also, no relationship was found between coercion interventions and day-to-day changes in pressure.

Next, a cluster analysis was used to analyze the identified groups of days and their weather conditions. The performed tests allowed the authors to conclude that four clusters should be identified. On this basis, the weather type, which favored a larger number of coercive interventions in particular months and groups, has been determinedto identify differences against the backdrop of the long-term daily mean (1981–2020) have been determined.

3.1. First group of days

The first and most numerous cluster (33.7% of all cases) included days occurring from October to May (in the cool part of the year) (*Table 2*). Air temperature was the factor which had the greatest influence on the occurrence of a large number of coercive interventions. In winter (between December and February), these were very atypical days for this season of the year, with a relatively high air temperature (Tmax>10 ºC). The mean values of temperature anomalies were 5.6–8.4 °C (*Table 2*). These days were also marked by lower pressure and langer cloudiness in January and February (altered by 5.5–7.7 hPa and 1.7–5.0% from the norm). In December, pressure was above the mean long-term value (by 6.4 hPa). The relative humidity was slightly below the average in three winter months (by 1.7–5.0%), while the wind speed was slightly higher (*Table 2*). The sunshine duration did not differ from the norm.

In spring (from March to May), the temperature on the days in this group was near the average (+/- 2 °C), with the exception of May, when they were on average 2.6–8.2 °C colder (*Table 2*). In March, these were days with less air pressure and in May with less humidity, but in both of these months, the cloud cover was greater and the sunshine duration shorter than the average. Days which were included in the first group but which occurred in October stood out more cloudiness, while those in November were characterised by less cloudiness (differing -12% from the norm), but were also the most sunny (the average cloud cover was around 60%).

Table 2. Mean monthly values of selected meteorological elements in the first cluster of days with an increased number of cases of aggressive behavior leading to coercive interventions in a psychiatric hospital in Krakow between January 1, 2015 and March 31, 2017

Elements	Jan	Feb	Mar	Apr	May	Jun	Jul	Aug	Sep	Oct	Nov	Dec
Mean monthly values												
Tmax (°C)	10.5	11.2	10.3	13.8	13.6	-	-	-	-	11.0	11.4	9.6
Tmin (°C)	2.0	2.5	1.8	4.4	7.1	-	-	-	-	4.5	2.5	3.8
Tmean (°C)	5.5	5.8	5.6	8.7	10.1	-	-	-	-	7.1	6.0	6.4
Pressure (hPa)	983.6	984.2	985.9	987.0	986.6	-	-	-	-	993.2	991.6	996.7
Humidity (%)	77.1	76.7	73.7	67.2	67.0	-	-	-	-	82.0	85.6	79.8
Wind speed (m/s)	2.7	2.1	2.3	1.9	2.3	-	-	-	-	2.3	1.3	3.0
Cloudiness (%)	73.9	77.3	76.7	65.8	75.0	-	-	-	-	77.0	60.3	75.7
SD (hours)	1.4	2.5	2.7	6.0	4.3	-	-	-	-	2.8	3.3	1.4
Mean monthly values of daily differences from 1981-2010 (anomalies)												
Tmax (°C)	8.4	7.4	1.9	-2.5	-8.2	-	-	-	-	-3.6	3.8	6.9
Tmin (°C)	6.1	5.6	2.0	-0.9	-2.6	-	-	-	-	-0.9	1.5	6.5
Tmean (°C)	6.8	5.9	2.0	-1.7	-5.2	-	-	-	-	-2.0	2.2	6.6
Pressure (hPa)	-7.7	-5.5	-2.2	0.3	-0.9	-	-	-	-	2.4	2.9	6.4
Humidity (%)	-5.0	-1.7	-0.1	0.6	-3.1	-	-	-	-	-0.2	1.5	-4.7
Wind speed (m/s)	1.0	0.3	0.3	0.2	1.0	-	-	-	-	1.0	-0.3	1.4
Cloudiness (%)	2.7	7.2	10.7	5.8	16.5	-	-	-	-	14.9	-12.8	-0.1
SD (hours)	-0.2	0.0	-0.4	0.4	-2.6	-	-	-	-	-0.6	1.6	0.3

-20 -10 0 10 20 anomaly
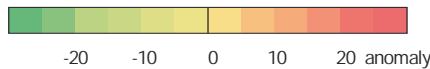
3.2. Second group of days

In the second group, (21.9% of all analyzed days), there were those which occurred in the ten months from February to November (*Table 3*). Air temperature, humidity, and cloud cover were the most significant differentiating factors in this group. In summer (from June to August), an increased number of coercive interventions was accompanied by weather which was relatively cool considering the season of the year (Tmean of 16 °C and Tmax of 21 °C; anomaly from -1.4 °C to -4.1 °C), overcast (cloud cover >75% and 12–21% above normal, sunshine duration of less than 4 hours per day; anomaly from -1.4 to -3.2 hours), and with high air humidity (>75%; 2.3–4.0% above normal). In the remaining months, these were days with (*Table 3*):

- a higher air temperature (in February with a Tmax above 16 °C on average; anomaly from 4.4 °C to 12.1 °C),

- most frequently, almost normal atmospheric pressure (980–990 hPa), but in February with low anomaly (-12.9 hPa by mean),

- low humidity in February, March, and November (with anomaly below -6.1%) and higher humidity in the remaining months (>72%),

- most frequently, more cloudiness and somewhat shorter sunshine duration.

Table 3. Mean monthly values of selected meteorological elements in the second cluster of days with an increased number of cases of aggressive behavior leading to coercive interventions in a psychiatric hospital in Krakow between January 1, 2015 and March 31, 2017.

Elements	Jan	Feb	Mar	Apr	May	Jun	Jul	Aug	Sep	Oct	Nov	Dec
Mean monthly values												
Tmax (ºC)	-	16.1	17.6	20.1	20.6	20.7	21.4	21.4	19.5	18.9	16.4	-
Tmin (ºC)	-	6.7	7.5	8.1	10.0	12.0	15.1	13.8	11.8	9.1	9.8	-
Tmean (ºC)	-	11.9	11.9	12.9	14.8	16.0	17.9	16.8	14.9	13.1	12.4	-
Pressure (hPa)	-	976.9	990.8	982.3	986.0	985.5	987.5	990.0	989.3	989.4	990.3	-
Humidity (%)	-	64.0	62.7	72.5	75.2	74.8	76.3	77.6	78.7	87.0	77.8	-
Wind speed (m/s)	-	2.3	1.8	1.5	1.7	1.6	2.2	1.7	2.0	0.7	3.1	-
Cloudiness (%)	-	66.7	72.2	71.9	67.0	75.9	79.9	75.8	79.2	68.8	59.2	-
SD (hours)	-	7.7	5.5	4.7	5.9	5.0	4.0	3.3	2.8	3.1	3.5	-
Mean monthly values of daily differences from 1981-2010 (anomalies)												
Tmax (ºC)	-	12.1	7.7	6.3	0.1	-2.4	-4.1	-4.1	-0.3	4.1	8.9	-
Tmin (ºC)	-	10.2	6.7	4.4	0.8	-0.5	0.7	-0.3	2.0	3.3	8.7	-
Tmean (ºC)	-	12.0	7.1	4.6	0.4	-1.4	-1.4	-2.1	1.0	3.8	8.5	-
Pressure (hPa)	-	-12.9	3.0	-3.4	-1.7	-1.6	0.0	1.9	-0.5	-1.4	1.1	-
Humidity (%)	-	-12.2	-10.7	3.9	5.5	3.2	4.0	3.8	-1.5	3.6	-6.1	-
Wind speed (m/s)	-	0.6	0.0	-0.3	0.1	0.0	0.7	0.5	0.6	-0.5	1.5	-
Cloudiness (%)	-	-3.9	9.0	6.5	7.7	12.7	21.3	19.8	19.6	9.8	-15.2	-
SD (hours)	-	4.8	1.9	0.2	-0.8	-1.4	-3.0	-3.2	-1.7	-0.3	1.8	-

-20   -10   0   10   20 anomaly
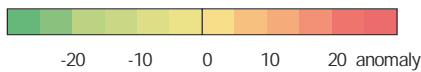
3.3. Third group of days

The third group consisted of days which occurred in the cool half of the year, from November to March (*Table 4*). They included 24.9% of all cases. An increased number of coercive interventions was accompanied by cool weather with a Tmax<4 °C and a Tmin <0 °C, with a slightly higher atmospheric pressure (990–1000 hPa) and smaller cloud cover (<70%), with the exception of February (74%; anomaly +3.7%).

Table 4. Mean monthly values of selected meteorological elements in the third cluster of days with an increased number of cases of aggressive behavior leading to coercive interventions in a psychiatric hospital in Krakow between January 1, 2015 and March 31, 2017

Elements	Jan	Feb	Mar	Apr	May	Jun	Jul	Aug	Sep	Oct	Nov	Dec
Mean monthly values												
Tmax (ºC)	0.9	3.1	8.3	-	-	-	-	-	-	-	3.9	3.9
Tmin (ºC)	-5.6	-3.0	-0.8	-	-	-	-	-	-	-	-2.1	-2.0
Tmean (ºC)	-2.7	-0.4	3.2	-	-	-	-	-	-	-	0.6	0.8
Pressure (hPa)	988.9	991.1	990.3	-	-	-	-	-	-	-	991.8	1000.1
Humidity (%)	81.4	80.3	63.8	-	-	-	-	-	-	-	82.7	82.7
Wind speed (m/s)	1.8	1.8	1.6	-	-	-	-	-	-	-	1.7	2.1
Cloudiness (%)	67.1	74.0	55.6	-	-	-	-	-	-	-	75.8	70.6
SD (hours)	2.2	2.2	6.7	-	-	-	-	-	-	-	2.1	1.9
Mean monthly values of daily differences from 1981-2010 (anomalies)												
Tmax (ºC)	-1.0	-0.7	-0.5	-	-	-	-	-	-	-	-2.2	1.0
Tmin (ºC)	-1.6	0.2	-0.9	-	-	-	-	-	-	-	-2.4	0.5
Tmean (ºC)	-1.4	-0.3	-0.6	-	-	-	-	-	-	-	-2.3	0.8
Pressure (hPa)	-1.4	2.0	3.2	-	-	-	-	-	-	-	3.6	10.4
Humidity (%)	-0.1	0.7	-9.3	-	-	-	-	-	-	-	-3.4	-1.8
Wind speed (m/s)	0.0	0.0	-0.4	-	-	-	-	-	-	-	0.3	0.4
Cloudiness (%)	-5.3	3.7	-12.0	-	-	-	-	-	-	-	-0.1	-4.8
SD (hours)	0.7	0.1	3.6	-	-	-	-	-	-	-	0.9	0.7

-20   -10   0   10   20 anomaly

3.4. Fourth group of days

The last group was that of days occurring from May to September (*Table 5*). There were 64 of them, i.e., 19.5% of all cases. The increased number of coercive interventions was then related to weather which was (*Table 5*):

- hot (Tmax>25 °C), with anomaly of maximum air temperature from 2.4 °C to 7.1 °C,
- with low air humidity (anomaly from -5.9% in September to -13.8% in May),
- very little cloud cover (<42%; anomaly <-18.2%) and long sunshine duration (>9 hours; anomaly >3.8 hours).

The other meteorological elements did not have a major impact on the identification of this cluster.

Table 5. Mean monthly values of selected meteorological elements in the fourth cluster of days with an increased number of cases of aggressive behavior leading to coercive interventions in a psychiatric hospital in Krakow between January 1, 2015 and March 31, 2017

Elements	Jan	Feb	Mar	Apr	May	Jun	Jul	Aug	Sep	Oct	Nov	Dec
Mean monthly values												
Tmax (ºC)	-	-	-	-	22.8	28.2	28.3	27.9	27.5	-	-	-
Tmin (ºC)	-	-	-	-	9.7	14.2	15.6	15.2	13.6	-	-	-
Tmean (ºC)	-	-	-	-	16.1	21.1	21.6	20.7	19.2	-	-	-
Pressure (hPa)	-	-	-	-	984.5	988.3	989.1	992.6	990.9	-	-	-
Humidity (%)	-	-	-	-	57.0	61.4	60.1	65.7	73.2	-	-	-
Wind speed (m/s)	-	-	-	-	1.7	1.8	2.0	1.7	1.3	-	-	-
Cloudiness (%)	-	-	-	-	41.7	42.9	38.5	29.9	21.7	-	-	-
SD (hours)	-	-	-	-	12.2	11.8	11.1	10.4	9.3	-	-	-
Mean monthly values of daily differences from 1981–2010 (anomalies)												
Tmax (ºC)	-	-	-	-	2,4	5,3	3,1	3,3	7,1	-	-	-
Tmin (ºC)	-	-	-	-	0.5	2.0	1.5	1.6	3.3	-	-	-
Tmean (ºC)	-	-	-	-	1.7	4.0	2.5	2.4	4.8	-	-	-
Pressure (hPa)	-	-	-	-	-1.8	0.7	1.3	4.7	2.1	-	-	-
Humidity (%)	-	-	-	-	-13.8	-9.8	-11.3	-9.0	-5.9	-	-	-
Wind speed (m/s)	-	-	-	-	0.0	0.1	0.4	0.4	-0.1	-	-	-
Cloudiness (%)	-	-	-	-	-28.6	-18.2	-18.6	-25.9	-37.7	-	-	-
SD (hours)	-	-	-	-	6.9	5.1	3.8	4.0	4.5	-	-	-

-20   -10   0   10   20 anomaly
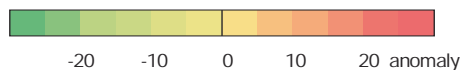
4. Discussion and conclusions

The aim of this study was to determine the weather conditions in days with a higher level of coercion measures in a psychiatric hospital. Studies on the impact of weather conditions on patients' aggressive behaviors are rarely undertaken in research (*Brandl et al.*, 2018). Detailed studies on the influence of the weather on aggressive behaviors and the use of coercive measures have not been often conducted. The relationship between meteorological factors and the intensity of mental health problems has been confirmed by the research of *Settineri et al.*, (2016). According to *Settineri*, the most abrupt weather change in spring and fall cause psychopathological emergencies.

Human behavior is the result of many factors. Some of them, like weather, may additionally burden the psychiatric patients. These include a drop in atmospheric pressure (*Schory et al.,* 2003). The research results suggest, that in some months of the year, an increase in the frequency of aggressive behavior leading to coercive interventions among the patients could be related to meteorological conditions. An increase in the frequency of the analyzed events co-occurred with low atmospheric pressure. *Schory et al.* also noted the impact of low atmospheric pressure on an increased number of psychiatric emergencies and cases of violent behavior (*Schory et al.*, 2003). Low atmospheric pressure may be a risk factor for aggressive behavior, and may be related with the number of coercive measures.

The research also showed the existence of weather patterns related to the number of coerces used. This study found that with lower pressure values, the incidence of aggressive behavior in patients leading to the use of coercive measures increases. For temperature (positive correlation) and relative humidity (negative correlation), there was a poor, but statistically insignificant correlation. Perhaps this should be attributed to the fairly short series of data. By contrast, no relationship was found between intraday and day-to-day changes in pressure and the values of the other individually considered meteorological elements, and there were likewise no seasonal variations in coercion.

A synergic impact of weather can be analyzed, inter alia, on the basis of the synoptic situation prevailing on a given day and in a given area. Information about synoptic situations is communicated by every weather forecast and is available on weather websites. An analysis of medical data with the use of a calendar of circulation types leads to the conclusion that an increase in the frequency of coercive interventions was accompanied by:

- low-pressure systems, and in particular by three types of circulation: cyclonic situations with an advection of air masses from north (Nc) and northwest (NWc) and anticyclonic situations with an advection of air masses from northwest (NWa),

- the passage of various air masses during one day and/or advection of Arctic air masses,

- and the passage of a cold front or several fronts during one day.

The use of cluster analysis made it possible to identify a group of days with weather which accompanied an increased frequency in the occurrence of the analyzed phenomena. Considering the selected meteorological elements, the clearest differentiating factors in the identified clusters were atmospheric pressure and thermal conditions, followed, to a lesser extent, by cloud cover and sunshine duration, while air humidity only had a very poor differentiating effect. Wind speed was irrelevant. An increased frequency in aggressive behavior leading to coercive interventions was accompanied by the following weather types:

- in winter: high temperature (Tmax>10 °C), i.e., days which were not typical for that season of the year, but also days with a smaller cloud cover (daily anomalies <-4%), i.e., extreme weather types in terms of the meteorological conditions typical for that season of the year,

- in spring: days with temperatures within the normal range but quite overcast and humid (anomalies >3%), with the exception of April, where in terms of the thermal conditions the days should be considered cool, and in terms of cloud cover, fairly sunny,

- in summer: cold, overcast, and humid, but also hot days, with low air humidity and little cloud cover, as well as long sunshine duration, i.e., extreme weather types in terms of the meteorological conditions typical for that season of the year,

- in autumn: the least differentiated and difficult in terms of unequivocal determination; however, most frequently warm, dry, and with little cloud cover.

The increase in the frequency of aggressive behaviors ended with the use of mechanical restrains was facilitated by anomalous weather (deviating from the norm), which was not typical for the season of the year. Similar results connected with the influence of temperature were indicated in the studies of *Shiue et al.* (2016). The correlations related mainly to personality disorders, schizophrenia, and sleep disorders. There was no effect of temperature on depression and anxiety disorders. It is consistent with previous research, because in the case of the three first disorders, the personnel have to more likely deal with aggressive behavior.

The results are similar to earlier researches. There were a significant increase in pharmacological coercion during spring and mechanical coercion during summer (*Reitan et al.*, 2018). Schory et al. stated that the greatest number of visits to an emergency psychiatric service occurred in the summer, when inclement weather (as a deviation from the norms) varies from pleasant to hot and was associated with very little precipitation (*Schory et al.*, 2003). Also Finnish

research shows that the prevalence of seclusion and restraint are marked by seasonality (*Kuivalainen et al.*, 2017).

The obtained results are consistent with the CLASH model (climate, aggression, and self control in humans), according to which a cooler climate correlates positively with self-restraint (*Van Lange, et al.*, 2017). Others publications also noted a larger number of emergency room visits by psychiatric patients on especially hot days (*Wang* and *Chen*, 2013; *Hansen et al.*, 2008) and on warm and humid ones (Vida et al., 2012), while a smaller number of such patients were treated on rainy days (*Santiago et al.*, 2005). Weather with lower temperatures, low humidity, and low atmospheric pressure correlated with the occurrence of non-fatal violence and psychiatric admissions, but not with suicide or homicide (*Talaei et al.*, 2014).

The study seems to have clinical applications. The knowledge about correlations between meteorological conditions, especially atmospheric pressure, may increase personnel awareness of the risk factors for aggressive behavior. It might influence more effective prevention of such incidents. The research allows us to determine meteorological risk factors, which are: high temperature, low air pressure, and generally – the occurrence of unusual weather in some seasons of the year.

Knowledge of the weather patterns occurring in certain months of the year would allow better preparation in the sense of the number of personnel on duty during shifts for a specific period of the year. This might be logistically difficult, however, an awareness of the risks allows for better preparation in the prevention of aggressive behavior.

The study limitations may lie in the differences between climatic and meteorological conditions in various areas of the globe as the results relate to the temperate zone of Central Europe. Specifying the patterns for other regions of the world requires additional research. The influence of atmospheric factors on the human body is universal, but an indication for future research would be the creation of similar patterns for those meteorological factors impacting on patients in other climatic zones. Earlier research has focused most often on one selected area of the globe (*Shiue et al.*, 2016). Research extension could also involve a more precise analysis of the impact of weather changes depending on the time of day. Meteorological factors can have different impacts at different periods of the day, a more frequent use of coercive measures during the day than at night may be involved.

However, it needs to be emphasized that the results presented here are an attempt at a statistical processing of the correlations. Weather may lead to an increased frequency of certain behavior types exhibited by patients and staff members but, certainly, it is not the only or the decisive cause of aggression by patients who had to be subjected to coercive interventions. However, taking preventive measures should be considered in psychiatric hospitals on days when the weather is not typical for a particular season of the year and is additionally accompanied by low atmospheric pressure systems. Such weather may have an

irritating impact and may contribute to an increased likelihood of the occurrence of aggressive behavior in patients.

References

Almendra, R., Loureiro, A., Silva, G., Vasconcelos, J., and *Santana, P.* 2019: Short-term impacts of air temperature on hospitalizations for mental disorders in Lisbon. *Scie. Total Environ. 647*, 127–133. https://doi.org/10.1016/j.scitotenv.2018.07.337

Belleville, G., Foldes-Busque, G., Dixon, M., Marquis-Pelletier, É., Barbeau, S., Poitras, J., … Marchand, A. 2013: Impact of seasonal and lunar cycles on psychological symptoms in the ED: an empirical investigation of widely spread beliefs. *Gen. Hospit. Psych. 35*, 192–194. https://doi.org/10.1016/j.genhosppsych.2012.10.002

Brandl, E. J., Lett, T. A., Bakanidze, G., Heinz, A., Bermpohl, F., and *Schouler-Ocak, M.* 2018: Weather conditions influence the number of psychiatric emergency room patients. *Int. J. Biometeorol. 62*, 843–850. https://doi.org/10.1007/s00484-017-1485-z

Chambers, M., Kantaris, X., Guise, V., and *Välimäki, M.* 2015: Managing and caring for distressed and disturbed service users: the thoughts and feelings experienced by a sample of English mental health nurses. *J. Psych. Mental Health Nurs. 22*, 289–297. https://doi.org/10.1111/jpm.12199

Dominiak, M., Swiecicki, L., and *Rybakowski, J.* 2015: Psychiatric hospitalizations for affective disorders in Warsaw, Poland: Effect of season and intensity of sunlight. *Psychiatry Research*, *229*(1), 287–294. https://doi.org/10.1016/j.psychres.2015.07.011

Hansen, A., Bi, P., Nitschke, M., Ryan, P., Pisaniello, D., and *Tucker, G.* 2008: The Effect of Heat Waves on Mental Health in a Temperate Australian City. *Environ. Health Perspec. 116*, 1369–1375. https://doi.org/10.1289/ehp.11339

Kuivalainen, S., Vehviläinen-Julkunen, K., Louheranta, O., Putkonen, A., Repo-Tiihonen, E., and *Tiihonen, J.* 2017: Seasonal variation of hospital violence, seclusion and restraint in a forensic psychiatric hospital. *Int. J. Law Psych. 52*, 1–6. https://doi.org/10.1016/j.ijlp.2017.05.004

Manning, C., and *Clayton, S.* 2018: Threats to mental health and wellbeing associated with climate change. In Psychology and Climate Change (pp. 217–244). https://doi.org/10.1016/B978-0-12-813130-5.00009-6

McWilliams, S., Kinsella, A., and *O'Callaghan, E.* 2014: Daily weather variables and affective disorder admissions to psychiatric hospitals. *Int. J. Biometeorol. 58*, 2045–2057. https://doi.org/10.1007/s00484-014-0805-9

Nastos, P.T., Bleta, A.G., and *Matsangouras, I.T.,* 2017: Human thermal perception related to Föhn winds due to Saharan dust outbreaks in Crete Island, Greece. *Theor. Appl. Climatol. 128*, 635–647. https://doi.org/10.1007/s00704-015-1724-3

Peluola, A., Mela, M., and *Adelugba, O. O.* 2013: A review of violent incidents in a multilevel secure forensic psychiatric hospital: is there a seasonal variation? *Medic. Sci. Law 53*, 72–79. https://doi.org/10.1258/msl.2012.012016

Niedźwiedź, T. 2020. Calendar of circulation types for territory of Southern Poland. http://www.kk.wnoz.us.edu.pl/nauka/kalendarz-typow-cyrkulacji/ [accessed 15 September 2020].

Reitan, S. K., Helvik, A.-S., and *Iversen, V.* 2018: Use of mechanical and pharmacological restraint over an eight-year period and its relation to clinical factors. *Nordic J.Psych. 72*, 24–30. https://doi.org/10.1080/08039488.2017.1373854

Santiago, P.N., McLay, R.N., and *Hammer, P.S.,* 2005: Meteorologic Factors in Emergency Evaluation, Admission, and Discharge. *Psych. Serv. 56*, 1625–1625. https://doi.org/10.1176/appi.ps.56.12.1625

Schory, T.J., Piecznski, N., Nair, S., and El-Mallakh, R.S., 2003: Barometric Pressure, Emergency Psychiatric Visits, and Violent Acts. *The Canadian J. Psych- 48*, 624–627. https://doi.org/10.1177/070674370304800909

Settineri, S., Mucciardi, M., Leonardi, V., Schlesinger, S., Gioffrè Florio, M., Famà, F., ... Mento, C. 2016: Metereological conditions and psychiatric emergency visits in Messina, Italy. *Int. J. Psycholog. Res. 9*, 72. https://doi.org/10.21500/20112084.2103

Shiloh, R., Shapira, A., Potchter, O., Hermesh, H., Popper, M., and Weizman, A. 2005: Effects of climate on admission rates of schizophrenia patients to psychiatric hospitals. *Eur. Psych. 20*, 61–64. https://doi.org/10.1016/j.eurpsyhttps://doi.org/10.1016/j.eurpsy.2004.09.0200

Shiue, I., Perkins, D.R., and Bearman, N., 2016: Physically equivalent temperature and mental and behavioral disorders in Germany in 2009–2011. *J. Mental Health 25*, 148–153. https://doi.org/10.3109/09638237.2015.1101431

Talaei, A., Hedjazi, A., Rezaei Ardani, A., Fayyazi Bordbar, M. R., and Talaei, A., 2014: The Relationship between Meteorological Conditions and Homicide, Suicide, Rage, and Psychiatric Hospitalization. *J. Forensic Sci. 59*, 1397–1402. https://doi.org/10.1111/1556-4029.12471

Van Lange, P. A.M., Rinderu, M.I., and Bushman, B.J., 2017: Aggression and violence around the world: A model of CLimate, Aggression, and Self-control in Humans (CLASH). *Behav. Brain Sci. 40*, e75. https://doi.org/10.1017/S0140525X16000406

Vida, S., Durocher, M., Ouarda, T.B.M.J., and Gosselin, P. 2012: Relationship Between Ambient Temperature and Humidity and Visits to Mental Health Emergency Departments in Québec. *Psych. Serv. 63*, 1150–1153. https://doi.org/10.1176/appi.ps.201100485

Wang, B., and Chen, D. 2013: Evidence for seasonal mania: a review. *J. Psychiatr Pract, 19*, 301–308. https://doi.org/10.1097/01.pra.0000432600.32384.c5

Weizmann-Henelius, G. 2000: Violence in a Finnish forensic psychiatric hospital. *Nordic J. Psych. 54*, 269–273. https://doi.org/10.1080/080394800448147

Yackerson, N.S., Zilberman, A., Todder, D., and Kaplan, Z. 2014: The influence of air-suspended particulate concentration on the incidence of suicide attempts and exacerbation of schizophrenia. *Int. J. Biometeorol. 58*, 61–67. https://doi.org/10.1007/s00484-012-0624-9

IDŐJÁRÁS

Spatiotemporal distribution of the climatological fronts over Europe in the modern climate period

Inna Semenova[1],* and **Katsiaryna Sumak**[2]

[1] *Odessa State Environmental University*
Department of Military Training
15 Lvivska Str., 65016, Odessa, Ukraine

[2] *Republican center for hydrometeorology,*
control of radioactive contamination
and environmental monitoring (BELHYDROMET)
Department of Meteorological forecasts
110, Nezavisimosti ave, 220114, Minsk, Belarus

*Corresponding author E-mail: in_home@ukr.net

Abstract— The geographical position of the Arctic front and two branches of the Polar front over Europe was determined during the period 1995–2015 using calculated grid fields of the thermal frontal parameter in the troposphere layer of 850–700 hPa. It was revealed that the geographical position of climatological fronts changed both in the cold and warm periods of the year in comparison with climate data. The most recent standard reference period of 1961–1990 recommended by WMO (*WMO*, 2017) was used for comparison. It is shown that in January there was a shift of the northern and southern branches of the Polar front to the north compared to the reference climate period, and in July the convergence of both branches of the Polar front in the middle latitudes was observed. The Arctic front was characterized by a northern location compared to the climate in both January and July. It is revealed that the main areas of frontogenesis in the cold period of the year were the sea surface, namely, the southern regions of the Norwegian Sea, the central part of the Baltic Sea, and the western half of the Mediterranean Sea. In the summer, more active atmospheric fronts were over the continent in the area of the mountain systems such as the south of the Scandinavian mountains, the north of the Alps and Pyrenees, the Urals, and the lower Volga region. The Arctic front intensified over the Barents and Norwegian Seas in all seasons of the year.

Key-words: thermal front parameter, climatological fronts, frontal zones, Polar front, Arctic front, temperature gradients

1. Introduction

The atmospheric front is one of the most complex objects in the atmosphere, which carries important weather-forming and climatic functions. Therefore, the use of methods that allow simulating the complex structure of the front in order to determine its position in space and time is an actual and not completely solved problem.

Objective identification of fronts usually requires 5 subjective choices (*Thomas* and *Schultz*, 2019): 1) a thermodynamic quantity (e.g., potential temperature, equivalent potential temperature, wind); 2) a mathematical function that operates the value to create a field for identifying the front (e.g., gradient, thermal frontal parameter, frontogenesis); 3) a level or layer where the analysis is performed (e.g., surface, 850 hPa, between 850 and 700 hPa); 4) a minimum threshold or tolerance of the field value for the feature that will be considered a front (e.g., value of the horizontal gradient of a potential temperature exceeding 8K (100 km)$^{-1}$); 5) an algorithm that allows to draw the front line or identify an area that represents the frontal zone in a field with a specified threshold, and classify the front as warm or cold.

The most common quantitative characteristics of atmospheric fronts are front parameters, which functionally link meteorological values and describe their behavior in the frontal zone, which allows setting some limit criteria specific to the fronts.

As a quantitative characteristic of atmospheric baroclinicity, the front parameter Ψ was proposed by *Huber-Pock* and *Kress* (1989), which is a horizontal gradient of the gradient modulus of the equivalent thickness of the *ZTE* (zero thermal expansion) layer enclosed between isobaric surfaces of 925-700 or 850-500 hPa:

$$\Psi = \nabla |\nabla \text{ZTE}| \cdot \vec{n}_{\text{ZTE}}, \tag{1}$$

where $\vec{n}_{\text{ZTE}}$ is a unit vector (normal to the *ZTE* contour line) directed to the area of minimum temperature and humidity values.

The equivalent layer thickness is a function of temperature and humidity on the corresponding isobaric surfaces and, therefore, it is a complex characteristic of air masses:

$$ZTE = -\sum_{Pl}^{Pu} \frac{R}{g} \, \overline{T}_e ln\left(\frac{P_u}{P_l}\right), \tag{2}$$

where R is the specific gas constant, g is the acceleration of gravity, u and l are the upper and lower isobaric surfaces, respectively. $\overline{T}_e$ is the function of the equivalent layer thickness bounded by isobaric surfaces P_u and P_l:

$$\overline{T}_e = T + \frac{Lq}{C_p}, \quad, \tag{3}$$

where q is the specific humidity, T is the air temperature, L is the specific heat of vaporization, and C_p is the specific heat capacity at constant pressure.

Taking into account the constant values $L = 2.5104$ J·kg^{-1} and $C_p = 1004.64$ J·kg^{-1}·K^{-1}, Eq.(3) takes the form for calculating the equivalent temperature:

$$T_e \cong T + 2.5q, \tag{4}$$

where q is expressed in g·kg^{-1}.

A new approach for expressing the front parameter Ψ was proposed in the studies of Russian scientists (*Shakina et al.,* 1998a,b). Due to the fact that the measure of atmospheric baroclinicity is the number of isobar-isosteric solenoids, which is associated with the horizontal gradient of the layer thickness, the areas where the baroclinicity gradient has a maximum in the direction of the layer thickness gradient should be defined as frontal zones. As a result, the formula for calculating the front parameter Ψ takes the form:

$$\Psi_{ZTE} = \nabla|\nabla \, ZTE| \cdot \vec{n}_{ZTE}. \tag{5}$$

Since the front line near the ground is located on the warm side of the zone of maximum gradients, it follows from Eq.(5) that only positive Ψ_{ZTE} values can be associated with the front. In order to take into account humidity in the zone of atmospheric fronts *Shakina et al.* (1998b) considered the humidity index, which is expressed by the ratio:

$$HIX = \frac{\nabla ZTE - \nabla ZT}{\nabla ZTES - \nabla ZT}, \tag{6}$$

where the *ZTES – ZTE* function is calculated for saturated air, *ZT* is an analogue of the *ZTE* function calculated by normal temperature.

The humidity index *HIX* allows identifying zones of atmospheric fronts, where cloud cover and precipitation are observed.

Further, *Shakina et al.* (2000) introduced a dimensionless front parameter *F*, which is a linear combination of cycloniticity and barocliniticy:

$$F = P + \Psi, \tag{7}$$

where parameter P is a characteristic of cyclonicity and baroclinicity of the lower troposphere (925–850 hPa), and Ψ is the characteristics of baroclinicity in layers 850–500 hPa or 925–700 hPa.

One of the most commonly used parameters in meteorological practice is the thermal front parameter (*TFP*), which is a quantitative characteristic that takes into account the distribution of temperature gradients (*Creswick*, 1967; *Hewson*, 1998; *Serreze et al.,* 2001).

The thermal front parameter reflects the basic definition of the atmospheric front, namely, on the cold front the temperature begins to decrease, and on the warm front its rise stops. The temperature for calculating the *TFP* can be taken at any level, or calculated in a certain layer of the atmosphere, which allows taking into account the three-dimensionality of the frontal zones. The equivalent temperature T_e is calculated instead of the usual temperature in order to take into account the moisture content. The position of the front line is determined through the zone with the maximum positive values of *TFP* (*Berry et al.,* 2011a; *Hewson,* 1998).

Using the average monthly temperature fields for calculating *TFP* allows identifying baroclinic zones that correspond to the main climatological fronts (*Semenova,* 2010). Moreover, the daily *TFP* fields taking into account humidity can be used to clarify the structure and position of the frontal systems in extratropical cyclones (*Semenova* and *Ivus*, 2011).

The *TFP* fields are in a good agreement with the cloud zones in satellite images: the bright areas of frontal clouds in the images correspond to the areas of positive *TFP* values. It is shown that the calculated *TFP* fields occupy a certain position relative to the cloud band of the cold front, and these positions remain constant for the next 12 h in most cases, which confirms the need to use numerical *TFP* calculations in operational practice (*Zwatz-Meise* and *Hufnagl*, 1990).

The method described by *Hewson* (1998) allows calculating several functions from thermodynamic variables to horizontal winds on isobaric surfaces at grid points, which makes it possible not only to identify fronts numerically, but also to determine their type. The same technique was applied in a study by *Berry et al.* (2011a), which allowed the authors to calculate objective global front climatology using ERA-40 reanalysis data with a spatial resolution of 2.5°×2.5° for the period 1958–2001. The wet bulb potential temperature fields (Θ_w) at the level of 850 hPa were used to calculate the *TFP*. It was found that in the Northern Hemisphere, the maximum frontal frequency is typical for the North Atlantic and Pacific Oceans, and the highest values are typical for the western parts of these basins. The direction of the fronts here is from southwest to northeast, which is consistent with the trajectories of extratropical cyclones.

The same authors (*Berry et al.,* 2011b) expanded their previous research by using four reanalysis datasets such as Era-Interim, NCEP 2, JRA, and MERRA, for studying global trends in objective atmospheric fronts for the period 1989–2009. There was a decrease in the average annual frequency of fronts (by 10–20%) between 30 and 50°N, from the USA to Central Europe. Towards the pole, a local increase was observed near Iceland. In the North Atlantic region, fronts have become less common.

A comparative analysis of two methods of objective identification of fronts in the lower troposphere for different synoptic situations was performed by *Schemm et al.,* 2015. The first method is thermal, based on a gradient of equivalent potential temperature at the level of 850 hPa, the second is based on temporary wind changes at the level of 10 m. It was found that the thermal method allows identifying both cold and warm fronts and quasi-stationary ones, especially in strong baroclinic situations, which include classical extratropical systems of low pressure. The second method is most appropriate for identifying fronts in weak baroclinic synoptic situations, when the frontal systems are induced by strong wind shear and convergence between two anticyclones. The authors also obtained the climatology of fronts for the winter and summer seasons of both hemispheres for the period 1979–2012 according to the Era-Interim reanalysis. The highest frequency of fronts in the Northern Hemisphere in winter was identified in the two main cyclonic regions of the North Atlantic and the Pacific Oceans. Almost complete absence of fronts prevailed over the continental part (Eurasia). In the summer, the maximum of frontal activity shifted northward with a noticeable decrease in frequency. There is an increase in cyclonic activity, especially over the Great Lakes and Hudson Bay, as well as in Western Europe. The orientation of the fronts identified by the thermal method has a more zonal component than the wind one (more meridional orientation of fronts).

Thomas and *Schultz* (2019) also used gradients of equivalent potential temperature and the wind field to determine the fronts and their location at the surface and 850 hPa during the period 1979–2016. The threshold of 2.0 K $(100 \text{ km})^{-1}$ was chosen as minimum, because it most closely corresponds to the surface analysis of DWD (Deutscher Wetterdienst). It was found that the regions with the highest *TFP* frequency exceeding the threshold value are located near mountain ranges, as well as in lower latitudes, especially over the tropical Eastern Pacific and the Indian Oceans. The *TFP* can not only represent fronts at mid-latitudes, but also represent air mass boundaries from the subtropics, which are largely the result of humidity gradients. Proof of the importance of taking humidity into account in *TFP* calculations is that the mathematical expression for *TFP* includes higher derivatives, and humidity contains much greater variability than temperature, especially in wetter low latitudes. As a result of global averaging, it is revealed that the fronts at the surface are more intense than at the level of 850 hPa. About 10% of the most intense fronts near the surface are more common over land than over the oceans.

The study of *Bitsa et al.* (2019) developed a scheme for identifying cold frontal systems in the Mediterranean basin based on the Frontal Tracking Scheme (FTS), which were developed in the University of Melbourne, Australia. This modified scheme takes into account the particular characteristics of the Mediterranean fronts and includes two criteria – total wind direction change and total wind magnitude for the better identifying of the positions and tilt of a Mediterranean cold front. Thermodynamic criteria were not included in this

scheme, meaning that wind shear is a prerequisite for the transition of the baroclinic zone to an organized cold front in the Mediterranean Sea. A good agreement was obtained between the objective cold fronts and the frequency of the fronts detected as a result of synoptic analysis over Greece.

Catto et al. (2014) estimated future changes (period of 2080–2100) in the frequency of atmospheric fronts using the high emission scenario RCP 8.5. Forecasts showed a decrease in frequency in the Northern Hemisphere, with a shift to the pole of maxima, and a significant decrease in high latitudes, where the temperature gradient decreases. Changes in the frequency of fronts in the future will be strongly associated with changes in the trajectories of cyclones, and these changes are not so clear due to the uncertainty of "their response" to climate warming.

The aim of this study is to determine the spatial and temporal distribution of the climatological frontal zones over Europe in the period of 1995–2015 using the thermal front parameter.

2. Materials and methods

The method of objective analysis of the climatological frontal zones was applied using the calculated grid fields of the thermal front parameter over the European sector, in restricted area 13°W – 62°E and 35–80°N, using the formula (*Creswick*, 1967; *Hewson,* 1998; *Serreze et al.,* 2001):

$$\text{TFP} = -\nabla |\nabla \text{T}| \frac{\nabla \text{T}}{|\nabla \text{T}|}, \tag{8}$$

where $\nabla = \vec{\imath}\, \frac{\partial}{\partial x} + \vec{\jmath}\, \frac{\partial}{\partial y}$ and $|\nabla \text{T}| = \sqrt{\left(\frac{\partial \text{T}}{\partial x}\right)^2 + \left(\frac{\partial \text{T}}{\partial y}\right)^2}$ is the module of temperature gradient.

The initial data for calculating the *TFP* were the daily temperature fields T (K) and specific humidity q (kg·kg^{-1}) at the 850 and 700 hPa pressure levels of the Era-Interim reanalysis data with a spatial resolution of 1.5°×1.5° (*ERA Interim, Daily datasets,* 2019).

Eq.(8) includes the equivalent temperature T_e averaged in the layer 850–700 hPa, determined by the formula:

$$\text{T}_{e\,(850\text{-}700)} \cong \text{T}_{850\text{-}700} + 2.5 q_{850\text{-}700}, \tag{9}$$

where q (specific humidity) is expressed in g·kg^{-1}.

As the calculated *TFP* fields have the order of magnitude of $10\text{–}11^{-2}\,\text{K·m}^{-2}$, in further analysis, we will operate with *TFP* units (without specifying the exponent).

To determine the average monthly position of the frontal zones, the frequency of positive *TFP* values in each point of the calculated grid and the average intensity of the front were analyzed. The latitudinal zone, within which the total number of points with positive values at each latitude was the largest with the simultaneous highest average value of the *TFP*, was taken as the position of the front. At the same time, information on the climatic position of the axes of altitudinal frontal zones was also taken into account (*Vorobyov*, 1991).

This article presents the results of an objective analysis of climatological fronts for the central months of the seasons and averaged by seasons.

3. Results and discussions

3.1. Geographical position of the frontal zones

The latitudinal zones defined by the described method, as well as the latitudes with maximum parameters that correspond to the average position of the climatological fronts (Arctic front, northern branch of the Polar front (further - NPF), southern branch of the Polar front (further - SPF)) for the central months of the seasons of the studied period are shown in *Table 1* and specified as 'fact'. Information on the position of climatological fronts was available only in January and July (*Khromov* and *Petrosyants*, 2006) for the reference climate period 1961–1990 (*WMO*, 2017) and provided as 'climate' in this table for comparison for the respective months. For April and October, a comparison of the geographical position of the fronts was performed only in comparison with the previous season within the study period.

Table 1. Geographical latitudes of the position of the frontal zones (°N) for the period 1995-2015 (fact) and according to climate data (climate)

Month	NPF		The interval of latitudes (fact)	SPF		The interval of latitudes	Arctic		The interval of latitudes (fact)
	fact	climate		fact	climate		fact	climate	
January	59.0	56.0	57.5-59.0	42.5	39.3	41.0-44.0	72.5	68.3	69.5-74.0
April	60.5	-	59.0-60.5	51.5	-	50.0-53.0	75.5	-	74.0-75.5
July	62.0	64.2	60.5-66.5	51.5	47.9	48.5-53.0	77.0	73.0	75.5-77.0
October	62.0	-	62.0-65.0	42.5	-	41.0-44.0	69.5	-	69.5-72.5

As seen, the position of the northern and southern branches of the Polar front in winter (January) has changed compared to the climate data, namely, there was a shift to the north by three degrees of latitude of both branches. In the summer

period (July), the northern branch, on the contrary, occupies a more southerly position compared to the previous period, and the southern branch has shifted to the north by more than three degrees of latitude. In the spring (April), the northern branch occupies an intermediate position between the winter and summer periods, while the southern branch is characterized by the greatest shift to the north (by 9 degrees of latitude) in comparison with the winter period, and thus, its position in April and July is identical. In the autumn (October), the northern branch did not change its position relative to the summer location, while the southern branch shifted south by almost 11 degrees of latitude.

The position of the Arctic front in the cold and warm periods of the year also changed in comparison with the previous climate period: it shifted to the north by four degrees of latitude. In April, there was a significant shift of the front to the northern latitudes in comparison with the cold period of the year, and in October, the Arctic front occupies its highest position among the considered months at longitude 69.5°N.

3.2. Spatiotemporal dynamics of frontal zones

The spatiotemporal cross sections of *TFP* fields were constructed as the Hovmöller diagrams for the identified latitudes corresponded to location of main climatological fronts, to determine the time dynamics of the intensity of the frontal zones during the study period.

In *Figs. 1–4*, the distribution of the thermal front parameter at fixed latitudes (which correspond to the described climatological fronts) for central months of the seasons is shown. At all latitudes, areas can be seen with longitudes and time intervals where the fronts are well expressed in the *TFP* fields.

January. The Arctic front is most pronounced over the areas of the Barents Sea and the eastern part of the Norwegian Sea (11–35°E). However, the position of the maximum *TFP* changes over the years (*Fig.1a*). Thus, the most intense section of the front was located in the longitude range of 11–19°E in 1997, 1999, and in the period 2002–2007, and over the central regions of the Barents Sea – from 2005 to 2009. At the beginning of the study period (1995–1996), the front also intensified (up to 3–5 TFP units) in the area of the Jan Mayen Island, which is located to east of Greenland. In the last five-year period, the Arctic front was weakly expressed over the entire longitude interval.

Fig. 1b shows that the northern branch of the Polar front (NPF) in January is the most intense over the southern regions of the Norwegian Sea (13° W-5°E), however, in different years, the position of the maximum *TFP* (up to 3–4 units) in this area changes. Thus, the highest intensity of this section of the front was observed in 1996–1997, 2001–2002, and 2006, as well as in the western part of the region in 2009 and in the eastern part in 2014. Further to the east, the intensity of the NPF decreases significantly, but it is possible to distinguish periods when the front intensified. The front's intensification (up to 1–2 TFP units) occurred at

longitudes of 20–33°E, i.e., over the areas of the central part of the Baltic Sea and the Gulf of Finland in the period from 1996 to 1998, as well as in 2006, 2008, and 2011–2012. The front was most intense in the Volga and Ural regions in 1998, 2001, 2003-2004, and 2012–2013. In general, it should be noted that over the sea surface no significant changes in the intensity of NPF were observed during the study period, and over the continental part the front was weaker than over the sea in almost all years.

The distribution of *TFP* at the latitude of the southern branch of the Polar front (SPF) is complex due to the alternation of sea and continental surfaces over longitudes (*Fig. 1c*). In almost all years, the front is well defined from 13°W to 19°E, which corresponds to the area of the Atlantic and the adjacent western half of the Mediterranean Seas. The most intense SPF in this region was in the periods from 2000 to 2006 and from 2009 to 2015, as well as in 1995, when the maximum *TFP* reached 2–3 units of *TFP*.

Further to the east, in the interval of longitude 28–44°E, i.e., over the mountainous areas of the northern part of the Peninsula of Asia Minor and the Lesser Caucasus, the front also intensified from 1995 to 1999 and in the period 2002–2015, and the maximum *TFP* also reached 2–3 units of *TFP*. Thus, in January, during the study period, there was an increase in the intensity of SPF in almost the entire region.
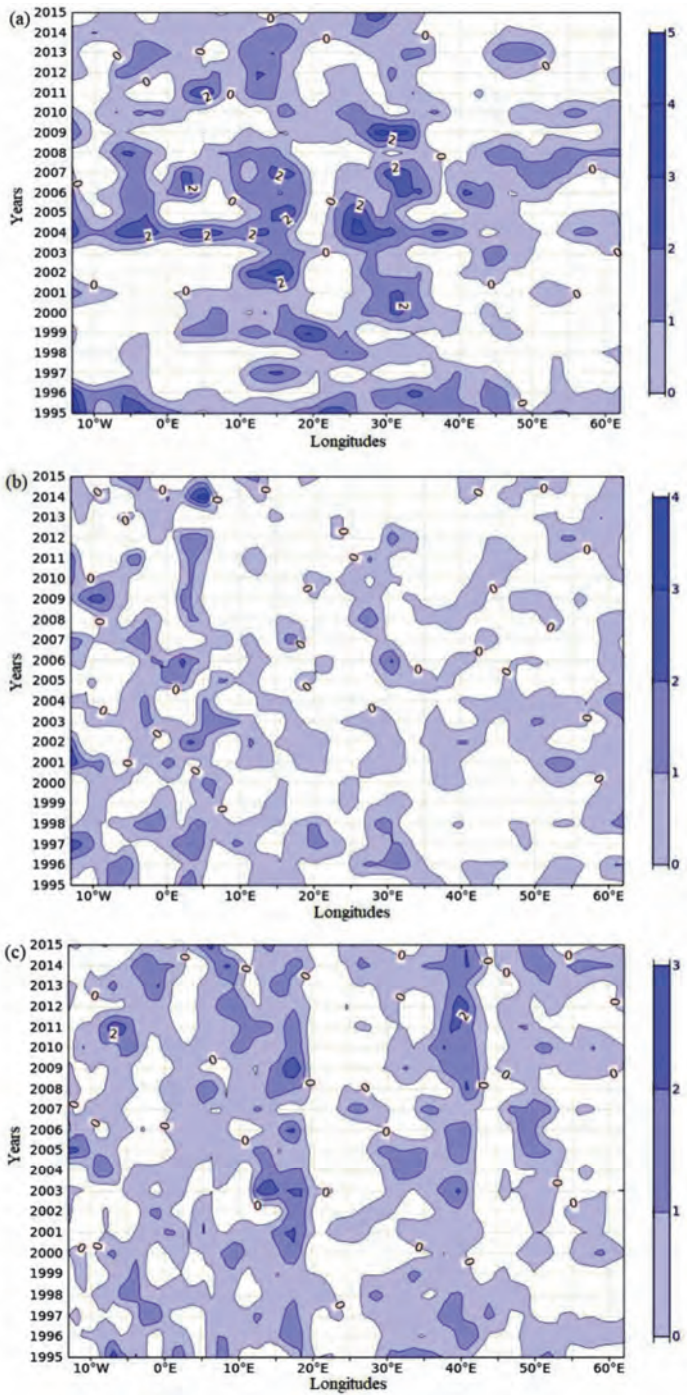
Fig. 1. Spatiotemporal distribution of *TFP* in January 1995–2015 at latitudes: a) 72.5°N (Arctic front); b) 59°N (NPF); c) 42.5°N (SPF).

April. The Arctic front is most intense over the northern areas of the Norwegian Sea (13°W-8°E), but in different years the position of the maximum *TFP* (up to 4–5 units of *TFP*) in this area changes. Thus, the highest intensity of this section of the front was observed from 2002 to 2006, as well as in 2015 in the western part of the region, and in 2011 in the eastern part. In 2002–2004 and 2006, the Arctic front was well defined not only over the Norwegian Sea, but also over the Barents Sea (20–45°E). The Arctic front also intensified over the western part of the Barents Sea in 2011. As it can be seen from *Fig. 2a*, in general, the Arctic front is weakly expressed, and its intensity in some areas decreases from west to east.

The distribution of *TFP* at the latitude of the northern branch of the Polar front is complex due to the predominance of the continental surface along this latitude (*Fig. 2b*). In almost all years, the NPF front section is well defined in the longitude range from 13°W to 10°E, which corresponds to the southern part of the Norwegian Sea and the south of the Scandinavian Peninsula. In this area, the front was most intense in 1999–2000, 2003–2004, and 2007–2011, when *TFP* values reached 3 units. Further to the east, the intensity of the NPF generally decreases, but it is possible to distinguish periods when the front intensified. In the period 1995–2001, the intensification of the front (up to 3–4 *TFP* units) occurred at longitudes 22–33°E, i.e., over the areas of the central part of the Baltic Sea. From 1999 to 2002, the most intense section of the NFP (3–4 *TFP* units) was located within 41–56°E, above the continental surface of the Non-Black Earth Region of Russia, and this section of the front was shifted even further to the east in 2005. In general, it should be noted that over the continental surface, there was a decrease in the intensity of NPF during the study period, while in the west, over the sea surface, no significant changes were observed.

The SPF in April was more intense over the continental surface, at longitudes 5–38°E. The position of the maximum *TFP* (up to 2–3 units of *TFP*) changes at different times. Thus, in the period 1999–2001, the front intensified over the central regions of Eastern Europe and the Black Earth Region of Russia, and from 2005 to 2009, the most intense section of the front passed over Central Europe (2–3 *TFP* units). At the end of the study period (2012–2015), the intensification of the front was observed at longitudes 8–15°E, 32–35°E, and the most intense section (up to 4 *TFP* units) was located over the Southern Urals (54–62°E). In general, as it can be seen from *Fig. 2c*, the southern branch of the Polar front in April is weakly expressed, especially over the sea surface.
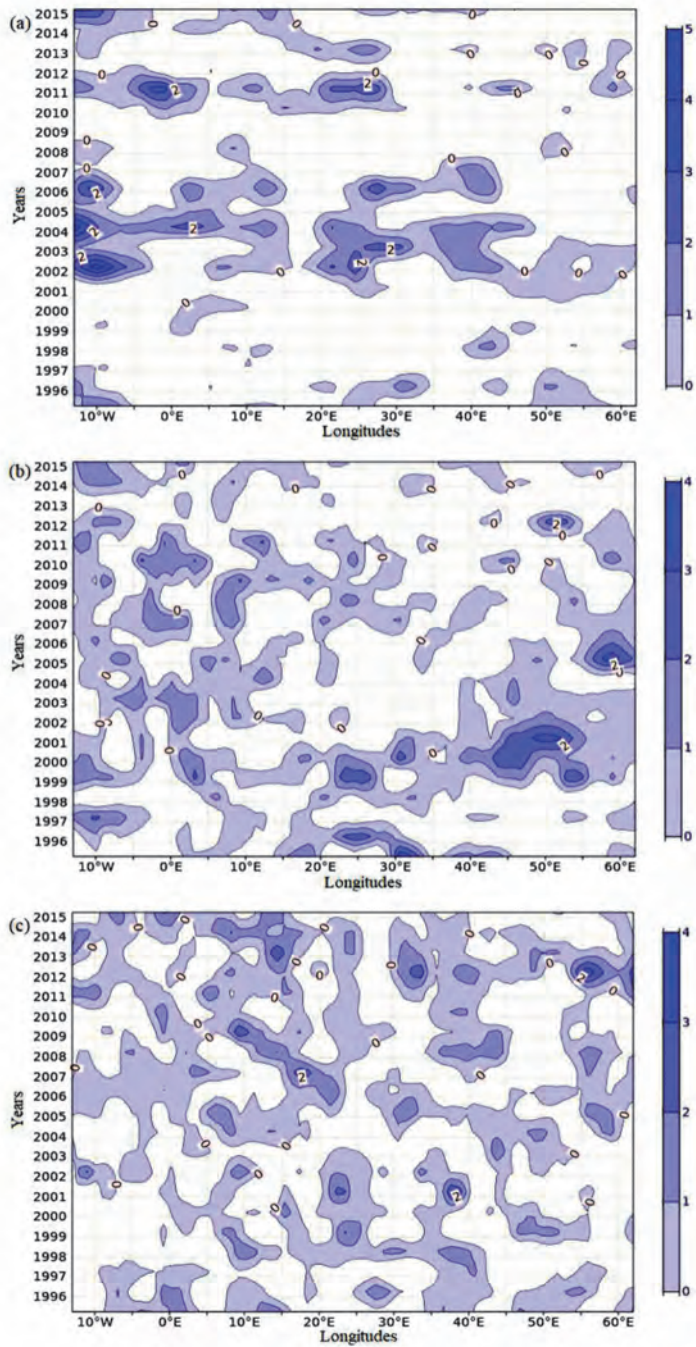
Fig. 2. Spatiotemporal distribution of *TFP* in April 1995–2015 at latitudes: a) 75.5°N (Arctic front); b) 60.5°N (NPF); c) 51.5°N (SPF).

July. In summer, the Arctic front is the most intense (up to 3–5 *TFP* units) in almost all years over the areas of Svalbard Island and the northwestern part of the Barents Sea (15–40°E), and only in the last five-year period this section of the front was weakly expressed. The highest intensity of the front (up to 2–3 units of *TFP*) over the northern part of the Greenland Sea was observed from 1995 to 1997, as well as from 2001 to 2007 and in 2011. In the eastern part of the study region at longitudes 45–62°E, the front intensified from 1997 to 2002, in 2005–2008 and 2012–2015. In general, as it can be seen from *Fig. 3a*, in July the Arctic front was well expressed in certain sections along the longitudes, and no significant changes in its intensity were observed during the study period.

The NPF branch in summer is most intense over the southern regions of the Scandinavian mountains (6–12°E), here in almost all years the maximum TFP reached 6–7 *TFP* units (*Fig. 3b*). Over the sea surfaces, i.e., over the southern part of the Norwegian Sea (13°W-5°E) and the central part of the Baltic Sea (18–22°E), the front is less intense. Further to the east, over the continental surface, in general, the intensity of NPF is low, but it is possible to distinguish periods of the highest intensification of the front. Thus, from 1999 to 2001, the front intensified (up to 6–7 TFP units) at longitudes of 35–60°E, i.e., over the northeast of the European part of Russia, the Volga region, and the Middle Urals. In 2010–2013, this was also the most intensive section of the NPF (3–6 *TFP* units).

As in winter, the SPF branch is well expressed at almost all longitudes (*Fig. 3 c*). The front was most intense (up to 3–5 TFP units) in 2006 and 2015 within 6–14°E, which refers to the region of Western Europe, as well as from 27 to 36°E, i.e., over the central part of Eastern Europe and the Black Earth of Russia in 1999 and 2007. Over the Atlantic (13–9°W), the front intensified from 2010 to 2014, when the values of the *TFP* reached 3 units. In the eastern part of the region (44 – 62°E), the front was most intense (up to 2–3 *TFP* units) in 1997, 2000, 2005, and 2010. In general, there were no trends in changes in the intensity of SPF in summer during the study period.

October. As it can be seen from *Fig. 4a*, in general, the Arctic front is relatively weak, but it is possible to distinguish periods and areas when the front was intensified. Thus, over the northwestern part of the Norwegian Sea (13°W - 0°), the front was well-defined (up to 4–5 *TFP* units) in 2002 and 2005. Over the northern part of the Scandinavian Peninsula, the highest intensity of the front (up to 2–4 *TFP* units) was observed in 2005, 2011, and 2013. Further to the east, over the southern part of the Barents Sea (35–62°E), the intensity of the Arctic front decreases sharply. It can be noted that no changes in the intensity of the Arctic front were detected during the study period.

The northern branch of the Polar front in October occupies the same position as in July (62°N, see *Table 1*), but it has become less intense. From 1995 to 2007, the front is expressed in almost all longitudes. The most intense areas were located over the sea surfaces during this period: over the southern regions of the Norwegian Sea (13°W – 0°), when the maximum *TFP* reached 3–5 units, as well as over the central part of the Baltic Sea and the Gulf of Finland (18–27°E).
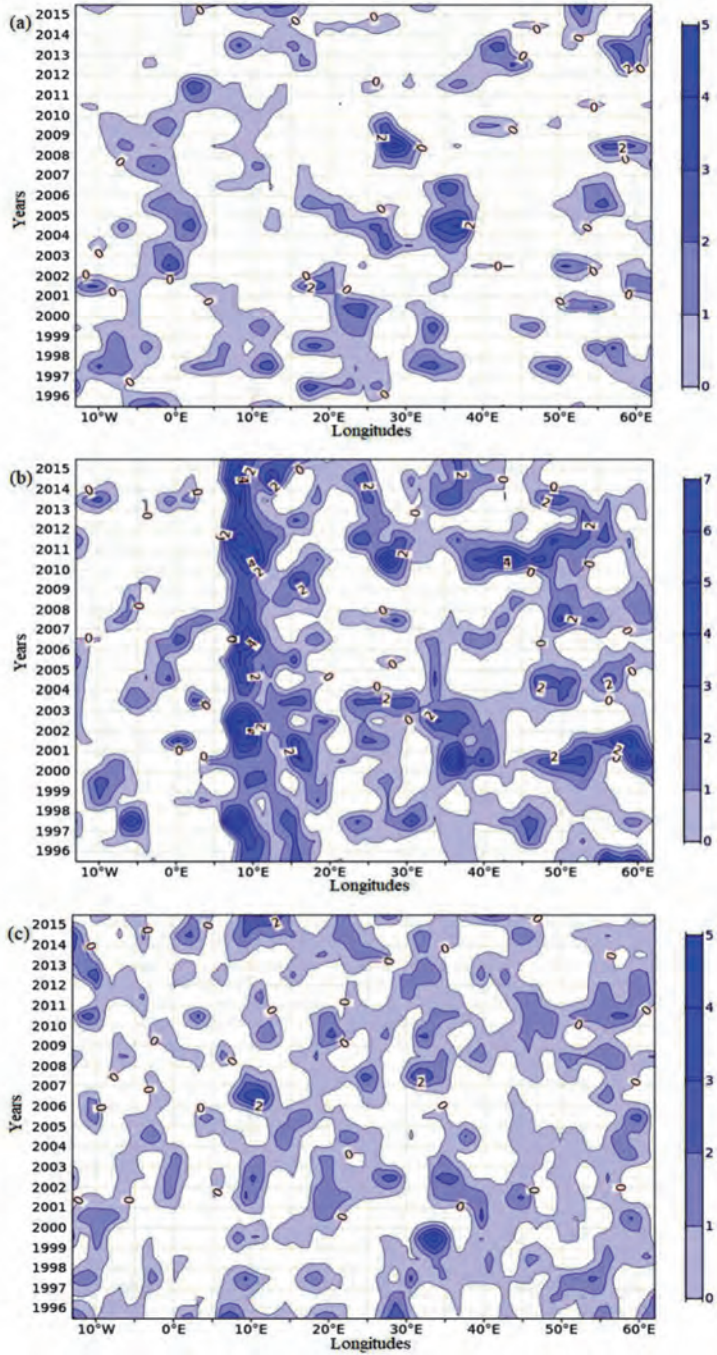
Fig. 3. Spatiotemporal distribution of TFP in July 1995–2015 at latitudes: a) 77°N (Arctic);
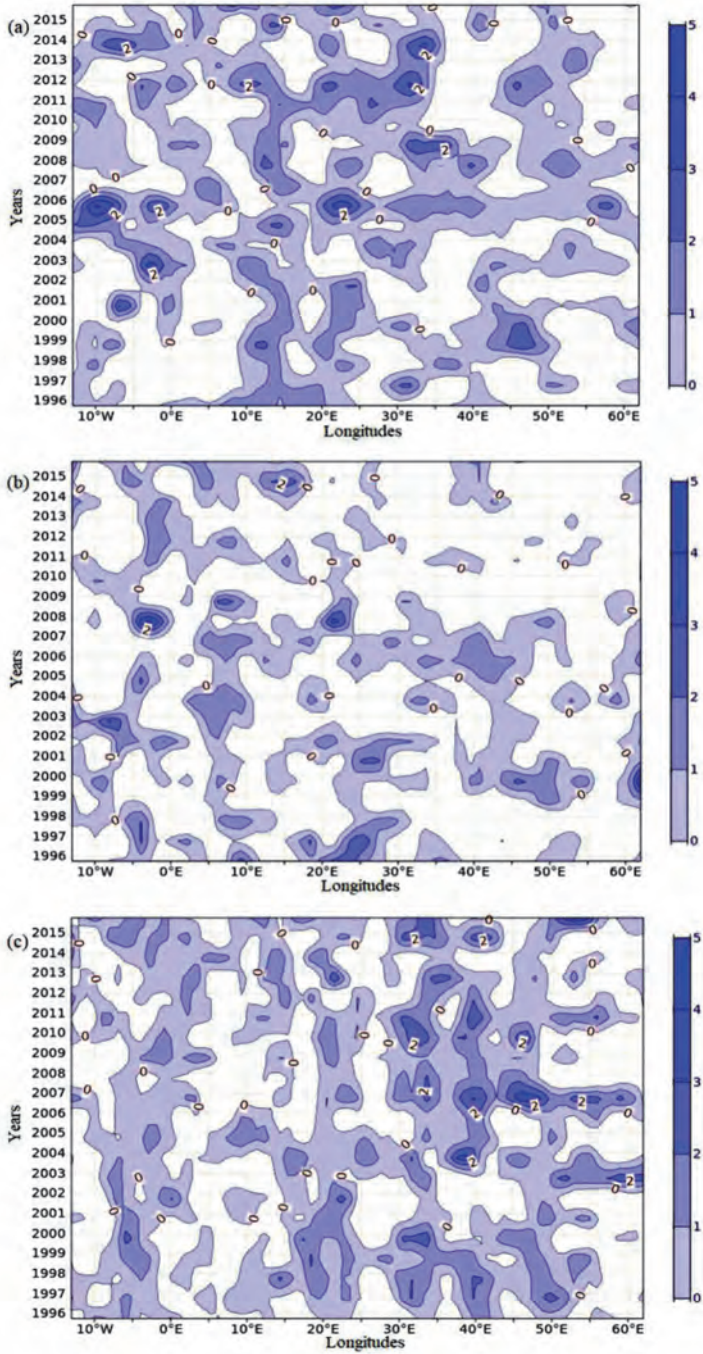b) 62°N (NPF); c) 51.5°N (SPF).

Fig. 4. Spatiotemporal distribution of TFP in October 1995–2015 at latitudes: a) 69.5°N (Arctic front); b) 62°N (NPF); c) 41°N (SPF).

The southern part of the Scandinavian mountains, in the interval of longitude 5–10°E, also turned out to be the area of intensification of the front (2–3 units of TFP). Over the continental surface (30–62°E) in general, the intensity of this section of the front weakens, but there are certain periods of intensification of the front. Thus, the highest activity of the front (2–3 units of *TFP*) was observed from 1998 to 2000 in the interval of longitude 39–62°E, which corresponds to the regions of the northeast of the European territory of Russia and the Pre-Urals. It should be noted that the intensity of NPF decreased during the study period (*Fig. 4 b*).

As it can be seen from *Fig. 4c*, the SPF branch is most intense over the mountainous areas of the northern part of the Asia Minor Peninsula and the Lesser Caucasus (28–48°E), but the position of the maximum *TFP* (up to 3–4 *TFP* units) changes in this area. Thus, the highest intensity of this section of the front was observed from 2003 to 2006, as well as in 2015. Over the Iberian, Balkan, and Apennines peninsulas, as well as the Mediterranean Sea, the front was almost not pronounced, in some years its intensity did not exceed 1–2 *TFP* units. In general, the southern branch of the polar front is relatively weak in October, and no noticeable trends in its intensity were observed during the study period.

3.3. *Seasonal spatial distribution of frontal zones*

The geographical distribution of frontal zones over Europe was averaged by season. *Figs. 5–8* show that in all seasons, certain geographical areas are distinguished, where the frontal zones are most intense in the *TFP* values.

Winter. In winter, within the study region, such zones of active frontogenesis are detected (*Fig. 5*). In the northwestern part, in the latitudes 72–80°N, an area located to the north-east of Greenland with maximum *TFP* of up to 1–2 units is distinguished, which is justified by baroclinicity conditions due to few factors: contrasts between the warm North Atlantic current and the cold East Greenland current, as well as the Arctic basin located to the north, filled with cold air. Over the Atlantic, the baroclinic zones associated with the Icelandic low are oriented in the meridian direction and take a latitudinal position over Arctic waters along the northern edge of the continent, which coincides with the average trajectories of extratropical cyclones and corresponds to sections of the Arctic front, which is constantly intensifying in this band.

The next zone of seasonal frontal activity extends from the British Isles through the North Sea and adjacent waters along the Scandinavian Peninsula. The maximum *TFP* (up to 1–2 *TFP* units) is located in the latitude band 63–69°N near the meridian 10°E, which corresponds to the transition zone between various underlying surfaces as cold land - warm ocean. Atmospheric fronts, approaching the Scandinavian mountains, slow down and intensify, undergoing orographic frontogenesis on the windward slopes.

Over most of the mainland Europe, frontal activity is low, due to the influence of anticyclonic formations, which have a high frequency in the winter season (*Semenova* and *Najmudinova*, 2019).
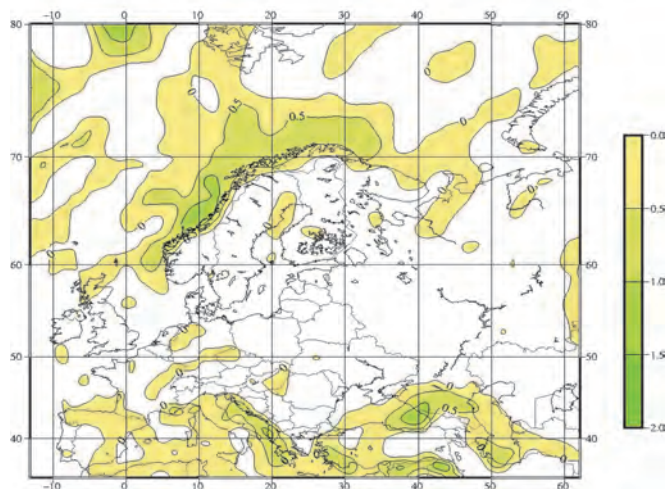
Fig. 5. Average *TFP* field in the winter (December-February) for the period 1995–2015.

Over the territory of Eastern Europe, in the north of the Eastern European plain, a weakened section of the front is revealed, which, according to *Zolotokrylin et al.* (2014), should be attributed to the secondary branch of the Arctic (subarctic) front, formed as a result of the branching of the main branch of the Arctic front over Scandinavia.

In the southern part of Europe, there is an extensive zone of frontal activity, which corresponds to the southern (Mediterranean) branch of the Polar front, which intensifies during the cold season and separates polar and subtropical air masses. The most intense areas of the fronts are over the Gulf of Genoa, the Adriatic Sea, the Eastern Mediterranean, as well as the southeastern part of the Black Sea and the Greater Caucasus mountain system with maximum *TFP* of 1–2 units.

Spring. Compared to the winter period, during the transition season, there is a significant weakening of frontal activity in northern latitudes, which is detected by a significant decrease in the area of zones of positive *TFP* values (*Fig. 6*). However, several of the most intense sections of the fronts can be identified here. As in winter, this is the area to the northeast of Greenland, corresponding to the

section of the Arctic front. The second section of the branch is less intense than in the previous season (the maximum *TFP* does not exceed 1 unit), there is no continuous zone of positive *TFP* values to the east of the Icelandic low, and only small areas are allocated near the northern part of the Scandinavian and Kola peninsulas, as well as the adjacent Arctic basin. It is characteristic that the frontal zones do not spread further to the east along 70°N.

In the spring, high frontal activity persists over the British Isles. The intensity of fronts is weak over areas of Central and Eastern Europe.

The southern (Mediterranean) branch of the Polar front remains acute, and the zone of positive *TFP* values covers a significant area in the southern part of this region. Thus, the maximum *TFP* reaches 1–2 units over the areas of the Iberian Peninsula, the Atlas mountain systems, the Alps, the Greater Caucasus, Zagros, the Armenian highlands, the Carpathians, and the peninsulas of Asia Minor. However, there are almost no fronts over the Mediterranean basin.
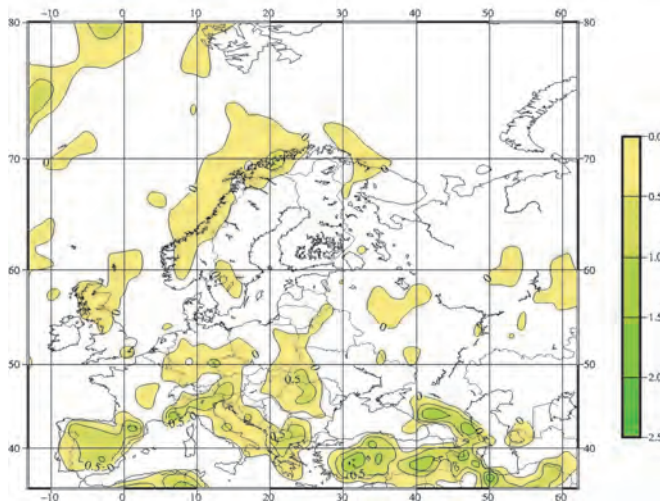
Fig. 6. Average *TFP* field in the spring (March-May) for the period 1995–2015.

Summer. In the summer, in northern latitudes, almost complete absence of frontal zones over the seas is observed, and only a weak section of the Arctic front is fixed over the Greenland Sea (*Fig. 7*). However, over the mainland, there is a significant intensification of the branches of the Polar front compared to the previous season, including the territory of Eastern Europe. As seen, the baroclinic zone is most clearly manifested in the regions with mountain systems, due to the local increase of the horizontal temperature gradients in the lower troposphere induced by the orografic impact under the general weakening advective processes that is typical for the summertime (*Semenova* and *Najmudinov*a, 2019).
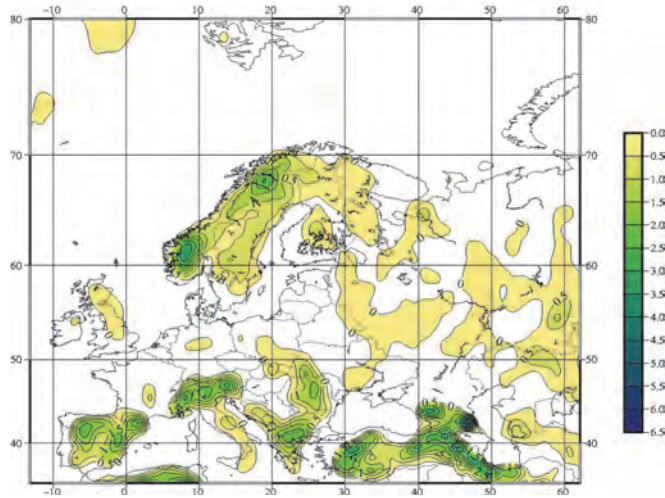
Fig. 7. Average *TFP* field in the summer (June-August) for the period 1995–2015.

The increased activity of fronts over the East European plain is also explained by the predominance of the low pressure field over the warmed continent in the summer season, which contributes to the formation of convergence zones in the lower layers of the troposphere, in which atmospheric fronts can sharpen. The most intense sections of the NPF branch are located above the Scandinavian mountains, with maximum *TFP* up to 3 units.

The southern (Mediterranean) branch of the Polar front is characterized by significant intensity over the land surface. The baroclinic zones (up to 1–3 *TFP* units) located over the Pyrenees, Alps, Carpathians, Atlas Mountains, as well as over the mountain ranges on the Balkan Peninsula and the Asia Minor Peninsula. The intensity of the baroclinic zone reaches 3–7 *TFP* units in the mountains of the Greater and Lesser Caucasus.

Autumn. In the autumn period, the geographical distribution of frontal activity in the study region almost coincides with the spring processes, and in comparison with the summer, there is a significant decrease in the intensity of *TFP* in the frontal sections over the continent (*Fig. 8*). Zones of positive *TFP* values (maximum up to 1 *TFP* unit) appear again over the waters of the seas in northern latitudes. As in previous seasons, the southern (Mediterranean) branch of the Polar front is distinguished, while the intensity of the maximum *TFP* decreases and does not exceed 1–2 units over the Iberian and Balkan peninsulas, Asia Minor, the mountain systems of the Alps, the Carpathians, and the Atlas. Over the territory of Eastern Europe, the activity of atmospheric fronts is low, which is associated with an increase in the frequency of anticyclonic formations over the continent in this season of the year.
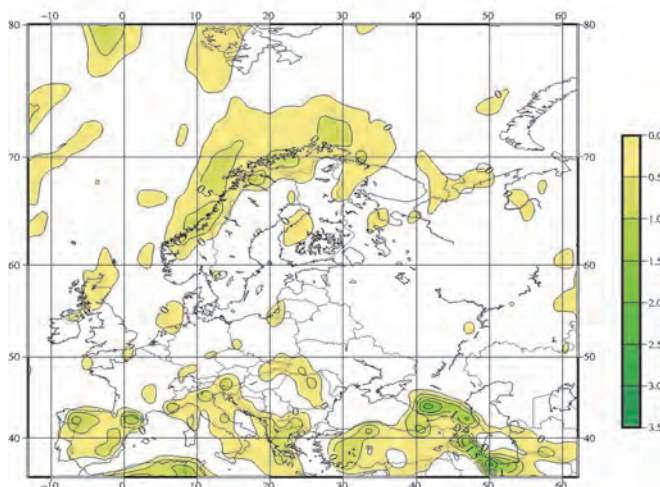
Fig. 8. Average *TFP* field in the autumn (September-November) for the period 1995–2015.

4. Conclusions

The average monthly position of the Arctic front and two branches of the Polar front over Europe in the modern period was established using the calculated fields of the thermal front parameter (*TFP*) in the layer 850–700 hPa. It is revealed that the geographical position of climatological fronts has changed in both the cold and warm periods of the year compared to the climate data. So, in January, both branches of the Polar front shifted to the north by three degrees of latitude. In July, the northern branch of the Polar front descended to the south, the southern branch took a more northerly position, which led to the convergence of the two branches of the Polar front in the middle latitudes. In spring (April), compared to winter, there was a northward shift of the two branches of the Polar front, while in autumn (October), the northern branch did not change its summer position, and the southern branch had the southernmost location during the year. The Arctic front was characterized by northerly location in both January and July compared to the climatic one. In April, a significant shift of the front to the northern latitudes was revealed compared to January, and from mid-autumn to January, the Arctic front occupied the southernmost position among the months of the year. Since cyclonic activity is directly related to atmospheric fronts, the detected front shifts indicate changes in regional synoptic processes over the European continent over the past 20 years, which were reflected in the climate regime of these territories (*Pachauri* and *Meyer,* 2014).

The main areas of intensification of the branches of the Polar front in the cold period of the year was the southern areas of the Norwegian Sea, central part of the Baltic Sea, the western half of the Mediterranean Sea, the Volga region,

106

and the mountain ranges of the Urals and Lesser Caucasus. In summer, these were the southern regions of the Scandinavian mountains, the northeast of the European territory of Russia, the Volga region, the Middle Urals, and the mountainous regions of Western Europe. In the spring and autumn, the most intense sections of the front were typical for the southern part of the Norwegian Sea and central part of the Baltic sea, the southern Urals, Central Europe, as well as for the mountainous regions of the northern part of the Asia Minor Peninsula and the Lesser Caucasus. The Arctic front in all seasons of the year intensified over the areas of the Barents and Norwegian Seas, in the summer over the north of the Greenland Sea, and in the autumn also over the northern part of the Scandinavian Peninsula.

In the seasonal distribution, the main zones of frontogenesis in the winter were the territories from the British Isles to the Scandinavian Peninsula, as well as the Gulf of Genoa, the Adriatic Sea, the Eastern Mediterranean, the southeastern part of the Black Sea, and the Caucasus mountain system. During the transition seasons, the most intense sections of fronts were typical for the southern part of the study region, namely, the Iberian Peninsula, mountain systems of Western Europe, North Africa, the Greater Caucasus, and the Asia Minor Peninsula. In the summer season, the intensification of fronts was detected over the continent, with intense baroclinic zones associated with mountain systems such as the Scandinavian mountains, Pyrenees, Alps, Carpathians, Atlas Mountains, the Caucasus. These *TFP* maxima, as shown in other studies (e.g., *Berry et al.*, 2011a), correspond to features of stable baroclinic zones connected with a change in the underlying or/and sloping land surface, but they are not atmospheric fronts in the classical sense (e.g., *AMS glossary,* 2012), although in some cases they can induce local cyclogenesis.

References

AMS Glossary of Meteorology, 2012: Available online: https://glossary.ametsoc.org/wiki/Front

Berry, G., Reeder, M.J., and *Jacob, Ch.,* 2011a: A global climatology of atmospheric fronts, *Geoph. Res. Let. 38.* https://doi.org/10.1029/2010GL046451

Berry, G., Jakob, C., and *Reeder, M.*, 2011b: Recent global trends in atmospheric fronts, *Geoph. Res. Let. 38.* https://doi.org/10.1029/2011GL049481

Bitsa, E., Flocas, H., Kouroutzoglou, J., Hatzaki, M., Rudeva, I., and *Simmonds, I.,* 2019: Development of a Front Identification Scheme for Compiling a Cold Front Climatology of the Mediterranean. *Climate 7(11),* 130. https://doi.org/10.3390/cli7110130

Catto, J.L., Nicholls, N., Jakob, C., and *Shelton, K.L.,* 2014: Atmospheric fronts in current and future climates. *Geoph. Res. Let. 41.* https://doi.org/10.1002/2014GL061943

Creswick, W.S., 1967: Experiments in objective frontal contour analysis, *J. Appl. Meteor. 6,* 774–781. https://doi.org/10.1175/1520-0450(1967)006<0774:EIOFCA>2.0.CO;2

ERA Interim, Daily datasets. 2019: Available online: https://apps.ecmwf.int/datasets/data/interim-full-daily/levtype=pl/ .

Hewson, T.D., 1998: Objective fronts, *Meteorol. Appl. 5,* 37–65. https://doi.org/10.1017/S1350482798000553

Huber-Pock, F. and *Kress, Ch.,* 1989: An operational model of objective frontal analysis based on ECMWF products. *Meteorol. Atmos. Phis. 40,* 170–180. https://doi.org/10.1007/BF01032457

Khromov, S.P, and *Petrosyants M.A.,* 2006: Метеорология и климатология: учебник. Москва, Изд-во Моск. ун-та, Наука, 582 с. (In Russian)

Pachauri, R.K. and *Meyer, L.A. (eds.),* 2014: IPPC. Climate Change 2014: Synthesis Report. Contribution of Working Groups I, II and III to the Fifth Assessment Report of the Intergovernmental Panel on Climate Change. Available online: https://www.ipcc.ch/report/ar5/syr/

Schemm, S., Rudeva, I., and *Simmonds, I.,* 2015: Extratropical fronts in the lower troposphere – global perspectives obtained from two automated methods, *Quart. J. Roy. Meteorol. Soc. 141,* 1686–1698. https://doi.org/10.1002/qj.2471

Semenova, I.G., 2010: Об'єктивний аналіз кліматологічних фронтів в Атлантико-Європейському секторі. *Причорноморський екологічний бюлетень 2 (36),* 47-51. (In Ukrainian)

Semenova, I.G. and. *Ivus, G.P.,* 2011: Использование термического фронтального параметра для моделирования бароклинных зон в процессах циклогенеза. *Наукові праці УкрНДГМІ, 261,* 56-71. (In Ukrainian)

Semenova, I.G. and Najmudinova, O.M, 2019: Регіональна синоптика: підручник. Одеса: ТЕС, 212 с. (In Ukrainian)

Serreze, M.C., Lynch, A.H., and *Clark, M.P.*, 2001: The arctic frontal zone as seen in the NCEP-NCAR reanalysis. *J. Climate, 14,* 1550–1567. https://doi.org/10.1175/1520-0442(2001)014<1550:TAFZAS>2.0.CO;2

Shakina, N.P., Kalugina, G.Yu., Skriptunova, E.N., and *Ivanova, A.R.,* 1998a: Субъективный и объективный анализы атмосферных фронтов. I. Объективные характеристики фронтов, проведенных синоптиками. *Метеорология и гидрология, 7,* 19-30. (in Russian).

Shakina, N.P., Skriptunova, E.N., Ivanova, A.R., and *Kalugina, G.Yu.,* 1998b: Субъективный и объективный анализы атмосферных фронтов. II. Объективное выделение зон фронтов. *Метеорология и гидрология, 8,* 5-15. (in Russian).

Shakina, N.P., Skriptunova, E.N., and *Ivanova, A.R.,* 2000: Объективный анализ атмосферных фронтов и оценка его эффективности. *Метеорология и гидрология, 7,* 5-16. (in Russian).

Thomas, C.M. and *Schultz, D.M.,* 2019: Global Climatologies of Fronts, Airmass Boundaries, and Airstream Boundaries: Why the Definition of "Front" Matters, *Month. Weather Rev. 147,* 691–717. https://doi.org/10.1175/MWR-D-18-0289.1

Vorobyov, V.I., 1991: Синоптическая метеорология. Ленинград: Гидрометеоиздат. 616 с. (In Russian)

WMO, 2017: Guidelines on the Calculation of Climate Normals. WMO Publisher No. 1203. Geneva. Avalable online: https://library.wmo.int/doc_num.php?explnum_id=4166

Zolotokrylin, A.N., Titkova, T.B., and *Mikhailov, A.Yu.,* 2014: Климатические вариации арктического фронта и ледовитости Баренцева моря. *Лёд и Снег, 1 (125),* 80-85. (In Russian) https://doi.org/10.15356/2076-6734-2014-1-85-90

Zwatz-Meise, V. and *Hufnagl, F.,* 1990: Some results about the relation between an objective front parameter and cloud bands in satellite images and its connection to classical cold front models, *Meteorol. Atmos. Phys. 42,* 77–89. https://doi.org/10.1007/BF01030580

IDŐJÁRÁS

Cloudiness and cloud genera variability at the turn of the 21st century in Poznań (Poland)

Katarzyna Szyga-Pluta

Department of Meteorology and Climatology
Institute of Physical Geography and Environmental Planning
Adam Mickiewicz University in Poznań
ul. Krygowskiego 10, 61-680 Poznań, Poland

*Corresponding author E-mail: pluta@amu.edu.pl

Abstract— The aim of this article was to investigate the effect of macroscale circulation types on total cloud cover in Poznań-Ławica (western Poland) in years 1951–2015. The analysis was preceded by the characteristics of the long-term, annual, and seasonal changes in total cloud cover and cloud genera (data regarding observations of cloud genera covered the period of 1971–2015). The effect of six macroscale circulation types (Arctic oscillation, North Atlantic Oscillation, East Atlantic, East Atlantic/West Russian, Scandinavian, and Polar/Eurasian Types) on the total cloud cover was examined. The amount of cloud cover in Poznań was influenced by the macroscale circulation types, mainly in the warm part of the year. The North Atlantic Oscillation, Arctic Oscillation and Scandinavian types had the strongest impact there.

Key-word: cloudiness, cloud genera, macroscale circulation, Poznań, Poland

1. Introduction

Clouds affect the environment in many ways, playing a significant role in the transfer of heat and water vapor towards the earth's surface and precipitation reaching the surface of the earth. In addition, they are the main factor influencing the earth's climate system through their share in the radiation balance, by modulating the solar radiation inflow to the earth's surface, and by absorbing long-wave radiation (*Ramanathan et al*., 1989, *Boucher et al.,* 2013). Cloudiness, its size and type depend on many meteorological elements, and its diversity is a factor that also determines climate change (IPCC, 2007). It is currently not possible to

ascertain whether recent multidecadal variations in clouds have mitigated or exacerbated anthropogenic global warming (*Norris*, 2008). Cloudiness is the most important meteorological element that reflects the state of the atmosphere, and it is largely shaped by its circulation (*Niedźwiedź* and *Ustrnul*, 1989). The local conditions play great role in spatial differentiation, especially in case of convective clouds and low-level layered clouds (*Okołowicz*, 1962; *Warakomski*, 1962, 1969).

For many decades, it has been the subject of observation allowing researchers to study long-term changes in cloud cover, in particular in connection with atmospheric circulation and synoptic conditions. The influence of clouds on the radiation balance of the planet is measured as the difference between the downward radiation streaming with clouds and without clouds, called radiative forcing (*Ramanathan et al.,* 1989; *Mace et al*., 2006; *Zelinka* and *Hartmann*, 2010). Individual elements of the climate affect the clouds by favoring the conditions that determine the types of clouds and their vertical and horizontal distribution, their composition, and radiation and hydrological properties. Studies of temperature and cloud cover indicate a strong relationship of a temperature increase in Europe with a decrease in cloudiness (*Tang* and *Leng*, 2012). Cloudiness is an element introducing uncertainty to the construction of climate models – the final effect of changes in the cloud amount and structure on the climate system is still unclear, which causes errors in estimating and forecasting the cloud amount in a given area (*Bartok* and *Imecs,* 2012).

The research on cloudiness in various spatial and temporal scales is, therefore, of great importance for understanding climate processes on a global scale. Examining cloud types as well as total cloud cover is essential, because it is a better measure of processes and radiative impacts (*Norris*, 2000). The study aim is the characteristics of the long-term, annual, and seasonal changes in total cloud cover and cloud types in the period 1951–2015. The objective of this study is to investigate the effect of macro-scale circulation patterns on total cloud cover in Poznań (western Poland).

2. *Data and methods*

The analysis was based on the values of total cloud cover and cloud amount at the Poznań-Ławica meteorological station located in western Poland (52°12'N, 18°40'E; 86 m above sea level). Data, verified in terms of quality and homogeneity, came from the database of the Institute of Meteorology and Water Management – National Research Institute (IMGW-PIB). According to *Hahn et al.* (1995), the diurnal cycle in surface-based climatologies can be biased, because visual cloud observations by human observers are less accurate at night. Therefore, observations of cloud cover made three times a day: at 6:00, 12:00, and 18:00 UTC in the period of 1951–2015 were considered for the purpose of the study. The total cloud cover was recorded during the period under consideration

at various scales in Poland (at a 0–10 scale during the period 1951–1965 and at a 0–8 scale during the period 1966–2015). Thus, all the values were converted into percents so that the data could be compared. Data regarding observations of cloud genera covered the period of 1971–2015. Ten basic types of clouds were considered in accordance with the International Cloud Atlas (WMO, 1975): *Cirrus (Ci), Cirrocumulus (Cc), Cirrostratus (Cs), Altocumulus (Ac), Altostratus (As), Stratocumulus (Sc), Stratus (St), Nimbostratus (Ns), Cumulus (Cu),* and *Cumulonimbus (Cb).* The frequency of the occurrence of cloud genera was used to describe the cloud structure. For the total cloud cover, the mean and the 1st and 3rd quartile were calculated on an annual, seasonal and monthly bases. The percentage share of the occurrence frequency of particular types of clouds in observation terms as well as their annual and daily changes were presented. The long-term changes in the occurrence of cloud genera with the trend of changes were determined and the significance of the trend was estimated using the Mann-Kendall test.

In the next step, the effect of macroscale circulation types on the total cloud cover was examined. For this purpose, the correlation coefficient was calculated between the average monthly cloud cover value and the index value of each type of circulation. Monthly indices of six patterns of circulation: Arctic Oscillation (AO), North Atlantic Oscillation (NAO), East Atlantic (EA), Scandinavian (SCAND), Polar/Euroasian (POLAR-E), and East Atlantic/West Russian (EA WR), relevant for Central Europe, were obtained from the databases of the Climate Prediction Center (CPC) of NOAA (1951–2015). The types of circulation specified in the CPC database were determined by means of the principal components analysis based on the monthly values of 500 hPa isobaric surface anomalies (*Barnston* and *Livezey*, 1987).

The positive phase of the Arctic Oscillation (AO) is associated with lower than normal pressure in the Arctic region and with a higher one at moderate latitudes. It causes the blockade of the Arctic air masses inflow to lower latitudes. The negative phase of the AO is associated with higher than average pressure in the Arctic, and with a lower one in moderate latitudes. This pressure pattern is slowing down and shifting the air stream to the south, which promotes the advection of the Arctic air masses to the south (*Higgins et al.*, 2002; *Kang et al.,* 2014). The North Atlantic Oscillation (NAO) is a regional indication of the Arctic Oscillation with centers in the region of Iceland and the Azores Islands. The positive phase of the NAO is associated with negative pressure anomalies in the area of the Icelandic Low and with positive anomalies in the Azores High. As a result, there is a high pressure gradient over the North Atlantic, which causes the intensive advection of humid and warm air masses from the west and the southwest over the northern, western, and central part of parts of Europe. The negative phase of the NAO is related to the opposite distribution of the pressure anomalies. Under these conditions the western flow is slowed down, and there is an inflow of dry and cool air masses from the northeast (*Hurrell*, 1995; *Hurrell*

and *Deser,* 2010). Shifted to the southeast towards the NAO is the East Atlantic (EA) type of circulation. Its southern center is associated with the intertropical circulation (*Barnston* and *Livezey*, 1987). The positive phase of the EA is connected with a deep system of low pressure over the Atlantic, causing the advection of warm air masses over Europe. In the negative phase, there is a high pressure system formed over the Atlantic that brings cool and dry air masses (*Josey et al.*, 2011; *Mikhailova* and *Yurovsky*, 2016). The Scandinavian circulation type (SCAND) is characterized by the presence of a strong high occurring in the positive phase over the Scandinavian Peninsula with its center over Finland, while the area of lower pressure extends from Western Europe to Eastern Russia and Western Mongolia. The positive SCAND phase is associated with a blocking situation with higher pressure over Scandinavia and Western Russia, while the negative phase is associated with lower pressure than the average over Northern Europe (*Bueh* and *Nakamura*, 2007; *Liu et al.,* 2014). Lower impact on the weather in Europe is shown by the Polar/Euroasian pattern (POLAR-E), which has one main center over the polar region and separate centers of the opposite sign over Europe and northeastern part of China. This system, according to CPC, has its influence in all seasons of the year at 700 hPa (*Gao et al.*, 2016). The positive phase of this system manifests itself in the negative values of the anomalies over the polar region (intensification of the polar vortex), which results, inter alia, in relatively high precipitation in Scandinavia, and the negative phase is associated with the weakening of the polar vortex (*Lorenzo* and *Taboada*, 2005). The least-affecting type of circulation in connection to weather in Central Europe is the Eastern European (EA WR) type characterized by two centers located latitudinally. In the positive phase, the low pressure area is located over the Caspian Sea, while the high is located over Western Europe and the British Isles. In the positive phase, such a system causes the advection of air masses from the northern sector, while the reverse system in the negative phase promotes advection from the southern sector (*Krichak* and *Alpert*, 2005; *Ionita et al.*, 2015; *Lim*, 2015).

3. Results

3.1. Total cloud cover

The average annual total cloud cover from the period of 1951–2015 in Poznań was 64% (*Table 1*). The highest annual total cloud cover was observed in 2013 (72%), and the lowest in 1982 (53%). The standard deviation was 3.5%, which indicates low year-to-year variation in the research period. Winter was the season of the year characterized by the highest cloud amount in Poznań. The average cloud cover was 74%, and the standard deviation was the lowest (5.0%). The highest average cloud amount in winter was observed in 2013 (86%), and the lowest in 1972 (64%). The sunniest season was summer, with the mean total cloud

cover of 58% and the highest year-to-year variability (standard deviation 5.6%). The lowest cloud amount in summer occurred in 1983 (43%), and the highest in 2013 (69%). The most overcast month in Poznań was December (77%), and the least was August (55%). The highest average monthly cloud cover was observed in December 1959 (93%). The lowest cloud amount occurred in April 2009 (26%).

Table 1. Mean monthly, seasonal, and annual total cloud cover (%) in Poznań in the period 1951–2015

MONTH	MEAN	Q₁	Q₃	MAXIMUM		MINIMUM	
				VALUE	DATE	VALUE	DATE
I	74	66	79	91	2013	56	1993
II	71	64	77	93	2013	51	1982; 1986
III	63	58	71	79	1981;1985	41	1953
IV	59	54	65	83	1956	26	2009
V	57	50	63	79	2010	38	1989
VI	59	53	65	75	2012	39	1992
VII	58	53	65	82	2000	33	1994
VIII	55	48	60	71	2006	35	1973
IX	56	48	63	79	1978	33	2006
X	62	54	68	81	1974	28	1951
XI	75	71	80	88	1958	55	1984
XII	77	71	82	93	1959	46	1972
YEAR	64	61	66	72	2013	53	1982
Spring	60	69	78	76	2013	45	1953
Summer	57	57	64	69	2013	43	1983
Autumn	64	53	60	77	1952	51	1952; 2005
Winter	74	59	68	86	2013	64	1972

Explanations: Q₁ – 1st quartile, Q₃ – 3rd quartile

The long-term changes showed significant fluctuations in the cloud amount in the subsequent years (*Fig. 1*); however, the decrease in cloud cover in the examined period in Poznań was small (-0.1%/10 years) and statistically insignificant. The deviations of the average annual cloudiness value from the average in the years 1951–2015 reached 11% (*Fig. 2*). In the first part of the research period, the cloud amount showed very considerable year-to-year fluctuations. At the end of the 1970s, significant positive deviations were noted. From 1982 until 1996, there was a period of reduced cloud cover. Next, there were short periods of increase and decrease, and since 2006 one could notice an increase in cloud cover.
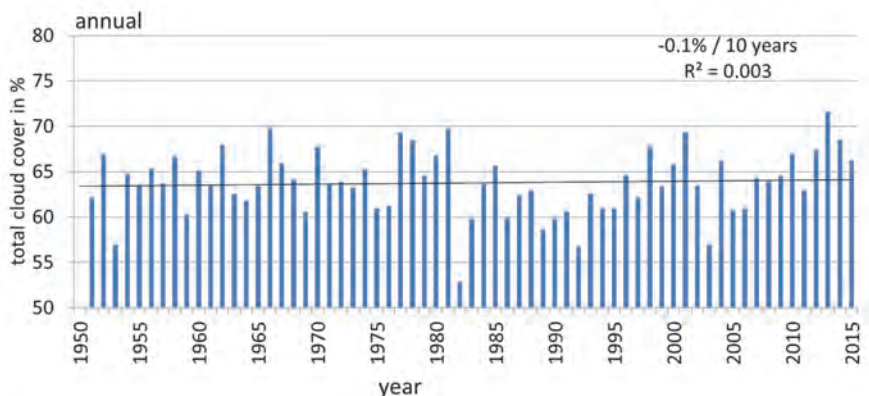
Fig. 1. The long-term course of mean annual cloud cover in Poznań with linear trend and the coefficient of determination R^2 (1951–2015).
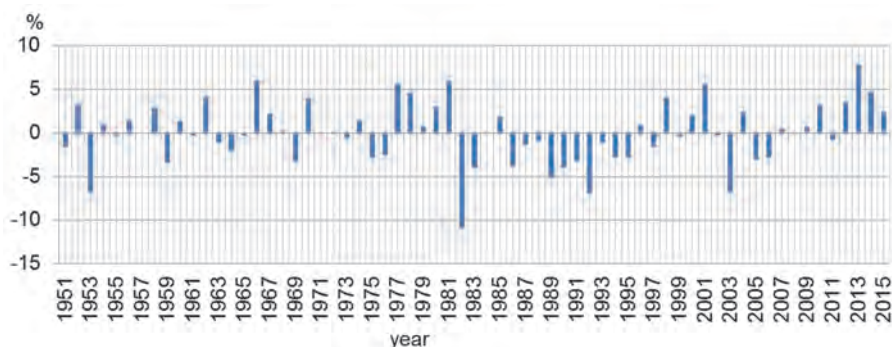
Fig. 2. Deviation of annual cloud cover in Poznań from the average of the period 1951–2015

The largest variations in cloud cover occurred in spring - the amplitude in the whole research period exceeded 30% (*Fig. 3*). The largest difference from year to year occurred in 2009 and 2010 (19.8%) and in 1958 and 1959 (18.8%). The lowest amplitude of cloud cover (aaproximately 21%) occurred in the studied period in winter. The maximum increase in cloud cover was observed in 1951 and 1952, and decrease in 1952 and 1953 (24.1% each). The amplitude of fluctuations in summer and autumn was approx. 28%. In the colder part of the year, a greater increase in cloud cover could be observed in the period of 1951–2015, however, it was not statistically significant.
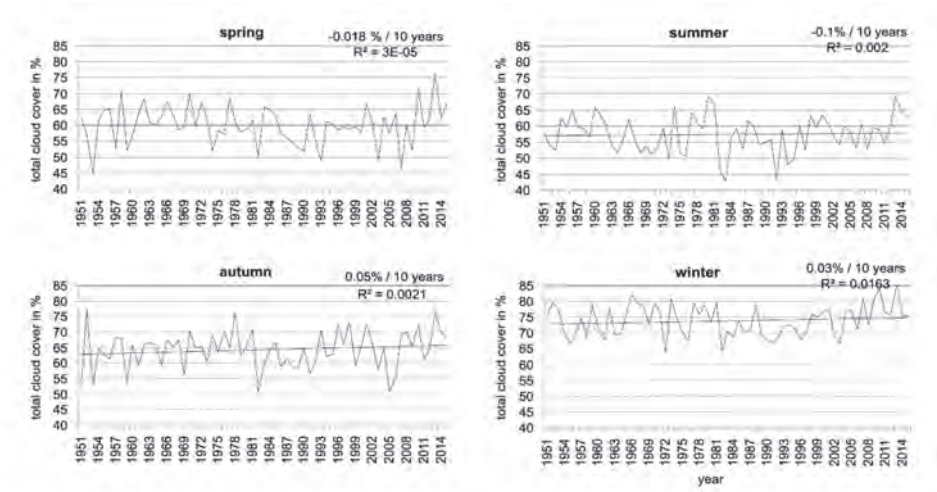
Fig. 3. The long-term course of mean seasonal cloud cover in Poznań with linear trend and the coefficient of determination R^2 (1951–2015).

3.2. Occurrence of cloud genera

The most common clouds in Poznań are *Stratocumulus* (25.6%), and the fewest are *Cirrocumulus* (*Table 2*). Next are: *Altocumulus* (18.7%), *Cirrus* (18.5%), and *Cumulus* (14.0%). The cloud cover structure changes throughout the year. In winter, *Stratocumulus* clouds had a much larger share than in other seasons. *Stratus* clouds were also more common then. The frequency of *Cirrus*, *Cumulus*, and *Cumulonimbus* clouds increased in spring and summer. Clouds that did not show significant variation in their frequency during the year are: *Cirrocumulus*, *Cirrostratus*, *Altostratus,* and *Nimbostratus*.

Table 2. Annual and seasonal frequency of occurrence (%) of cloud genera in Poznań (1971–2015)

Months	Cloud genera									
	Ci	Cc	Cs	Ac	As	Ns	Sc	St	Cu	Cb
Year	18.4	0.8	1.3	18.7	3.7	3.3	25.6	9.8	14.0	4.4
Spring	22.9	0.8	1.7	18.9	3.9	3.3	21.8	5.1	16.0	5.6
Summer	22.5	1.2	1.1	23.9	3.2	2.9	14.2	2.8	21.8	6.4
Autumn	17.2	0.7	1.1	19.8	3.8	3.6	28.9	10.9	11.1	2.9
Winter	11.4	0.3	1.2	12.3	3.9	3.2	37.5	20.5	7.1	2.6

High clouds did not change the frequency of occurrence during the day (*Table 3*). Similarly, *Altostratus* and *Nimbostratus* formed with the same frequency at different times of the day. *Altocumulus* and *Stratus* clouds appeared most often in the morning, and least often in the evening. Distinctive daily changes characterized *Cumulus* clouds, which were the most numerous at noon. *Cumulonimbus* was least often observed in the morning, more often at noon and in the evening.

Table 3. Diurnal frequency of occurrence (%) of cloud genera in Poznań (1971–2015)

Cloud Type	Hour		
	6 UTC	12 UTC	18 UTC
Cirrus	17.8	16.3	17.5
Cirrocumulus	1.0	0.5	0.5
Cirrostratus	1.2	1.4	1.2
Altocumulus	20.3	14.7	18.8
Altostratus	3.7	3.8	3.6
Nimbostratus	3.4	3.2	3.2
Stratocumulus	**28.1**	20.7	**33.1**
Stratus	14.6	8.8	10.6
Cumulus	8.0	**25.3**	6.6
Cumulonimbus	1.9	5.3	4.9

Bold indicates the highest values.

The cloud cover structure in Poznań changed over the period under consideration (*Fig. 4*). Types of clouds that tended to increase their occurrence frequency were *Ci, Ac, Sc,* and *Cu*. Only in the case of *Ac*, these were statistically insignificant changes. Decreasing trend concerning the frequency in the years 1971–2015 was shown by clouds *As, Ns, St,* and *Cb*. On the other hand, the frequency of *Cs* clouds, in the first part of the analyzed period, was decreasing, followed by a period of equal frequency until 2007, and since then *Cs* has been observed increasingly often. *Cc* clouds were characterized by very high year-to-year variability of occurrence.

Changes in the annual frequency of occurrence of particular types of clouds at different times of the day are shown in *Fig. 5*. The annual changes in frequency of *Cirrus* were not considerable during the day. It formed more often in the warm part of the year, and much less frequently in the cold part of the year. It was most often observed in spring and autumn, especially in the evening. It was difficult to determine the annual changes of *Cirrocumulus* clouds due to their low frequency, although it could be seen that they were more often observed in the warm period of the year. In the case of *Cirrostratus* clouds, there was a higher frequency in spring, especially in the morning and at noon.

Fig. 4. Multiannual course of the frequency of occurrence of particular types of clouds in Poznań with the trend line and the coefficient of determination R^2 (1971–2015).

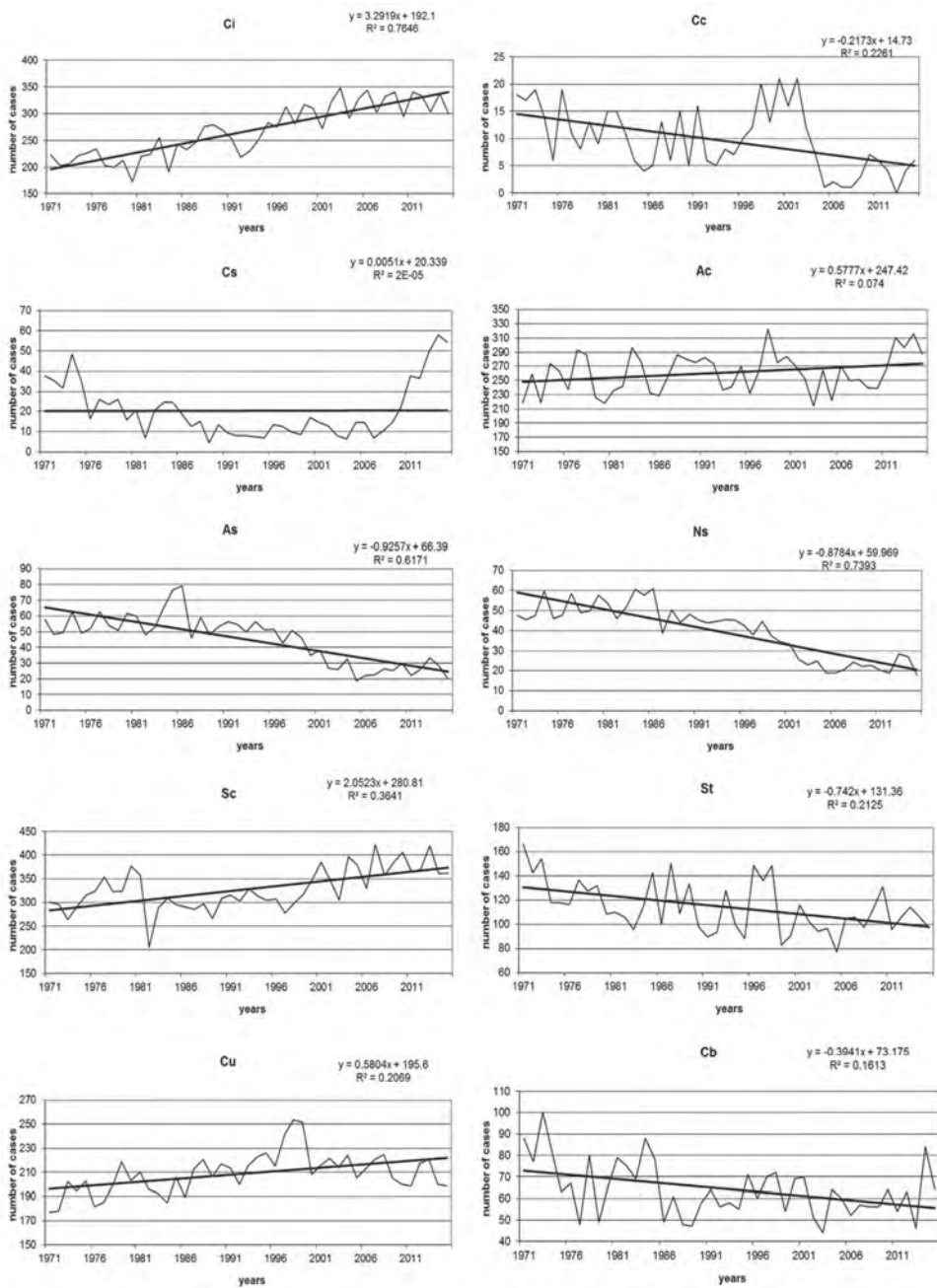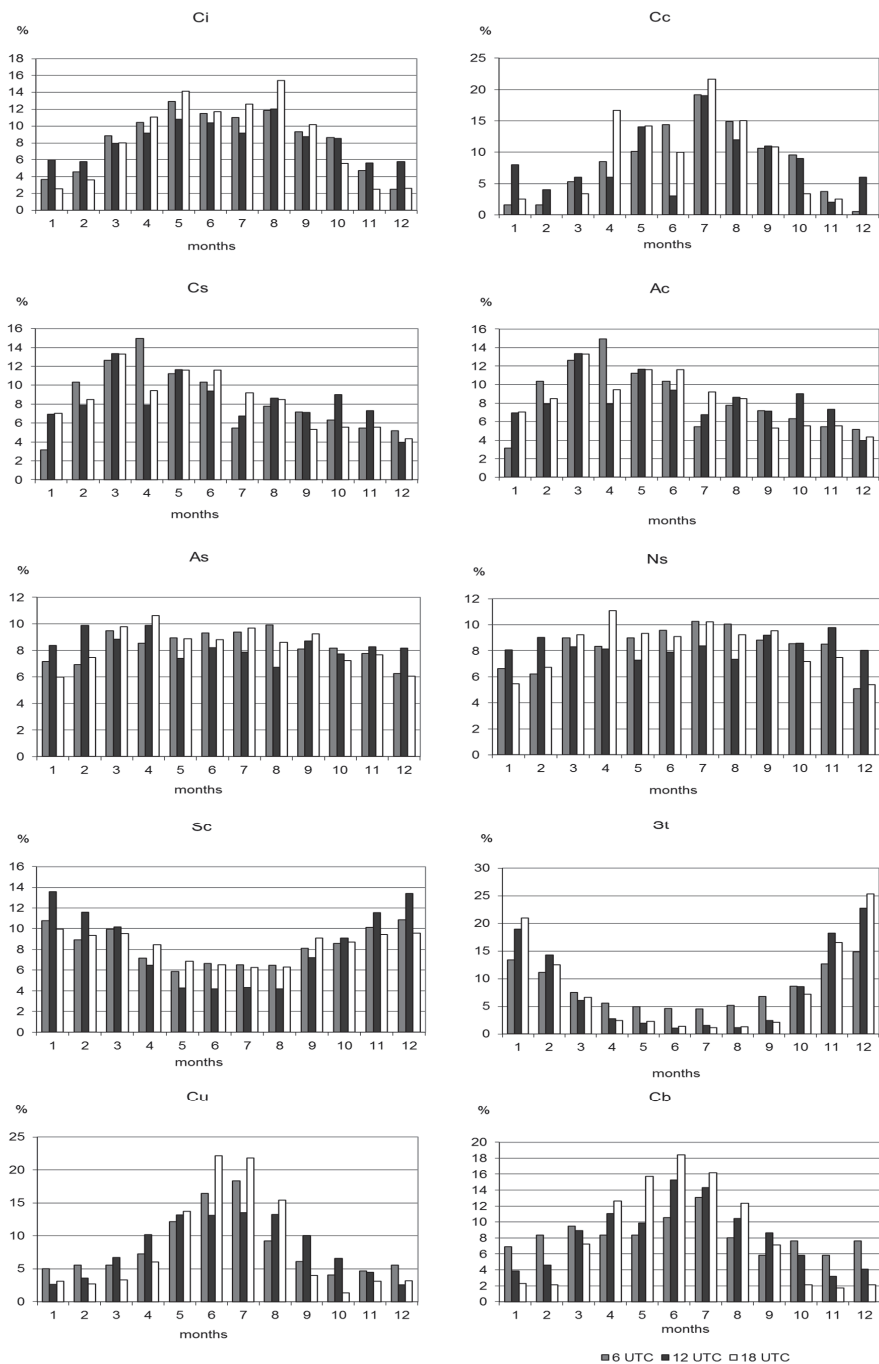*Fig. 5.* The annual course of the frequency of occurrence of particular types of clouds in three observation periods in Poznań in the years 1971–2015.

Clear annual changes, varied during the day, with lower frequency in winter and higher in summer, were shown by *Altocumulus* clouds. The highest amplitude of the frequency characterized the evening time; it was slightly lower in the morning, while at noon, the annual course was the most uniform. *Altostratus Nimbostratus* clouds occurred with a similar frequency throughout the year, regardless of the time of day. Annual changes in the frequency of occurrence of *Stratocumulus* clouds was the most diverse at midday - the summer minimum and the winter maximum were clearly marked then. In the morning and evening, *Stratocumulus* also more often appeared in the cold than the warm part of the year, however, the amplitude of the frequency was definitely lower. *Stratus* on the other hand, showed a clear differentiation of the annual changes, especially at noon and in the evening, with the highest frequency in winter and the lowest in summer. The annual changes in towering vertical clouds, *Cumulus* and *Cumulonimbus*, were exactly opposite. They formed much more often in the warm half of the year. *Cumulus* was usually observed the most frequently at noon, and *Cumulonimbus* could be found equally often at midday and in the evening.

3.3. Influence of macroscale circulation types on cloud cover

The Arctic Oscillation (AO) is a type of atmospheric circulation in the Northern Hemisphere, dominating during the winter, in particular. The strongest influence of AO on cloudiness, however, was visible in the warm half of the year (*Table 4*). The correlation in this period was negative and statistically significant. It assumed the highest of values the correlation coefficient in August and September (> -0.4), and slightly lower in June and July.

The North Atlantic Oscillation system, observed throughout a year, was of great importance in shaping the cloud cover in Poznań. The Pearson correlation coefficient was negative and statistically significant from June to October. In December, January, and April the amount of cloudiness did not show any connection with NAO.

The EA pattern had a much smaller impact on the shaping of the cloud cover in Poznań and the correlation coefficient did not exceed -0.3. A somewhat greater influence of EA on cloud cover occurred in June and July.

The Scandinavian pattern was negatively correlated with the amount of cloud cover in Poznań for the most part of the year, which means that a drop in pressure below the average over Northern Europe in the negative SCAND phase caused an increase in cloud cover in the studied area.

The POLAR-E system had a small influence on the amount of cloudiness in Poznań. Only in September, the correlation assumed a statistically significant negative value (-0.5).

The East European pattern did not have a statistically significant impact on the shaping of the cloud cover over Poznań for most of the year. Only in December there was a positive, statistically significant correlation.

Table 4. Coefficients of correlation of the average total cloud cover in Poznań with selected indices of circulation types for the North Atlantic and Eurasia after the Climate Prediction Center (1951–2015)

Index	Months											
	I	II	III	IV	V	VI	VII	VIII	IX	X	XI	XII
AO	-0.12	-0.26	-0.20	0.09	-0.09	**-0.27**	**-0.18**	**-0.36**	**-0.42**	-0.17	-0.19	-0.17
NAO	0.06	-0.18	-0.14	0.02	-0.15	**-0.38**	**-0.27**	**-0.39**	**-0.29**	**-0.29**	-0.14	0.09
EA	-0.21	-0.19	-0.15	-0.18	-0.20	**-0.27**	**-0.30**	-0.21	-0.12	-0.11	-0.27	-0.18
SCAND	**-0.20**	-0.07	**-0.29**	-0.01	0.01	**-0.29**	**-0.50**	**-0.16**	**-0.36**	**-0.27**	0.18	0.11
POLAR-E	-0.07	-0.09	-0.07	0.03	-0.17	-0.07	-0.01	0.10	**-0.49**	-0.05	-0.14	-0.17
EA WR	-0.05	-0.09	-0.08	-0.01	-0.03	-0.15	0.16	-0.03	-0.14	-0.10	0.07	**0.23**

Explanations: NAO – North Atlantic Oscillation, AO – Arctic Oscillation, EA – East Atlantic, SCAND – Scandinavia, POLAR-E – Polar/Eurasia, EA WR – East Atlantic/West Russia

bold – statistically significant correlation

4. Discussion and summary

On the basis of the conducted research it was found, that the annual values of the total cloud cover in Poznań showed a statistically insignificant downward trend, and among the seasons, its increase was visible in autumn. In Łódź (central Poland), as in Poznań (western Poland), there was a slight decrease in total cloud cover (*Wibig*, 2008). The results of *Wibig* (2008), however, indicated a decrease in the amount of cloud cover in winter and spring in the morning and at noon in Łódź, while a drop in its amount in the evening. In the warm seasons of the year in Poznań, the amount of cloud cover did not change much in the long-term, while in Łódź, in summer, the decrease in the cloud cover was observed (*Wibig*, 2008). In the second half of the twentieth century, in all seasons except autumn, a decrease was found in the amount of cloud cover in Poland (*Żmudzka*, 2003). *Żmudzka* (2007) explained that, probably, an increase in the frequency of lows in this part of Europe, as well as along the North Atlantic - North Sea - Southern Baltic Sea track, areas located to the east of Poland, were the direct cause of the increase in the cloud cover over Poland in autumn. In Lithuania, there was a decrease in low cloud cover in the cold seasons of the year and an increase in the cold seasons in the second half of the 20th century (*Stankûnavičius,* 1998). In the second half of the 20th century, a few percent increases in cloud cover were observed in the area of moderate and high latitudes (*Houghton et al*., 2001). The analysis of *Warren et al*. (2007) on the basis of metadata, showed a slight decrease in total cloud cover in Central and Southern Europe in 1971–1996. The decreasing

cloudiness in Europe (apart from Northern Europe) in 1984–2007 was confirmed by *Tang et al.* (2012). The increase in total cloud cover was found in Central Europe (*Henderson-Sellers,* 1986, 1992), Fennoscandian countries and Denmark (*Cappelen*, 2004) as well as in the former USSR (*Sun* and *Groisman*, 2000) and Russia (*Chernokulsky et al.,* 2011, 2013). A similar trend was recorded in Moscow (*Abakumova et al.*, 1996) and Estonia (*Keevallik* and *Rusak*, 2001). However, in the area of the Black, Caspian and Aral Sea in the years 1991–2010, no changes in total cloud cover were found (*Calbó et al.*, 2016). The increase in total cloud cover was visible in Spain in the period of 1866–2010, although a decreasing trend was found since the 1960s (*Sanchez-Lorenzo et al.*, 2012). The decrease in total cloud cover was observed in other regions, i.e., over the Mediterranean region (*Maugeri et al.,* 2001; *Sanchez-Lorenzo et al.*, 2017). In Kraków (southern Poland), in the period from 1906 to the 40s of the twentieth century, there was an increase in total cloud cover observed; then for two decades it remained at the same level, and since 1961 there was a decrease in cloud cover before the increase from 1983 to 2000 (*Matuszko,* 2003). The spatial variability of long-term changes in cloud cover was found in Poland (*Filipiak* and *Miętus,* 2009) and on the Iberian Peninsula (*Calbó* and *Sanches-Lorenzo,* 2009). *Żmudzka* (2007) stated that the decreasing trends of changes in cloud cover could be explained primarily by the increase in the frequency of anticyclonic patterns over Central Europe. The decrease in the amount of cloud cover in Central Europe as a consequence of the intensification of the activity of highs was indicated also by *Henderson-Sellers* (1986).

Norris (2005), based on the analysis of data from terrestrial and satellite observations, found a relatively small drop in the amount of high clouds, which was not confirmed by the results for Poznań. In Kraków (southern Poland) an increase in the amount of *Ci* clouds was found based on a long series of observations (1906–2000), while *Cs* clouds appeared less and less often (*Matuszko*, 2003; *Matuszko* and *Węglarczyk*, 2018). *Wibig* (2008) found no significant changes in the amount of high clouds in Łódź in the second half of the twentieth century. According to *Eerme* (2004) low average cirrus amounts in spring-summer period were often recorded when the spring was dry, and high cirrus amounts - when it was wet in Estonia. An increase in the amount of cumulus clouds, as in Poznań, in the former USSR was reported by *Sun* and *Groisman* (2000). This confirms as well the previous results obtained by both *Warren et al.* (2007) for Central and Southern Europe, as well as *Sun et al.* (2001) for Eastern Europe. Cumulus clouds that formed more often were also observed in various parts of Poland (*Matuszko* 2003; *Żmudzka* 2007; *Wibig*, 2008). In southern Poland (Kraków) the frequency of occurrence of the *Cu* alone increases in the 1930s, then decreases in the 1950s and again increases (slightly) until 2015 (*Matuszko* and *Węglarczyk,* 2018). As in Poznań, the amount of stratus clouds in the former USSR (*Sun et al.*, 2001) and decreased which was also confirmed by the results of *Matuszko* (2003) and *Matuszko* and *Węglarczyk* (2018) for Kraków in southern

Poland and of *Wibig* (2008) for Łódź in central Poland, as well as by the earlier results of *Warren et al.* (2007). Interannual variations in stratiform cloud amount are related to changes in static stability as explained by *Klein* and *Hartmann* (1993).

Most research on the North Atlantic Oscillation has focused on the winter season. However, studies by *Barnston* and *Livezey* (1987) or *Portis et al.* (2001) showed that NAO is the leading type of teleconnection in all months of the year, including summer. On the other hand, *Wibig* (2008) pointed out that despite the strong influence of NAO on weather conditions in Poland, its impact on the shaping of the cloud cover over Poland was small in all months except April and September. The amount of cloud cover in Poznań was influenced by macroscale circulation types, mainly in the warm part of the year. The North Atlantic Oscillation, Arctic Oscillation, and Scandinavian types had the strongest impact on cloudiness in Poznań. Long-term variability of cloudiness over Europe, and especially of *Nimbostratus* clouds, dependent on NAO, was noticed by *Warren et al.* (2007). *Klein* and *Hartmann* (1993) explain that the amount of stratus clouds appear to be closely tied to aspects of the general circulation of the atmosphere and ocean.

5. *Conclusions*

In Poznań, in the years 1951–2015, the annual values of the total cloud cover showed a statistically insignificant downward trend, and among the seasons, its increase was visible in autumn. Types of clouds that tended to increase their occurrence frequency were *Ci, Ac, Sc,* and *Cu,* and only in the case of *Ac*, these were statistically insignificant changes. The decrease trend concerning the frequency in the years 1971–2015 was shown by *As, Ns, St,* and *Cb* clouds. On the other hand, the frequency of *Cs* clouds was decreasing in the first part of the analyzed period, followed by a period of equal frequency until 2007, since *Cs* has been observed increasingly often. The amount of cloud cover in Poznań was influenced by macroscale circulation types, mainly in the warm part of the year. The North Atlantic Oscillation, Arctic Oscillation and Scandinavian type had the strongest impact there.

References

Abakumova, G.M., Feigelson, F.M., Russak, V., and *Stadnik, V.V.,* 1996: Evaluation of long-term changes in radiation, cloudiness, and surface temperature on the territory of the former Soviet Union. *J. Climate 9,* 1319–1327.
https://doi.org/10.1175/1520-0442(1996)009<1319:EOLTCI>2.0.CO;2
Barnston, A.G. and *Livezey, R.E.,* 1987: Classification, seasonality, and persistence of low-frequency atmospheric circulation patterns. *Mon. Weather Rev. 115*, 1083–1126.
https://doi.org/10.1175/1520-0493(1987)115<1083:CSAPOL>2.0.CO;2

Bartok, B. and *Imecs, Z.,* 2012: Verification of statistical cloudiness estimations for Europe. Aerul si Apa. Componente ale Mediului, 289–296.

Boucher, O., Randall, D., Artaxo, P., Bretherton, C., Feingold, G., Forster, P., Kerminen, V-M., Kondo, Y., Liao, H., Lohmann, U., Rasch, P., Satheesh, S.K., Sherwood, S., Stevens, B., and *Zhang X-Y.,* 2013: Clouds and aerosols. In (*T.F. Stocker, D. Qin, G-K. Plattner, M. Tignor, S.K. Allen, J. Doschung, A. Nauels, Y. Xia, V. Bex, P.M. Midgley*) Climate Change 2013: The Physical Science Basis. Contribution of Working Group I to the Fifth Assessment Report of the Intergovernmental Panel on Climate Change., Eds. Cambridge University Press, 571–657.

Bueh, C. and *Nakamura, H.,* 2007: Scandinavian pattern and its climatic impact. *Quart. J Roy. Meteor. Soc. 133,* 2117–2131. https://doi.org/10.1002/qj.173

Calbó, J. and *Sanchez-Lorenzo A.,* 2009: Cloudiness climatology in the Iberian Peninsula from three global gridded datasets (ISCCP, CRU TS 2.1, ERA-40). *Theor. Appl. Climatol. 96,* 105–115 https://doi.org/10.1007/s00704-008-0039-z

Calbó, J., Badosa, J., González, J.A., Dmitrieva, L., Khan, V., Enríques-Alonso, A., and *Sanches-Lorenzo, A.,* 2016: Climatology and changes in cloud cover in the area of the Black, Caspian, and Aral seas (1991-2010): a comparison of surface observations with satellite and reanalysis products. *Int. J. Climatol. 36,* 1428–1443. https://doi.org/10.1002/joc.4435

Cappelen, J., 2004: Yearly temperature, precipitation, hours of bright sunshine and cloud cover for Denmark as a whole 1873–2003. *DMI Techn. Rep. 4–6.*

Chernokulsky, A.V., Bulygina, O.N., and *Mokhov, I.I.,* 2011: Recent variations of cloudiness over Russia from surface daytime observations. *Environ. Res. Lett. 6,* 035202. https://doi.org/10.1088/1748-9326/6/3/035202

Chernokulsky, A., Mokhov, I.I., and *Nikiyina, N.,* 2013: Winter cloudiness variability over Northern Eurasia related to the Siberian High during 1966-2010. *Environ. Res. Lett. 8,* 045012. https://doi.org/10.1088/1748-9326/8/4/045012

Eerme, K., 2004: Changes in spring-summer cirrus cloud amount over Estonia, 1958–2003. Int. *J. Climatol. 24,* 1543–1549. https://doi.org/10.1002/joc.1055

Filipiak, J. and *Miętus M.,* 2009: Spatial and temporal variability of cloudiness in Poland, 1971-2000. *Int. J. Climatol. 29,* 1294–1311. https://doi.org/10.1002/joc.1777

Gao, Y., Lu, J., and *Leung, L.R.,* 2016: Uncertainties in projecting future changes in atmospheric rivers and their impacts on heavy precipitation over Europe. *J. Climate 29,* 6711–6726. https://doi.org/10.1175/JCLI-D-16-0088.1

Hahn, C.J., Warren, S.G., and *London, J.,* 1995: The effect of moonlight on observations of cloud cover at night, and application to cloud climatology. *J. Climate 8,* 1429–1446. https://doi.org/10.1175/1520-0442(1995)008<1429:TEOMOO>2.0.CO;2

Henderson-Sellers, A., 1986: Increasing clouds in a warming world. *Climate Change 9,* 267–309. https://doi.org/10.1007/BF00139074

Henderson-Sellers, A., 1992: Continental cloudiness changes this century. *Geo. J. 27,* 255–262. https://doi.org/10.1007/BF02482666

Higgins, R.W., Leetmaa, A., and *Kousky V.E.,* 2002: Relationships between climate variability and winter temperature extremes in the United States. *J. Climate, 15,* 1555–1572. https://doi.org/10.1175/1520-0442(2002)015<1555:RBCVAW>2.0.CO;2

Houghton, J.T., Ding, Y., Griggs, D.J., Noguer, M., van der Linden, P.J., and *Dai, X. (eds),* 2001: Climate Change 2001: The Scientific Basis. Contribution of Working Group I to the Third Assessment Report of the International Panel on Climate Change (IPCC). Cambridge University Press: Cambridge UK and New York, NY, USA.

Hurrell, J.W., 1995: Decadal trends in the North Atlantic Oscillation: regional temperatures and precipitation. *Science, 269,* 676–679. https://doi.org/10.1126/science.269.5224.676

Hurrell, J. and *Deser, C.,* 2010: North Atlantic climate variability: the role if the North Atlantic Oscillation. *J. Marine Syst. 79,* 231–244. https://doi.org/10.1016/j.jmarsys.2008.11.026

Ionita, M., Boroneanţ, C., and *Chelcea, S.,* 2015: Seasonal modes of dryness and wetness variability over Europe and their connections with large scale atmospheric circulation and global sea surface temperature. *Clim. Dynam, 45,* 2803–2829. https://doi.org/10.1007/s00382-015-2508-2

IPCC, 2007: Climate Change 2007 The Physical Science Basis. Contribution of Working Group I to the Fourth Assessment Report of the Intergovernmental Panel on Climate Change [*S Solomon, D Qin,*

M Manning, Z Chen, M Marquis, K B Averyt, M Tignor and H L Miller (eds.)]. Cambridge University Press, Cambridge, United Kingdom and New York, NY, USA

Josey, S.A., Somot, S., Tsimplis, M., 2011: Impacts of atmospheric modes of variability on Mediterranean Sea surface heat exchange. *J. Geophys. Res., 116*, C02032.
https://doi.org/10.1029/2010JC006685

Kang, D., Lee, M.I., Im, J., Kim, D., Kim, H.M., Kang, H.S., Schubert, S.D., Arribas, A., and *MacLachlan, C.,* 2014: Prediction of the Arctic Oscillation in boreal winter by dynamical seasonal forecasting systems. *Geophys. Res. Lett. 41,* 3577–3585. https://doi.org/10.1002/2014GL060011

Keevallik. S. and *Russak. V.,* 2001: Changes in the amount of low clouds in Estonia (1955–1995). *Int J of Climatol, 21,* 389–397. https://doi.org/10.1002/joc.618

Klein, S.A. and *Hartmann, D.L.,* 1993: The seasonal cycle of low stratiform clouds. *J. Climate 6,* 1587–1606. https://doi.org/10.1175/1520-0442(1993)006<1587:TSCOLS>2.0.CO;2

Krichak, S.O. and *Alpert P.,* 2005: Signatures of the NAO in the atmospheric circulation during wet winter months over the Mediterranean region. *Theor. Appl. Climatol. 82,* 27–39.
https://doi.org/10.1007/s00704-004-0119-7

Lim, Y.K., 2015: The East Atlantic/West Russia (EA/WR) teleconnection in the North Atlantic: climate impact and relation to Rossby wave propagation. *Clim. Dynam 44,* 3211–3222.
https://doi.org/10.1007/s00382-014-2381-4

Liu, Y.Y., Wang, L., and *Zhou W.,* 2014: Three Eurasian teleconnection patterns: spatial structures, temporal variability, and associated winter climate anomalies. *Clim. Dynam. 42,* 2817–2839.
https://doi.org/10.1007/s00382-014-2163-z

Lorenzo, M.N. and *Taboada J.J.,* 2005: Influences of atmospheric variability on freshwater input in Galician Rı́as in winter. *J. Atmos. Ocean Sci. 10,* 377–387.
https://doi.org/10.1080/17417530601127472

Mace, G.G., Benson, S., and *Kato, S.,* 2006: Cloud radiative forcing at the Atmospheric Radiation Measurement Program Climate Research Facility: 2. Vertical distribution of radiant energy by clouds. *J. Geophys. Res. 111,* D11S91. https://doi.org/10.1029/2005JD005922

Matuszko, D., 2003: Cloudiness changes in Cracow in the 20th century. *Int. J. Climatol. 23,* 975–984
https://doi.org/10.1002/joc.887

Matuszko, D. and *Węglarczyk S.,* 2018: Long-term variability of the cloud amount and cloud genera and their relationship with circulation (Kraków, Poland). *Int. J. Climatol. 38,* 1205–1220.
https://doi.org/10.1002/joc.5445

Maugeri, M., Bagnati, Z., and *Brunetti, M.,* 2001: Trends in Italian total cloud amount, 1951–1996. *Geophys. Res. Lett. 28,* 4551–4554. https://doi.org/10.1029/2001GL013754

Mikhailova, N.V. and *Yurovsky, A.V.,* 2016: The East Atlantic Oscillation: mechanism and impact on the European climate in winter. *Phys. Oceanograph. 4,* 25–33.
https://doi.org/10.22449/1573-160X-2016-4-25-33

Niedźwiedź, T. and *Ustrnul, Z.,* 1989: Wpływ cyrkulacji atmosferycznej na kształtowanie się zachmurzenia w Hornsundzie [: Influence of synoptic situations on cloud formation in Hornsund]. XVI Sympozjum Polarne, Wydawnictwo Uniwersytetu w Toruniu, Toruń. 158–160. (in Polish)

Norris, J.R., 2000: What can clouds observations tell us about climate variability? *Space Sci Rev, 94,* 375–380. https://doi.org/10.1023/A:1026704314326

Norris, J.R., 2005: Multidecadal changes in near-global cloud cover and estimated cloud cover radiative forcing. *J. Geophys. Res. 110,* 1–17. https://doi.org/10.1029/2004JD005600

Norris, J.R., 2008: Observed interdecadal changes in cloudiness: real or spurious? In: Climate Variability and Extremes During the Past 100 Years, Springer, Netherlands, 169–178.
https://doi.org/10.1007/978-1-4020-6766-2_11

Okołowicz, W., 1962: Zachmurzenie w Polsce [Cloudiness in Poland]. *Prace Geograficzne,* 34, IG PAN Warszawa, 9-107. (in Polish)

Portis, D.H., Walsh, J.E., Hamly, M.E., and *Lamb P.J.,* 2001: Seasonality of the North Atlantic Oscillation. *J. Climate 14,* 2069–2078.
https://doi.org/10.1175/1520-0442(2001)014<2069:SOTNAO>2.0.CO;2

Ramanathan, V., Cess, R.D., Harrison, E.F., Minnis, P., Barkstrom, B.R., Ahmad, E., and *Hartmann, D.,* 1989: Cloud-Radiative Forcing and Climate: Results from the Earth Radiation Budget Experiment. *Science. New Series, 243,* 57–63. https://doi.org/10.1126/science.243.4887.57

Sanchez-Lorenzo, A., Calbó, J., and *Wild, M.,* 2012: Increasing cloud cover in the 20th century: review and new findings in Spain. *Clim. Past. 8,* 1199–1212. https://doi.org/10.5194/cp-8-1199-2012

Sanchez-Lorenzo, A., Enriquez-Alonso, A., Calbó, J., Gonzales, J-A., Wild, M., Folini, D., Norris, J.R., and *Vicente-Serrano, S.M.,* 2017: Fewer clouds in the Mediterranean: consistency of observations and climate simulations. *Nature, Sci. Rep. 7,* 41475. https://doi.org/10.1038/srep41475

Stankûnavičius, G., 1998: Debesuota. In: Klimato elementų kaitos kintamumas Lietuvos teritorijoje [Cloudiness. In: The Variability of Changes of Climatic Elements in Lithuanian Territory]. Vilnius, 110–132. (in Lithuanian)

Sun, B. and *Groisman, P.Y.,* 2000: Cloudiness variations over the former Soviet Union. *Int. J. Climatol. 20,* 1097–1111. https://doi.org/10.1002/1097-0088(200008)20:10<1097::AID-JOC541>3.0.CO;2-5

Sun, B., Groisman, P.Y., and *Mokhov, I.I.,* 2001: Recent changes in cloud-type frequency and inferred increases of convection over the United States and the former USSR. *J. Climate 14,* 1864–1880. https://doi.org/10.1175/1520-0442(2001)014<1864:RCICTF>2.0.CO;2

Tang, Q. and *Leng, G.,* 2012: Damped summer warming accompanied with cloud cover increase over Eurasia from 1982 to 2009. *Environ. Res. Lett. 7,* 014004. https://doi.org/10.1088/1748-9326/7/1/014004

Tang Q., Leng G., Groisman P.Y., 2012: European hot summers associated with a reduction of cloudiness. *J. Climate 25,* 3637–3644. https://doi.org/10.1175/JCLI-D-12-00040.1

Warren, S.G., Eastman, R.M., and *Hahn, C.J.,* 2007: A survey of changes in cloud cover and cloud types over land from surface observations, 1971-1996. *J. Climate 20,* 717–738. https://doi.org/10.1175/JCLI4031.1

Warakomski, W., 1962: O częstości występowania poszczególnych rodzajów chmur w Polsce [On frequency of occurrence of particular cloud genera in Poland]. *Przegląd Geofizyczny 7,* 185–192. (in Polish)

Warakomski, W., 1969: Zachmurzenie i rodzaj chmur w zależności od mas powietrznych w Polsce [Cloud cover and cloud types depending on air masses in Poland]. Rozprawy habilitacyjne Wydział BiNOZ UMCS. (in Polish)

Wibig, J., 2008: Cloudiness variations in Łódź in the second half of the 20th century. *Int. J. Climatol. 28,* 479–491. https://doi.org/10.1002/joc.1544

WMO, 1975: International Cloud Atlas. Manual on the observation of clouds and other meteors. Vol. 1, No. 407, Geneva.

Zelinka, M.D. and *Hartmann, D.L.,* 2010: Why is longwave cloud feedback positive? *J. Geophys. Res. 115,* D16117. https://doi.org/10.1029/2010JD013817

Żmudzka, E., 2003: Wielkość zachmurzenia w Polsce w drugiej połowie XX wieku [Cloudiness in Poland in the second half of 20th century]. *Przegląd Geofizyczny 48,* 159–185. (in Polish)

Żmudzka, E., 2007: Zmienność zachmurzenia nad Polską i jej uwarunkowania cyrkulacyjne (1951-2000) [Variability of cloudiness over Poland and its circulation-related conditioning (1951-2000)]. Wydawnictwo Uniwersytetu Warszawskiego, Warszawa. (in Polish with English summary)

IDŐJÁRÁS

Statistical analysis of annual and seasonal temperature regime change in Rasina River basin, Serbia

Ljiljana Stričević [1],*, **Mila Pavlović** [2], **Ivan Filipović** [1],
Aleksandar Radivojević[1], **Milena Gocić** [1], and **Nataša Martić Bursać** [1]

[1] *University of Niš*
Faculty of Sciences and Mathematics
Department of Geography
Višegradska 33, 18000 Nis, Republic of Serbia

[2] *University of Belgrade*
Faculty of Geography
Studentski trg 3/III, 11000 Belgrade, Republic of Serbia

Corresponding author E-mail: ljiljana.s.stricevic@gmail.com

(Manuscript received in final form October 16, 2020)

Abstract— In this research, changes in annual and seasonal trends of mean temperatures were analyzed on the territory of the Rasina River basin (central Serbia). We used data from four meteorological stations during three periods: 1961–1989, 1990–2018, and 1979–2013. The change detection analysis has been conceded using the Pettitt's test, von Neumann ratio test, Buishand's range test, and standard normal homogeneity (SNH) test, while the linear regression, Mann-Kendall, and Sen's slope tests have been applied for trend analysis. The results show that the change in summer temperatures occurred shortly after 1980. The analysis results showed that inhomogeneous structures are generally observed between 1976 and 1984, between 1997 and 1998, and in 2006. The trend of all the data on annual basis showed positive increasing trend. The analysis indicated that the average annual, winter, and summer temperatures show significant increasing trend both in the longer period (1961–2018) and in the second part of the period (1990–2018). In the first part of the period (1961–1989), autumn temperatures in Kruševac, summer and autumn temperatures in Blace, as well as winter and autumn temperatures in Goč showed significant decreasing trend. The significant rising trend in the summer and winter months in the last 30 years may affect water availability and water demands in the region.

Key-words: annual and seasonal temperature, statistical homogeneity tests, Mann-Kendall test, Rasina River, Serbia

1. Introduction

Climate change, particularly temperature trend and variation, is an important topic in climate research. Climate change is a well-known threat to the social, economic, and environmental spheres (*Croitoru et al.,* 2011; *Tan et al.,* 2019). Recent climate changing is the result of both natural and anthropogenic influence. The number and intensity of recorded natural hazards such as flood, drought, heatwave, and wildfire have increased as climate change exacerbates in several regions of the world (*Emmanuel et al.,* 2019, *Tan et al.,* 2019; *Mahmood et al,* 2019). In recent years, potential impacts of climatic change and variability have received a lot of attention from researchers. The studies include different regions in the world, and the result shows that there is an air temperature growth trend at all temperature variables (maximum, minimum, and mean temperatures) (*Jain et al.,* 2013; *Zarenistanak et al.,* 2014; *Chattopadhyay* and *Edwards*, 2016; *Hadi* and *Tombul,* 2018; *Tan et al.,* 2019; *Emmanuel et al.,* 2019; *Mahmood et al*., 2019; *Cherinet et al.,* 2019; *Panda* and *Sahu,* 2019).

According to the *IPCC* (2013) report, the average global surface temperature of the world has increased by 0.74 °C± 0.18 °C in the past 100 years. Available records show that the 1990s have been the warmest decade of the millennium in the Northern Hemisphere. The analysis of historical series of mean monthly and annual temperatures in different parts of the globe suggested, that 2005 was the warmest year in the historical series. Other warm years in the series that have occurred after 1990 were 1998, 2003, 2002, 2004, 2001, 1999, 1995, 1990, 1997, 1991, and 2000 (*Jaiswal et al.,* 2015).

This increase in global temperature is not homogeneously distributed over the Earth's surface. It varies among regions and locations. The seasonal and annual European series of the mean temperature exhibited an increasing trend during the twentieth century. Maximum and minimum temperatures in Europe have increased more in winter (1.0 °C / 100 years) than in summer (0.8 °C / 100 years) (*Moberg et al.,* 2006). Temperatures have risen faster than the global average in the Mediterranean region in the last decades with strong enhancement in the occurrence of extremely warm events (*Lionello et al.,* 2014)**.** *Brunetti et al.* (2004) noted that the temperature trend in Italy was positive for each season in the south, and for autumn and winter in the north. They found that Greece, in general, exhibits a cooling trend in winter, whereas in summer it exhibits an overall warming trend. *Hadi* and *Tombul* (2018) examined trends of annual and seasonal surface air temperature time series for 81 stations in Turkey for the period 1901–2014. They found that annual temperature has a significant, increasing trend, and 1993 was observed as the year of the most probable change. Seasonal temperature showed an increasing trend in all the seasons, and the highest increasing trend was observed in the summer. Analysis of the surface air temperature observed in Bulgaria indicated a decreasing trend in average air temperature in the northeast, east, and south regions, while the west, northwest,

and central regions have a positive trend (*Alexandrov et al.,* 2004). Seasonal air temperature for the period 1984–2010 in Bulgaria have also positive trend (*Chenkova* and *Nikolova*, 2015). Analysis of temperature changes in Slovenia showed statistically significant positive trend of mean temperatures in the period 1961–2011 (of around 0.3–0.4 °C/decade). Temperature rise has been particularly pronounced in summer, spring, and winter (*Milošević er al.,* 2017). Mean annual air temperature in Croatia in the period 1981–2018 has a clear upward trend. Higher mean annual air temperature (0.7–1.5 °C higher) occurs between 1998 and 2006 (*Tadić et al.,* 2019).

Along with the rest of the world, Serbia has experienced temperature changes during recent decades. The annual mean surface air temperature has increased significantly in almost all parts of Serbia, except the southeast part of the country. The rises in temperatures were higher in the northern than in the southern parts of Serbia, and the increase was the highest in spring (*Malinović-Milićević et al,* 2016. The regions with the greatest increase in temperature are Eastern Serbia and the region Vojvodina (*Radivojević et al.* 2015*; Gavrilov et al,* 2015, 2016). According to *Unkašević* and *Tošić* (2013), extreme temperature in Serbia increased in the period 1949–2009. The warmest summers with regards to heat wave duration and severity occurred within the periods 1951–1952, 1987–1998 (especially in 1996), and 2000–2007 (*Popović et al.,* 2009). Because Serbian regions are not always covered in European studies, the analysis of temperature tendencies can contribute to better understanding of the temperature changes. In addition to these results, the climate in Serbia was studied in other recent papers (*Radovanović* and *Ducić,* 2004; *Ducić et al.,* 2009; *Tošić et al.,* 2014; *Gavrilov et al.,* 2015, 2016, 2018; *Ruml et al.,* 2017; *Vukoičić et al.,* 2018).

In the present study, statistical methods of trend detection and change point analysis have been used for annual and seasonal temperature in the Rasina River basin from 1961 to 2018. Mean annual and monthly data were used to identify general trends in the temperature regime. These data were provided by the Republic Hydrometeorological Service of Serbia. The objective of the research was to examine homogeneity of the data during the period of observation, and to pinpoint the components of a trend in the data on annual and seasonal average air temperatures. This would allow us to determine of the moment t_c for marking a shift of the annual average air temperatures, implicating a statistically significant difference between the average temperatures in the period before and after this break-point moment (*Radivojević et al.,* 2015).

2. Study area

The basin of is situated in the south part of the middle Serbia connecting Dinaric and Serbian – Macedonian masses (*Fig. 1*). It covers an area of 979.6 km^2 (*Dimitrijević,* 2010). The largest part of the Rasina River basin is situated in the

zone of temperate continental climate with continental pluviometric regime, while mountainous climate is represented on the mountain edge of the basin. In the north, the basin is wide open towards Župa and the valley of the Zapadna Morava, from where continental air masses penetrate unhindered. The basin is surrounded by the mountain massifs of Goč, Željin, Kopaonik, and Jastrebac from the west, southwest, and east (*Stričević,* 2015).

Fig. 1. Geographical location of the research area and position of meteorological stations in the Rasina River basin.

According to the Kepen's classification, most of the basin belongs to the so-called C climate, i.e., it is moderately warm, because the average temperatures in the coldest month are higher than -3 ºC, while the average temperatures of the warmest month are higher than 18 ºC. The exception is the mountainous area of Kopaonik, which belongs to the D climate, that is, has a moderately cold climate with temperature lower than -3 ºC in the coldest month, while the temperature is higher than 10 ºC in the warmest month. According to the climatic regionalization of *T. Rakićević* (1980), the Rasina basin belongs to the West Moravian climate region in its middle and lower course, while the upper part of the basin, which includes the mountain massifs of Kopaonik, Goč, and Željin belongs to the Kopaonik climate region.

3. Data

Annual and seasonal average temperature data recorded at 4 stations in the Rasina River basin in the period 1961–2018 were analyzed. Selected stations are located on the territory of different climatic regions of Serbia: temperate continental climatic region (Kruševac and Blace) and mountainous climatic region (Goč and

Kopaonik). The locations of the stations are presented in *Fig. 1*, and their main parameters are given in *Table 1*. Monthly temperature was provided by the Republic Hydrometeorological Service of Serbia. Seasons were defined as follows: winter – W (December–February), spring – S_p (March–May), summer – S_m (June–August), and autumn – A (September–November). The average seasonal temperature for each station was calculated using the standard season definition. All the seasons correspond to the calendar year except for the winter season, which corresponds to January-February of the calendar year and to December of the previous year.

Table 1. List of stations with the basic geographical information

Meteorological station	Latitude (°N)	Longitude (°E)	Elevation (m)	Climate type
Kruševac	43°34'	21°20'	166	Temperate continental
Blace	43°18'	21°18'	395	Temperate continental
Goč	43°33'	20°51'	990	Mountainous
Kopaonik	43°17'	20°48'	1711	Mountainous

4. Methodology

A number of methods were applied to determine change points of a time series by many researchers such as *Buishand* (1982), *Radivojević et al.,* (2015), *Ming Kang and Yusof*, (2012), *Zarenistanak et al.* (2014), *Jaiswal et al.* (2015), *Palaniswami* and *Muthiah* (2018), *Hadi* and *Tombul* (2018), *Emmanuel et al.* (2019), *Javari* (2016), *Kocsis et al.* (2020), and many more. The change point detection is an important aspect to assess the period from which significant change occurred in a time series. The Pettitt's test, Buishand range test, standard normal homogeneity test, and von Neumann ratio test have been applied for change point detection in climatic series. The details of various change point tests applied in the study are presented here.

The Pettitt's test for change detection, developed by *Pettitt* (1979), is a non-parametric test, which is useful for evaluating the occurrence of abrupt changes in climatic records. The Pettitt's test is the most commonly used test for change point detection because of its sensitivity to breaks in the middle of any time series (*Wijngaard, et al.*, 2003; *Jaiswal et al.,* 2015). According to Pettitt's test, if there is a change point in a series of n observed data, the distribution function of first t samples (F_1) will be different from the distribution function of the second part of

the series (F_2). Null hypothesis H_0 implies that the data are homogeneous throughout the period of observation, and alternative hypothesis H_1 implies the presence of a non – accidental component among data causes a shift of the location parameter at a particular moment. The non-parametric test statistics Ut for this test may be described as follows:

$$Ut = \sum_{i=1}^{t} \sum_{j=i+1}^{n} \text{sgn}(x_i - x_j) \tag{1}$$

$$\text{sgn}(x_i - x_j) = \begin{bmatrix} 1, if\,(x_i - x_j) > 0 \\ 0, if\,(x_i - x_j) = 0 \\ -1, if\,(x_i - x_j) < 0 \end{bmatrix}. \tag{2}$$

The test statistic K and the associated confidence level (ρ) for the sample length (n) may be described as:

$$K_T = \max \left| U_t \right|, \tag{3}$$

$$p = \exp\left(\frac{-K}{n^2 + n^3} \right). \tag{4}$$

When ρ is smaller than the specific confidence level, the null hypothesis is rejected. The approximate significance probability (p) for a change-point is defined as:

$$P = 1 - p. \tag{5}$$

When there is a significant change point, the series is segmented at the location of the change point into two subseries. The test statistic K can also be compared with standard values at different confidence levels for the detection of a change point in a series. The critical values of K at 5% confidence level has been presented in *Tables 2* and *3*.

Table 2. Homogenity test's statistic – Kruševac and Blace

Test	Period	Variable	Kruševac					Blace				
			T_{av}	W	S_p	S_m	A	T_{av}	W	S_p	S_m	A
Pettitt's test	1961-2018	Kt	696	379	488	743	324	620	269	320	558	303
		tc	1997	1993	1998	1991	1999	1997	1993	1998	1991	1969
		p	0.0001	0.015	0.0002	0.0001	0.505	0.0001	0.168	0.058	0.0001	0.083
		T1	10.876	0.682	11.224	20.055	11.560	9.876	0.412	10.405	18.994	10.628
		T2	12.076	1.744	12.500	21.822	11.560	10.847	0.412	10.405	20.185	10.628
	1961-1989	Kt	80	111	35	107	156	92	88	80	161	153
		tc	1968	1969	1972	1972	1969	1968	1965	1972	1972	1970
		p	0.286	0.059	0.980	0.065	0.001	0.155	0.196	0.291	0.0006	0.002
		T1	10.807	0.738	11.259	20.038	12.511	9.845	0.161	10.269	19.708	11.440
		T2	10.807	0.738	11.259	20.038	10.610	9.845	0.161	10.269	18.518	9.953
	1990-2018	Kt	141	112	131	127	111	174	99	123	162	74
		tc	2006	2006	1998	2006	2007	2006	2006	1998	2006	2007
		p	0.004	0.052	0.011	0.016	0.054	0.0001	0.108	0.025	0.001	0.374
		T1	11.438	1.541	11.111	21.30	11.921	10.20	0.662	9.478	19.612	10.790
		T2	12.333	1.541	12.500	22.308	11.921	11.190	0.662	11.020	20.758	10.790
SNH test	1961-2018	Tt	32.963	10.689	15.500	29.178	7.689	28.5118	7.4161	8.0815	18.9030	9.0431
		t	1998	1969	1998	1991	1999	2006	1965	1998	2006	1969
		p	0.0001	0.016	0.0004	0.0001	0.075	0.0001	0.084	0.054	0.0001	0.037
		T1	10.889	-0.022	11.224	20.055	11.560	9.976	0.412	10.405	19.233	11.567
		T2	12.110	1.390	12.500	21.822	11.560	11.190	0.412	10.405	20.758	10.455
	1961-1989	Tt	5.470	7.175	1.823	4.315	13.235	6.278	6.673	3.993	11.321	12.051
		t	1968	1969	1988	1964	1969	1968	1965	1972	1972	1969
		p	0.160	0.063	0.872	0.371	0.0005	0.101	0.077	0.373	0.0019	0.002
		T1	10.807	0.738	11.259	20.038	12.511	9.845	0.161	10.269	19.708	11.567
		T2	10.807	0.738	11.259	20.038	10.610	9.845	0.161	10.269	18.518	9.979
	1990-2018	Tt	11.223	4.329	10.751	6.278	5.243	13.61	3.605	10.060	10.213	2.284
		t	1999	2006	1998	2006	2007	2006	2006	1998	2006	2007
		p	0.003	0.323	0.006	0.161	0.233	0.0003	0.486	0.009	0.013	0.781
		T1	11.156	1.541	11.111	21.717	11.921	10.20	0.662	9.478	19.612	10.790
		T2	12.137	1.541	12.500	21.717	11.921	11.190	0.662	11.020	20.758	10.790
Buishand test	1961-2018	Q	21.082	11.210	14.376	20.699	10.117	18.7091	8.4432	10.3804	16.0233	8.3645
		t	1997	1993	1998	1991	1998	1997	1993	1998	1991	1969
		p	0.0001	0.016	0.0002	0.0001	0.037	0.0001	0.130	0.030	0.0001	0.125
		R	21.082	11.209	14.376	20.699	17.395	18.709	9.534	14.304	18.411	14.125
		T1	10.876	0.682	11.224	20.055	11.247	9.876	0.412	10.082	18.994	10.628
		T2	12.076	1.744	12.500	21.822	12.155	10.847	0.412	11.020	20.185	10.628
	1961-1989	Q	5.729	6.792	1.867	5.161	9.224	6.137	5.348	5.394	9.082	8.802
		t	1968	1969	1968	1972	1969	1968	1965	1972	1972	1969
		p	0.131	0.045	0.994	0.204	0.001	0.085	0.191	0.181	0.0008	0.002
		R	6.167	7.727	3.700	7.209	9.224	6.394	7.135	6.452	9.807	8.802
		T1	10.807	-0.022	11.259	20.038	12.511	9.845	0.161	10.269	19.708	11.567
		T2	10.807	1.170	11.259	20.038	10.610	9.845	0.161	10.269	18.518	9.979

Table 2. Continued

Test	Period	Variable	Kruševac						Blace				
			T_{av}	W	S_p	S_m	A		T_{av}	W	S_p	S_m	A
Buishand test	1990-2018	Q	8.642	5.616	8.314	6.723	6.089		9.958	5.125	8.042	8.626	4.019
		t	2006	2006	1998	2006	2007		2006	2006	1998	2006	2007
		p	0.003	0.150	0.006	0.044	0.090		0.0004	0.229	0.009	0.002	0.492
		R	8.642	8.322	8.314	6.875	6.452		9.958	6.543	8.042	8.626	5.610
		T1	11.438	1.541	11.111	21.300	11.921		10.20	0.662	9.478	19.612	10.790
		T2	12.333	1.541	12.500	22.308	11.921		11.190	0.662	11.020	20.758	10.790
von Neumann test	1961-2018	N	0.789	1.415	1.504	0.973	1.475		0.966	1.511	1.709	1.058	1.715
		p	0.0001	0.012	0.028	0.0001	0.021		0.0001	0.030	0.137	0.001	0.133
	1961-1989	N	2.05	1.333	2.303	1.459	1.289		2.133	1.172	2.322	1.241	1.428
		p	0.556	0.033	0.796	0.063	0.022		0.647	0.009	0.804	0.014	0.053
	1990-2018	N	0.997	1.758	0.983	1.934	2.125		1.093	1.874	1.159	1.514	2.223
		p	0.002	0.254	0.001	0.421	0.637		0.005	0.374	0.009	0.087	0.721

Table 3. Homogenity test's statistic – Goč and Kopaonik

Test	Period	Variable	Goč					Kopaonik				
			T_{av}	W	S_p	S_m	A	T_{av}	W	S_p	S_m	A
Pettitt's test	1961-2018	Kt	663	528	485	706	310	766	589	644	790	237
		tc	1997	1987	1998	1986	2007	1984	1986	1980	1986	2007
		p	0.0001	0.0001	0.0003	0.0001	0.072	0.0001	0.0001	0.0001	0.0001	0.274
		T1	7.211	-1.785	6.608	15.265	8.672	2.621	-5.615	0.510	10.308	4.664
		T2	8.440	-0.306	7.950	16.803	8.672	4.665	-4.031	2.571	12.563	4.664
	1961-1989	Kt	57	106	29	88	145	199	113	120	149	62
		tc	1968	1969	1972	1973	1970	1976	1976	1980	1974	1974
		p	0.684	0.077	0.997	0.196	0.004	0.0001	0.047	0.030	0.003	0.587
		T1	7.179	-1.634	6.655	15.383	9.32	2.213	-5.856	0.510	9.879	4.345
		T2	7.179	-1.634	6.655	15.383	7.789	3.662	-4.885	2.178	11.020	4.345
	1990-2018	Kt	199	56	158	182	126	171	69	134	142	112
		tc	2006	2012	2005	2006	2008	2006	2012	1998	2006	2008
		p	0.0001	0.707	0.0006	0.0002	0.023	0.0001	0.459	0.011	0.004	0.051
		T1	7.571	-0.355	6.863	16.247	8.653	4.347	-4.062	1.622	12.141	4.983
		T2	8.928	-0.355	8.254	17.692	9.740	5.383	-4.062	3.175	13.333	4.983
SNH test	1961-2018	Tt	37.589	14.649	15.731	26.763	9.912	39.689	19.310	25.306	33.703	7.139
		t	2006	1987	2000	2006	2008	1980	1986	1980	1986	2008
		p	0.0001	0.001	0.0005	0.0001	0.019	0.0001	0.0001	0.0001	0.0001	0.158
		T1	7.324	-1.785	6.638	15.702	8.450	2.375	-5.615	0.510	10.308	4.664
		T2	8.928	-0.306	8.033	17.692	9.740	4.579	-4.031	2.571	12.563	4.664
	1961-1989	Tt	2.837	6.282	2.273	5.446	10.270	19.949	8.038	10.294	10.105	3.026
		t	1987	1969	1988	1986	1969	1978	1986	1980	1974	1973
		p	0.620	0.095	0.795	0.266	0.006	0.0001	0.032	0.014	0.012	0.589
		T1	7.179	-1.634	6.655	15.383	9.433	2.283	-5.615	0.510	9.879	4.345
		T2	7.179	-1.634	6.655	15.383	7.815	3.809	-3.733	2.178	11.020	4.345

Table 3. Continued

Test	Period	Variable	Goč					Kopaonik				
			T_{av}	W	S_p	S_m	A	T_{av}	W	S_p	S_m	A
SNH test	1990-2018	*Tt*	19.925	3.588	11.632	13.077	8.101	13.225	4.234	10.970	9.585	7.132
		t	2006	2012	2000	2006	2011	2006	2012	1998	2006	2008
		p	0.0001	0.503	0.003	0.007	0.034	0.0005	0.347	0.003	0.022	0.067
		T1	7.571	-0.355	6.591	16.247	8.732	4.347	-4.062	1.622	12.141	4.983
		T2	8.928	-0.355	8.033	17.692	9.957	5.383	-4.062	3.175	13.333	4.983
Buishand test	1961-2018	*Q*	20.773	14.666	14.307	19.286	9.331	23.004	16.789	18.369	22.179	8.671
		t	1998	1987	1998	1995	2007	1980	1986	1980	1986	1998
		p	0.0001	0.0003	0.0006	0.0001	0.0680	0.0001	0.0001	0.0001	0.0001	0.109
		R	20.773	14.666	14.307	19.286	15.192	23.004	16.789	18.369	22.180	9.960
		T1	7.218	-1.785	6.608	15.466	8.672	2.375	-5.615	0.510	10.308	4.664
		T2	8.487	-0.306	7.950	17.100	8.672	4.579	-4.031	2.571	12.563	4.664
	1961-1989	*Q*	3.741	6.355	1.508	3.895	8.125	11.877	6.515	8.135	8.706	4.741
		t	1968	1969	1988	1986	1969	1978	1976	1980	1974	1973
		p	0.585	0.072	0.999	0.521	0.008	0.0001	0.061	0.007	0.002	0.306
		R	6.398	6.355	2.705	7.368	8.125	11.877	6.611	8.135	9.218	6.788
		T1	7.179	-1.634	6.655	15.383	9.433	2.283	-5.421	0.510	9.879	4.345
		T2	7.179	-1.634	6.655	15.383	7.815	3.809	-5.421	2.178	11.020	4.345
	1989-2018	*Q*	12.049	4.205	9.190	9.761	7.308	9.816	4.568	8.398	8.357	6.973
		t	2006	2012	2005	2006	2008	2006	2012	1998	2006	2007
		p	0.0001	0.436	0.001	0.0001	0.016	0.0001	0.354	0.003	0.003	0.033
		R	12.049	5.281	9.190	9.761	9.424	9.816	5.248	8.398	8.357	7.891
		T1	7.571	-0.355	6.863	16.247	8.653	4.347	-4.062	1.622	12.141	4.567
		T2	8.928	-0.355	8.254	17.692	9.740	5.383	-4.062	3.175	13.333	5.664
von Neumann test	1961-2018	*N*	0.587	1.264	1.806	0.837	1.364	0.202	1.133	0.928	0.578	1.336
		P	0.0001	0.0009	0.237	0.0001	0.008	0.001	0.0001	0.0001	0.0001	0.004
	1961-1989	*N*	2.123	1.128	2.732	1.460	1.492	0.237	1.057	1.747	0.881	1.335
		P	0.637	0.006	0.981	0.064	0.081	0.0001	0.003	0.246	0.0001	0.038
	1990-2018	*N*	0.507	1.882	1.157	1.247	1.438	0.906	1.839	0.888	1.602	1.466
		p	0.0001	0.367	0.011	0.023	0.055	0.0005	0.335	0.0001	0.137	0.071

The Buishand range (BR) test is also a non-parametric test which checks the presence of a change point in the given data marking a change of the location parameter (average values) distribution. The null hypothesis H_0 implies data homogeneity in terms of the location parameter, i.e., absence of a change regarding the said parameter over time. The alternative hypothesis H_1 implies presence of a change-point involving an increase or decrease of the average value of the observed feature. The adjusted partial sum (S_k), that is, the cumulative deviation from mean for *k*th observation of a series *x1, x2, x3,….,xk,….xn* with mean $\bar{x}$ can be calculated using the following equation:

$$S_k = \sum_{i=1}^{k}(x_i - \overline{x}).$$

(6)

A series may be homogeneous without any change point if $Sk \cong 0$, because in random series, the deviation from mean will be distributed on both sides of the mean of the series. The significance of shift can be evaluated by computing rescaled adjusted range (R) using the following equation:

$$R = \frac{max(S_k) - min(S_k)}{\overline{x}}.$$

(7)

The computed value of $R = R/\sqrt{n}$ is compared with critical values given by *Buishand* (1982) and *Wijngaard et al.* (2003) and has been used for detection of possible change.

The standard normal homogeneity (SNH) test, is a statistical test which also checks if the data originate from the same population with the same distribution or indicate presence of a significant difference in the location parameter between the data before and after a specific change-point t_c bringing an increase or decrease of the value of the observed feature. The test statistic (T_t) is used to compare the mean of first t observations with the mean of the remaining (n-t) observations with n data points (*Alexandersson,* 1986; *Toreti et al.,* 2011; *Ming Kang and Yusof*, 2012; *Jaiswal et al.,* 2015):

$$T_t = tZ_1^2 + (n - t)Z_2^2,$$

(8)

$$Z_1 = \frac{1}{t}\sum_{i=1}^{t}\frac{x_i - \overline{x}}{\sigma},$$

(9)

$$Z_2 = \frac{1}{n-t}\sum_{i=t+1}^{n}\frac{x_i - \overline{x}}{\sigma},$$

(10)

where $\overline{x}$ and σ are the mean and standard deviations of the series. The year t can be considered as a change point and comprises a break where the value of T_t attains the maximum value. To reject the null hypothesis, the test statistics should be greater than the critical value, which depends on the sample size (n).

The von Neumann test (*Neumann,* 1941) also tests the null hypothesis H_0 implying data homogeneity in terms of the location parameter and absence of its change over the period of observation, as opposed to the alternative hypothesis H_1, which implies the presence of the moment t_c when the change of the location parameter occurs. If the alternative hypothesis is accepted, the von Neumann test

cannot pinpoint the moment t_c marking the change of the location parameter. The test statistics used in this test are as follows:

$$N = \frac{\sum_{i=1}^{n-1}(x_i - x_{i-1})^2}{\sum_{i=1}^{n}(x_i - \overline{x})^2}.$$

(11)

There are some differences between the SNH, BR, and Pettitt tests. SNH test is sensitive in detecting the breaks near the beginning and the end of the series. BR test and Pettitt test are easier to identify the break in the middle of the series. Besides, the SNH and BR tests assume X_i is normally distributed, whereas the Pettitt test does not need this assumption, because it is a non-parametric rank test (*Kang* and *Yusof*, 2012).

The trends in historical series of meteorological data have been assessed using the linear regression test and the Mann-Kendall test.

In the linear regression test, a straight line is adjusted to the data, and the slope of the line may or may not be significantly different from zero. For a series of observations *xi, i*=1, 2, 3,…,*n*, a straight line in the form of *y = a + bx* can be calculated as:

$$a = \frac{\sum X_i Y_i - \frac{1}{n}\sum X_i \sum Y_i}{\sum X_i^2 - \frac{1}{n}(\sum X_i)^2},$$

(12)

$$b = \frac{(\sum Y_i)(\sum X_i^2) - (\sum X_i)(\sum X_i Y_i)}{n \sum X_i^2 - (\sum X_i)^2},$$

(13)

where *y* is the temperature in °C, *a* and *b* are the intercept and slope of the fitted line, *x* is the time in years (*Jaiswal et al.,* 2015; *Gavrilov et al.,* 2016). This approach gives results which are simple to interpret; both graphically and analytically on the basis of the shape and parameters of the trend equation. The sign of the temperature trend depends on the value of the slope: when the slope is higher than zero, less than zero, or equal to zero, the sign of the trend is positive (increase), negative (decrease), or there is no trend (no change), respectively (*Gavrilov et al.,* 2015, 2016, 2018).

The statistical significance of the trend in annual and seasonal series was analyzed using the non-parametric Mann-Kendall (MK) test (*Mann,* 1945; *Kendall,* 1975). The MK test has been used in the analysis of a number of researchers to ascertain the presence of a statistically significant trend in hydrological climatic variables, such as temperature, precipitation, and

streamflow, for example: temperature: *Mohorji et al.,* 2017, temperature and precipitation *Jain et al.,* 2013; *Chattopadhyay* and *Edwards,* 2016; *Bhuyan et al.,* 2018; *Emmanuel et al.,* 2019; *Tan et al.,* 2019; *Mosase et al.,* 2019; *Panda* and *Sahu,* 2019; precipitation: *Kumar et al.* 2010; *Burić et al.,* 2015; *Hussain,* 2015; *Merabtene et al.,* 2016; *Kocsis et al.,* 2020; *Meena,* 2020; *Ramezani et al,* 2020; *Borse* and *Agnihotri,* 2020; precipitation and streamflow: *Da Silva et al.,* 2015; streamflow: *Radevski et al.,* 2018; temperature, precipitation, and flow: *Cherinet et al.,* 2019; evapotranspiration – *Sharma et al.,* 2020.

The MK test checks the null hypothesis of no trend versus the alternative hypothesis of the existence of increasing or decreasing trend (*Kumar et. al.,* 2010). A positive MK value indicates an increasing trend, while a negative MK value shows a decreasing trend. The Mann-Kendall statistics can be presented as:

$$S = \sum_{i=1}^{n-1} \sum_{j=i+1}^{n} sign(X_j - X_i), \tag{14}$$

where n is the total length of data, x_i and x_j are the time series of the annual and/or seasonal values of the temperatures in years $j = i + 1, i + 2, i + 3,...,n$ and $i = 1, 2, 3,..., n-1$, where $j > i$, and n is the last year in the time series. Function sign $(x_i–x_j)$ assumes the following values:

$$sign(X_j - X_i) = \begin{bmatrix} 1, if\,(X_j - X_i) > 0 \\ 0, if\,(X_j - X_i) = 0 \\ -1, if\,(X_j - X_i) < 0 \end{bmatrix}. \tag{15}$$

According to this test, the statistic S is approximately normally distributed with the mean $E(S)$ and the variance $Var(S)$ can be computed as follow (*Jaiswal et al.l,* 2015):

$$E[S = 0],$$

$$Var(S) = \frac{n(n-1)(2n+5) - \sum_{k=1}^{n} t_k(t_k-1)(2t_k+5)}{18}, \tag{16}$$

where n is the number of data in the time series, and t_k is the number of data in the kth tied group. (*Kocsis et al.,* 2020). The standardized statistics Z for this test can be calculated by the following equation:

$$Z = \begin{bmatrix} \frac{S-1}{\sqrt{Var(S)}}, if\,S > 0 \\ 0, if\,S = 0 \\ \frac{S+1}{\sqrt{Var(S)}}, if\,S < 0 \end{bmatrix}. \tag{17}$$

The positive values of Z indicate upward (increasing) trends in time series, and the negative values show downward (decreasing) trends. Trends are then tested against some critical values ($Z1-\alpha$) to show t whether they are statistically significant or not. For example, if $|Z| > Z1-\alpha$, (e.g., $Z1-\alpha$ at $\alpha = 0.05$); the null hypothesis of no-trend is rejected, and alternative hypothesis of a significant trend is accepted. In this study to represent the confidence level ***, **, *, and + signs have been used to represent 100%, 99%, 95%, and 90% levels of confidence, respectively.

The magnitude of the trend in the time series was determined using the Sen's slope test (*Sen*, 1968). The Sen's method assumes a linear trend in the time series and has been widely used for determining the magnitude of a trend in hydro-meteorological time series (*Hirsch et al.,* 1991; *Hussain et al.,* 2015; *Mahmood et al.,* 2019; *Cherinet et al.,* 2019; *Kocsis et al.,* 2020). In this method, the slopes (T_i) of all data pairs are first calculated by:

$$T_i = \frac{X_j - X_k}{j-k}, \text{ for } i = 1,2,..., N,$$ (18)

where x_j and x_k are data values at time j and k ($j>k$), respectively. The median of these N values of T_i is the Sen's estimator of slope, which is calculated as follows:

$$\beta = \left[\begin{array}{c} \frac{T_{N+1}}{2} \\ \frac{1}{2}\left(\frac{T_N}{2} + \frac{T_{N+2}}{2}\right) \end{array} \right].$$ (19)

A positive value of β indicates an upward (increasing) trend, while a negative value indicates a downward (decreasing) trend in the time series.

5. Results and discusion

In the present study, the first various change point tests, including the Pettitt's test, von Neumann's ratio test, Buishand's range test and SNH test, have been applied to detect a change point in annual and seasonal series of temperature in the Rasina River basin. For each of the tests, we failed to reject the null hypothesis when the estimated *p*-value was greater than the significance level of 0.05. After detecting the change point, the trend analysis was applied by using the linear regression and Mann-Kendall tests.

The test statistics of various tests and acceptance or rejection of null hypothesis for annual and seasonal temperatures are presented in *Tables 2* and *3*. *Figs. 2–5* show the change points of average annual and seasonal temperatures during the period 1961–2018.
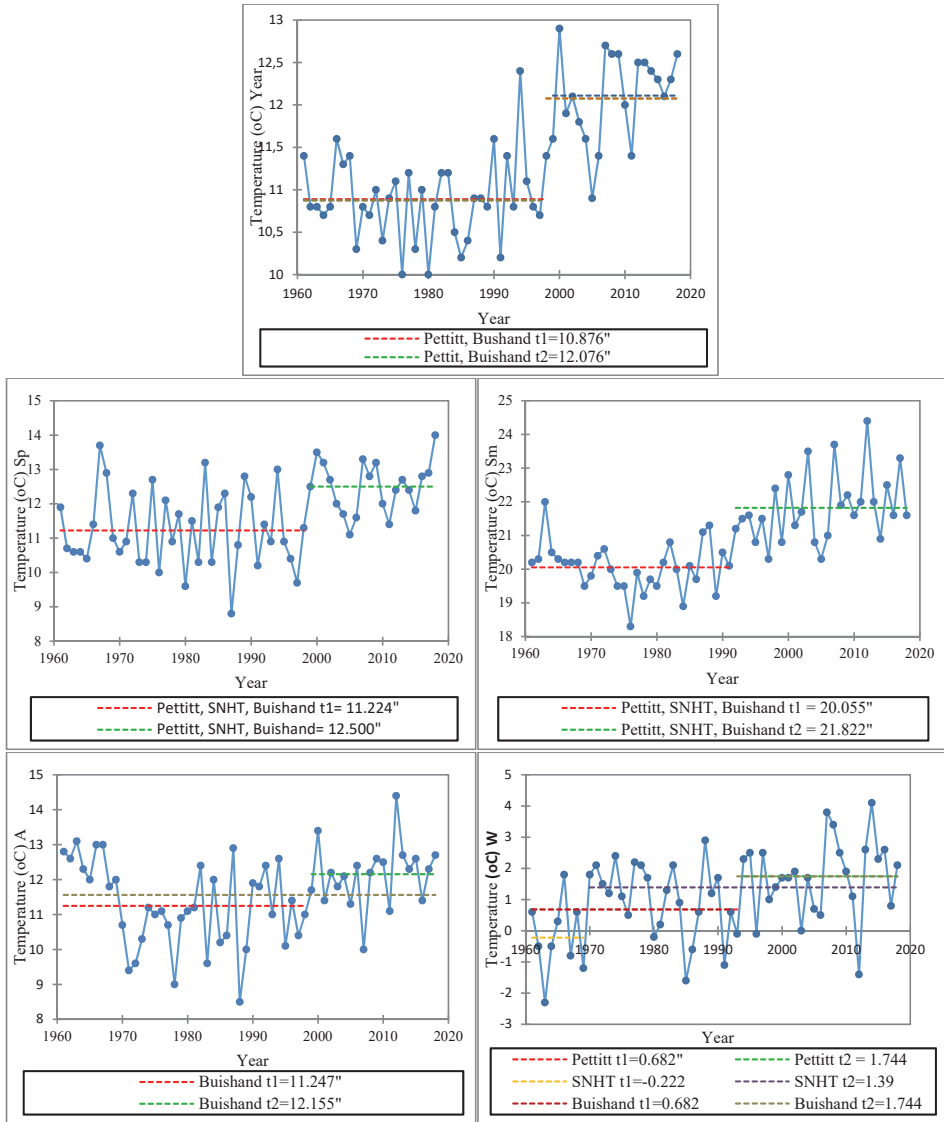
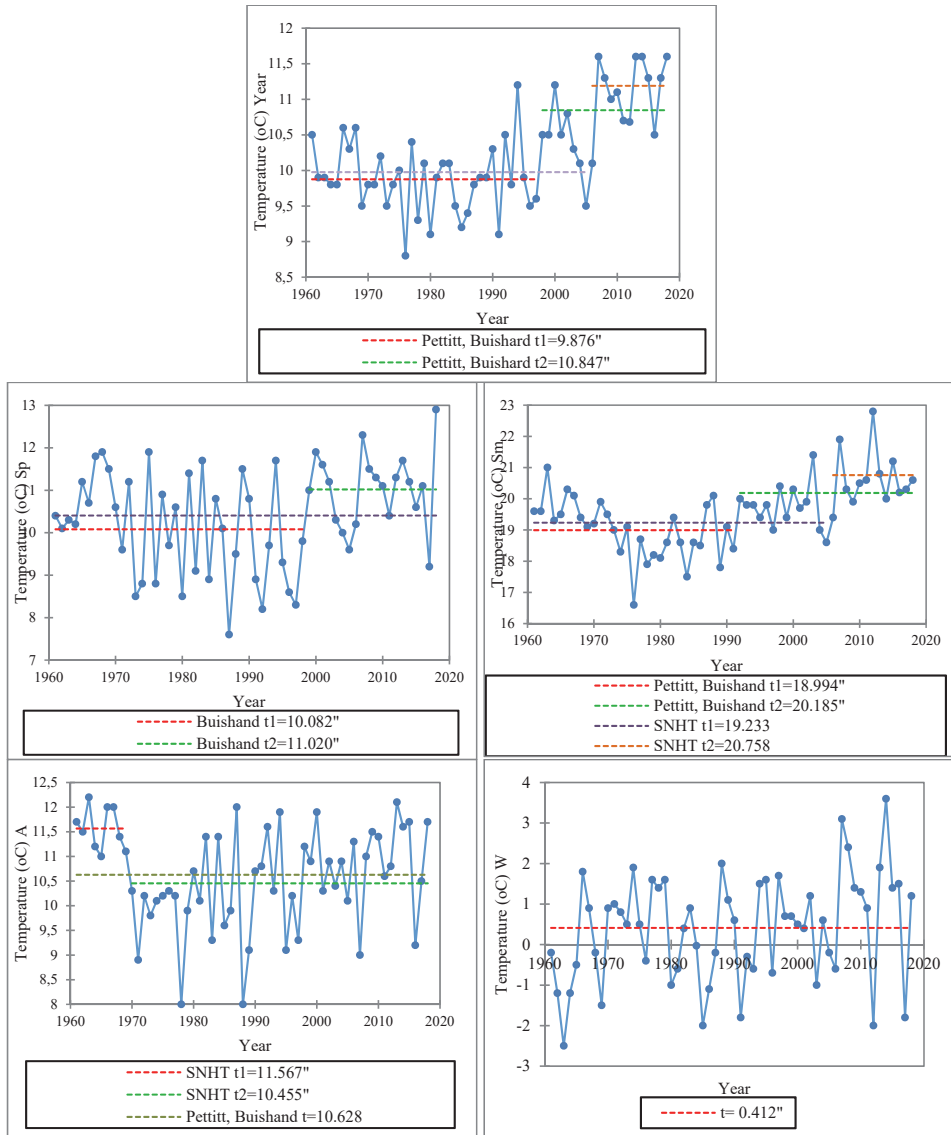*Fig. 2*. Change points of average annual and seasonal temperatures in Kruševac.

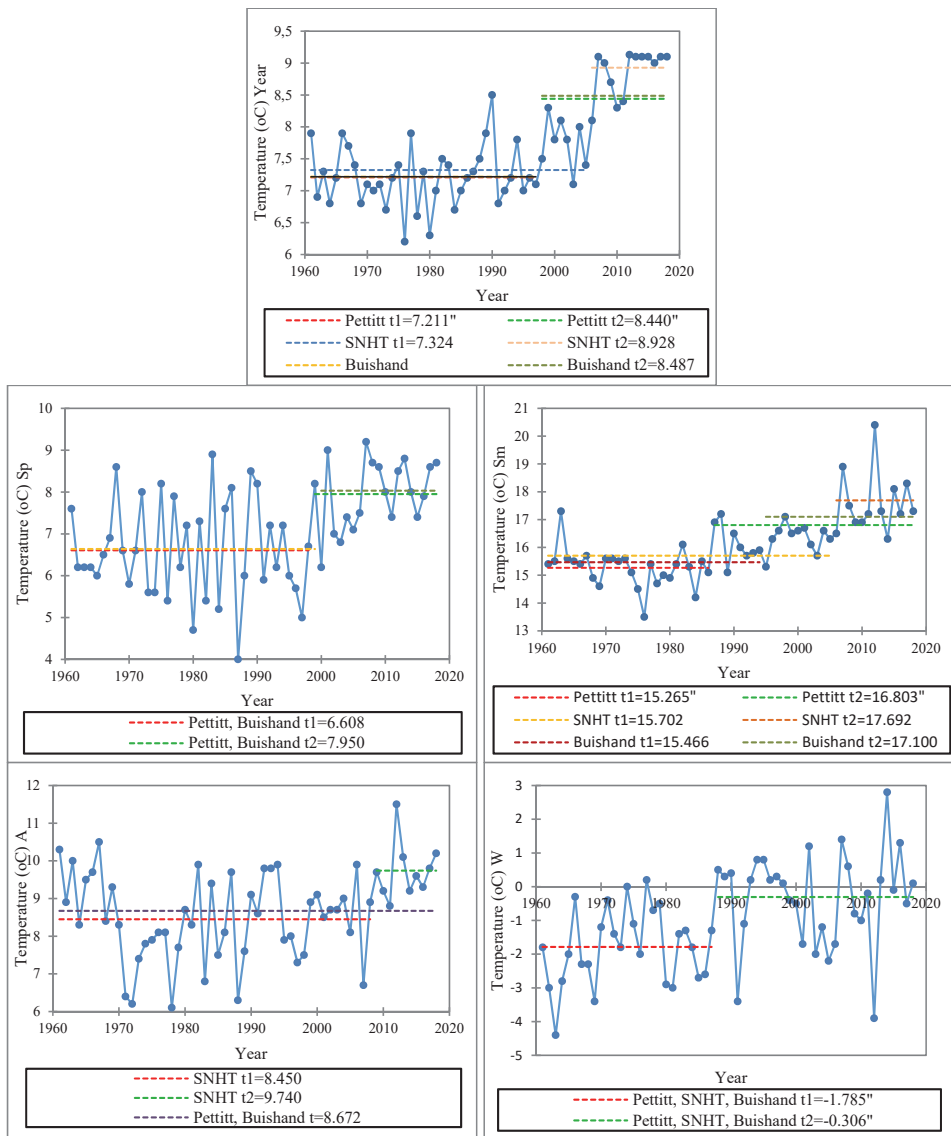*Fig. 3.* Change points of average annual and seasonal temperatures in Blace.

Fig. 4. Change points of of average annual and seasonal temperatures in Goč.
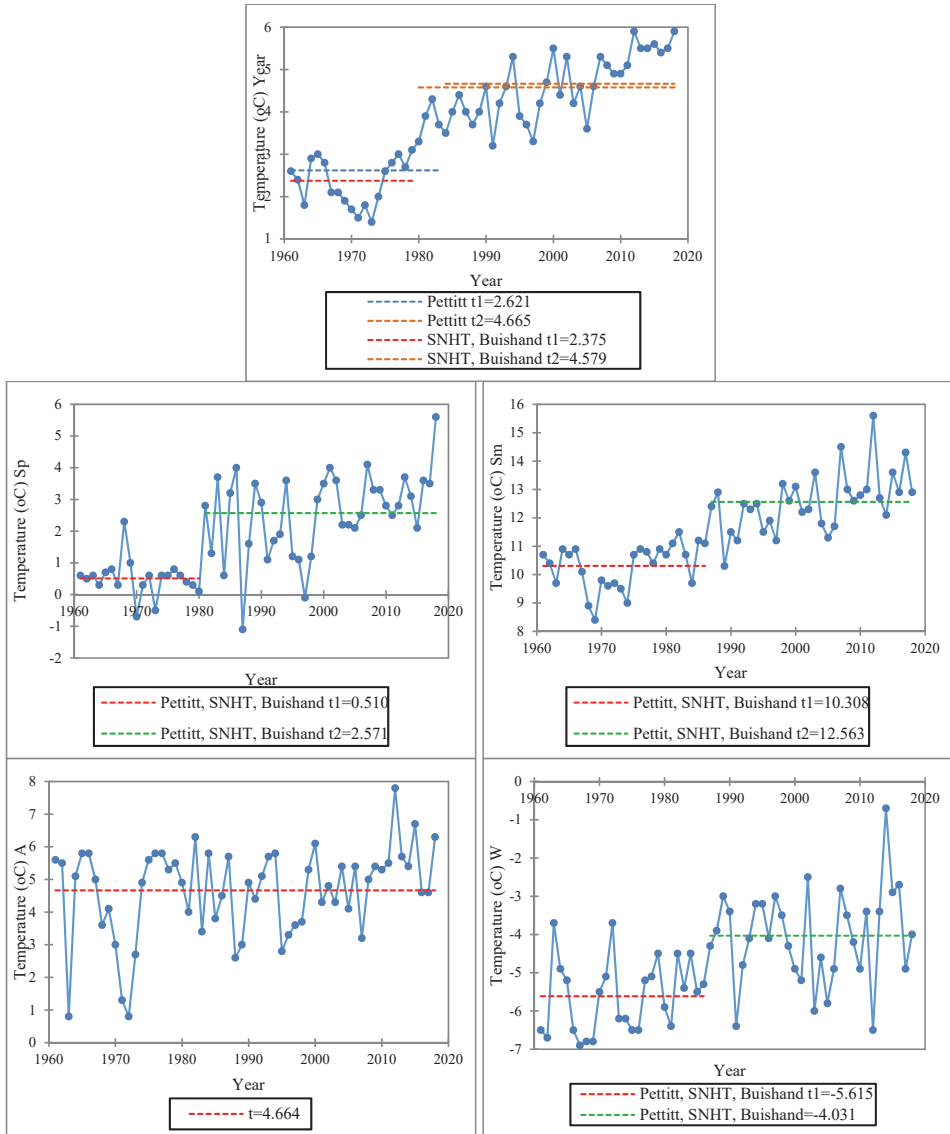
Fig. 5. Change points of of average annual and seasonal temperatures in Kopaonik.

The average annual, winter, summer, and spring temperature series in the period 1961–2018 on all the stations indicated a significant change point, except in Blace, where spring and winter data can be considered as homogeneous in nature. All the analyzed stations have passed the critical test value at a 95% significance level as a result of the application of Pettitt,SNH and Buishard tests.

The analysis results shown in *Tables 2* and *3* indicate that the inhomogeneous structure is generally observed between 1976 and 1984, between 1997 and 1998, and in 2006. All the tests on Kruševac and Blace stations indicate that the change in annual temperature occured in 1997, except for SNH test, which identifies the year of 1998 as a changing point in Kruševac and 2006 as a changing point in Blace. In the mountainous parts of the basin, on Goč station, the change in annual temperature occured in 1997 and 1998, according to the Pettitt's and Buishand tests, while in Kopaonik, the change in average temperature occured in 1980 and in 1984. The average annual temperature in the period 1961–2018 increased in Kruševac from 10.88 ºC to 12.08 ºC, in Blace from 9.88 ºC to 10.85 ºC, in Goč from 7.21 ºC to 8.44 ºC, whereas in Kopaonik it increased from 2.62 ºC to 4.67 ºC.

The Pettitt's and Buishand tests indicate an increase in average winter temperatures in Kruševac and Blace from 1993, while in Goč and Kopaonik, the increase started in 1987 and 1986.

The analysis of spring temperature confirmed that the change point may have occured in 1998 in Kruševac, Blace, and Goč, while it may have occurred in in 1980 in Kopaonik.

All the tests on Kruševac and Blace stations indicate that the change in the average summer temperature occured in 1991, except for the SNH test, which identifies the year of 2006 as a changing point in Blace. On the Kopaonik station, the change in the average summer temperature occurred in 1986. The average summer temperature in Kruševac increased from 20.06 ºC to 21.82 ºC, in Blace from 18.99 ºC to 20.19 ºC, in Goč from 15.27 ºC to 16.80 ºC, while in Kopaonik, it increased from 10.31 ºC to 12.56 ºC.

The results of the von Neumann test of homogeneity call for acceptance of the alternative hypothesis too, i.e., they lead to a conclusion that in the series of average annual temperatures there is a change point regarding the location parameter.

As the time series was 58-year-long, it was long enough to be divided it into two equal 29-year-long periods, in order to gain a better insight. The first half of the period occurred between 1961 and 1989, while the second occurred between 1990 and 2018.

In the first half of the period (1961–1989), all the tests indicated a significant change point in the average autumn temperatures in Kruševac, average autumn and summer temperatures in Blace and Goč, and average annual, winter, summer, and spring temperatures in Kopaonik.

All the tests on the Blace station indicate that a decrease of the average summer temperature occurred in 1972, while in Kopaonik, an increase of the summer temperature was observed from 1974. The average summer temperature in Blace decreased from 19.71 ºC to 18.52 ºC, and in Kopaonik increase from 11.02 ºC to 11.55 ºC.

In the second half of the period 1990–2018, all test in all stations detected year 2006 as changing point of the average annual and summer temperatures and

1998 as changing point of the annual spring temperature (except in Goč, where the change in annual spring temperature occured in 2005).

The main conclusions derived from the presented results are that the temperature is increasing with accelerated rate, with more pronounced increase in maximum temperatures, especially during the summer. According to the used data, the hottest year on the territory of the Rasina basin was 2000, while out of 10 hottest years, 9 have occurred since the year of 2000. The hottest summer was during 2012, same as on the territory of the whole Serbia (*Vuković et al.,* 2018). The mean annual temperature for the period of 1990–2018 increased by 1.3 ºC with respect to the period of 1961–1989. The highest increase of 1.5 ºC is recorded for the summer season. The season with the second highest increase in temperatures is spring.

These results may be the basis for the future analysis of the reasons for inhomogeneity in these stations and of the question whether the inhomogeneity of these stations are caused by variations of natural meteorological conditions or by other environmental conditions.

To determine a trend, the linear regression test and the Mann-Kendall test have been applied in the different series of meteorological variables. *Figs. 6–9* show annual and seasonal mean temperatures during the period 1961–2018 with three trend equations: above (1961–2018) and below (1961–1989 and 1990–2018); and three trend lines: for longer and two shorter periods, respectively.

In strictly formal terms, some trends can be observed in all cases. However, all the trends do not have the same sign, magnitude, and probability. To obtain a final evaluation of the temperature trends in the Rasina River basin, all the numerical parameters, visual representation of trends, and results of the MK test were used (*Gavrilov et al.,* 2015, 2016, 2018). The MK test statistics for annual and seasonal temperature are presented in *Tables 4–7*.

In the first period (1961–1989), the trend is negative for average annual, spring, summer, and autumn temperatures at all the stations, except Kopaonik. MK testing proves whether these statements are true. As the computed probability values p are greater than the significance level α in cases: Y-T_{av}, W, S_p, S_m (Kruševac), Y-T_{av}, S_m, W (Blace), Y-T_{av}, S_p, S_m,A (Goč), Y-T_{av}, W, S_p, S_m (Kopaonik), the H_0 cannot be rejected. Probability values p for A (Kruševac), S_p and A (Blace), W (Goč), and A (Kopaonik) are lower than α, so the H_0 should be rejected, and the H_a should be accepted for all of these cases. The MK test indicated a non-significant decrease in the trend of the annual temperature in Kruševac, Blace, and Goč and significant increase in the trend of the annual temperature in Kopaonik.

The average annual and seasonal temperatures in the second period (1990–2018) show a positive trend at all the stations. The MK test indicated a significant increase in temperature during all the seasons in Kruševac, in spring and summer in Blace and Goč, and during spring, summer, and autumn in Kopaonik, with very high certainty (α=0.005-0.0001). The annual temperature exhibits an increasing

trend from 0.5 ºC/decade in Kruševac and Blace, 0.8 ºC/decade in Goč and 0.7 ºC/decade in Kopaonik. Spring mean temperature increased from 0.7 ºC/decade in Kruševac and Blace, 0.9 ºC/decade in Goč, and 0.8 ºC/decade in Kopaonik, while summer temperature increased from 0.5 ºC/decade in Kruševac and Blace, 0.6 ºC/decade in Goč and Kopaonik.
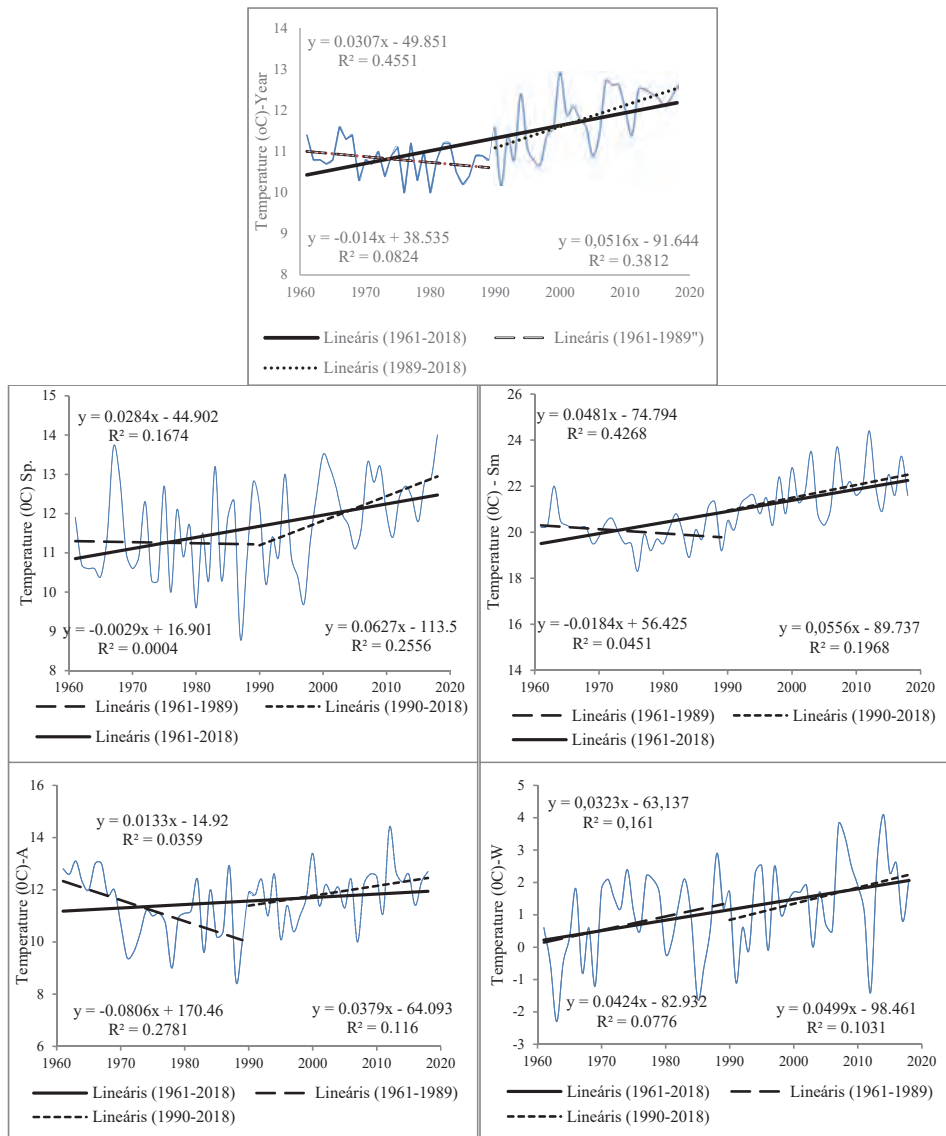

Fig. 6. Average annual and seasonal temperatures, trend equations, and trend lines for Kruševac.
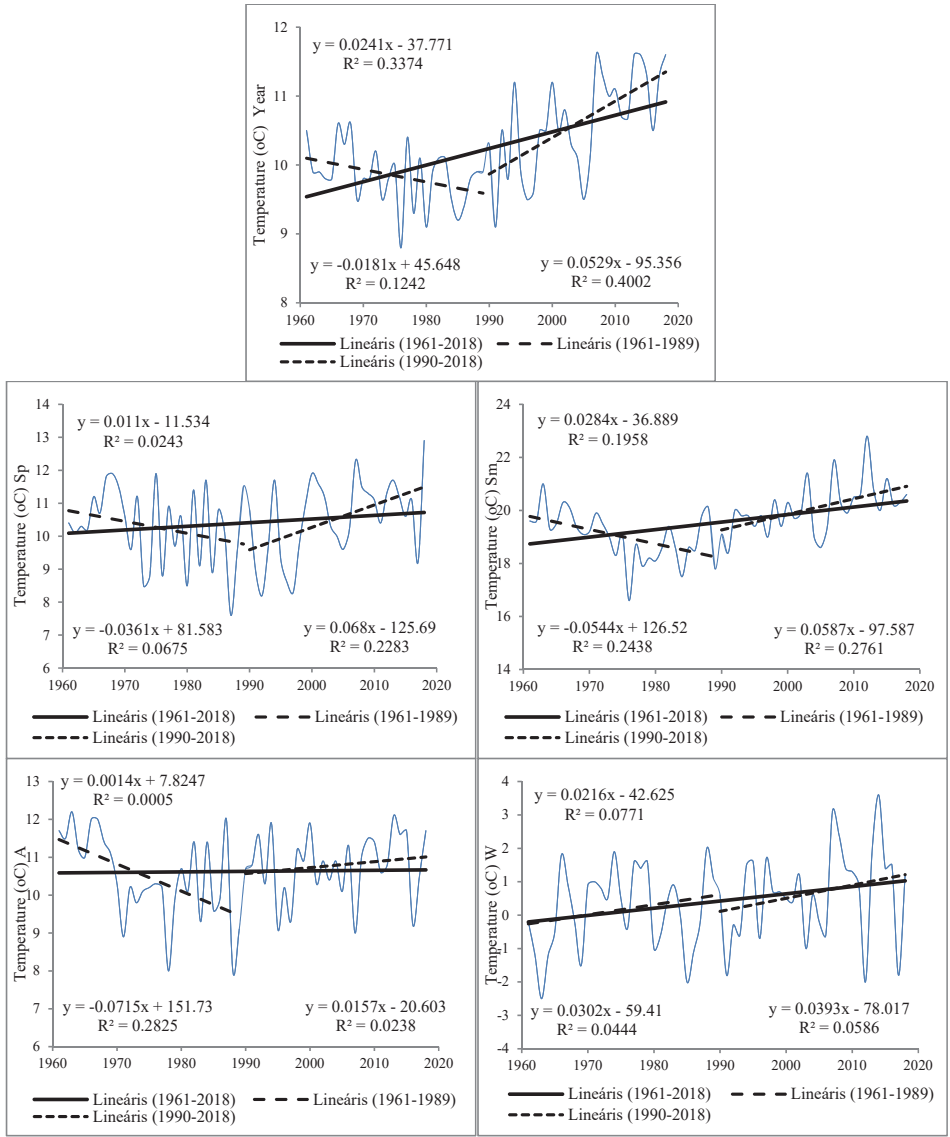
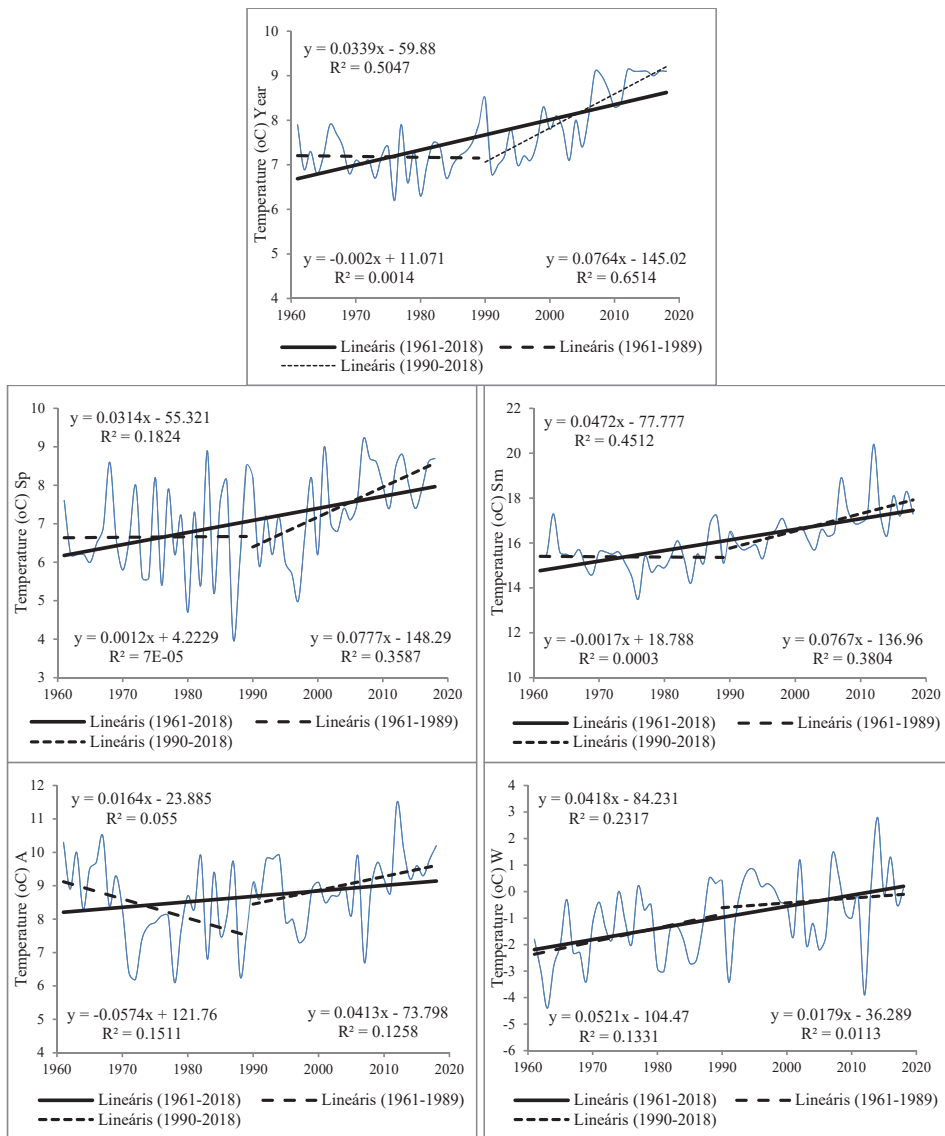*Fig. 7.* Average annual and seasonal temperatures, trend equations, and trend lines for Blace.

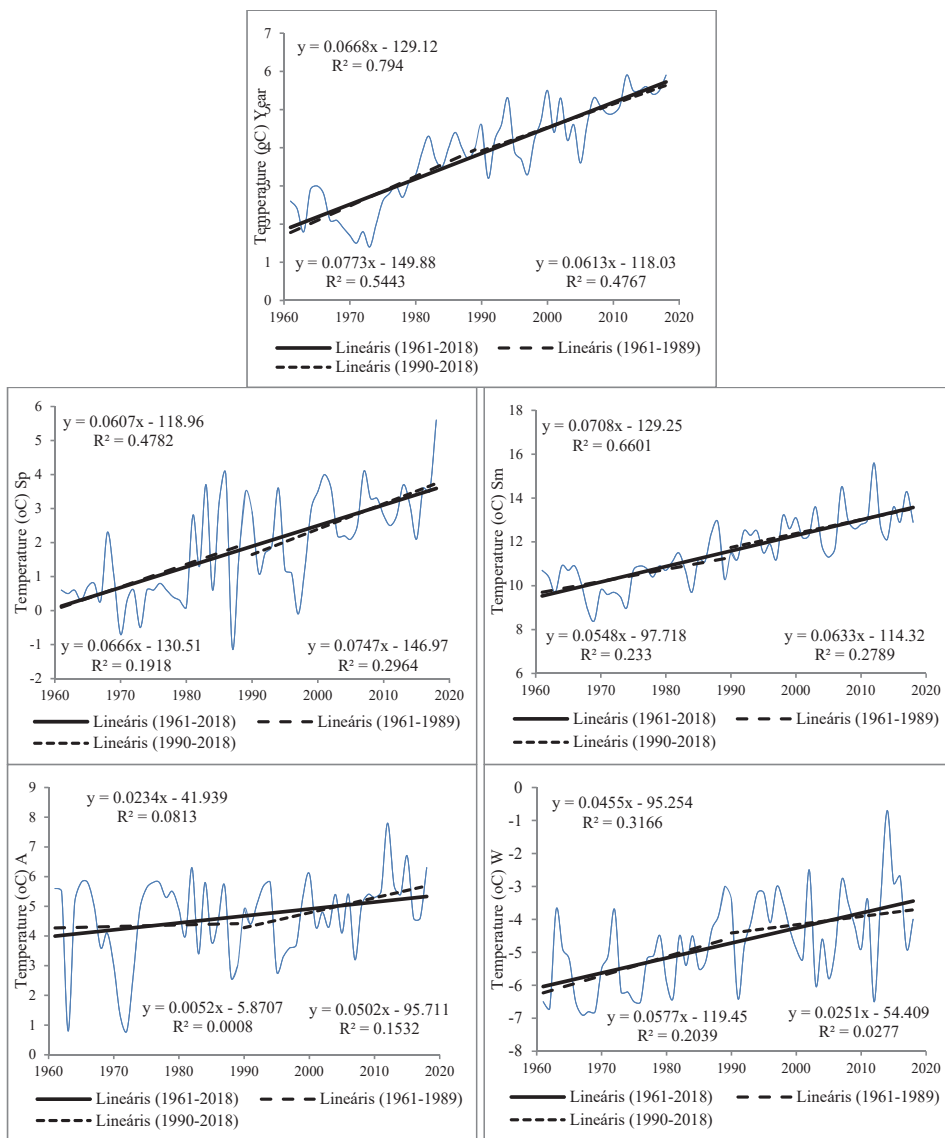*Fig. 8.* Average annual and seasonal temperatures, trend equations, and trend lines for Goč.

Fig. 9. Average annual and seasonal temperatures, trend equations and trend lines for Kopaonik.

Table 4. Man – Kendall test's statistics for Kruševac

Period		Min.	Max.	Mean	St.dev.	Z – value of trend	B	Sen's slope	α – level of significance
1961–2018	T_{av}	10.0	12.9	11.31	0.769	4.86	10.53	0.030	***
	W	-2.3	4.1	1.140	1.359	3.01	0.37	0.032	**
	S_p	8.8	14.0	11.66	1.174	3.08	10.76	0.029	**
	S_m	18.3	24.4	20.88	1.243	5.16	19.68	0.043	***
	A	8.5	14.4	11.56	11.560	1.44	11.31	0.014	-
1961–1989	T_{av}	10.0	11.6	10.8	0.417	-1.13	11.07	-0.14	-
	W	-2.30	2.90	0.74	1.295	1.17	0.34	0.038	-
	S_p	8.80	13.70	11.26	1.161	-0.21	10.94	-0.002	-
	S_m	18.30	22.0	20.04	0.738	-1.53	20.32	-0.024	-
	A	8.50	13.10	11.20	1.302	-2.80	12.53	-0.091	**
1990–2018	T_{av}	10.20	12.90	11.814	0.712	2.94	11.12	0.053	**
	W	-1.40	4.10	1.54	1.323	1.88	0.91	0.056	+
	S_p	9.70	14.0	12.07	1.055	2.44	11.12	0.065	*
	S_m	20.10	24.40	21.72	1.067	2.61	20.89	0.053	**
	A	10.0	14.40	11.92	0.948	2.09	11.54	0.037	*

*** - α=0.001 ; ** - α=0.01; * - α=0.05; + - α=0.1

Table 5. Man – Kendall test's statistics for Blace

Period		Min.	Max.	Mean	St.dev.	Z – value of trend	B	Sen's slope	α – level of significance
1961–2018	T_{av}	8.8	11.6	10.23	0.701	4.13	9.62	0.023	***
	W	-2.5	3.6	0.41	1.316	1.93	-0.08	0.023	+
	S_p	7.6	12.9	10.41	1.195	1.09	10.39	0.012	-
	S_m	16.6	22.8	19.55	1.083	3.30	18.90	0.025	***
	A	8.0	12.2	10.63	1.019	0.28	10.68	0.002	-
1961–1989	T_{av}	8.8	10.6	9.84	0.438	-1.57	10.03	-0.178	-
	W	-2.5	2.0	0.16	1.219	0.98	-0.20	0.030	-
	S_p	7.6	11.9	10.27	1.184	-0.94	10.85	-0.030	-
	S_m	16.6	21.0	19.01	0.939	-3.10	19.69	-0.055	**
	A	8.0	12.2	10.47	1.146	-3.16	11.49	-0.080	**
1990–2018	T_{av}	9.1	11.6	10.61	0.712	3.36	10.05	0.05	***
	W	-2.	3.6	0.66	1.381	1.31	0.31	0.043	-
	S_p	8.2	12.9	10.54	1.211	2.16	9.50	0.066	*
	S_m	18.4	22.8	20.07	0.952	3.08	19.27	0.052	**
	A	9.0	12.1	10.79	0.865	1.18	10.62	0.237	-

*** - α=0.001; ** - α=0.01; * - α=0.05; + - α=0.1

Table 6. Man – Kendall test's statistics for Goč

Period		Min.	Max.	Mean	St.dev.	Z – value of trend	B	Sen's slope	α – level of significance
1961–2018	T_{av}	6.2	9.13	7.66	0.807	5.33	6.7	0.033	***
	W	-4.4	2.8	-0.99	1.468	3.65	-2.27	0.043	***
	S_p	4.0	9.2	7.07	1.240	3.24	6.15	0.032	**
	S_m	13.50	20.40	16.11	1.186	5.68	14.83	0.043	***
	A	6.10	11.50	8.67	1.179	1.86	8.16	0.020	+
1961–1989	T_{av}	6.20	7.90	7.18	0.453	0.09	7.20	0	-
	W	-4.40	0.50	-1.63	1.216	1.78	-2.43	0.051	+
	S_p	4.0	8.90	6.66	1.245	-0.11	6.50	0	-
	S_m	13.50	17.30	15.38	0.797	-0.77	15.51	-0.008	-
	A	6.10	10.50	8.32	1.258	-2.14	8.98	-0.059	*
1990–2018	T_{av}	6.80	9.13	8.13	0.806	4.70	6.83	0.083	***
	W	-3.90	2.80	-0.36	1.435	0	0.10	0	-
	S_p	5.0	9.20	7.49	1.105	3.16	6.14	0.085	**
	S_m	15.30	20.40	16.84	1.059	3.99	15.82	0.064	***
	A	6.70	11.50	9.03	0.992	2.24	8.33	0.048	*

*** - α=0.001 ; ** - α=0.01; * - α=0.05; + - α=0.1

Table 7. Man – Kendall test's statistics for Kopaonik

Period		Min.	Max.	Mean	St.dev.	Z – value of trend	B	Sen's slope	α – level of significance
1961–2018	T_{av}	1.4	5.9	3.82	1.266	7.89	1.90	0.067	***
	W	-6.9	-0.7	-4.74	1.365	4.53	-6.05	0.048	***
	S_p	-1.1	5.6	1.86	1.483	5.30	0.05	0.058	***
	S_m	8.4	15.6	11.50	1.471	7.04	9.57	0.067	***
	A	8.5	14.4	11.56	11.560	1.44	11.31	0.014	-
1961–1989	T_{av}	1.4	4.4	2.86	0.893	3.95	1.63	0.083	***
	W	-6.9	-3.0	-5.42	1.089	2.60	-6.50	0.063	**
	S_p	-1.1	4.0	1.03	1.295	1.76	0.21	0.039	+
	S_m	8.4	12.9	10.47	0.966	2.45	9.85	0.05	*
	A	0.8	6.3	4.34	1.585	-0.38	5.02	-0.006	-
1990–2018	T_{av}	3.2	5.9	4.78	0.756	4.07	3.70	0.067	***
	W	-6.5	-0.7	-4.06	1.286	0.58	-4.19	0.016	-
	S_p	-0.1	5.6	2.69	1.168	2.67	1.48	0.075	**
	S_m	11.2	15.6	12.63	1.021	2.80	11.64	0.055	**
	A	2.8	7.8	4.98	1.093	2.09	4.35	0.05	*

*** - α=0.001 ; ** - α=0.01; * - α=0.05; + - α=0.1

The trend pattern indicated a significant increase in the average annual, winter, and summer temperatures in the whole series from 1961 to 2018 at all the stations. Statistical significant increase is also detected in spring in Kruševac, Goč and Kopaonik. The annual temperature for the Rasina River basin exhibits an increasing trend of annual temperature from 0.2ºC / decade in Kruševac, 0.3 ºC/decade in Blace and Goč and 0.7 ºC/decade in Kopaonik. The spring mean temperature increased from 0.3 ºC/decade in Kruševac and Goč, to 0.6 ºC/decade in Kopaonik. The summer temperature increased from 0.4 ºC/decade in Kruševac and Goč, 0.3 ºC/decade in Blace, and 0.7 ºC/decade in Kopaonik. In the analyzed period, a significant increase in winter temperature from 0.3 ºC/decade in Kruševac, 0.2 ºC/decade in Blace, 0.4 ºC/decade in Goč, and 0.5 ºC/decade in Kopaonik was observed. The autumn temperature showed statistically significant increase of 0.2 ºC/decade only in Goč.

Higher temperatures occurred at the beginning and the end of the period, while lower temperatures occurred in the middle of the period from the 1970s until the mid-1980s. Our results are in accordance with the results of *Unkašević* and *Tošić* (2009) and *Gavrilov et al.,* (2015, 2016). Analyzing the temperature data from 1949 to 2007 and from 1949–2013, they found that the slow decrease in the summer temperatures until 1975 was followed by temperature increase that lasted until the end of the analyzed periods (Serbia).

Similar results in temperature changes were observed in the neighboring areas. According to a report of the *Slovenian Environment Agency* (2011), in the period 1961–2011, the most significant change of climate in Slovenia is the increase of the mean air temperature by about 0.36 °C per decade. The most evident warming is observed in spring and summer, which is about 0.4 or 0.5 °C per decade in most of Slovenia. Conversely, the autumn temperature change is not statistically significant.

Chenkova and *Nikolova* (2015) found that the trend of the seasonal air temperature for the period 1984-2010 in Bulgaria is positive. A statistically significant positive trend was observed during the summer season with the values of 0.7 ºC to 0.8 ºC/decade. *Croitoru et al.* (2011) found that increasing average trend slopes for four summit stations in the Romanian Carpathians amount to 0.683 °C / decade.

6. Conclusion

The variability of temperature, due to the change in the climate or due to human involvement can influence different human activities: agriculture, planning and managing water resources, tourism, and ecosystems. In the present study, change point detections followed by trend analyses have been carried out using different non-parametric statistical tests.

On the basis of the statistical tests used, it can be concluded that there is a change point marking occurrence of an increase in the average annual and seasonal air temperatures in the Rasina River basin. Depending on the test used, different values regarding the year of temperature break have been obtained. The results of the Pettitt and Buishard range tests show, that the change points in the annual temperature data in the period 1961–2018 were identified in 1997 and 1998 at all the stations, except Kopaonik, where the change in the annual temperature occurred in 1980 and 1984. The SNH test identifies 2006 as the year of changing point in Blace. *Piticar* and *Ristoiu* (2012) obtained similar results for the temperatures in Romania, where 1988, 1995, and 1998 were detected as break-point years. The obtained results are also compliant with numerous other researches carried out in Europe.

Except for the average annual temperatures, an increasing trend was observed in the average winter, spring, and summer temperatures. The Pettitt's and Buishand tests indicate increase of average winter temperatures in Kruševac and Blace from 1993, while in Goč and Kopaonik, the increase started in 1987 and 1986. For spring temperatures, the change point may have occurred in 1998 in Kruševac and Blace, while it occurred in in 1980 Goč and Kopaonik. At the Kopaonik station, the change in the average summer temperature occured in 1986, while at all other stations, the years of change were 1991 and 2006.

In the first half of the period 1961–1989 all the tests indicate a significant change point in the average autumn temperature in Kruševac, in the average autumn and summer temperatures in Blace and Goč, and in the average annual, winter, summer and spring temperatures in Kopaonik. All tests in Blace indicate that the decrease in the average summer temperature occured in 1972, while in Kopaonik, an increase of the summer temerature was observed from 1974.

In the second half of the period (1990–2018) all the tests in all the stations detect 2006 as a changing point in average annual and summer temperatures and 1998 and 2005 as changing points in annual spring temperature.

The whole data trend on annual basis showed a positive increasing trend. The analysis indicated that the average annual, winter and summer temperature, have significant increasing trends due to positive values of both Z and Sen's statistics in the longer period (1961–2018) and in the second part of the period 1990–2018. In the first part of the period 1961–1989, the autumn temperatures in Kruševac, summer and autumn in Blace, as well as winter and autumn temperatures in Goč showed a significant decreasing trend due to the negative value of Z and Sen's statistics. All the other seasons have a non-significant decreasing trend. The exception is the Kopaonik station, where the average annual spring and summer temperatures show a positive increasing trend, while winter temperatures shows a significant decreasing trend.

The effects of climate change may exacerbate the existing social and economic states across the country, mainly where people are reliant on resources

sensitive to climate variability. Improved capacity to cope with future climate variability extremes can lessen the extent of economic and social losses.

The results of this research can be helpful for further analysis of temperature changes and other climatic elements, primarily from the aspect of their impact on natural resources and human activities.

References

Alexandersson, H.A., 1986: Homogeneity Test Applied to Precipitation Data, *J. Climatol. 6,* 661–675. https://doi.org/10.1002/joc.3370060607

Alexandrov, V., Schneider, M., Koleva, E.J., and *Moisselin, J.M.,* 2004: Climate variability and change in Bulgaria during the 20th century. *Theor. Appl. Climatol. 79,* 133–149. https://doi.org/10.1007/s00704-004-0073-4

Bhuyan, I.D., Islam, M., and *Khalil Bhuiyan, E.,* 2018: A Trend Analysis of Temperature and Rainfall to Predict Climate Change for Northwestern Region of Bangladesh, *Amer. J. Climate Change 7,* 115–134. https://doi.org/10.4236/ajcc.2018.72009

Borse, K. and *Agnihotri, G. P.,* 2020: Trends of Rainfall, Temperature and Rice Yield of Nashik Region of Maharashtra, *Int. J. Innov. Technol. Explor. Engineer. 9,* 395–398. https://doi.org/10.35940/ijitee.E2276.039520

Brunetti, M., Buffoni, L., Mangianti, F., Maugeri, M., and *Nanni, T.,* 2004: Temperature, precipitation and extreme events during the last century in Italy. *Glob. Planet. Change 40,* 141–149. https://doi.org/10.1016/S0921-8181(03)00104-8

Buishand, T.A., 1982: Some Methods for Testing the Homogeneity of Rainfall Data, *J. Hydrol. 58,* 11–27. https://doi.org/10.1016/0022-1694(82)90066-X

Burić, D., Luković, J., Bajat, B., Kilibarda, M., and *Živković, N.,* 2015: Recent trends in daily rainfall extremes over Montenegro (1951–2010), *Nat. Hazards Earth Syst. Sci. 15,* 2069–2077. https://doi.org/10.5194/nhess-15-2069-2015

Chattopadhyay, S. and *Edwards, R.D.,* 2016: Long-Term Trend Analysis of Precipitation and Air Temperature for Kentucky, United States. *Climate 4(10),* 1–15. https://doi.org/10.3390/cli4010010

Chenkova, N. and *Nikolova, N.,* 2015: Air temperature and precipitation variability in Northeastern Bulgaria on the background of climate change, *Thermal Sci. 19, Suppl. 2,* 381–390. https://doi.org/10.2298/TSCI150430104C

Cherinet, A.A., Yan, D, Wang, H., Song, X., Qin, T., Kassa, T.M., Girma, A., Dorjsuren, B., Gedefaw, M., Wang, H., and *Yadamjav, O.,* 2019: Climate Trends of Temperature, Precipitation and River Discharge in the Abbay River Basin in Ethiopia. *J. Water Resour. Protect. 11,* 1292–1311. https://doi.org/10.4236/jwarp.2019.1110075

Slovenian Environment Agency, 2011: Climate change and variability in Slovenia in the period 1961–2011., 2011, Summary, Ministry of the Environment and Spatial Planning, Ljubljana, 4-7.

Croitoru, A.E., Drignei, D., Holobaca, J.H., and *Dragota, C.S.,* 2011: Change-point analysis for serially correlated summit temperatures in the Romanian Carpathians. *Theor. Appl. Climatol. 108,* 9–18. https://doi.org/10.1007/s00704-011-0508-7

Da Silva, R.M., Santos, A.G.C., Moreira, M., Corte Real, J., Silva C.L.V., and *Medeiros C.I.,* 2015: Rainfall and river flow trends using Mann–Kendall and Sen's slope estimator statistical tests in the Cobres River basin, *Nat. Hazards 77,* 1205–1221. https://doi.org/10.1007/s11069-015-1644-7

Dimitrijević, Lj., 2010: Hidrogeografska studija reke Rasine, Magistarski rad, Geografski fakultet, Univerzitet u Beogradu.

Ducić, D., Luković, J., and *Milovanović, B.,* 2009: Promene temperature i padavina u Srbiji u drugoj polovini XX veka u sklopu globalnih klimatskih promena, *Zaštita prirode, 60,* 1-2, 541–652.

Emmanuel, L.A., Hounguè, N.R., Biaou, C.A., and *Badou, D.F.,* 2019: Statistical Analysis of Recent and Future Rainfall and Temperature Variability in the Mono River Watershed (Benin, Togo), *Climate 7(8);* 1–17. https://doi.org/10.3390/cli7010008

Gavrilov, B.M., Marković, B.S., Jarad, A., and *Korać,M.V.,* 2015: The analysis of temperature trends in Vojvodina (Serbia) from 1946 to 2006, *Thermal Sci. 19,* 339–350. https://doi.org/10.2298/TSCI150207062G

Gavrilov, B.M., Tošić, I., Marković, B.S., Unkašević, M., and *Petrović, P.,* 2016: Analysis of annual and seasonal temperature trends using the Mann-Kendall test in Vojvodina, Serbia. *Időjárás 120,* 183–198.

Gavrilov, M., Marković,S., Janc, N., Nikolić, M., Valjarević, A., Komac, B., Zorn, M., Punišić,M., and *Bačević, N.,* 2018: Assessing average annual air temperature trends using the Mann-Kedell test in Kosovo, *Acta Geographica Slovenica, 58,* 7–25. https://doi.org/10.3986/AGS.1309

Hadi, J.S. an*d Tombul, M.,* 2018: Long-term spatiotemporal trend analysis of precipitation and temperature over Turkey. *Meteoeological 25,* 445–455. https://doi.org/10.1002/met.1712

Hirsch, R.M., Alexander, R.B., and *Smith R.A.,* 1991: Selection of methods for the detection and estimation of trends in water quality. *Water Resour. Res. 27,* 803–813. https://doi.org/10.1029/91WR00259

Hussain, F., Nabi, G., and *Boota, W.M.,* 2015: Rainfall trend analysis by using the Mann-Kendell test and Sen's slope estimates: a case study of district Chakwal Rain gauge, Barani area, Northern Punjab province, Pakistan, *Sci.Int.(Lahore) 27,*3159–3165.

IPCC. Climate Change 2013: The Physical Science Basis. Contribution of Working Group I to the Fifth Assessment Report of the Intergovern-mental Panel on Climate Change 1535. Cambridge University Press, Cambridge, United Kingdom and New York, NY, USA, 2013.

Jain, K.S., Kumarbc, V., and *Sahariad, M.,* 2013: Analysis of rainfall and temperature trends in northeast India. *Int. J. Climatol. 33,* 968–978. https://doi.org/10.1002/joc.3483

Jaiswal, K.R., Lohani, K.A., and *Tiwari, L.H.,* 2015: Statistical Analysis for Change Detection and Trend Assessment in Climatological Parameters. *Environ. Process, 2,* 729–749. https://doi.org/10.1007/s40710-015-0105-3

Javari, M., 2016: Trend and Homogeneity Analysis of Precipitation in Iran. *Climate*, *4*(3), 44. https://doi.org/10.3390/cli4030044

Kang, M.H. and *Yusof, F*., 2012: Homogeneity Tests on Daily Rainfall Series in Peninsular Malaysia, *Int. J. Contemp. Math. Sci. 7,* 9–22.

Kendall, M.G., 1975: Rank correlation methods, 4th ed. Charles Griffin, London.

Kocsis, T., Kovács-Székely, I., and *Anda, A.,* 2020: Homogeneity tests and non-parametric analyses of tendencies in precipitation time series in Keszthely, Western Hungary. *Theor. Appl. Climatol. 139,* 849–859. https://doi.org/10.1007/s00704-019-03014-4

Kumar, V., Jain, K.S., and *Singh, Y.,* 2010: Analysis of long-term rainfall trends in India. *Hydrol. Sci. J. 55,* 484–496. https://doi.org/10.1080/02626667.2010.481373

Lionello, P., Abrantes, F., Gacic, M., Planton, S., Trigo, R., and *Ulbrich, U.,* 2014: The climate of the Mediterranean region: research progress and climate change impacts, *Reg. Environ. Change 14,* 1679–1684. https://doi.org/10.1007/s10113-014-0666-0

Mahmood, R., Jia, S., and *Zhu, W.,* 2019: Analysis of climate variability, trends, and prediction in the most active parts of the Lake Chad basin, Africa, *Sci. Rep. 9, 6317,* 1–18. https://doi.org/10.1038/s41598-019-42811-9

Mann, H.B., 1945: Non-parametric tests against trend. *Econometrica 13,* 245–259. https://doi.org/10.2307/1907187

Malinović-Milicević, S., Radovanović, M., Stanojević, G., and *Milovanović, B.,* 2016: Recent changes in Serbian climate extreme indices from 1961 to 2010, *Theor. Appl. Climatol, 124,* 1089–1098. https://doi.org/10.1007/s00704-015-1491-1

Meena, M., 2020: Rainfall Statistical Trend and Variability Detection Using Mann-Kendall Test, Sen's Slope and Coefficient of Variance - A Case Study of Udaipur District (1957-2016). *Appl. Ecol. Environ. Sci. 8,* 34–37.

Merabtene, T., Siddique, M., and Shanableh, A., 2016: Assessment of Seasonal and Annual Rainfall Trends and Variability in Sharjah City, UAE. *Hindawi Publ. Corpor. Adv. Meteorol. 3*, 1–13. https://doi.org/10.1155/2016/6206238

Milošević, D., Savić, S., Stankov, U., Žiberna, I., Pantelić, M., Dolinaj, D., and Leščešen, I., 2017: Maximum temperatures over Slovenia and their relationship with atmospheric circulation patterns. *Geografie 122*, 1–20. https://doi.org/10.37040/geografie2017122010001

Moberg, A., Jones, P., Lister, D., Walther, A., Brunet, M., Jacobeit, J., Alexander, L., Della-Marta, P., Luterbacher, J., Yiou, P., Chen, D., Klein Tank, A., Saladie, O., Sigro, J., Aguilar, E., Alexandersson, H., Almarza, C., Auer, I., Barriendos, M., Begert, M., Bergstrom,H., Bohm, R., Butler,C. J., Caesar, J., Drebs, A., Founda, D., Gerstengarbe, F.W., Micela, G., Maugeri, M., Osterle, H., Pandzic, K., Petrakis, M., Srnec, L., Tolasz, R., Tuomenvirta, H., Werner, P., Linderholm, H., Philipp, A., Wanner, H., and Xoplaki E., 2006: Indices for daily temperature and precipitation extremes in Europe analyzed for the period 1901–2000. *J. Geophys. Res. 111*, D22106, 1–25. https://doi.org/10.1029/2006JD007103

Mohorji, M.A., Zeka, S., and Almazroui, M., 2017: Trend Analyses Revision and Global Monthly Temperature Innovative Multi-Duration Analysis, *Earth Syst. Environ. 1*, 9. https://doi.org/10.1007/s41748-017-0014-x

Mosase, E., Ahiablame, L., Light, F., and Dwomoh, F., 2019: A Case Study of Rainfall and Temperature Trends in San Diego Region, 1985–2017, *Hydrology 6, 87*; 1–20. https://doi.org/10.3390/hydrology6040087

Neumann, von J., 1941: Distribution of the Ratio of the Mean Square Successive Difference to the Variance, *Ann. Math. Stat. 12*, 367–395. https://doi.org/10.1214/aoms/1177731677

Panda, A. and Sahu, N., 2019: Trend analysis of seasonal rainfall and temperature pattern in Kalahandi, Bolangir and Koraput districts of Odisha, India, *Atmos. Sci. Lett., 20*, 1–10. https://doi.org/10.1002/asl.932

Palaniswami, S. and Muthiah, K., 2018: Change Point Detection and Trend Analysis of Rainfall and Temperature Series over the Vellar River Basin, *Pol. J. Environ. Stud.* 27, 1673–1681. https://doi.org/10.15244/pjoes/77080

Pettitt, A.N., 1979: A Non-Parametric Approach to the Change-Point Problem, *Appl. Stat. 28*, 126–135. https://doi.org/10.2307/2346729

Popovic, T., Djurdjevic, V., Zivkovic, M., Jović, B., and Jovanović, M., 2009: Promena klime u Srbiji i očekivani uticaji. Ministarstvo zastite zivotne sredine, Agencija za zastitu zivotne sredine Republike Srbije, Peta regionalna konferencija "EnE09—Zivotna sredina ka Evropi".

Piticar, A. and Ristoiu, D., 2012: Analysis of Air Temperature Evolution in Northeastern Romania and Evidence of Warming Trend, *Carpathian J. Earth Environ. Sci. 7, 4*, 97–106.

Radevski, I., Gorin, S., Taleska, M., and Dimitrovska, O., 2018: Natural regime of streamflow trends in Macedonia. *Geografie 123*, 1–20. https://doi.org/10.37040/geografie2018123010001

Radivojević, A., Martić Bursać, N., Gocić, M., Filipović, I., Pavlović, M., Radovanović, M., Stričević, Lj., and Punišić, M., 2015: Statistical analysis of temperature regime change on the example of Sokobanja basin in Eastern Serbia. *Thermal Sci. 19, Suppl. 2*, 323–330. https://doi.org/10.2298/GSGD0401019R

Radovanović, M. and Ducić, D., 2004: Kolebanje temperature vazduha u Srbiji u drugoj polovini XX veka, *Glasnik Srpskog geografskog društva 84,1*, 19–29.

Rakićević, T. 1980: Klimatska rejonizacija Srbije. Posebno izdanje Geografskog institute Srbije, 27, 29–42.

Ramezani, Y., Khashei-Siuki, A., and Nazeri Tahroudi, M., 2020: Spatial distribution of the daily, monthly, and annual precipitation concentration indices in the Lake Urmia basin, Iran. *Időjárás 124*, 73–95. https://doi.org/10.28974/idojaras.2020.1.4

Republic Hydrometeorological Service of Serbia (RHSS), 2020: Website of the RHSS, http://www.hidmet.gov.rs/ (accessed 29 July 2020).

Ruml, M., Gregorić, E., Vujadinović, M., Radovanović, S., Matović, G., Vuković, A., Počuča, V., and Stojičić Dj., 2017: Observed changes of temperature extremes in Serbia over the period 1961−2010, *Atmos. Res. 183*, 26–41. https://doi.org/10.1016/j.atmosres.2016.08.013

Sen, P.K., 1968: Estimates of the regression coefficient based on Kendall's tau. *J. Amer. Stat. Assoc. 63,*1379–1389. https://doi.org/10.1080/01621459.1968.10480934

Sharma, V., Nicholson, C., Bergantino, A., Irmak, S., and *Peck, D.,* 2020: Temporal Trend Analysis of Meteorological Variables and Reference Evapotranspiration in the Inter-Mountain Region of Wyoming. *Water, 12,* 21–59. https://doi.org/10.3390/w12082159

Stričević, Lj., 2015: Vodni resursi Rasinskog okruga i njihov uticaj na regionalni razvoj, Doktorska disertacija, Prirodno-matematički fakultet, Univerzitet u Nišu.

Tadić, L.,Brleković, T., Hajdinger, A.,Španja, S., 2019: Analysis of the Inhomogeneous Effect of Different Meteorological Trends on Drought: An Example from Continental Croatia, *Water 11,* 2625. https://doi.org/10.3390/w11122625

Tan, M., L., Samat, N., Chan, W., N., Lee, A., J., and *Li, C.,* 2019: Analysis of Precipitation and Temperature Extremes over the Muda River Basin. Malaysia, *Water 11,* 283–299. https://doi.org/10.3390/w11020283

Toreti, A., Kuglitsch, G. F., Xoplaki, E., Della Marta, P., Aguilar, E., Prohom, M., Luterbacher, J., 2011: A note on the use of the standard normal homogeneity test (SNHT) to detect inhomogeneities in climatic time series. *Int. J. Climatol. 31* 630–632. https://doi.org/10.1002/joc.2088

Tošić, I., Hrnjak, I., Gavrilov, M.B., Unkašević, M., Marković, S.B., and *Lukić, T.,* 2014: Annual and seasonal variability of precipitation in Vojvodina, Serbia. *Theor. Appl. Climatol. 117,* 331–341. https://doi.org/10.1007/s00704-013-1007-9

Unkašević, M. and *Tošić, I.,* 2009: An analysis of heat waves in Serbia. Glob. *Planet. Change 65,* 17–26. https://doi.org/10.1016/j.gloplacha.2008.10.009

Unkašević, M. and *Tošić, I.,* 2013: Trends in Temperature Indices over Serbia: Relationship to Large Scale Circulation Patterns. *Int. J. Climatol. 33,* 3152–3161. https://doi.org/10.1002/joc.3652

Vukoičić, D., Milosavljević, S., Penjišević, I., Bačević, N., Nikolić, M., Ivanović, R., and *Jandžiković, B.,* 2018: Spatial analysis of air temperature and its impact on the sustainable development of mountain tourism in Central and Western Serbia. *Időjárás 122,* 259–283. https://doi.org/10.28974/idojaras.2018.3.3

Vuković, A., Vujadinović, M., Rendulić, S., Djurdjević, V., Ruml, M., Babić, V., and *Popović, D.,* 2018: Global warming impact on climate change in Serbia for the period 1961–2100. *Thermal Sci. 22,* 2267–2280. https://doi.org/10.2298/TSCI180411168V

Wijngaard, B.J., Klein Tank, G.M.A. and *Konneh P.G.,* 2003: Homogeneity of 20th century European daily temperature and precipitation series. *Int. J. Climatol. 23,* 679–692. https://doi.org/10.1002/joc.906

Zarenistanak, M., Dhorde, G.A. and *Kripalani, H.R.,* 2014: Trend analysis and change point detection of annual and seasonal precipitation and temperature series over southwest Iran, *J. Earth Syst. Sci. 123,* 281–295. https://doi.org/10.1007/s12040-013-0395-7

INSTRUCTIONS TO AUTHORS OF *IDŐJÁRÁS*

The purpose of the journal is to publish papers in any field of meteorology and atmosphere related scientific areas. These may be

- research papers on new results of scientific investigations,
- critical review articles summarizing the current state of art of a certain topic,
- short contributions dealing with a particular question.

Some issues contain "News" and "Book review", therefore, such contributions are also welcome. The papers must be in American English and should be checked by a native speaker if necessary.

Authors are requested to send their manuscripts to

Editor-in Chief of IDŐJÁRÁS
P.O. Box 38, H-1525 Budapest, Hungary
E-mail: journal.idojaras@met.hu

including all illustrations. MS Word format is preferred in electronic submission. Papers will then be reviewed normally by two independent referees, who remain unidentified for the author(s). The Editor-in-Chief will inform the author(s) whether or not the paper is acceptable for publication, and what modifications, if any, are necessary.

Please, follow the order given below when typing manuscripts.

Title page should consist of the title, the name(s) of the author(s), their affiliation(s) including full postal and e-mail address(es). In case of more than one author, the corresponding author must be identified.

Abstract: should contain the purpose, the applied data and methods as well as the basic conclusion(s) of the paper.

Key-words: must be included (from 5 to 10) to help to classify the topic.

Text: has to be typed in single spacing on an A4 size paper using 14 pt Times New Roman font if possible. Use of S.I.

units are expected, and the use of negative exponent is preferred to fractional sign. Mathematical formulae are expected to be as simple as possible and numbered in parentheses at the right margin.

All publications cited in the text should be presented in the *list of references*, arranged in alphabetical order. For an article: name(s) of author(s) in Italics, year, title of article, name of journal, volume, number (the latter two in Italics) and pages. E.g., *Nathan, K.K.,* 1986: A note on the relationship between photo-synthetically active radiation and cloud amount. *Időjárás 90,* 10–13. For a book: name(s) of author(s), year, title of the book (all in Italics except the year), publisher and place of publication. E.g., *Junge, C.E.,* 1963: *Air Chemistry and Radioactivity.* Academic Press, New York and London. Reference in the text should contain the name(s) of the author(s) in Italics and year of publication. E.g., in the case of one author: *Miller* (1989); in the case of two authors: *Gamov* and *Cleveland* (1973); and if there are more than two authors: *Smith et al.* (1990). If the name of the author cannot be fitted into the text: *(Miller,* 1989); etc. When referring papers published in the same year by the same author, letters a, b, c, etc. should follow the year of publication. DOI numbers of references should be provided if applicable.

Tables should be marked by Arabic numbers and printed in separate sheets with their numbers and legends given below them. Avoid too lengthy or complicated tables, or tables duplicating results given in other form in the manuscript (e.g., graphs). *Figures* should also be marked with Arabic numbers and printed in black and white or color (under special arrangement) in separate sheets with their numbers and captions given below them. JPG, TIF, GIF, BMP or PNG formats should be used for electronic artwork submission.

More information for authors is available: journal.idojaras@met.hu